MAX-PLANCK-INSTITUT
FÜR HERZ- UND LUNGENFORSCHUNG

JUSTUS-LIEBIG-
UNIVERSITÄT
GIESSEN

Investigation of a Protein Complex Essential for Vascular Smooth Muscle Cell Function

Untersuchung eines Proteinkomplexes, der für die Funktion der glatten Gefäßmuskelzellen essentiell ist

INAUGURAL-DISSERTATION

For the award of the degree of Doctor of Natural Sciences
- Doctor rerum naturalium -
(Dr. rer. nat.)

Presented to the Department of Biology and Chemistry (FB 08)
of the Justus Liebig University Giessen

Submitted by

M. Sc. Salma Hachim

Bad Nauheim, April 2024

First reviewer: Prof. Dr. Thomas Böttger

Second reviewer: Prof. Dr. Dr. Thomas Braun

Declaration

I declare that I have completed this dissertation single-handedly without the unauthorized help of a second party and only with the assistance acknowledged therein. I have appropriately acknowledged and referenced all text passages that are derived literally from or are based on the content of published or unpublished work of others, and all information that relates to verbal communications. I have abided by the principles of good scientific conduct laid down in the charter of the Justus Liebig University of Giessen in carrying out the investigations described in the dissertation.

Salma Hachim

Department of Cardiac Development and Remodelling (Prof. Dr. Dr. Thomas Braun)
AG Böttger (Prof. Dr. Thomas Böttger)
Max Planck Institute for Heart and Lung Research,
Bad Nauheim

Publications

Schutt C, Hallmann A**, Hachim S**, Klockner I, Valussi M, Atzberger A, Graumann J, Braun T, Boettger T. Linc-MYH configures INO80 to regulate muscle stem cell numbers and skeletal muscle hypertrophy. EMBO J. 2020; 39 (22):e105098. doi: 10.15252/embj.2020105098

Weiss M, Hettrich S, Hofmann T, **Hachim S**, Günther S, Braun T, Boettger T. Mitolnc controls cardiac BCAA metabolism and heart hypertrophy by allosteric activation of BCKDH. Nucleic Acids Res. 2024 Apr 3:gkae226. doi: 10.1093/nar/gkae226. Epub ahead of print. PMID: 38567728.

Summary

INO80 is an evolutionary conserved chromatin remodelling complex composed of over 15 different subunits organized in structural modules. The INO80 complex acquires different subunits, including the transcription factor YY1, contingent on the tissue specific function the complex may carry out. INO80 alters DNA accessibility of chromatin in an ATP-dependent manner through histone variant exchange, nucleosome spacing, nucleosome sliding and nucleosome eviction. These INO80 dependent processes contribute to various fundamental nuclear DNA based functions classified through transcriptional regulation, DNA replication as well as DNA damage repair at double strand breaks. INO80 has been shown to be essential for embryonic development and to play a role in several cell types. Germline deletion of Ino80 leads to early embryonic lethality due to failure in gastrulation, growth retardation, and significant cell death as a consequence of the loss of INO80-dependent transcriptional regulation. In addition to this, INO80-dependent transcriptional regulation has been shown to control cell cycle in cardiac endothelial cells as well as proliferation in hepatocytes, satellite cells and cardiac endothelial cells. Nonetheless, the functions of INO80 on a molecular level and its contribution in the development, contractility and regeneration of smooth muscle cells in the cardiovascular system are yet to be understood.

To characterize the functions of INO80 in vascular smooth muscle cells (VSMCs), the Ino80-encoding gene was inactivated in smooth muscle cells of mice using the Cre-loxP system. This work demonstrates for the first time how two essential functions of the INO80 chromatin remodelling complex contribute to different aspects of the INO80 loss of function phenotype in VSMCs**.** Global analysis of the function of INO80 in VSMCs transcriptional regulation revealed that loss of INO80 led to major changes in transcriptional programs and that YY1 is an essential co-factor of INO80 transcriptional regulation. We report that INO80 binds to the myocardin promoter to transcriptionally activate myocardin and thereby maintains VSMCs contractility most likely through recruitment by YY1. Loss of this function leads to a decrease in VSMCs contractility, altered migration, as well as blunted or unsuited responsiveness to environmental cues. Moreover, we show that the DNA repair function of INO80 controls VSMCs metabolism by regulating FOXO1 activity through a cascade of defined regulatory events involving an increase in DNA damage induced ROS production. Finally, we

propose that changes in the VSMCs phenotype upon loss of INO80 culminate in the acceleration of atherosclerosis development as reported in humans upon homozygous missense mutation of Ino80d, a subunit of the INO80 complex.

In summary, this study demonstrates how two distinct molecular functions of a chromatin remodeler affect VSMCs physiological performance and progression of atherosclerosis.

Zusammenfassung

Der INO80-Komplex ist ein evolutionär konservierter Chromatin-Remodeller-Komplex, der aus über fünfzehn verschiedenen, in Modulen organisierten Untereinheiten zusammengesetzt ist. Die Interaktion zwischen dem INO80-Komplex und den verschiedenen Untereinheiten erfolgt dynamisch, beispielsweise mit dem Transkriptionsfaktor YY1, um gewebespezifische Funktionen zu realisieren. INO80 verändert die Zugänglichkeit der DNA im Zellkern in ATP-abhängiger Weise durch Veränderung des Nukleosomenabstandes, den Austausch von Histonen, sowie durch die Verschiebung und den Ausschluss von Nukleosomen aus dem Chromatin. Auf der Basis dieser Prozesse trägt der INO80-Komplex zu verschiedenen grundsätzlichen Funktionen im Chromatin bei, unter anderem zur transkriptionellen Regulation, der DNA-Replikation und der Reparatur von DNA-Doppelstrangbrüchen. Diese Funktionen sind essentiell für die embryonale Entwicklung und treten in unterschiedlichen Zellarten auf. Die Deletion von INO80 in der Keimbahn führt zu einer Störung der Gastrulation, zur Wachstumshemmung, vermehrtem Zelltod und letztlich zur embryonalen Letalität, als Resultat des Verlusts der INO80-abhängigen transkriptionellen Regulation. Zellspezifisch wurde die INO80-abhängige transkriptionelle Regulation des Zellzyklus in kardialen Endothelzellen beschrieben, sowie Störungen der Proliferation in Hepatozyten und Satellitenzellen beobachtet. Die molekularen und zellulären Funktionen von INO80 bei der Entwicklung und Funktion der glatten Muskelzellen des kardiovaskulären Systems sind bisher jedoch nicht verstanden.

Um die Funktion des INO80-Komplexes in vaskulären glatten Muskelzellen (VSMCs) zu untersuchen, wurde das für die zentrale Untereinheit des INO80-Komplexes kodierende INO80-Gen mittels des Cre-loxP Systems in Mäusen inaktiviert. Diese Untersuchung demonstriert zum ersten Mal, wie zwei essentielle molekulare Funktionen des INO80-Komplexes zum Phänotyp der VSMCs beitragen. Die globale Analyse der Funktion von INO80 bei der transkriptionellen Regulation zeigte wesentliche Veränderungen von transkriptionellen Programmen und dass YY1 ein essentieller Kofaktor von INO80 in VSMC ist. Die Arbeit zeigt, dass INO80 am Promoter des Myocardin Gens bindet und die Expression dieses Gens durch die Rekrutierung von YY1 aktiviert. Der Verlust dieser Regulation führt zu verminderter Kontraktion der VSMCs, veränderter Migration dieser Zellen und massiver

Abschwächung der Reaktion der Zellen auf gefäßspezifische Reize. Des Weiteren wird gezeigt, dass die DNA-Reparaturfunktion von INO80 den Metabolismus von VSMC kontrolliert, in dem die Aktivität von FOXO1 über eine definierte Kaskade an regulatorischen Ereignissen reguliert wird, die eine von DNA-Schäden abhängige Erhöhung der ROS Produktion beinhaltet.

Der Verlust von INO80 führt in letzter Konsequenz zu einer verstärkten Atherosklerose, welche in Korrelation zum beschriebenen Phänotyp bei missense Mutationen der humanen INO80d Untereinheit steht.

Zusammenfassend zeigt diese Studie, wie zwei unterschiedliche molekulare Funktionen eines Chromatin-Remodeller-Komplexes die physiologische Leistungsfähigkeit von vaskulären glatten Muskelzellen ermöglichen und den Verlauf von Atherosklerose beeinflussen.

Table of Contents

List of figures

List of tables

List of Abbreviations

AAV8	Adeno Associated virus 8
Acta1	Actin alpha 1
Acta2	Smooth muscle actin
Actg2	Actin gamma 2
AKT	Protein kinase B
AP-1	Activator protein 1
Arp	Actin-related protein
aSMA	Alpha smooth muscle actin
aSMA pos. layer	Alpha smooth muscle actin positive layer
aSMCs	Aortic smooth muscle cells
$AT_{1/2}$	Angiotensin receptor 1/2
ATP	Adenosine triphosphate
AutoN	Autoinhibitory N-terminal
AV	Aortic valve
BIN1	Bridging integrator 1
bp	Basepair
Bromo	Bromodomain
C	Celsius
C.thermophilum	Chaetomium thermophilum
Ca^{2+}	Calcium ions
Cald1	Caldesmon 1
CEBPB	CCAAT enhancer binding protein beta
CEBPD	CCAAT enhancer binding protein delta
CHD	Chromodomain helicase DNA-binding

ChIP -exo	Chromatin immunoprecipitation with lambda exonuclease digestion
CI-V	Complexes I-V
CMV	Cytomegalovirus
Cnn	Calponin
CnR/ Cut & Run	Cut and Run
CNS	Central nervous system
CRC	Chromatin remodelling complex
Cre	Tyrosine recombinase enzyme derived from the P1 Bacteriophage
Cryo-EM	Cryogenic electron microscopy
DAG	Diacylglycerol
DBD	DNA-binding domain
DCF	Dichlorodihydrofluorescein
DCFDA	Dichlorofluorescin Diacetate
Des	Desmin
DNA	Deoxyribonucleid acid
dNTP	Deoxyribonucleotide
DPI	Diphenyleneiodonium chloride
DSB	Double strand break
DTT	Dithiothreitol
DUSP1	Dual specificity phosphatase 1
EB	Extraction buffer
EDTA	Ethylenediaminetetraacetic acid
EdU	5-ethynyl-2´-deoxyuridine
Edu+	5-ethynyl-2′-deoxyuridine positive
eGFP	Enhanced green fluorescent protein
EtOH	Ethanol
$FADH_2$	Flavin adenine dinucleotide

FAO	Fatty acid oxidation
FC	Fold change
FCS	Fetal calf serum
fos	Fos proto-oncogene
FOXO	Forkhead box
FOXO1	Forkhead box O1
FOXO4	Forkhead box O4
FST	Follistatin
fwd	Forward
FWER	Family-wise error rate
Gapdh	Glyceraldehyde 3-phosphate dehydrogenase
GPCR	G protein-coupled receptors
GRP	Glucose-Regulated Protein
GSEA	Gene set enrichment analysis
H	Histone
H_20_2	Hydrogen peroxide
H2CFDA	Dichlorodihydrofluorescein diacetate
HCl	Hydrochloric acid
HFD	High fat diet
HOXB8	Homeobox B8
HSA	Helicase/SANT-associated
HSA/PTH	helicase-SANT-associated/Post-HSA
HSS	HAND–SANT–SLIDE
IGV	Integrative genomics viewer
INO80	Inositol requiring 80
INO80C	INO80 complex subunit c
INO80D	INO80 complex subunit d
INO80E	INO80 complex subunit e
IP_3	Inositol trisphosphate
ISWI	Imitation switch

JNK	c-Jun N-terminal kinases
JNK1	Mapk8: mitogen-activated protein kinase 8/ C-Jun N-Terminal Kinase 1
JNK2	Mapk9: mitogen-activated protein kinase 9/ C-Jun N-Terminal Kinase 2
Jun/ c-Jun	Jun proto-oncogene
kB	Kilobase
KCl	Potassium chloride
KCNJ15	Potassium inwardly rectifying channel subfamily j member 15
kDa	Kilodalton
KEGG	Kyoto Encyclopedia of Genes and Genomes
KO	Knockout
L	Litre
L-Asc. Acid	L-ascorbic acid
L-NAME	N (gamma)-nitro-L-arginine methyl ester
LB	Lysogeny broth
LDL	Low density lipoprotein
lox	LoxP
loxP	Locus of X-over P1
LSA	Left subclavian artery
M	Molar
MAPK	Mitogen-activated protein kinase
MCRS1	Microspherule protein 1
Mg	Magnesium
$MgCl_2$	Magnesium chloride
Min	Minute
ml	Millilitre

MLC kinase	Myosin light-chain kinase
MLCK	Myosin light chain kinase
MLCP	Myosin light-chain phosphatase
mm	Millimetre
mM	Millimolar
mmHg	Millimetre mercury
Mmol	Millimol
MMS	Methyl methane sulfonate
MNase	Micrococcal Nuclease
Myocd	Myocardin
NADH	Nicotinamide
NFR	Nucleosome-free region
NFRKB	Nuclear factor related to κB
Nhp10	Non-histone protein 10
NIH	National institute of health
nm	Nanometer
NOX/ Nox	NADPH oxidase
NR4A2	Nuclear receptor 4A2
NRG1	Neuregulin 1
NTD	N-terminal domain
Nucleotide/base A	Adenosine
Nucleotide/base C	Cytosine
Nucleotide/base G	Guanine
Nucleotide/base T	Thymine
OARD1	O-acyl-ADP-ribose deacylase 1
OE	Overexpression
Oligo	Oligonucleotide
ORF	Open reading frame
OXPHOS	Oxidative phosphorylation
P-AKT	Phospho protein kinase B
P-c-JUN	Phospho jun proto-oncogene
P-FOXO1	Phospho Forkhead box protein O1

P-RPA	Phospho replication protein A
P53	Tumor protein p53
PA	Phosphatidic acid
PASMCs	Pulmonary arterial smooth muscle cells
PBS	Phosphate buffered saline
PCR	Polymerase Chain Reaction
PCSK9	Proprotein Convertase Subtilisin / Kexin type 9
PFA	Paraformaldehyde
PHO	Pleiohomeotic
PKC	Protein kinase C
PLA_2	Phospholipase A_2
PLC	Phospholipase C
PLD	Phospholipase D
Pos. layer	Positive layer
PROX1	Prospero Homeobox 1
PS	Penicillin/streptomycin
PTM	Post-translational modification
qPCR	Quantitative polymerase chain reaction
RAAS	Renin-angiotensin-aldosterone system
Rac1	Ras-related C3 botulinum toxin substrate 1
RAD 51/52	RAD recombinase 51/52
Ras	Rat sarcoma virus
RCA	Right common carotid artery
rev	Reverse
Rho	Ras homologous
RhoA	Ras homolog family member A
RNA	Ribonucleic acid
ROS	Reactive oxygen species

RPA	Replication protein A
rpm	Revolutions per minute
RSA	Right subclavian artery
RT	Real-time, reverse transcriptase
RUNX1	RUNX family transcription factor 1
RuvBL1/Rvbl1	RuvB Like AAA ATPase 1
RuvBL2/Rvbl2	RuvB Like AAA ATPase 2
s	seconds
S. cerevisiae	Saccharomyces cerevisiae
scRNA seq	Single cell RNA sequencing
Ser	Serine
siRNA	Small interfering RNA
SM22	Transgelin
SMCs	Smooth muscle cells
SnAC	Snf2 ATP coupling
Snf2	Sucrose non fermenting 2
Snf2ATPase	Sucrose non fermentable 2 ATPASE
SRCAP	Snf2 Related CREBBP Activator Protein
SRF	Serum response factor
SWI/SNF	Switch/sucrose non-fermentable
SWR1	SWI2/SNF2-Related 1 Chromatin Remodeling Complex
T1/10E	Tris (hydroxymethyl)aminomethane) -EDTA buffer diluted 1:10
Taf9	TATA-Box Binding Protein Associated Factor 9
Taq	Thermus aquaticus

TBHP	Tert-Butyl hydroperoxide
TBS-T	Tris Buffered Saline with Tween
TF	Transcription factor
TFPT	TF3 fusion partner
Tgln	Transgelin
Thr	Threonine
Tris	Tris (hydroxymethyl)aminomethane
TSS	Transcription start site
U	Unit
UTR	Untranslated region
UV	Ultraviolet
VSMCs	Vascular smooth muscle cells
w/v	Weight per volume
WB	Western Blot
wt	Wildtype
YY1	Yin yang 1
γ-H2AX	Gamma H2A.X variant histone
µl	Microliter
µM	Micromolar

1. Introduction

Complex organisms are highly organized assemblies of different cell types determined by their genomic DNA. Genomic DNA is compacted and organized with proteins to form chromatin. Various mechanisms control accessibility of the genome on the chromatin level, thereby regulating essential processes such as gene transcription, DNA replication and DNA repair(Luger et al., 2012). This thesis analyses the roles of an ATP-dependent chromatin remodeler INO80 in adult vascular smooth cells (VSMCs). Thus, it is fundamental to give a short overview on chromatin remodelers, INO80 itself, essential transcription factors which we found to be involved in INO80 dependent VSMCs regulation as well as the cell type of interest, VSMCs.

1.1 Chromatin structure in eukaryotes

Walther Flemming coined the term “chromatin” for the stainable fibrous structures observed in the nucleus (Flemming, 1882). Nucleosomes in simple terms, are the basic repeating unit of chromatin and consist of DNA wrapped around a histone core. Histones, namely H1, H2A, H2B, H3 and H4, are positively charged proteins which are able to tightly bind with the negatively charged DNA and compact it (Annunziato, 2008). The canonical nucleosome structure is formed by tightly wrapping 146 bp of DNA fragment around a globular compact histone octamer core made of two copies each of the unmodified major type histones H2A, H2B, H3 and H4 (figure 1) (Tyagi et al., 2016; Zhou et al., 2019). The nucleosome is stabilized by numerous protein-to-protein interactions within the histone octamer as well as through multiple electrostatic and hydrogen bonds between the histone proteins and the DNA(Davey et al., 2002; Luger et al., 1997; Rohs et al., 2009). Histones and DNA are in contact through structurally conserved histone-fold domains which organize the majority of DNA wrapped around the nucleosome (120 bp of DNA). The remaining DNA at each end is bound by the N-terminal alpha-helix, which is specific to H3 (Luger et al., 1997). These interactions are essential for maintaining nucleosome stability (Iwasaki et al., 2013). H3 and H4 form a symmetric heterotetramer inside the histone core by hydrophobic insertion of a four-helix-bundle structure between two H3 proteins (figure 1) (Zhou et al., 2019). Two H2A-H2B dimers then interact with the H3-H4 tetramer through several interactions including but not limited to, a four-helix-bundle structure between H2B and H4 as well as additional interactions between the H2A docking domain and H3-H4

(Zhou et al., 2019). Nucleosomes are then connected by 20 - 90 bps of DNA segments (termed “linker DNA”) together forming nucleosomal arrays (figure 1) (Annunziato, 2008; Beshnova et al., 2014; Luger et al., 2012; Olins & Olins, 1974; Weintraub, 1978).

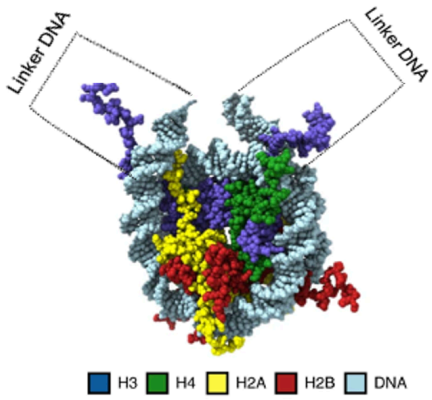

Figure 1. Nucleosome structure (Adapted from (Zhou et al., 2019)).
Nucleosome disc view, model of histone octamer derived from protein data bank 1KX5(Davey et al., 2002) and model of DNA from protein data bank 1ZBB(Schalch et al., 2005).

Finally, nucleosomes are arranged in a beads-on-a-string organization and are connected through binding of linker histones, including multiple H1 variants, to turn chromatin fibers into chromatosomes (figure 2) (Annunziato, 2008; Woodcock et al., 1976). One linker histone associates with linker DNA (Shen & Gorovsky, 1996; Thoma & Koller, 1977). Eventually, further looping, compression and coiling lead to the formation of chromosomes (figure 2).

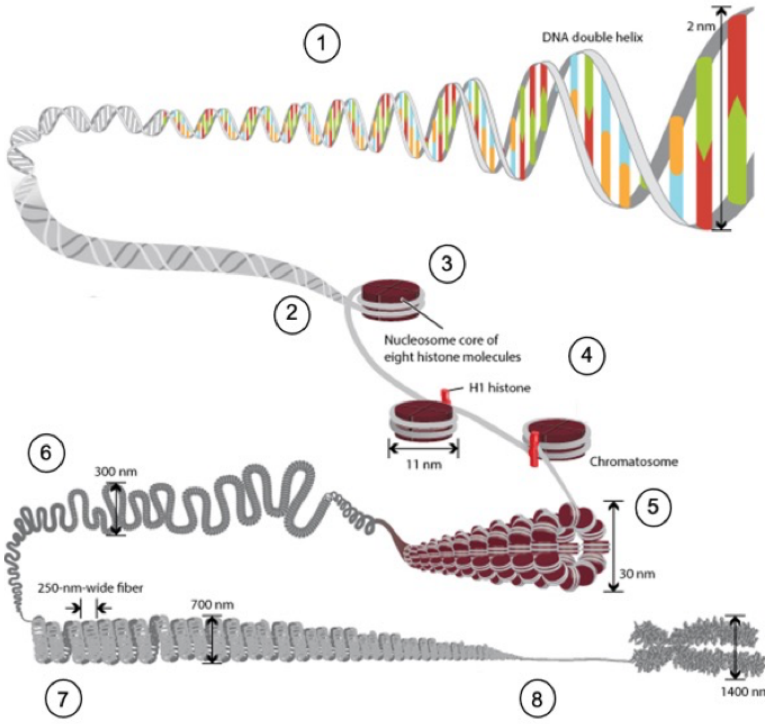

Figure 2. Nucleosome assembly and DNA packaging in eukaryotic cells (Adapted from (Annunziato, 2008)).
1 On the basic level, chromatin is a double-stranded helical structure of DNA and protein. **2** DNA is compacted with histones to form nucleosomes. **3** Nucleosomes are made of eight histone proteins around which 146 bp of DNA wraps itself. **4** A chromatosome consits of a nuclesomome (11 nm) attached to a H1 histone protein. **5** Nucleosomes are folded in on each other and organised into forming a hollow tube like 30 nm fiber. **6** The chromatin fibers compacts and forms loops averaging 300 nm in length. **7** The 300 nm fibers are further compressed and folded to produce a 250 nm wide and 700 nm long fiber. **8** Tight coiling of the 250-nm fibers form the chromatid of a chromosome. Top right vertical double–ended arrow indicates that DNA double helix strands are 2 nm apart. DNA strands are shown as gray ribbons connected by vertical red/green or yellow/cyan coloured bars which represent the 4 types of bases (A C T G) found in a DNA molecule.

In contrast to the canonical nucleosome structure detailed above, non-canonical nucleosomes present either partially detached DNA, partially detached histones, fewer than eight histones or a combination of these features (Zlatanova et al., 2009).

In eukaryotes, higher-order chromatin can be classified into two major structures: heterochromatin and euchromatin. The majority of chromatin is present as heterochromatin which is characterized by a tightly packed, condensed structure and thereby an inactive transcriptional status due to a lack of DNA accessibility for other DNA binding proteins (Lee et al., 2020). Heterochromatin is initially formed and regulated during embryogenesis and can be further categorized into constitutive and facultative heterochromatin. Constitutive heterochromatin comprehends permanent domains of heterochromatin which are usually found in centromeric or telomeric

regions containing satellite sequences (small regions which are repeated many times) and transposable elements (Allshire & Madhani, 2018). Facultative heterochromatin is characterized by genes which are transcriptionally regulated in a cell specific modus and according to morphogenesis and differentiation signals (Trojer & Reinberg, 2007). In contrast to this, euchromatin is characterized by actively transcribed genes and is commonly found in the inside of the interphase nucleus (Morrison & Thakur, 2021).
Euchromatin, has an open, unfolded structure, contains wider spacing between nucleosomes, as well as histone modifications and variants permitting the transcriptional machinery to bind the DNA and consequently facilitating subsequent activation of transcription (Adam et al., 2001; DiFiore et al., 2020; Draker et al., 2012; Jin et al., 2009; Morrison & Thakur, 2021; Smale & Kadonaga, 2003; Venkatesh et al., 2012; Venkatesh & Workman, 2015). Euchromatin is in the vast majority found on transcriptionally active gene bodies as well as on regulatory elements such as promoter and enhancer elements (Venkatesh & Workman, 2015). Euchromatin is organized into transcriptionally inactive domains intermixed with pockets of transcriptional activity, called the active nuclear compartment (Morrison & Thakur, 2021). Euchromatin contains the highest proportion of nucleosomes with precise nucleosomal positions relative to the underlying DNA sequence (Radman-Livaja & Rando, 2010). In fact, nucleosome positioning is directly linked to the precise recognition of DNA sequence motifs by their protein partners which plays an essential role in transcription regulation close to transcription initiation sites (K. Struhl & E. Segal, 2013).

1.2 Chromatin dynamics and functions

Although the nucleosome is stabilized through the numerous interactions described in part 1.1, it is not a static ‘disc’ as the crystal structure in figure 1 might suggest. Conversely, nucleosomes are highly dynamic in terms of both structural composition and nucleosome arrangement. The spacing between nucleosomes can vary depending on the underlying DNA sequence, activity of chromatin remodelers and other DNA binding factors (such as transcription factor binding). These changes in chromatin structure affect gene expression and thereby modulate cell specific gene regulatory networks (van Holde & Zlatanova, 2007).
Nucleosomes undergo intrinsic structural dynamics through fast transient DNA unwrapping and re-wrapping commonly termed “DNA breathing” (Zhou et al., 2019).

Spontaneous unwrapping of DNA (occurring 2-10% of the time) from the histone octamer is an essential feature of nucleosome dynamics as this expose's protein-binding sites in nucleosomal DNA which are otherwise hidden away (Li & Widom, 2004). Following protein binding on these sites, the unwrapping equilibrium shifts allowing for further unwrapping of the DNA to take place (Zhou et al., 2019). This process allows for protein-sequence specific DNA binding to take place in the presence of nucleosomes (Zhou et al., 2019). This process similarly takes place for nucleosomes also contained within a nucleosomal array. Indeed, these nucleosomes also experience spontaneous DNA unwrapping alike single nucleosomes, rendering their DNA equally accessible to DNA binding proteins likely as an answer to different biological cues (Poirier et al., 2008; Poirier et al., 2009; Zhou et al., 2019).

Furthermore, different states of histone post-translational modifications (PTMs) (commonly also called epigenetic marks) as well as variations in the composition of histone protein variants alter nucleosome structure and thus DNA interaction properties (Luger et al., 2012; Zhou et al., 2019).

Histones are decorated with a plethora of PTMs which regulate chromatin structure and thereby DNA-templated processes (Millan-Zambrano et al., 2022). Histone PTMs can be found on the flexible histone tails (consisting of 15 to 38 amino acids from each histone N terminus) away from nucleosomal DNA, as well as in their core globular domains (Cosgrove et al., 2004). The most common histone PTMs are methylation, phosphorylation, acetylation and ubiquitin like modifications (Millan-Zambrano et al., 2022). Different types of PTMs operate through various direct and indirect mechanisms and certain combinations of PTMs display strong synergetic effects adding another layer of complexity (Brehove et al., 2015). Histone PTMs which act directly initiate a local structural alteration of the chromatin leading to a direct genomic response such as transcriptional activation (Millan-Zambrano et al., 2022). Indirectly acting histone PTMs require an intermediate step such as binding of an effector protein or chromatin remodeling complex but also ultimately generate DNA-templated processes (Millan-Zambrano et al., 2022).The most characterized PTM to date is lysine acetylation, a modification which is mainly associated with chromatin accessibility and transcriptional activity, and which can be reversed by deacetylation through deacetylases which mediate transcriptional repression (Sterner & Berger, 2000). Histone methylation is the second best characterized PTM, and takes place on the side chains of lysines and arginines (Bannister & Kouzarides, 2011). Histone

methylation consists of methyltransferases with a distinctive extended catalytic active site which catalyses the transfer of a methyl group from S-adenosylmethionine to a lysine's ε-amino group or to a he ω-guanidino group of arginine. Lysines might be mono-, di- or tri-methylated by histone lysine methyltransferases (HKMTs), meanwhile arginines can be mono-, symmetrically or asymmetrically di-methylated by arginine methyltransferases (PRMTs) (Bannister & Kouzarides, 2011; Bedford & Clarke, 2009; Lan & Shi, 2009; Ng et al., 2009). Histone methylation is considered to be a stable static modification, nonetheless lysine and arginine methylation can be reversed by different demethylase enzymes such as JMJD2 demethylase (Bannister & Kouzarides, 2011; Whetstine et al., 2006).

1.3 Chromatin remodelers

In addition to the action of histone modifying enzymes, another class of enzymes contributes to higher order chromatin compaction and nuclear organization. Chromatin dynamics include the action of specialized ATP-dependent chromatin-remodeling complexes (CRCs) commonly termed chromatin remodelers. Nucleosome remodelers are multi-subunit complexes containing an Snf2 (sucrose non fermenting 2) type ATPase catalytic core which transforms the energy of ATP hydrolysis to disrupt the contacts between histones and DNA. In answer to various biological needs, specialized groups of remodelers adapt genome-wide nucleosome occupancy and composition altering thereby DNA accessibility to make it directly available during cellular processes (Clapier C. R., 2014; Hargreaves & Crabtree, 2011; Ho & Crabtree, 2010). Various genetic experiments have shown that ATP-dependent CRCs are fundamental regulators of the majority of chromosomal processes, and that their deregulation causes a variety of diseases, including but not limited to cancer (Clapier C. R., 2014; Lai & Wade, 2011; Rhee et al., 2018; Wilson & Roberts, 2011). As previously mentioned, a set of CRCs exploit the energy of ATP to interrupt nucleosome DNA contacts, move nucleosomes along DNA, as well as remove or exchange nucleosomes (Hargreaves & Crabtree, 2011). Other CRCs however, collaborate with site-specific transcription factors and histone-modifying enzymes to move or eject histones thereby enabling binding of transcription factors to DNA. Lastly, another family of remodelers creates specialized chromosomal regions where canonical histones are replaced by histone variants.

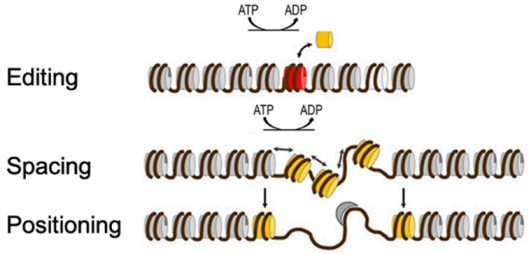

Figure 3. Representation of the general functions of chromatin remodeler complexes. (adapted from *https://www.genzentrum.uni-muenchen.de/research-groups/hopfner/research/chromatin-remodeller/index.html*, last accessed 24.04.24).
Chromatin remodeling complexes can perform different ATP-dependent functions. CRCs can edit the chromatin through histone variants exchange (editing) (red histone variant is exchanged by a yellow one). Additionally, CRCs can achieve changes in nucleosome spacing and positioning through nucleosome sliding and nucleosome ejection.

Phylogenic and functional studies have classified all chromatin remodeler ATPases within the RNA/DNA helicase superfamily 2 into four distinct subfamilies: imitation switch (ISWI), chromodomain helicase DNA-binding (CHD), switch/sucrose non-fermentable (SWI/SNF) and inositol requiring 80 (INO80) (Clapier C. R., 2014; Clapier & Cairns, 2009; Flaus et al., 2006) (figure 4).

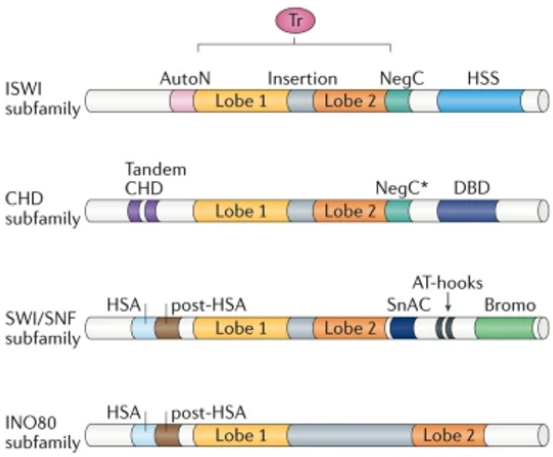

Figure 4. Domain organization of chromatin remodeling complex subfamilies (Clapier et al., 2017).
The ATPase-translocase domain (Tr) can carry out DNA translocation on its own. The Tr domain is made of two RecA-like lobes (lobe 1 and lobe 2). These lobes can be separated by either short (ISWI, CHD, SWI/SNF families) or long (INO80) insertions (grey). NegC* is a region with structural similarity to the ISWI negative regulator of coupling (NegC) domain; AutoN: autoinhibitory N-terminal; Bromo: bromodomain; DBD: DNA-binding domain; HSAhelicase/SANT-associated; HSS: HAND–SANT–SLIDE; SnAC: Snf2 ATP coupling (adapted from (Clapier et al., 2017)).

1.4 Structural organization of the chromatin remodeler INO80

The INO80 family includes the INO80 and the SWR1 chromatin remodeling complexes (SRCAP in mammals), which both contain a long insertion within the Snf2-ATPase domain (between lobe 1 and lobe 2) (figure 4) (Poli et al., 2017).

The INO80 chromatin remodeler is a large megadalton central multi-subunit enzyme complex with over 15 subunits, organized in structural modules (Jin et al., 2005; Shen et al., 2000). Ino80 is located on chromosome 2 in M*us musculus* and contains 37 exons (Gene ID: 68142, NIH). Ino80 is highly conserved and is located on chromosome 15 of the human genome, where it also contains 37 exons (Gene ID: 54617, NIH). The INO80 complex from yeast to humans was found to be composed of three different modules: the Snf2 -like ATPase/helicase domain as well as the helicase-SANT-associated/Post-HAS (HAS/PTH) domains flanked by non-conserved N- and C- terminal regions (figure 5) (Conaway & Conaway, 2009; Flaus et al., 2006). The ATPase/helicase domain has been proposed to provide a binding site for Arp5 and RuvBL1 and RuvBL2, a hexameric subcomplex consisting of two functionally associated AAA+ ATPases RuvBL1/2 (also commonly called Tip49a/b, or pontin/reptin in mammals) (Jonsson et al., 2004; Kunert et al., 2022; Poli et al., 2017). In S. cerevisiae, the HSA/PTH domain is required for ATP-dependent nucleosome remodeling and operates as a docking site for actin and actin-related proteins Arp4 and Arp8 (Shen et al., 2003; Szerlong et al., 2008). Prior reports have shown that the catalytic activity of the INO80 Snf2-like-ATPase domain is required for ATP-dependent nucleosome remodeling by the *S. cerevisiae* INO80 complex. Indeed, S. cerevisiae missing either a single or several actin related proteins (Arp), or the RuvBL1 and RuvBL2 AAA+ ATPase revealed strong reduction of nucleosome remodeling activities, thereby suggesting that these subunits either play a role in nucleosome remodeling activities and/or are essential to appropriate assembly of the INO80 complex (Jonsson et al., 2004; Shen et al., 2003). The human INO80 complex shares eight evolutionary conserved subunits with the S. cerevisiae INO80 complex comprising Snf2- family ATPase, the AAA+ ATPases RuvBL1 and RuvBL2, Arp4, Arp5, Arp8, Ino80B, Ino80C (figure 5) (Jin et al., 2005).

A

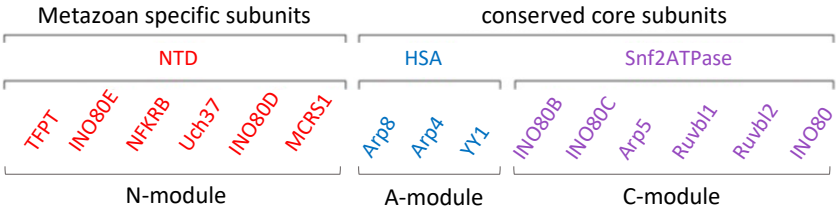

B

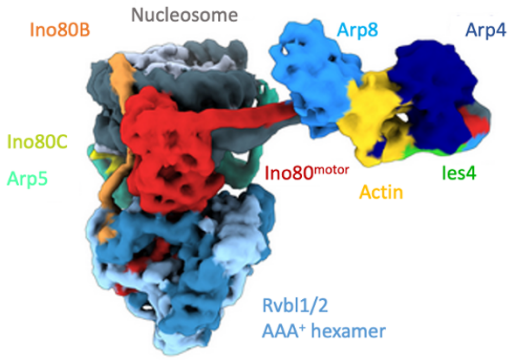

Figure 5. Modular organization of the INO80 complex (adapted from (Chen et al., 2011; Kunert et al., 2022)).

A Schematic diagram showing the domain and subunit organization of the INO80 complex. **B** Multibody refined Cryo-EM reconstitution of the C.thermophilum A and C modules binding to nucleosomal and extra-nucleosomal DNA.

In contrast to this, hIno80 lacks other orthologs of the S. cerevisiae INO80 complex subunits including Nhp10, Taf9, Ies1, Ies3 Ies4, Ies5, and contains instead several seemingly metazoan-specific subunits TFPT, INO80E, and nuclear factor related to κB (NFRKB), INO80D and the forkhead associated domain containing MCRS1 proteins (Jin et al., 2005; Yao et al., 2008). Both human and drosophila INO80 complexes contain the GLI- Kruppel family zinc finger transcription factor Yin-Yang-1 (YY1) (referred to as PHO in drosophila (Y. Cai et al., 2007; Klymenko et al., 2006; Wu et al., 2007). Another GLI-Kruppel family zinc finger protein referred to as Iec1 has been characterized in *Schizosaccharomyces pombe* INO80 complex and has also been suggested to be orthologous to YY1 and PHO (Hogan et al., 2010).

1.5 Dynamics and functions of INO80

The INO80 complex acquires divergent subunits in the holo-complex in different species and tissues relating with the extent of tissue and/or species-specific functions

the complex may carry out. INO80 contributes to various fundamental DNA based functions classified through transcriptional regulation (both basal and inducible), DNA replication as well as DNA damage repair (Poli et al., 2017).

1.5.1 Functions of INO80 in chromatin remodeling and transcriptional regulation

INO80 ATPase was initially reported in a genetic screen in S. cerevisiae where inositol depletion revealed defects in Inositol/choline responsive dependent gene activation (Ebbert et al., 1999). Further inter-species studies described that INO80 has a remodeling function which promotes transcriptional activation of genes induced by different signaling pathways. For instance, activation of PHO5 in yeast, upon phosphate depletion and induction of transcriptional activation by INO80 together with YY1 at the GRP78 locus, upon endoplasmic reticulum stress induction (Barbaric et al., 2007; Y. Cai et al., 2007; Steger et al., 2003).

In contrast to these findings, further studies reported that INO80 does not primarily respond to stress but rather regulates transcription more generally. Investigation of transcriptional changes under stress conditions showed that several genes were transcriptionally regulated (either up or down) in the presence or absence of INO80 (Mizuguchi et al., 2004; van Attikum et al., 2004). Indeed, transcriptome analysis of the loss of Ino80 in isogenic yeast strains revealed that 668 genes were upregulated and 488 genes were reduced by at least 1.5-fold. After exposure to the alkylating agent methyl methane sulfonate (MMS) an analogous Affymetrix-based analysis of gene expression found that 2500 genes were altered (upregulated and downregulated) by at least 1.5-fold in the WT background, of which only 80 responded differentially in the Ino80 mutant (van Attikum et al., 2004).

Recent studies have proposed that INO80 regulates transcription of genes on promoters through both transcriptional activation and repression by remodeling the position and composition of nucleosomes at promoters. Loss of the catalytic Ino80 subunit or Arp5-Ies6 core subcomplex in yeast reveled misregulation of 15% of the yeast genome (half of which was upregulated and the other half downregulated), in line with the findings from van Attikum et al., and Mizuguchi et al. (Mizuguchi et al., 2004; van Attikum et al., 2004; Yao et al., 2016).

Furthermore, this study could also correlate the observed transcriptional changes with occupancy by Ino80, Arp5 and Ies6 at the +1 nucleosome of the transcription start site

(TSS) of these regulated genes (Yao et al., 2016). Accordingly, a genome-wide study revealed that INO80 can bind over 90% of budding yeast's gene promoters (Yen et al., 2013). In human cells, transcription expression analysis in HeLa cells following RNA interference against the hINO80 subunit revealed mis-regulation of a similar number of genes (1936 ORFs in total with a comparable balance to yeast in terms of percentage of upregulated and downregulated genes) (Cao et al., 2015).

Investigation of Arp5/Ies6 (subunits of the INO80 complex) dependent genes in budding yeast indicates that INO80 has a general effect on metabolic genes related to glycolysis. In fact, upon loss of INO80, glycolysis related genes were found to be decreased whilst mitochondrial electron transport chain genes were increased (Yao et al., 2016). Additionally, INO80 was found to regulate the yeast inositol pathway and osmotic-stress-regulated yeast genes (Cao et al., 2015; Ebbert et al., 1999). Furthermore, INO80 aids repression of ecdysone regulated genes during pre-pupal development in Drosophila (Neuman et al., 2014). Human INO80 regulates expression of cell cycle genes, including p53 dependent genes (Cao et al., 2015). The mechanisms by which INO80 affect cell cycle genes could either be direct, through direct transcriptional regulation, or indirect, through accumulation of DNA damage (Poli et al., 2017).

Besides, INO80 determines chromatin structure at large nucleosome-free regions (NFRs) and nucleosome depleted regions (NDRs) (Jin et al., 2005; Shen et al., 2000; Udugama et al., 2011). ChIP-exo experiments mapped INO80 subunits across the genome on the near-nucleotide level and showed that the INO80 complex occupies NFRs, TSSs and over 90% of budding yeast promoters (Xue et al., 2015; Yen et al., 2012). Interestingly, INO80 is also recruited to transcription termination sites (TTSs), confirming that INO80 preferentially binds NFRs (Xue et al., 2015; Yen et al., 2012). INO80 appears to favorably bind/associates to nucleosomes containing extra-nucleosomal linker DNA in comparison to nucleosomes without additional linker DNA (Udugama et al., 2011).

Enrichment of INO80 at promoters doesn’t always correlate with changes in transcription (Klopf et al., 2017). For instance, upon activation of stress-response genes, INO80 recruitment correlates with recruitment of RNA polymerase II (RNAPII) (Klopf et al., 2009). INO80 interacts both with a subunit of RNAPII Rpb1 as well as with the transcription elongation complex PAF1, suggesting that the transcription machinery aids in INO80 recruitment at NFRs (Lafon et al., 2015; Poli et al., 2017; Poli

et al., 2016). So far, no INO80 subunit deletion mutant was able to fully nullify INO80 chromatin binding. To date, the precise mode of action by which INO80 is recruited to the chromatin remains unclear. It has however been suggested that instead of recognizing histone modifications, INO80 recruitment creates the NFR or is required by it, followed by other factors and/ or histone marks further stabilizing the NFR (Poli et al., 2017). Recently, Kunert et al., using cryo-electron microscopy and functional assays reported that binding of the INO80 A module (figure 5A) to DNA puts light on the INO80 linker DNA binding and illustrates the mechanism by which INO80 sliding may be controlled by extra-nucleosomal DNA features (Kunert et al., 2022). The A module of INO80 is connected to the motor unit of INO80 through an HSA/post-HSA lever element which chemo-mechanically couples the motor and linker DNA sensing (Kunert et al., 2022). Their work identified two sites of curved DNA recognition through the cooperative work of four actin/actin-related proteins and the motor INO80 subunit (Kunert et al., 2022).

As previously mentioned, INO80 utilizes the energy of ATP hydrolysis to intrinsically organize nucleosomes in *cis* and spaces them around 30 bp apart (Jin et al., 2005; Shen et al., 2003; Udugama et al., 2011). In yeast, INO80 was shown to recognize and establish NFRs, to correctly position the -1 and +1 nucleosomes relative to the TSS, as well as reposition nucleosomes after their mobilization by the elongation transcription machinery (Krietenstein et al., 2016; Yen et al., 2013).

In addition to moving canonical nucleosomes and hexasomes such as nucleosomes lacking a H2A-H2B dimer, INO80 has been reported to exchange H2A.Z with H2A, a function which is evolutionary conserved (Brahma et al., 2017; Papamichos-Chronakis et al., 2011). H2A.Z is a H2A variant which is found at promoter and enhancer elements and which serve various critical regulatory functions such as transcriptional control and DNA repair, centromeric heterochromatin and cancer (Albert et al., 2007; Giaimo et al., 2019). INO80 was found to be essential for efficient nucleosome remodeling during PHO5 gene activation, thereby ensuring PHO5 transcriptional activation (Barbaric et al., 2007; Mizuguchi et al., 2004). Furthermore, INO80 was also found to increase chromatin mobility at the PHO5 promoter (Neumann et al., 2012). These findings suggest that INO80-mediated exchange of H2A.Z enhances chromatin mobility at promoters and makes them accessible for transcriptional factors to allow for gene activation to take place. The pre-initiation complex of RNAPII also enhances removal of H2A.Z from the TSS and the INO80 interaction with the elongating RNAPII

machinery fosters its recruitment to inducible promoters. This suggests that H2A.Z removal by INO80 occurs post-initiation potentially to facilitate RNAPII passage through the +1 nucleosome (Hintermair et al., 2012; Klopf et al., 2009; Klopf et al., 2017; Lafon et al., 2015; Poli et al., 2016; Tramantano et al., 2016; Weber et al., 2014). In contrast to these findings, two studies in yeast, reported no changes in the distribution and occupancy levels of H2A.Z on chromatin upon the loss of INO80 (Jeronimo et al., 2015; Tramantano et al., 2016).

In addition to the regulation of protein coding genes, INO80 can inhibit bi-directional transcription at functional promoters and increase transcriptional silencing within heterochromatin (Marquardt et al., 2014; Xue et al., 2015). Similarly, to protein coding genes, the INO80 complex regulates expression of LncRNAs through nucleosome editing but suppresses heterochromatin associated transcripts through mechanisms which are yet to be clearly identified (Bure & Nemtsova, 2023).

On the other hand, lncRNAs have also been reported to regulate the function and composition of INO80 in a tissue specific manner. For example, lncRNA HAND2-AS1 recruits INO80 to the promoter of BMPR1A in order to allow for transcriptional activation of BMP signaling (Wang et al., 2019). Schutt et al. also described that the lncRNA linc-MYH acts as a selective molecular switch for INO80 by controlling the composition of the INO80 complex in skeletal muscle stem cells (Schutt et al., 2020).

Taken together, INO80 regulates transcription, organizes and repositions nucleosomes as well as defines chromatin accessibility at promoters in a context, specie and tissue-dependent manner. To achieve these functions, INO80 acquires divergent subunits such as the transcription factor YY1, makes the chromatin accessible for further transcription factor binding, or interacts with other proteins such as RNAPII.

1.5.2 Functions of INO80 in DNA damage and maintenance of genome stability

Early evidence for a function of INO80 in DNA damage and genome stability became apparent following the observation that yeast cells lacking key INO80 subunits were very sensitive to physical DNA damage and that INO80 was rapidly recruited to double strand breaks (DSBs). Furthermore, INO80 was also found to maintain genome stability by allowing for replication fork progression at stalled or damaged replication forks during replication or early S-phase (Morrison et al., 2004; Shen et al., 2000; van

Attikum et al., 2004). In yeast, the INO80 complex was mapped to around half of the known replication origins of hydroxyurea (HU) treated S-phase cells (HU inhibits ribonucleotide reductase (RNR) which normally catalyzes the rate-limiting step in the de novo deoxyribonucleotides (dNTP) biosynthesis pathway, resulting in a decrease in intracellular dNTP levels and inhibition of DNA synthesis) and in cells undergoing normal S-phase progression (Falbo et al., 2009; Lee et al., 2014; Shimada et al., 2008; Vincent et al., 2008). In mammalian cells, INO80 is also recruited to replication forks but through ubiquitinylated H2A and the BRCA1-associated protein 1 (BAP1) (Lee et al., 2014). Moreover, INO80 was found to directly interact with the replication protein A (RPA) implying that several factors or pathways might influence or direct INO80 binding to replication forks (Au et al., 2011). Moreover, replication-stress leads to lethality in Ino80 mutants, a lethality found to be unrelated to impairments in the checkpoint response or to inhibition of the transcriptional reaction (Morrison, 2017; van Attikum et al., 2004).

Further studies reported that INO80 mutants fail to resume replication after treatment with other genotoxic drugs (Falbo et al., 2009; Papamichos-Chronakis & Peterson, 2008; Shimada et al., 2008; Vassileva et al., 2014). Depending on the lesion encountered by the DNA, Rad-51 strand evasion takes place allowing the replication fork to restart (Bjergbaek et al., 2005; Lambert et al., 2010). ATPase-dead Ino80 mutants failed to recruit Rad18 and Rad51 to MMS-stalled replisomes, thereby avoiding adequate ubiquitinylation of PCNA and impaired recruitment of the recombination machinery (Falbo et al., 2009).

Collectively, these findings suggest that INO80 might play a direct role in restarting stalled replication forks by removing complexes which block fork progression or recruiting essential factors and/or processes for repair and recovery at damage sites including but not limited to formation of sister chromatid cohesion (Ogiwara et al., 2007; Poli et al., 2017). Alternatively, INO80 could also allow for replication fork progression through nucleosomes ejection ahead of the replication fork, since it is known to fulfill this function around double strand breaks (DSBs) (Tsukuda et al., 2005; van Attikum et al., 2007).

Long range chromatin movements to achieve transfer of a transcribed gene, clustering of active replication forks during S-PHASE, shift DSBs or collapsed replication forks to the nuclear envelope also preserve genome stability (Chagin et al., 2016; Horigome et al., 2014; Nagai et al., 2008; Taddei et al., 2006). INO80 is essential for DSB-

induced mobility of chromatin both in *cis* and in *trans* and presence of INO80 at an undamaged locus was found to be sufficient for enhancing proximal chromatin mobility (Amitai et al., 2017; Neumann et al., 2012; Seeber et al., 2013; Strecker et al., 2016). Indeed, INO80 has been shown to play a function in the degradation of 30% of four core histones upon DNA damage induction (Hauer et al., 2017). In mammalian cells, INO80 was reported to displace/eject rather than degrade core histones at DNA damage sites (Adam et al., 2016). INO80 mediated reduction of histone density through histone degradation and eviction, facilitates chromatin decompaction and enhances chromatin fiber flexibility and dynamics (Poli et al., 2017). This feature of INO80 is not only applicable to histone proteins but also to RNAPII. Indeed, during DNA damage and HU-induced replication stress conditions the INO80 complex contributes to removal of RNAPII from the chromatin (Lafon et al., 2015; Poli et al., 2016). The ejection of RNAPII relies on the collaboration of the INO80 complex, PAF1 and Cdc48 which facilitate RNAPII degradation by the 26S proteasome (Lafon et al., 2015; Poli et al., 2016). It must be noted, that under stress conditions, both histone and RNAPII degradation require activation of the Mec1-Ddc2 checkpoint kinase (ATR-ATRIP) (Bastos de Oliveira et al., 2015; Hustedt et al., 2015; Morrison et al., 2007). In addition to removal and degradation of histone proteins and RNAPII during under damage and stress conditions, INO80 also binds DSBs and together with other factors initiates DNA damage repair. In endonuclease-induced persistent DSBs, INO80 binds to at least two distinct sites at the nuclear periphery, eliciting a site-specific impact on repair. In order for DSBs repair to ensue, ATP-dependent remodelers (SWR1 in yeast) deposit histone variant Htz1/H2A.Z at the site of the break (Horigome et al., 2014; Papamichos-Chronakis et al., 2006). Marking DNA damage sites/breaks with Htz1/H2A.Z is required for their successful recruitments by the nuclear pore complex (NPC) or by Mps3 (a SUN-domain protein anchored in the nuclear envelope) (Seeber & Gasser, 2017). DSBs preferentially associate with Mps3 during S- and G2- phase where the INO80 complex along with other factors are required for removal of the break and repair to take place (Horigome et al., 2014). For instance, INO80 complex plays a role in the processing of resected ends. The Ruvbl1/2 subunits of the INO80 complex display a 3’ to 5’ helicase activity which unwinds 3’ ssDNA (single stranded DNA) overhangs *in vitro* and thereby contribute to processing of resected DNA ends (Papin et al., 2010). In coherence with this, INO80 mutants present defects in HR-mediated repair but not in NHEJ repair (Papamichos-Chronakis et al., 2006; van

Attikum et al., 2007). Recruitment of DSBs to the NPC takes place in G1 and S-phase and requires poly-SUMO chain deposition or successful recruitment of the SUMO-dependent ubiquitin ligase complex Slx5-Slx8 which is fundamental for interaction with the Nup84 subcomplex of the NPC (Nagai et al., 2008; Poli et al., 2017; Ryu et al., 2015). DSB recruitment to the NPC favors alternative recombination pathways such as microhomology-mediated recombination or break-induced replication (BIR) (Burgess et al., 2007; Horigome et al., 2016). DSBs association with Mps3 stops illegitimate recombination processes, thereby conserving equal sister chromatid recombination and preserving genetic information (Horigome et al., 2014).

Although these data clearly show important roles for Ino80-mediated DNA repair and recovery from replication stress, whether this function is required in all cells of a multicellular organisms or in specific cellular or environmental contexts only is not clear. For instance, loss of Ino80 in endothelial cells did not report any changes in DNA damage, or DNA repair (Rhee et al., 2018) This might be attributed to the fact that other chromatin remodeling complexes such as SWR1 and Htz1/H2A.Z which also play a role in DNA repair may compensate for the role of INO80 in certain cellular contexts (van Attikum et al., 2007; Xu et al., 2012)

In summary, the precise molecular mechanism by which INO80 maintains genomic stability is unclear. Poli *et al*. suggest that it could be a ramification of end-resection and chromatin remodeling events which ensue through DSB repair or that chromatin dynamics could facilitate relocation of sub-nuclear sites supporting bias particular repair outcomes over others (Poli et al., 2017).

1.6 The transcription factor Yin-Yang-1 and its function with INO80

Yin-Yang-1 (YY1) is a transcriptional factor first described in 1991 which is ubiquitously expressed throughout mammalian cells (Verheul et al., 2020). YY1 forms homodimers which bind a small sequence motif (5′-CCGCCATNTT-3′), often found in enhancers and promoter regions, through the four C2H2 zinc fingers contained within its C-terminal domain (figure 6) (Hyde-DeRuyscher et al., 1995; Yant et al., 1995). YY2 is the paralog of YY1, together they share 56% homology on the amino acid sequence level and display 86% conservation of the zinc fingers region (Verheul et al., 2020). These two paralogs bind the same motif which might also explain their high degree of homology (Nguyen et al., 2004). YY1 and YY2 act as both, transcriptional activators

and repressors hence the choice for their name (Yin-Yang) which expresses their dual activity (Nguyen et al., 2004; Shi et al., 1991; Wang et al., 2018; Zhang et al., 2017).

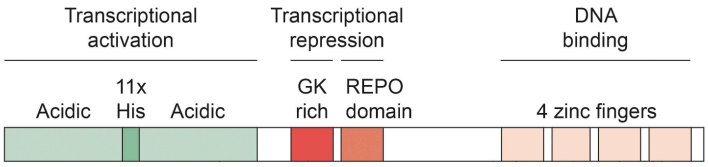

Figure 6. Schematic diagram of human YY1 domains (adapted from (Verheul et al., 2020)).

YY1 binds DNA through the four C2H2-type zinc fingers stationed at the C-terminal of the protein. The REPO domain and the glycine-lysine rich domain convey transcriptional repression. The REPO domain conducts the interaction with polycomb group proteins. Meanwhile, the GK rich domain is responsible for the interaction with histone deacetylases (HDAC). Finally, the N-terminal region of the protein is responsible transcriptional activation (adapted from (Verheul et al., 2020)).

The DNA binding domain at the C-terminal of the YY1 protein overlaps in part with transcriptional repression. On the other hand, the N-terminal region contains a transcriptional activator domain (figure 6) (Shi et al., 1991). YY1 regulates transcription by recruiting different co-factors. For example, the REPO domain of YY1 recruits repressive co-factors to target genes through interaction with polycomb group proteins (Wilkinson et al., 2010; Wilkinson et al., 2006).

YY1 is involved in different tissue specific functions in various regulatory mechanisms and regulates cell proliferation, differentiation, apoptosis and cell cycle control (Deng et al., 2010; Liu et al., 2007; Nicholson et al., 2011; Schutt et al., 2020). In order to fulfill its various functions, YY1 associates with different co-factors and chromatin modifiers. YY1 has been found to be closely associated with the chromatin remodeler complex INO80 (Y. Cai et al., 2007). On one hand, YY1 was found to recruit INO80 to YY1 activated genes where INO80 acts as a co-activator (Y. Cai et al., 2007; Schutt et al., 2020). On the other hand, INO80 through shifting and remodeling of nucleosomes was described to make YY1 target genes available for YY1 binding, allowing for successive transcriptional activation (Y. Cai et al., 2007; Wu et al., 2007). In addition to its interaction with INO80, YY1 can associate with other chromatin remodelers in a context specific or cell specific manner. For instance, in embryonic cells, YY1 associates with the BAF complex (BRG1/HBRM associated factors) and binds to super enhancers which transcriptionally activate proliferation and pluripotency related genes (Wang et al., 2018).

1.7 The transcription factor family Forkhead-Box-O-1

The Forkhead-Box-O-1 (FOXO1) gene was identified in the 1990's and belongs to the large transcription factor (TF) family Forkhead-Box-O (Foxo) genes. FOXO proteins are evolutionary conserved in metazoans. In mammals, four Foxo genes were identified (figure 7) (Avila-Flores et al., 2019; Burgering, 2008). FOXO1 and FOXO3 consist of approximately 650 amino acids whilst FOXO4 and FOXO6 have a length of 500 amino acids (figure 7) (Obsil & Obsilova, 2008).

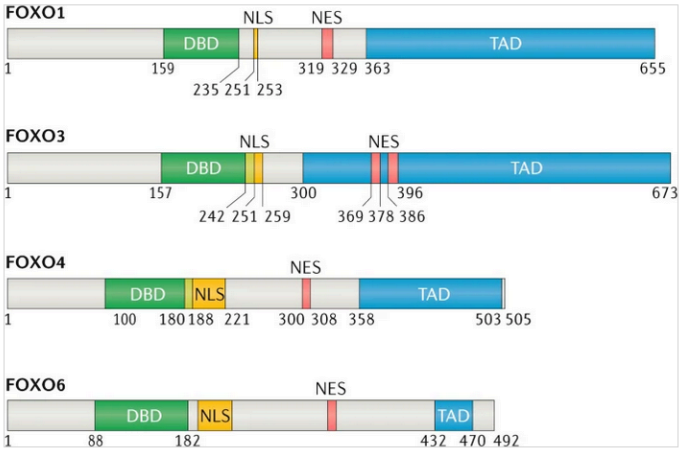

Figure 7. Mammalian FOXO isoforms (Calissi et al., 2021)
All four FOXO isoforms contain a DNA-binding domain (DBD), nuclear localization signal (NLS), nuclear export signal (NES) and the transactivation domain (TAD). The amino acid positions are indicated.

FOXO proteins comprise four domains, a highly conserved DNA-binding domain (DBD), a nuclear localization signal (NLS) positioned downstream of the DNA binding domain and a nuclear export sequence (NES) as well as a transactivation domain (TAS) at the N terminus. The rest of the FOXO proteins is predicted to be highly disorganized (Link, 2019; Obsil & Obsilova, 2008). FOXO1, 3 and 4 are ubiquitously expressed, nonetheless their expression levels changes between different cell types. For instance, FOXO1 is highly expressed in adipocytes whilst FOXO4 is highly expressed in skeletal and smooth muscle cells (Furuyama et al., 2000). The FOXO proteins have redundant as well as isoform-specific regulatory mechanisms and display differential target genes (Potente et al., 2005; Salih & Brunet, 2008). FOXO transcription factors have been proposed as homeostasis regulators to coordinate the responses to environmental changes, including growth factor deprivation as well as metabolic and oxidative stress, and to maintain tissue homeostasis (Eijkelenboom & Burgering, 2013).

Upon changes in environmental signals, FOXO proteins are both regulated by modifications on its mRNA and protein levels in order to adapt transcription of its downstream target genes (Essaghir et al., 2009; Yamagata et al., 2008). FOXO proteins are tightly regulated through various PTMs such as phosphorylation, acetylation, ubiquitylation and methylation (Eijkelenboom & Burgering, 2013; van der Horst & Burgering, 2007). The main form of PTMs which regulates FOXO protein is phosphorylation. Kinases which can phosphorylate FOXO proteins have been classified into either FOXO-activating kinases and include AMPK, JNK and MST1 or into FOXO-inactivating kinases and comprise AKT, SGK, ERK, p38, DYRK, IKK, CDK1/2 and CK1 (Brown & Webb, 2018; Brunet et al., 1999; Brunet et al., 2001; Essers et al., 2004; Flotow et al., 1990; Greer et al., 2007; Ho et al., 2012; Hong et al., 2012; Hu et al., 2004; Huang et al., 2006; Lehtinen et al., 2006; Liu et al., 2008; Rena et al., 2002; Soundararajan et al., 2013; Sunayama et al., 2005; Woods et al., 2001; Yang et al., 2008; Yuan et al., 2008).

FOXO1 has been reported to play a role in oncogenesis and to transcriptionally activate various metabolic diseases (including gluconeogenesis, glycogenolysis, adipogenesis and thermogenesis) (Dong, 2017; Eijkelenboom & Burgering, 2013; Link & Fernandez-Marcos, 2017; Maiese, 2015; Wagatsuma et al., 2016; Xing et al., 2018). The Phosphoinositide 3-kinase/protein kinase B (PI3K/PKB) mediated phosphorylation of FOXO1 in response to insulin or growth factors is a very well-established and evolutionary conserved form of FOXO1 regulation (Biggs et al., 1999). PI3K and PKB (also known as AKT and c-AKT) negatively regulate FOXO1 by phosphorylating it at three conserved residues, Threonine 24, Serine 256, and Serine 319 (Biggs et al., 1999; Peng et al., 2020). These modifications lead to the translocation of the FOXO1 protein from the nucleus to the cytoplasm thereby abolishing FOXO1-dependent transcription. In the presence of oxidative stress, the c-Jun N-terminal kinase (JNK) was also found to be able to phosphorylate FOXO1 and FOXO4 proteins resulting in FOXO1/4 translocation from the cytoplasm to the nucleus thereby counteracting the PI3K/PKB pathway (Essers et al., 2004; Grabiec et al., 2015).

1.8 Vascular smooth muscle cells in health and disease

Smooth muscle cells (SMCs) are non-striated, non-voluntary, contractile cells which can be found in various tissue types including the blood vessels, the urinary bladder, the iris, the trachea and the digestive tract (Durham et al., 2018).

Vascular smooth muscle cells (VSMCs) are highly specialized cells which primary functions are contraction and regulation of blood vessel tone, blood flow, and blood pressure, in response to diverse physiological stimuli. Additionally, VSMCs also contribute to blood vessel structural integrity through extracellular matrix generation (Campbell, 1995; Owens, 1995). Blood vessels can be subdivided into two subgroups: elastic and muscular arteries. Elastic arteries have large diameters and localize close to the heart (ie. aorta) (Rhodin, 1980; Silver et al., 1989). Muscular arteries on the other hand are found in the periphery (ie. femoral artery). In terms of microscopical structure, both groups are composed of three distinct layers: the tunica intima, the tunica media and the tunica externa (figure 8) (Holzapfel G A, 2000; Rhodin, 1980).

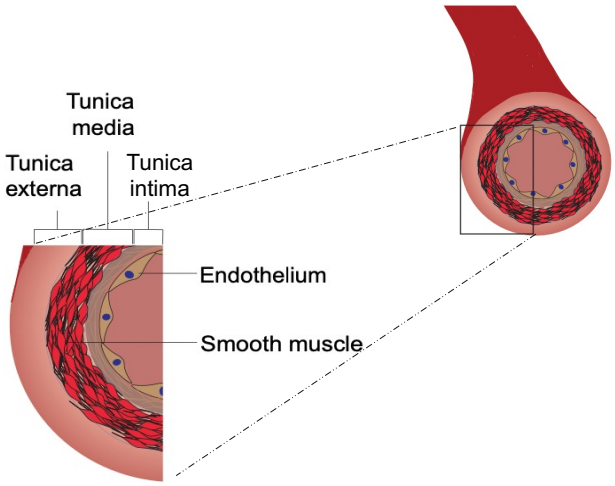

Figure 8. Structure of the arterial wall.
The arterial wall is made of 3 different layers: Tunica externa (also named adventitia), Tunica media and Tunica intima (also called interna). The inner most layer is the tunica interna and is composed of endothelial cells and is in direct contact with the blood flow. The tunica media is primarily composed of smooth muscle cells. The tunica externa, the outermost layer of the artery, consists of connective tissue (thick bundles of collagen and fibrils arranged in helical structures) (Holzapfel G A, 2000).

VSMCs are the pre-dominant and most essential cell type in the tunica media of the vasculature. In healthy adult blood vessels, VSMCs are found in a contractile phenotype. Contractile VSMCs, exhibit low proliferation and migration rates, are functionally contractile, respond to small molecule signals such as acetylcholine and norepinephrine and express a collection of contractile proteins including but not limited

to smooth muscle-alpha actin (ACTA2), myocardin (MYOCD), transgelin (SM22-alpha), smooth muscle myosin heavy chain (MYH11), smooth muscle basic calponin (CNN1) and smoothelin (SMTN) (Miano, 2015; Owens, 1995; Wang et al., 2003). In culture, contractile VSMCs exhibit a slender and dense fusiform morphology (Campbell, 1987; Rzucidlo et al., 2007). Contractile VSMCs are characterized by little connective tissues, presence of an ultrastructure composed of tight bundles of myofilaments (thick myofilaments: myosin filaments and thin myofilaments: actin filaments), ovoid dense body structures, mitochondria and minimal rough endoplasmic reticulum, Golgi or free ribosomes (Campbell, 1987; Chamley-Campbell J, 1979; Dikalov & Ungvari, 2013; Hedin & Thyberg, 1987; Zhuge et al., 2020). The spacers occur on the inner side of the cell membrane and turn into dense regions. Cell membranes of two adjacent VSMCs are connected to each other by maintaining close proximity, thereby founding a mechanical coupling to achieve transfer of inter-cell tension. Concurrently, gap junctions can also be found between VSMCs to complete electric and chemical coupling between the cells. Protein components resembling those found in the z-band of skeletal muscle can be found in the dense body and dense region (Herrera et al., 2005; Herzog & Ait-Haddou, 2002). These protein components together with a filamentous polymer localized between the dense body and dense region form a complete intracellular framework through filamentous binding of the dense body and dense region. The thick filament of SMCs expands the cross-bridge in different opposite directions in order for the thin myofilament coming from different directions to approach each other. In order to increase the contractility range of SMCs, the sliding range between the thick and think myofilaments can extend the whole length of the thin myofilament (figure 9) (Herrera et al., 2005; Herzog & Ait-Haddou, 2002).

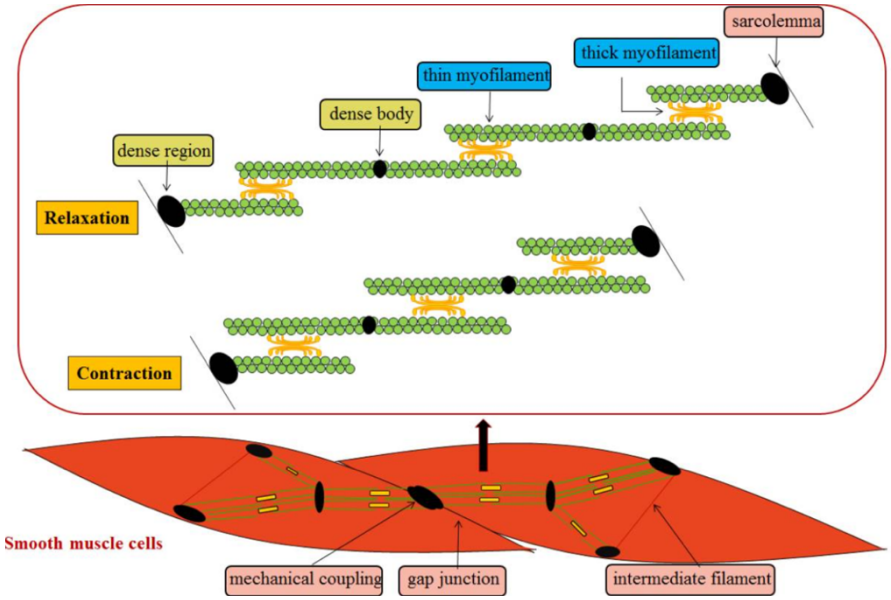

Figure 9. Vascular smooth muscle contraction and relaxation (Zhuge et al., 2020). Thick myofilaments are also called myosin filaments. Thin myofilaments are interchangeably named actin filaments. The dynamic rearrangement of actin cytoskeleton, cross-bridge formation of actin and myosin, intermediate filaments regulate vascular contraction, tone and plasticity.

VSMCs contract slowly due in part to a slower rate of action potential delivery on the cell membrane. VSMCs contraction is triggered by Ca^{2+} through two different pathways. First through action potential which is produced by chemical signals or stretch stimuli, thereby stimulating extracellular Ca^{2+} entry into the intracellular cytosol. Upon VSMC activation, Ca^{2+} goes into the cell through electro-mechanical coupling and pharmaco-mechanical coupling. The second path of SMC contractility induction is based on chemical activation of the G-protein coupled receptor PLC-IP3 pathway, leading to activation of IP3R in the SR membrane and inducing Ca^{2+} release into the cytosol (Billups et al., 2006; Zamponi & Currie, 2013). Even though SMCs display minimal quantities of sarcoplasmic reticulum (SR), Ca^{2+}-sensitive ryanodine receptor (RYR) and Inositol 1,4,5-trisphosphate (IP3)-sensitive receptors (IP3R) in the SR membrane act as calcium releasing channels (Taylor & Tovey, 2010). In both pathways, increased cytosolic Ca^{2+} associates with calmodulin (CaM) to form Ca^{2+}-CaM compounds which in turn combine with and activate cytoplasmic myosin light chain kinase (MLCK). This interaction promotes the phosphorylation of myosin light chain (MLC) and allows VSMC contraction to take place (figure 10) (He et al., 2008). The majority of cytosolic Ca^{2+} originates from extracellular sources, a small part is

however also released by the RYR from the SR membrane (figure 10) (Zhuge et al., 2020).

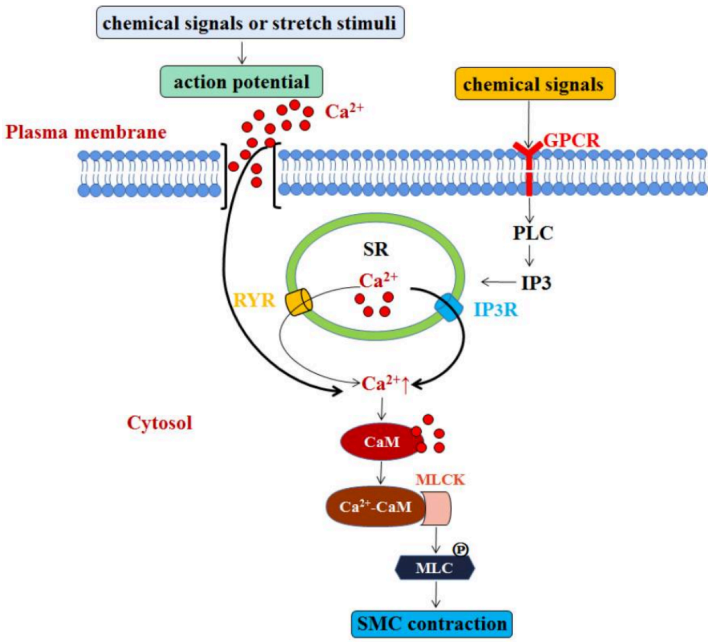

Figure 10. Smooth muscle contraction (Zhuge et al., 2020).
Smooth muscle contraction is induced through two pathways both involving Ca^{2+} release into the cytosol. Chemical signals or stretch stimuli induce action potential induced Ca^{2+} influx into the intracellular cytosol. Alternatively, chemical signals activate IP3R in the sarcoplasmic reticulum (SR) through the G-protein coupled receptor-PLC-IP3 pathway. This also then leads to release of Ca^{2+} into the cytosol. Regardless of the pathway by which Ca^{2+} enters the cytosol, Ca^{2+} combines with calmodulin (CaM) and form Ca^{2+}-CaM compounds. These compounds associate and activate myosin light chain kinase (MLCK) which in turn phosphorylates myosin light chain leading to SMC contraction.

Besides calcium-dependent mechanisms, vascular contractility is regulated by calcium-independent mechanisms such as remodeling of the actin cytoskeleton and reactive oxygen species (Cheng et al., 2013; Matchkov et al., 2012; Tang, 2015). Conversely, during VSMCs relaxation, cytosolic Ca^{2+} is reinstated back out to the SR, either through the SR membrane calcium pump or is carried out of the cells via the muscle membrane Na^{+}-Ca^{2+} exchanger and the plasmalemmal calcium pump. This leads to a drop in intra-cytosolic Ca^{2+} concentrations, which causes deactivation of MLCK, de-phosphorylation of MLC through MLC phosphotase (MLCP), and ultimately leads to slow relaxation of VSMCs (Lacolley et al., 2012). In addition to this, VSMCs relaxation can be achieved by enhancing MLCP though modulation of cyclic guanosine monophosphate, cyclic adenosine monophosphate and protein kinase A (Bolz et al., 2003; Vanhoutte et al., 2017).

Contraction and relaxation of VSMCs rapidly change the diameter of blood vessels, thereby influencing blood flow velocity and changing blood vessel wall pressure. Variations in vascular diameter is an acute and fast adaptive process, based in majority on the activation and deactivation of SMC constrictor proteins and dynamic rearrangement of the actin cytoskeleton as described above (Touyz et al., 2018; Zhuge et al., 2020). Pro-hypotensive or pro-hypertensive stimuli, such as oxidative stress, mechanical forces, the renin-angiotensin-aldosterone system (RAAS), the sympathetic nervous system as well as hemodynamic changes, alter SMC signaling and thereby lead to structural and functional vascular changes to adapt blood pressure (Dikalov & Ungvari, 2013; Esler et al., 2010; Kim et al., 2016; Te Riet et al., 2015).
VSMCs however, are not terminally differentiated and retain phenotypic plasticity. Indeed, in response to local environmental cues such as vascular injury (ie. angioplasty), VSMCs can de-differentiate from the contractile phenotype into a highly synthetic fibroblast-like phenotype (Sinha et al., 2014) (figure 11). This switch is characterized by a decrease in contractile proteins, an increase in the expression of genes involved in SMC proliferation and remodeling of the ECM to facilitate migration including but not limited to vimentin (VIM), non-muscle myosin heavy chain B (MYH10), tropomyosin 4 (TPM4), cellular retinol biding-protein-1 (RBP1) (Campbell, 1987; Owens et al., 2004; Sobue et al., 1999). The ultrastructure of synthetic VSMCs reveals a cytoplasm lacking contractile bundles but with plenty rough endoplasmic reticulum, Golgi and ribosomes (Campbell, 1987; Chamley-Campbell J, 1979; Hedin & Thyberg, 1987). *In vitro*, synthetic VSMCs originally exhibit a broad and spread shape but then begin to grow over one another in a “hill-and-valley” pattern (Campbell, 1987); (Rzucidlo et al., 2007). This phenotypic de-differentiation from a contractile to a synthetic state is considered a binary process which implicates VSMCs returning to the contractile *in vivo* physiological state once repair is completed (re-differentiation) (figure 11) (Durham et al., 2018). Nonetheless, VSMCs can maintain a variety of phenotypes upon different environmental/disease states and can display characteristics of osteoblasts, chondrocytes, adipocytes and macrophage foam cells (figure 11) (Durham et al., 2018). These different VSMCs phenotypes contribute to the development of various diseases including atherosclerosis, hypertension, vascular calcification, and neointima formation (Allahverdian et al., 2018; Campbell & Campbell, 1985; Rzucidlo et al., 2007).

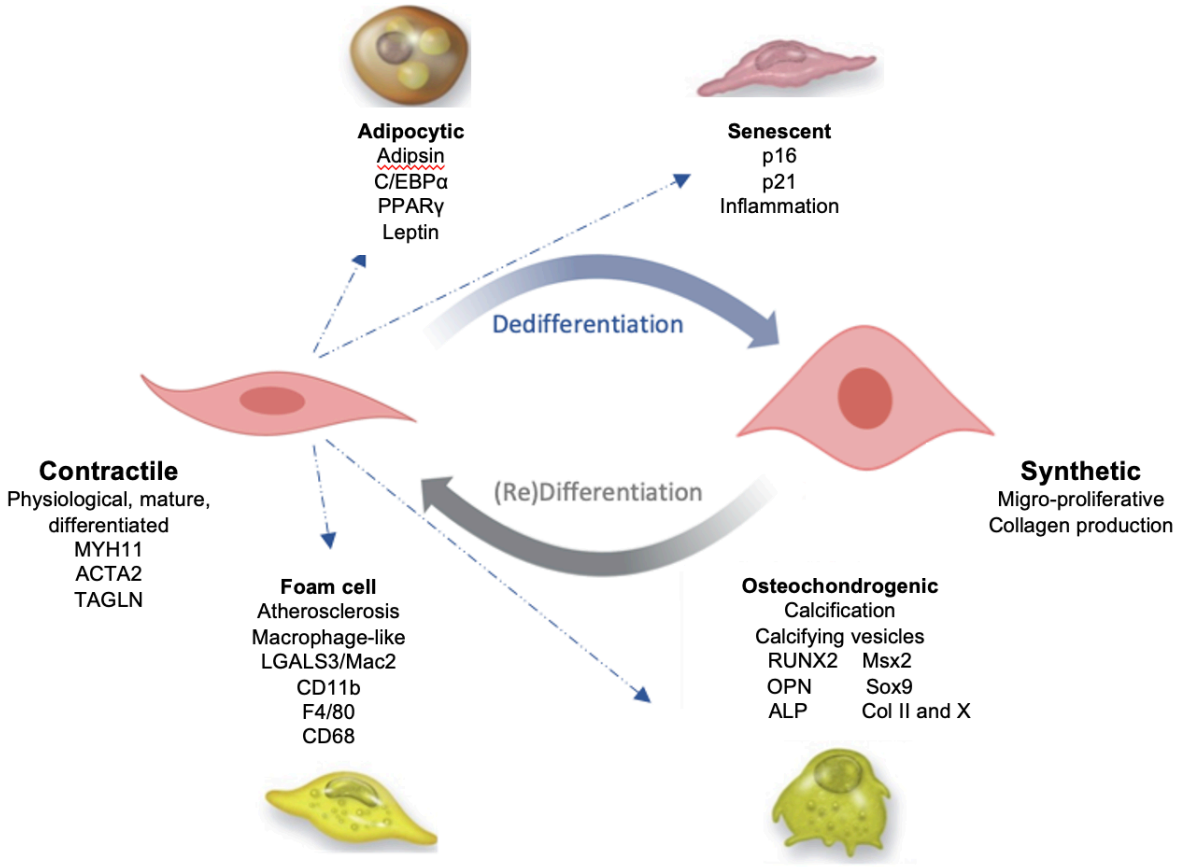

Figure 11. Diagram of the spectrum of VSMCs phenotypes identified in health and disease (adapted from (Durham et al., 2018)).

SMC phenotypes identified are in bold and their cellular markers are highlighted below that. The alteration of VSMC phenotype from contractile to synthetic phenotype occurs upon tissue damage and is accompanied by a decrease in contractile genes (such as Myh11, acta2, tagln) and concomitant increase in collagen production and migro-proliferative genes. On the other hand, the shift to an osteochondrogenic phenotype is caused by an increase in calicum/phosphate. Osteochondrogenic phenotype is characterized by the development of calcifying vesicles, down-regulation of mineralization inhibitory molecules, and elaboration of a calcification prone matrix together with loss of SMC markers and gain of osteochondrogenic markers (Shanahan et al., 2011). Treatment of VSMCs with aggregated low-density lipoprotein (agLDL) leads VSMCs to switch toward a foam cell like SMCs phenotype characterized by the downregulation of elastogenic capacity and an increase in macrophage foam cell markers (Swirski & Nahrendorf, 2014); (Samouillan et al., 2012). Likewise, VSMCs treated with adipogenic differentiation media (dexamethasone, methylisobutylxanthine and insulin) develop adipocyte markers (Davies et al., 2005). Finally, upon DNA damage and ageing, VSMCs can switch to a senescence associated secretory phenotype where they no longer go through mitosis and alternatively produce cytokines, growth factors and proteases (Nakano-Kurimoto et al., 2009).

Atherosclerosis is a chronic progressive inflammatory disease which is a leading underlying cause of cardiovascular disease and a major reason for mortality worldwide (Chen et al., 2010; Zhuge et al., 2020). Atherosclerosis is characterized by the deposition and accumulation of lipids between the intimal and medial layers of blood vessels (Chen et al., 2010). Subsequently, macrophages infiltrate the blood vessels

and VSMCs differentiate into foam cell like VSMCs (figure 11) (Gistera & Hansson, 2017; Libby et al., 2019). More recent studies reported that 40% of foam cells found within advanced human coronary atherosclerotic lesions express both SMC marker ACTA2 and the macrophage marker CD68 (figure 11) (Allahverdian et al., 2014). Moreover, plaque formation is accompanied by inflammation, apoptosis, oxidative stress, enhanced aerobic glycolysis, and VSMCs differentiation into an osteoblast-like cell phenotype (Chen et al., 2018; Durham et al., 2018; Mulvihill et al., 2004). This leads to deposition of microcalcification within the intimal wall thereby reducing wall stability and increasing the risk of atherosclerotic plaque rupture (Durham et al., 2018). Furthermore, VSMC inflammatory activation plays an important role in blood vessel pathophysiology, vascular disease and progression (Orr et al., 2010; Sprague & Khalil, 2009). For instance, Myocardin (Myocd) a “guardian” of the contractile, non-inflammatory VSMC contractile phenotype is a critical regulator of blood vessel inflammation and associated atherosclerosis (Ackers-Johnson et al., 2015). Furthermore, premature atherosclerosis has been associated with the INO80 complex. Indeed, Ser818Cys missense mutation in Ino80d, a subunit of the INO80 complex, was identified as the likely cause behind premature atherosclerosis amongst other symptoms related to accelerated arterial ageing (Khader Shameer et al., 2014).

1.9 Aims and Objectives

The ATP dependent chromatin remodeler INO80 contributes to various fundamental DNA based functions classified through transcriptional regulation, DNA replication as well as DNA damage repair which result in a plethora of cell specific subsequent changes. Nonetheless, the functions of INO80 on a molecular level and which roles it plays in the development, contractility and regeneration of smooth muscle cells (SMCs) in the cardiovascular system are yet to be understood. The aim of this work is to comprehensively characterize the molecular functions of INO80 in adult smooth muscle cells and their subsequent physiological implications in the cardiovascular system. For this purpose, the Ino80-encoding gene was inactivated in smooth muscle cells of mice using the Cre-loxP system. The consequences of the loss of INO80 in SMCs were investigated *in vivo* and *in vitro* by means of physiological, morphological and histological analysis. Additionally, molecular biological analysis tools were exploited to determine transcriptomic changes upon loss of INO80. Furthermore, interaction partners and target genes of INO80 in vascular smooth muscle cells were identified to understand the molecular pathways behind the observed physiological changes. Both *in vivo* and *in vitro* rescue experiments were designed and performed to validate the identified INO80 interactions. Lastly, based on our findings, phenotypical analysis of the role of INO80 in atherosclerotic plaque development was conducted. Further molecular analysis of the function of INO80 on the chromatin level would give more insight into how INO80 shapes nucleosome positioning in adult VSMCs.

2. Material and Methods

2.1 Animal maintenance

Mice were kept in ventilated cages (Aero Cage – mM) at a temperature of 22 - 23°C with 45 - 48% relative air humidity. Circadian rhythm was maintained by keeping the animals in the dark from 6 pm to 7 am including 1 hour of dawn. All animal experiments were performed in accordance with German animal protection laws and were approved by the local governmental animal protection committee (Regierungspraesidium Darmstadt) through applications TVA B2/1150 and TVA B2/2027.

2.2 Ino80 and Foxo1 smooth muscle cell specific knockout mouse lines

Conditional Ino80, Foxo1 mutant mice were generated as described (Qiu et al., 2016); (Stöhr et al., 2013). For constitutive Cre-mediated recombination in smooth muscle cells, $Ino80^{lox/lox}$ were bred with SM22-Cre transgenic mice. SM22-Cre express Cre recombinase under the control of the mouse smooth muscle protein 22-alpha promoter and were generated as described (Holtwick et al., 2002). For generating a double knock out (dKO) of $Foxo1^{lox/lox}$ and $Ino80^{lox/lox}$ in smooth muscle cells, the $Foxo1^{lox/lox}$ mutant mice were mated to the $Ino80^{lox/lox}$ SM22-Cre^{pos} mice. For detailed schematic representation of these mouse lines please refer to appendix (figure 35).

2.3 Organ isolation

Animals were sacrificed by cervical dislocation following isoflurane exposure. The thorax was dissected to expose the heart. The left ventricle of the heart was perfused with 1x PBS (137 mM NaCl, 2.7 mM KCl, 10 mM Na_2HPO_4, and 1.8 mM KH_2PO_4). Isolated organs were: aorta (including abdominal aorta), bladder, femoral artery, carotid artery as specified.

2.4 Partial carotid ligation assay and EdU injection in adult mice

$Ino80^{lox/lox}$ SM22Cre^{neg} and $Ino80^{lox/lox}$ SM22Cre^{pos} mice around 10 weeks of age weighting no less than 18g were used for a partial ligation of the left carotid artery under anesthesia and analgesia (Nam et al., 2010) according to TVA B2/1150. Shortly,

the left external cortical artery and the left internal carotid artery were tied off above the carotid bifurcation using a non-absorbable suture 6-0. The occipital artery as well as the superior thyroid artery were spared. Blood supply was maintained via the right carotid artery. The vessel proximal to the ligation site was dissected after three weeks and examined histologically and molecularly. Surgery was performed by Marion Wiesnet. For histological examination, EdU (5-ethynyl-2' -deoxyuridine) was used to investigate the proliferation rate of vascular smooth muscle cells in adult mice which underwent carotid ligation. Two days post-surgery, animals were weighted and daily injected with Click-It EdU (5-ethynyl-2' -deoxyuridine) (Thermo Scientific # E10187) for a duration of three days at a final concentration of 5 µg per µl. For every 10 g mouse body weight, 100 µl of solution were applied, to a maximum of 300 µl. For the Edu solution preparation, 500 mg Click-It EdU (5-ethynyl-2' -deoxyuridine) (Thermo Scientific # E10187) was initially dissolved in 30 ml 0.9 % NaCl. This solution was incubated in a heated shaker for 30 min at 50°C until all particles were dissolved. The solution was further diluted at a ratio of 1:3.33 with 0.9 % NaCl (Braun #3570350) to a total of 99 ml and then aliquoted to 1 ml in 1.5 ml Eppendorf tubes and stored at -20°C. Before use, the corresponding amount of aliquot was thawed at 37°C. Following thawing, the solution was resuspended several times by vortexing. The solution was administered intraperitoneally into the mouse using a syringe and needle.

2.5 EdU staining

The purpose of this experiment was to examine vascular smooth muscle cell proliferation in adult mice after partial carotid ligation. Animals were first injected intraperitoneally with EdU (Thermo Scientific # E10187) as described in the section for partial carotid ligation assay and EdU injection in adult mice. The mice were then killed by CO_2, together with cervical dislocation. Carotid sections were handled and stored as described in the section for cryosections. The cryosections were prepared as described in the section for cryosections. The EdU staining was carried out according to the manufacturer's instructions and stained with antibodies as described in the immunohistochemistry section. The number of EdU positive vascular smooth cells was quantified from ligated carotid sections using alpha smooth muscle actin staining.

2.6 Wire myography assay

A wire myography assay was performed to evaluate the effects of INO80 on arterial contractility. For performing wire myography assay the following stock solutions were prepared in advance of the experiment: 20x Krebs-Henseleit buffer (20x KH stock) (NaCl 278.16 g, KCl 14 g, $MgSO_4$ $7H_2O$ 11.56 g, KH_2PO_4 6.44 g, EDTA 0.4 g, H_20 2 l), 20x Ca^{2+} stock solution ($CaCl_2$ $2H_2O$ 14.72 g, H_20 2 l) and 20x K^+ buffer (NaCl 74.88 g, KCl 89.4 g, $MgSO_4$ $7H_2O$ 5.78 g, KH_2PO_4 3.22 g, EDTA 0.2 g, H_20 1 l). The following buffers had to be freshly prepared on the day of the experiment: Glucose-$NaHCO_3$ solution ($C_6H_{12}O_6$ 8.4 g, $NaHCO_3$ 10.9 g, H_20 500 ml), KH buffer (H_20 1600 ml, Glucose-$NaHCO_3$ solution 200 ml, 20x K-H stock 100 ml, 20x Ca^{2+} stock solution 100 ml), Hypertension buffer (KCl 100 mM in water, Angiotensin II 10^{-2} µM in water, 10^{-3}M noradrenaline in water and 10^{-5}M phenylephrine in water).

KH buffer was aerated with carbogen (95% O_2 and 5% CO_2) at 37°C for at least 20 minutes. In the meanwhile, $Ino80^{lox/lox}$ $SM22Cre^{neg}$ and $Ino80^{lox/lox}$ $SM22Cre^{pos}$ mice were sacrificed, a 2 mm segment of femoral artery was isolated from each and transferred into a petri dish containing aerated KH buffer on ice. 2x 40 µm metal wires were inserted into each 2mm artery segment without damaging the arterial wall. Calibration and mounting of the femoral artery pieces were performed as described by the user manual (version 3.3) of Auto Dual Wire Myography System Model 510A, DMT. Optimal stretching of the femoral arteries was optimized for each artery and was found to be around 250 µm stretch for femoral arteries. Two femoral artery segments were simultaneously mounted and recorded. Following 3x KH buffer washing, the femoral arteries were stimulated with Angiotensin II 10^{-2} µM, 100 mM KCl, 10^{-3} M noradrenaline and 10^{-5} M phenylephrine, one at a time. Contractility was recorded and further analyzed using the Lab Chart 7 Software.

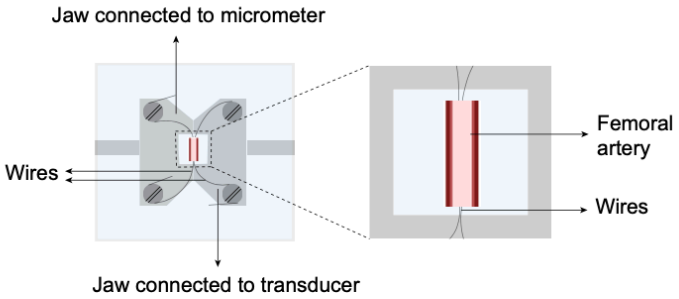

Figure 12. Schematic representation of wire myograph

The micrometer jaw is used to establish the initial conditions of active tension of the artery. On the other hand, the force transducer is connected to an interface and chart recorder, allowing for the force across the artery to be recorded.

2.7 Telemetric blood pressure measurement

A calibrated telemetric arterial pressure transducer TA11PA-C10 from DSI was inserted into the left carotid artery of Ino80$^{lox/lox}$ SM22Cre^{neg} and Ino80$^{lox/lox}$ SM22Cre^{pos} mice (minimum weight 25 g) under anesthesia and analgesia as described by the PA Device Surgical Manual for Mouse Copyright 2005 Transoma Medical All Rights Reserved, Part Number 391-0066-001 Rev.51. Surgery was performed by Marion Wiesnet. Seven days post implantation surgery, arterial pressure signals of mice unrestrained and untreated were recorded every 15 minutes for 2 minutes for 7 days. Captopril 600 µg/ml (in drinking water) and L-NAME 500 µg/ml (in drinking water) were respectively used to investigate arterial blood pressure changes. The mice drank compound-containing water *ad libitum* for seven days each time. The water was daily changed to ensure that no degradation of the compounds took place. A one-week period of rest was given to the animals so that their blood pressure returned to basal levels, mice only received compound free water during this time. Arterial pressure was sampled using Dataquest A.R.T 4.0 with a sample rate of 500 Hz and with a filter cut-off of 100 Hz. Recorded data was summarized by Dataquest A.R.T 4.0 by calculating a reduced mean for sample signals at a given time point. This generated diastolic, systolic, pulse pressure, activity, blood pressure and heart rate measurements which were then separated between night and day time (due to the activity change of mice during night versus day time).

2.8 Atherosclerosis development

2.8.1 AAV8-PCSK9 and AAV8-Luc vectors preparation

Using the 2-plasmid system, AAV8/ D377Y-mPCSK9 (gift from Jacob Bentzon; Addgene plasmid #58376) (Bjørklund et al., 2014) or pSSV9-CMV-luc together with helper plasmid pDP8(Sonntag et al., 2011) were co-transfected in HEK293T cells using polyethylenimine (Sigma). Next, the AAV vector preparations were purified using iodixamol step gradients concentrated and titrated as previously reported (Jungmann A, 2017). Vector preparations were a gift from Oliver J. Mueller, Kiel University,

attending physician at the Department of Internal Medicine III at University Hospital Schleswig-Holstein.

2.8.2 Atherosclerotic lesion development

For atherosclerosis induction, Ino80$^{lox/lox}$ SM22Cre^{neg} (control mice) and Ino80$^{lox/lox}$ SM22Cre^{pos} male mice were injected with 1x10^{11} vector genome copies (VG) of AAV8-PCSK9 (in 1x PBS) via single tail vein injection under Isoflurane anesthesia as per TVA B2/2027. As a control, mice were injected with 1x10^{11} vector genome copies (VG) of AAV8-luc via a single tail vein injection. On the next day, animals injected with AAV8-PCSK9 were challenged with Western type diet containing 21% butterfat and 1.5% cholesterol (Ssniff, #TD88137) and continued receiving this diet for a consecutive fourteen weeks. Tail vein injections were performed with a maximal volume of 5 µl /g body weight by Tanja Enders, Max-Planck Institute for Heart and Lung Research.

2.8.3 Luciferase assay

Liver and heart were isolated from AAV8-Luc injected animals and instantly shock frozen in liquid nitrogen then stored at - 80°C. Luciferase was extracted from heart and livers as described (Manthorpe M 1993). Shortly, frozen tissues were pulverized into a fine powder by hand grinding with a dry ice-chilled porcelain mortar and pestle.
Tissue powders were next lysed using 500 µl of Promega lysis buffer (Dual-Luciferase Reporter Assay System, Promega #E1910). The samples were subsequently vortexed for 15 minutes, frozen and thawed three times using altenating liquid nitrogen and 37°C water baths. Samples were centrifuged for 3 minutes at 10,000 x g and supernatants were transferred to a fresh 1.5-ml Eppendorf tube. The extraction process was then repeated (without freeze-thawing) after adding another 500 µl of lysis buffer to the pellet. The second supernatant was combined with the first one and the total extract (about 1 ml) stored at - 80°C. Luciferase expression was measured from supernatants by bioluminescence as instructed by the Dual-Luciferase Reporter Assay Protocol (Dual-Luciferase Reporter Assay System, Promega #E1910) using the Mithras LB940 plate reader (Berthold).

2.9 Molecular methods

2.9.1 DNA preparation and PCR for genotyping from murine ear punches and tail biopsies

For genotyping, DNA was isolated from tail biopsies or ear plugs of transgenic mice. Tail segments or ear punches were incubated overnight in lysis buffer (100mM Tris/HCl pH8.5, 5 mM EDTA, 200 mM NaCl, 0.2% SDS, 2% 10 mg/µl Proteinase K) at 56°C. Following centrifugation, at 14,000 RPM for 15 minutes, supernatants were then transferred into a fresh Eppendorf tube. In order to precipitate genomic DNA, 400 µl Isopropanol was then added onto the supernatants and subjected to centrifugation at 14,000 RPM for 15 minutes at 4°C. The DNA pellets were next washed with 70% ethanol and centrifuged at 14,000 RPM for 5 minutes. Finally, the DNA was dissolved in 100 µl T1/10E (10 mM Tris/HCl (pH 8.0), 0.1 mM EDTA (pH 8.0)) and incubated overnight at 56°C.

To establish the genotype of each transgenic mouse, PCRs using specific primer pairs (table 1) to amplify genomic areas of interest were performed. For visualization, the amplified DNA fragments of interest were then loaded onto an agarose gel electrophoresis using ethidium bromide.

Table 1. Primer list for genotyping

Name	Sequence	Primer Description	Annealing temperature
CS597	GCACTTCCTGGTTTTGCTGT	fwd Ino80	
CS598	CACTGACTGGCGTGTTCAGA	rev Ino80	62°C
SH 81	GCTTAGAGCAGAGATGTTCTCACATT	fwd Foxo1	
SH82	CCAGAGTCTTTGTATCAGGCA AATAA	rev Foxo1 WT	62°C
SH83	CAA GTCCATTAA TTC AGCACATTG A	rev Foxo1 mut	
TB95	CTAAACATGCTTCATCGTCGGTCCG	fwd Cre	
TB97	CGTAACAGGGTGTTATAAGCAATCC	rev Cre	62°C
TB879	AAAGTCGCTCTGAGTTGTTAT	fwd Rosa	
TB880	GGAGCGGGAGAAATGGATATG	rev Rosa	62°C
SH124	TATGCATCCCCAGTCTTTGG	fwd ldlr	
SH125	CTACCCAACCAGCCCCTTAC	rev ldlr WT	65°C
SH126	ATAGATTCGCCCTTGTGTCC	rev ldlr mut	
SH20	TAGAATTCATCTGCACCACCGGCAAGCTGC	fwd GFP	

SH21	AGAAAGCTTGTGCCCCAGGATGTTGCCG	rev GFP	62°C

Table 2. PCR program for genotyping

Step	Temperature	Time
Initial denaturation	94°C	5 min
Denaturation	94°C	30 sec
Annealing	*°C	30 sec
Elongation	72°C	60 sec/kb
Final elongation	72°C	7 min
Hold	10°C	∞

35 cycles

*The optimal annealing temperature was established for each primer mix and is detailed above in table 1.

Table 3. PCR reaction for genotyping

Reagent	Volume (µl)
2x Taq Master mix (Vazyme biotech, #P111/P112)	12.5
Primer 1	1
Primer 2	1
Primer 3*	1
DNA	1
H_20	8.5
Total	25

*Primer 3 added only if needed to discern for WT and mutant in the same PCR, the volume of primer 3 was replaced by water when no third primer was used.

2.9.2 RNA isolation from cells and tissue

Animal tissues were extracted as described in the organ isolation section. The tissue of interest was then shock frozen in liquid nitrogen. 1 ml Trizol (Thermo Scientific #15596026) and an autoclaved metal bead were added in an Eppendorf tube containing the tissue of interest. The tissue was homogenized using a vibrating mill (Retsch, MM301) at maximal intensity for 5 minutes. In the instance where RNA was isolated from cells, the cells were washed with 1 x PBS and 1 ml Trizol was directly added onto the cells. The rest of the procedure was followed exactly as for the RNA

isolation from tissues. Following homogenization, RNA was extracted as per manufacturer's protocol from Trizol (Thermo Scientific #15596026) or using the miRNeasy Mini Kit (Qiagen #217004). Concentration of dissolved RNA was measured using the Nanodrop-2000 UV/Vis Spectrometer (Thermo Scientific).

2.9.3 cDNA synthesis

In order to catalyze RNA into DNA the enzyme reverse transcriptase was used. The RNA was extracted as detailed in the section for RNA isolation from cells and tissue. The PrimeScript RT Reagent Kit (TaKaRa #RR047A) was then used according to manufacturer's instructions to achieve cDNA synthesis from RNA.

2.9.4 SYBR Green Quantitative Real Time-PCR (RT-qPCR)

Following cDNA synthesis, RT-qPCR was used for qualitative and quantitative analysis of the expression of specific genes. Transcriptomic expression levels, target specific RT-qPCR primers were used.

10 ng cDNA were used for RT-qPCR and each sample was tested in triplicates. Set up of the Blue S'Green qPCR reaction using the Blue S´Green qPCR Kit (Biozym #F410-L/F415-L) and procedure as well as used oligonucleotides which were used are listed below (RT-qPCR reaction and table 4). RT-qPCR was performed using the StepOnePlusTM RealTime PCR System (Applied Biosystems) and the comparative ΔΔCT method. The expression of the target genes was normalized to an endogenous reference gene (gapdh) and relative to the calibrator using the StepOne Software v2.3 based on the following equation:

Amount of target gene = 2 –ΔΔCT (Livak & Schmittgen, 2001).

RT-qPCR reaction	**µl**
Blue S´Green qPCR Kit	10
H_2O	6.4
forward primer [10µm]	0.8
reverse primer [10µm]	0.8
cDNA	2
Total volume	20

RT-qPCR cycling parameters

95°C	15 min	
95°C	30 sec	**Cycling stage**
60°C	30 sec	
72°C	30 sec	
95°C	15 sec	
50°C	1 min	**Melt curve stage**
95°C	15 sec	

Table 4. RT-qPCR oligonucleotides

Gene	Oligonucleotide sequence	Annealing temperature
Gapdh forward	ACCACAGTCCATGCCATCAC	62°C
Gapdh reverse	CATGCCAGTGAGCTTCCCGT	62°C
Ino80 forward	TGGACCACTTTCTGCGACAAAC	62°C
Ino80 reverse	TGTATTAAGGGATCCCCAGACTC	62°C

2.9.5 Taqman assays

Following cDNA synthesis as described in the cDNA synthesis section, Taqman assay (RT-qPCR), was used for qualitative and quantitative analysis of the expression of specific genes. Expression levels of the gene of interest was quantified using fluorophore-labeled (FAM) Taqman probes (Table 5). VIC-labeled probes for gapdh were used for normalization purposes. All Taqman experiments were run on the Step One Plus System (Thermo Fischer #4376600). All samples were tested as technical triplicates. Relative expression was calculated using the StepOne Software v2.3 (Applied Biosystems).

Table 5. Taqman probes

Target Gene	Label	Catalog number
Acta1	FAM	Thermo Fischer Mm00808218_g1
Acta2	FAM	Thermo Fischer Mm00725412_s1
Actg2	FAM	Thermo Fischer Mm00656102_m1
Gapdh	VIC	Thermo Fischer Mm999999915_g1
Ino80	FAM	Thermo Fischer Mm01328744_m1

Myocd	FAM	Thermo Fischer Mm01325105_m1
Transgelin	FAM	Thermo Fischer Mm00441660_m1
Yy1	FAM	Thermo Fischer Mm00456392_m1

2.9.6 Microarrays

Using this method, a large part of the transcriptome of a tissue or cell lysate can be analyzed. RNA was prepared as described in the section for RNA isolation from cells and tissue. For RNA quality control, the Agilent Bioanalyzer 2100 (Agilent Technologies Model # G2938B) and the RNA 6000 Nano Kit (Agilent Technologies # 5067-1511) were used according to manufacturer's instructions. For RNA quality assessment, RNA integrity number (RIN) was used, only RNA with an RIN > 8.0 was used. For total aorta transcriptome, 150 - 200 ng of RNA were used per sample. RNA was labelled according to the GeneChip Whole Transcprit (WT) Sense Target Labeling assay (P/N 701880 Rev. 5). For mRNA expression analysis, the Affymetric GeneChip Mouse transcriptome array 1.0 ST (P/N 902513) from Affymetrix was used. Hybridization, and staining were performed as described in the GeneChip Whole Transcprit (WT) Sense Target Labeling assay (P/N 701880 Rev. 5 Affymetrix) using the Affymetrix Fluidics Station according to manufacturer’s instructions.
The primary analysis of the data was performed using the Affymetrix Expression Console, and the statistical analysis (modified t-test) of the data was done using DNAStar ArrayStar12 using the RMA quantile method. This procedure was carried out by Sylvia Thomas, Max-Planck-Institute for Heart and Lung Research, and the raw data initial analysis was carried out by Thomas Böttger, Max-Planck-Institute for Heart and Lung Research.

2.9.7 RNA seq

RNA was extracted from aortas as described in the RNA isolation from cells and tissue section using the miRNeasy Mini Kit (Qiagen #217004). RNA and library preparations integrity were verified by Dr. Stefan Günther at the Bioinformatics facility of the Max-Planck-Institute for Heart and Lung Research. Whole transcriptome single end RNA sequencing was also performed by Dr. Stefan Günther at the Bioinformatics facility of the Max-Planck-Institute for Heart and Lung Research. In brief, trimmomatic version 0.39 was employed to trim reads after a quality drop below a mean of Q15 in a window

of 5 nucleotides and keeping only filtered reads longer than 15 nucleotides (Bolger et al., 2014). Reads were aligned versus Ensembl mouse genome version mm10 (Ensembl release 101) with STAR 2.7.9a (Dobin et al., 2013). Alignments were filtered to remove: duplicates with Picard 3.0.0 (Picard: A set of tools (in Java) for working with next generation sequencing data in the BAM format), multi-mapping, ribosomal, or mitochondrial reads. Gene counts were established with featureCounts 2.0.2 by aggregating reads overlapping exons on the correct strand excluding those overlapping multiple genes (Liao et al., 2014). The raw count matrix was normalized with DESeq2 version 1.30.1 (Love et al., 2014). Contrasts were created with DESeq2 based on the raw count matrix. Genes were classified as significantly differentially expressed at average count > 5, multiple testing adjusted p-value < 0.05, and -0.585 < log2FC > 0.585. The Ensemble annotation was enriched with UniProt data (Activities at the Universal Protein Resource (UniProt)).

2.9.8 Gene set enrichment analysis

To further analyze transcriptomics data, Gene Set Enrichment Analysis (GSEA) was performed in order to evaluate significant differences in diverse pre-defined and thematized gene sets between two biological states thus facilitating the identification of relevant biological processes (Mootha et al., 2003; Subramanian et al., 2005). This analysis was performed using the GSEA Java Desktop Software v3.0 for gene set enrichment analysis of the microarray generated data set and GSEA Java Desktop Software v4.2.3 for the RNA seq generated data set, both with default settings with the permutation type set as "Geneset".

2.9.9 ATAC seq

ATAC sequencing was used to evaluate whether and how promoter accessibility was altered upon the loss of Ino80 in smooth muscle cells. For this purpose, isolated aortic smooth muscle cells from Ino80$^{lox/lox}$ SM22Cre^{neg} and Ino80$^{lox/lox}$SM22Cre^{pos} were subjected to ATAC sequencing. Primary aortic smooth muscle cells were isolated according to isolation of primary murine aortic vascular smooth muscle cells section. Following isolation, cells were trypsinized and washed with PBS. Counting of cells was performed with MOXI Z Mini Automated Cell Counter Kit (Orflo) and 50.000 cells were used for ATAC Library preparation using Tn5 Transposase from Nextera DNA Sample Preparation Kit (Illumina). Cell pellet was resuspended in 50µl PBS and mixed with

25µl TD-Buffer, 2.5µl Tn5, 0.5µl 10% NP-40 and 22µl water. Cell/Tn5 mixture was incubated at 37°C for 30min with occasional snap mixing. Transposase treatment was followed by 30min incubation at 50°C together with 500mM EDTA pH8.0 for optimal recovery of digested DNA fragments. For neutralization of EDTA 100µl of 50mM MgCl2 was added followed by purification of the DNA fragments by MinElute PCR Purification Kit (Qiagen). Amplification of Library together with Indexing was performed as described elsewhere (Buenrostro et al., 2013). Libraries were mixed in equimolar ratios and sequenced on NextSeq2000 platform using P3 flowcell and 2x 36bp paired-end setup.

Trimmomatic version 0.39 was employed to trim reads after a quality drop below a mean of Q15 in a window of 5 nucleotides and keeping only filtered reads longer than 15 nucleotides (Bolger et al., 2014). Reads were aligned versus Ensembl mouse genome version mm10 (Ensembl release 101) with STAR 2.7.10a (Bolger et al., 2014). Aligned reads were filtered to remove: duplicates with Picard 3.0.0 (Picard: A set of tools (in Java) for working with next generation sequencing data in the BAM format), spliced, multi-mapping, ribosomal, or mitochondrial reads. Peak calling was performed with Macs version 3.0.0a7 with FDR < 0.0001 (Zhang et al., 2008). Peaks overlapping ENCODE blacklisted regions (known misassemblies, satellite repeats) were excluded. Remaining peaks were unified to represent a common set of regions for all samples and counts were produced with bigWigAverageOverBed (UCSC Toolkit). The raw count matrix was normalized with DESeq2 version 1.36.0 (Love et al., Moderated estimation of fold change and dispersion for RNA-Seq data with DESeq2). Peaks were annotated with the promoter (TSS +- 5000 nt) of the nearest gene based on Ensembl release 101. Contrasts were created with DESeq2 based on the normalized count peak matrix with all size factors set to one. Peaks were classified as significantly differential at average count > 10 and -1 < log2FC > 1. All downstream analyses are based on the normalized peak count matrix. The DNA isolation, enzymatic treatment, sequencing as well as mapping of the reads were performed Stefan Günther at the Bioinformatics facility of the Max-Planck-Institute for Heart and Lung Research.

2.9.10 CUT & RUN

In order to determine which genes were direct binding targets of INO80 in smooth muscle cells a CUT & RUN experiment was performed. Approximately 100,000 cells

from C57BL/6 mouse primary aortic smooth muscle cells (PELOBiotech #PB-C57-6080) grown in in Complete Smooth Muscle Cell Medium /w kit (PELOBiotech #PB-M2268) were subjected to the CUT & RUN protocol using the CUT & RUN assay kit (Cell Signaling #86652) as per manufacturer's protocol using an INO80 specific antibody (Abcam #ab105451) at a 1:50 dilution, each reaction was rotated overnight at 4°C. DNA purification was performed using phenol/chloroform extraction. Precipitated DNA was measured by Qubit and a maximum of 1-10ng was used as input for SMARTer® ThruPLEX® DNA-seq Kit (Takara Bio). Resulting Libraries were sequenced on NextSeq2000 with P3 flowcell and 2x 36bp paired-end setup.
Trimmomatic version 0.39 was employed to trim reads after a quality drop below a mean of Q15 in a window of 5 nucleotides and keeping only filtered reads longer than 15 nucleotides(Bolger et al., 2014). Reads were aligned versus Ensembl mouse genome version mm10 (Ensembl release 101) with STAR 2.7.7a (Dobin et al., 2013). Aligned reads were filtered to remove: duplicates with Picard 2.21.7 (Picard: A set of tools (in Java) for working with next generation sequencing data in the BAM format), spliced, multi-mapping, ribosomal, or mitochondrial reads. Peak calling was performed with Macs version 2.1.1 with FDR < 0.0001 (Zhang et al., 2008). Peaks overlapping ENCODE blacklisted regions (known misassemblies, satellite repeats) were excluded. Remaining peaks were unified to represent a common set of regions for all samples and counts were produced with bigWigAverageOverBed (UCSC Toolkit). The raw count matrix was normalized with DESeq2 version 1.30.0 (Love et al., 2014). Peaks were annotated with the promoter (TSS +- 5000 nt) of the nearest gene based on Ensembl release 101. Contrasts were created with DESeq2 based on the normalized count peak matrix with all size factors set to one. Peaks were classified as significantly differential at average count > 10 and -1 < log2FC > 1. All downstream analyses are based on the normalized peak count matrix. Sequencing and mapping of reads were performed by Stefan Günther at the Bioinformatics facility of the Max-Planck-Institute for Heart and Lung Research.

2.9.11 CUT & RUN peaks motif analysis

MEME-ChIP version 5.3.3 (https://meme-suite.org/meme/tools/meme-chip)(Bailey et al., 2015) was applied on all peaks (center +- 250 nt) from the INO80 CUT & RUN described above, using default parameters. This analysis was performed by Carsten

Kuenne at the Bioinformatics facility of the Max-Planck-Institute for Heart and Lung Research.

2.9.12 Western blot

Protein from aorta was extracted by adding 250 µl of extraction buffer (0.1M Tris/HCl pH 8.0, 0.01 M EDTA pH 8.0, 10% SDS, 1 Complete Mini Protease inhibitor tablet (Sigma #04693132001),1x Phospho stop tablet, H_20) followed by sonication at 20 power/5cycle/20 sec. Protein extracts were then centrifuged at 14 000 RPM for 5min at RT. The supernatant was transferred to a fresh Eppendorf tube, and protein concentration measured using the BioRad DC-Kit assay and a bovine serum albumin (BSA) 0-30 µg/µl. 0.04 M DTT (Roth #6908.2) was added onto the protein lysates samples after protein concentration measurement.

10 µg of protein in 4x laemmli buffer (2.4 ml 1M Tris HCl pH 8.0, 0.8 g SDS, 4 ml 100% glycerin, 1ml beta-mercaptoethanol, 200 µl 1% bromphenol blue, 2.6 ml H_20) were boiled at 95°C for 1 min and loaded on 4-12% Bis-Tris polyacrylamide gels (ThermoFischer #NP0321BOX). The gels were run using 1x MES buffer (50 mM MES, 0,1 % SDS, 50 mM Tris, 1 mM EDTA) and placed in the chamber (ThermoFischer #EI0001). The prestained protein ladder (ThermoFischer #BP3603500) was used as a protein marker. The gels were initially run at 70V for 15 min and then increased to 180V for around 1 hour. The separated proteins were blotted from the gel onto a nitrocellulose membrane (Merck #WHA10402506) at 30V for 2 hours in the Xcell Blot Module (ThermoFischer #EI9051). For blotting a transfer buffer solution (20% methanol, 0.5 M Bicine, 0.5 M BisTris, 20.5 mM EDTA) was used. In order to confirm correct blotting and loading the membrane was stained with RedAlert (Merck #71078) and scanned following blotting. When required, the membrane was cut around the protein sized of interest.

The membrane was blocked using 5% BSA (Roth #8040.3) in 1x TBS-T (Sigma Aldrich #T6664-10PAK, 1%Tween20 Sigma Aldrich #P1379) for 1 hour shaking at RT. Following blocking, the membrane was incubated with the primary antibody (table 6) in 3% BSA in 1x TBS-T overnight shaking at 4°C.

The following day, the membrane was washed by shaking five times for 5 min each using 1x TBS-T at RT. Next, the membrane was incubated with the respective secondary antibody in 3% BSA in 1x TBS-T (table 7) for one hour at RT. The

membrane was then subsequently washed through shaking at RT five time for 10 min each using 1x TBS-T.

Finally, proteins were detected using the WesternBright Chemiluminescence Substrate Sirius (Biozym Scientific #541020) in the ChemiDoc-Imaging System (Bio-Rad #1708280). Further analysis was performed using the ImageLab software (Bio-Rad Laboratories).

Table 6. Primary antibody list

Description	Species	Dilution
C-fos (Cell Signaling #2250)	Rabbit	1:1000
Gapdh (Cell Signaling #2118)	Rabbit	1:1000
JNK1 (Cell Signaling #3708)	Mouse	1:1000
JNK2 (Cell Signaling #9258)	Rabbit	1:1000
Myocd (Covalab, pab0604)	Rabbit	1:200
p-C-fos (Cell Signaling #5348)	Rabbit	1:1000
p-C-Jun (Abcam #ab273417)	Rabbit	1:1000
p-RPA32 (Bethyl #A300-245A-M)	Rabbit	1:1000
y-H2AX (Cell Signaling #2577)	Rabbit	1:1000

Table 7. Secondary antibody list

Description	Species	Dilution
Anti-mouse-HRP (ThermoFischer #31450)	Rabbit	1:5000
Anti-rabbit-HRP (ThermoFischer #31460)	Goat	1:5000

2.10 Cell Culture

2.10.1 Isolation of pulmonary arterial smooth muscle cells (PASMCs)

PASMCs were isolated from Ino80^{lox} SM22Cre^{neg} (control) and Ino80^{lox} SM22Cre^{pos} (Ino80 KO) as described (Lee et al., 2013). In brief, animals were anesthetised, and a small incision in the abdominal aorta was performed. The right heart ventricle was then perfused with 1 x PBS until the lungs were cleared of blood and became white. The right heart ventricle was subsequently perfused with at least 3 ml of an iron-agarose solution (0.5% Iron III Oxide (Merck #310069) and 0.5% agarose low gelling temperature (Merck #A9414) in Medium 199 (Merck #M4530) containing 1% penicillin streptomycin (PS) warmed in the microwave at 70°C until the agarose particles were dissolved but without allowing the solution to boil. This solution should be kept warm at 40°C until perfusion in the animal. Special care should be taken when instilling this solution: the iron-agarose solution needs to be mixed before use and carefully perfused to avoid oedema and a perfusion block. Next, a small incision was made in the trachea at the level of the mandible and a small catheter or tracheal tube was inserted through this incision. A loose ligature was then made around the catheter. A minimum of 3 ml agarose solution (agarose low gelling temperature (Merck #A9414) dissolved in Medium 199 (Merck #M4530) containing 1% PS at a concentration of 10mg/ml) and warmed in the microwave at 70°C until the agarose particles were dissolved but without allowing the solution to boil. This solution was kept warm at 40°C until perfusion into the animal, and then instilled through the catheter into the lungs until the lungs were completely filled. After one to two minutes, the catheter was removed and the ligature closed assuring the agarose solution does not leak out from the lungs. The lungs were then dissected out and incubated in cold 1 x PBS for 10 minutes.

Under the cell culture hood, 1-2 ml of 1xPBS were added onto the lung lobes which were subsequently cut into very small pieces. The pieces of lung were washed using 10-30 ml 1x PBS in a 50 ml falcon using a magnetic holder (ThermoFischer Scientific #12001D). The lung pieces containing Iron III attached to the wall of the falcon where the magnet was whilst the remaining supernatant containing the rest of the lung was aspirated and discarded. This washing procedure was repeated three times. Next, the washed lung pieces were incubated in collagenase solution (80U/ml collagenase II in M199 medium containing 1% penicillin streptomycin) (10ml were required per lung)

and placed in a 5% CO_2, at 37°C in HeraCell150i (ThermoScientific) incubator for 45 minutes. Following incubation, the tissue was homogenized by aspirating and releasing the tissue using an 18 G or 20 G needle several times. The homogenized tissue was finally washed three times with M199 medium containing 1% PS using a magnetic holder as described above. Finally, the iron-containing pellet was resuspended in Smooth Muscle Cell Growth Medium 2 (Ready to use) (PromoCell #22062) and the resuspended cells were transferred onto a 6 well gelatin (PELOBiotech #PB-6950) coated plate (coating time 2 minutes, coating solution was removed before transfer of cell suspension). After one week, the supernatant containing the homogenized tissue was transferred into a fresh 6 well gelatin (PELOBiotech #PB-6950) coated plate. Cells which were attached to the initial 6 well plate were discarded (fibroblasts). These two steps were repeated twice. Finally, PASMCs were allowed to grow out from the iron-containing homogenized tissue until they reached 70-80% confluency.

2.10.2 Isolation of primary murine aortic vascular smooth muscle cells

Isolation of primary murine aortic vascular smooth muscle cells from aorta was performed as described (O'Rourke et al., 2016). In short, the isolated aorta (including abdominal aorta) was placed in cold HBSS buffer until all dissections were completed. Any remaining periaortic fat and soft tissue were also removed. Under a sterile hood, the cleaned aorta was transferred into an aortic digestion solution (DMEM medium, 175 U/ml type 2 collagenase, 1.25 U/ml Elastase) in a 35 mm x 10 mm tissue culture dish and placed in a 5% CO_2, at 37°C in HeraCell150i (ThermoScientific) incubator with gentle intermittent rocking for 30 minutes. Following incubation, the adventitial layer was removed using a microscope and forceps all whilst preserving the medial layer intact. The adventitial layer was peeled away of the aorta at one end like a sock could be peeled back and removed. Next, the remaining aorta was placed into a fresh tissue culture dish containing cell culture media (500 ml of Dulbecco's Modified Eagle Medium (DMEM) were supplemented with 10% fetal bovine serum, 100 units/ml penicillin, and 100 µg/ml streptomycin. the media was kept warm at 37 °C prior to use) and placed in a 5% CO_2, at 37°C in HeraCell150i (ThermoScientific) incubator for 3 hours. Next, the aorta was cut into 1-2 mm wide rings using a scalpel. The rings were then placed into a new tissue culture dish with aortic digestion solution (DMEM

medium, 175 U/ml type 2 collagenase, 1.25 U/ml Elastase) and incubated for 120 min with intermittent gentle rocking in a 5% CO_2, at 37°C in HeraCell150i (ThermoScientific) incubator. The solution was pipetted up and down several times during this incubation step to resuspend the cells. Following the incubation time, 5 ml of warm cell culture media (500 ml of Dulbecco's Modified Eagle Medium (DMEM) were supplemented with 10% fetal bovine serum, 100 units/ml penicillin, and 100 µg/ml streptomycin) was added to the digestion solution, transferred to a 15ml conical tube and centrifuged for 5 minutes at 200 x g. Following centrifugation, the media was removed and cells were resuspended in 5 ml warm cell culture media and transferred to a 25 cm^2 cell culture flask and incubate at 37 °C with 5% CO_2 in a HeraCell150i (ThermoScientific) incubator. During the initial seven to ten days of incubation, media was changed every 72 - 96 hours. When the cells approached confluence, media was replenished every 48 hours. Once confluent, cells were propagated using standard techniques. In brief, cells were incubated in at 37 °C with 5% CO_2 HeraCell150i (ThermoScientific) incubator in a film of trypsin (0.5 – 1 ml) to lift off the plate for 5 minutes. The flask was tapped every 30 - 60 seconds to help detach the cells from the surface of the flask. Once the cells detached from the bottom of the flask, 10 ml of warm cell culture media was added and cells were centrifuged at 200 x g for 5 minutes. Media was then removed and the cell pellet was resuspended in 5 – 10 ml of fresh cell media and transfered to a fresh flask and placed in at 37 °C with 5% CO_2 HeraCell150i (ThermoScientific) incubator.

2.10.3 Transfection of mouse primary aortic smooth muscle cells (aSMCs) and PASMCs

For optimal transfection conditions, aSMCs (PELOBiotech #PB-C57-6080) were grown in Complete Smooth Muscle Cell Medium /w kit (PELOBiotech #PB-M2268) and PASMCs in Smooth Muscle Cell Growth Medium 2 (Ready to use) (PromoCell #22062) on a 6 well gelatine (PELOBiotech #PB-6950) coated plate to 70% confluency. Transfection of smooth muscle cell specific Myocardin overexpressing construct pIRES2-EGFP-Myocd-V3 construct (appendix figure 36), control vector pX335-copGFP as well as siRNA mouse Ino80 mouse yy1, and non-targeting control siRNAs (respectively Dharmacon/Horizon #J-047137-08-0005 together with #J-047137-06-0005, #J-050273-08-0002, and #D-001810-01-05) were performed with

Lipofectamine 3000 (ThermoFischer #L3000015). Transfections were performed according to manufacturer's recommendations. All transfections were performed in triplicates unless stated otherwise. 48 hours post transfection, cells were harvested for RNA or Protein isolation.

2.10.4 H_20_2 assay on primary aortic smooth muscle cells

PASMCs from Ino80$^{lox/lox}$ SM22Cre^{neg} mice were isolated and grown as described in the isolation of pulmonary arterial smooth muscle cells section, to around 70-80% confluency. Cells were washed with 1 x PBS pH 7.4, detached using 1x Trypsin (Sigma #T4049) for two and half minutes in 5% CO_2, at 37°C. The cells were then centrifuged and resuspended in fresh medium then replated on a gelatin coated 6 well plate. H_20_2 was then added onto the cells at 30 µM, 100 µM, 500 µM, and 1000 µM concentrations. Cells were put back into a HeraCell150i (ThermoScientific) incubator with the following setting 5% CO_2, at 37°C for three hours.

2.10.5 DCFDA/H2DCFDA cellular reactive oxygen species (ROS) assay using doxorubicin, l-ascorbic acid and diphenyleneiodonium (DPI) treatments

The DCFDA/H2DCFDA cellular ROS assay kit (Abcam #ab113851) was used as per manufacturer's protocol to quantitively asses ROS in live aSMCs samples as well as PASMCs isolated from Ino80$^{lox/lox}$ SM22Cre^{neg} and SM22Cre^{pos} mice. DCFDA/H2DCFDA is a fluorogenic dye which measures hydroxyl, peroxyl as well as other ROS production in the cell. This assay is based on the staining of cells with DCFDA, whereby the dye diffuses into the cell and is deacetylated by cellular esterases rendering DCFDA non-fluorescent. Upon ROS production, DCFDA is oxidized into 2',7'-dichlorofluorescein (DCF), and becomes highly fluorescent. In these experiments, DCF was detected by fluorescence spectroscopy (excitation 485nm/ emission 535nm) using the Mithras LB940 plate reader (Berthold). For analysis, the respective recorded luminescence for the treated cell samples were normalized to the untreated DCFDA stained controls.

25 000 aSMCs or PASMCs were counted using a Neubauer chamber (Superior Marienfeld #0640110) and added onto each well of a gelatin coated (PELOBiotech #PB-6950) black flat bottom 96 well plate (Merck #M5811-40EA) (25 000 cells per well). Cells were allowed to attach overnight.

The following reagents were freshly prepared on the day of the experiment (volumes required were calculated for 100 µl/well, all treatments were performed in triplicates):
-1x supplemented buffer (2ml FBS, 18ml 1x buffer) and was allowed to equilibrate at 37°C before use.
-30 µM DCFDA solution (20mM DCFDA, 1x supplemented buffer)
-8.5 µM Doxorubicin (Santa Cruz #25316-40-9) in 1x supplemented buffer
-15 µM l-ascorbic acid in 1x supplemented buffer
-15 µM l-ascorbic acid + 8.5 µM doxorubicin in 1x supplemented buffer
- 70 µM DPI + 8.5 µM doxorubicin in 1 x supplemented buffer
- 70 µM DPI in 1x supplemented buffer
Media was removed from cells, and cells were washed using 1x supplemented buffer. (100 µl/well). Cells were then subsequently incubated with 30 µM DCFDA solution for 45 minutes in 5% CO_2 at 37°C. Following the incubation period, the DCFDA solution was removed and the cells were once again washed with 100 µl 1x supplemented buffer. Finally, different treatment combinations (detailed above) were added onto the cells of interest and incubated for 4 hours in a 5% CO_2, 37°C HeraCell150i (ThermoScientific) incubator. Next, plate was measured, DCF was detected by fluorescence spectroscopy (excitation 485nm/ emission 535nm) using the Mithras LB940 plate reader (Berthold).

2.10.6 FOS inhibitor T5224 treatment of PASMCs

T5224 specifically inhibits the transcription factor complex activator protein -1 (AP-1 is a heterodimer composed of c-Fos and c-Jun) and thereby reduces the DNA binding activity of c-Fos and c-Jun (Aikawa et al., 2008). PASMCs isolated from $Ino80^{lox/lox}$ $SM22Cre^{neg}$ and $SM22Cre^{pos}$ mice were used for this experiment. Medium was removed from the cells and replaced with fresh medium containing 30 µM and 60 µM T5224 (MedChemExpress #HY-12270), or a DMSO vehicle control. Cells were then incubated for 24 hours in a 5% CO_2, 37°C HeraCell150i (ThermoScientific) incubator.

2.11 Morphological analysis

2.11.1 Cryosections

Tissues were dissected and fixed using 4% PFA (Sigma #6148-1KG) in 1x PBS for two hours at RT. Next, tissues were incubated in 15% Sucrose in 1x PBS overnight for three hours followed by 30% sucrose in 1 xPBS overnight at 4°C. Afterwards, the samples were transferred into Tissue Tek™ (Leica) overnight at 4°C, aligned and embedded in Tissue Tek™ in cryomolds (Weckert). Samples were finally frozen on dry ice and subsequently stored at -20°C. 10 µm thick sections were cut from the frozen samples using the Superfrost slides (ThermoFischer #J3800AMNZ) at -25°C. Cryosections were stored at -80°C awaiting further use.

2.11.2 Immunohistochemistry

10 µm thick cryosections were fixed using 4% PFA (Sigma #6148-1KG) in 1x PBS. Next, the sections were washed twice with 3% BSA in 1x PBS for 5 minutes each time at RT followed by three washing steps using 0.3% Triton X-100 (Sigma #X100-100ML) in 1x PBS for 10 minutes each at RT. The sections were then washed again twice with 3% BSA in 1x PBS for 5 minutes each time at RT followed by a 1x PBS washing step for five minutes at RT. Blocking solution (0.01% Triton X-100 in 1xPBS diluted 1:10 in Blocking One (Nacalai #03953-95) was added on the cryosections for one hour at RT. If the primary antibody which was to be added originated from mouse, Mouse on Mouse Blocking Reagent (Vektorlabs #MKB-2213) was added into the blocking solution at 1:25 ratio. Following blocking, sections were washed with 1x PBS for five minutes at RT. Sections were subsequently incubated with primary antibodies (table 7) in Solution A (Nakalai #02272-74) overnight at 4°C.

On the next day, samples were washed three times with 0.01% Triton X-100 in 1x PBS for 10 min each time at RT. After washing, the sections were incubated with the respective secondary antibody (table 8) diluted in Solution B (Nakalai #02297-64) for one hour at RT. When a conjugated antibody was used at the same time as non-conjugated antibodies, the antibody was added at the same time as the secondary antibody. Secondary antibody was removed and sections were washed twice with 0.01% Triton X-100 in 1x PBS for 10 minutes each at RT. Sections were next stained with DAPI solution (Merck #D9542) diluted 1:1000 in 1x PBS for five minutes and then washed again with 1x PBS for another five minutes at RT. Finally, tissue sections were

covered with Fluoromount W (Serva #21634.01) and sealed using nail vanish on the next day. Immunohistochemistry samples were stored at 4 °C. Microscopic pictures were acquired using the fluorescence microscope Zeiss Axio Imager Z1.

2.11.3 Immunocytochemistry

PASMCs or aSMCs were fixed using 4% PFA (Sigma #6148-1KG) in 1x PBS. Next, cells were washed twice with 3% BSA in 1x PBS for 5 minutes each time at RT followed by permeabilization through three washing steps using 0.3% Triton X-100 (Sigma #X100-100ML) in 1x PBS for 10 minutes each at RT. Cells were once more rehydrated twice using 3% BSA in 1x PBS for 5 minutes each time at RT followed by a 1x PBS washing step for five minutes at RT. Blocking solution (0.01% Triton X-100 in 1xPBS diluted 1:10 in Blocking One (Nacalai #03953-95) was added on the cells for one hour at RT. If the primary antibody which was to be added originated from mouse, Mouse on Mouse Blocking Reagent (Vektorlabs #MKB-2213) was added into the blocking solution at 1:25 ratio. Following blocking, cells were washed with 1x PBS for five minutes at RT. Samples were subsequently incubated with primary antibodies (table 8) in Solution A (Nakalai #02272-74) overnight at 4°C.

On the next day, samples were washed three times with 0.01% Triton X-100 in 1x PBS for 10 min each time at RT. After washing, cells were incubated with the respective secondary antibody (table 9) diluted in Solution B (Nakalai #02297-64) for one hour at RT. When a conjugated antibody (table 9) was used at the same time as non-conjugated antibodies, the antibody was added at the same time as the secondary antibody. Specific fluorochrome labeled binding proteins were also added to the secondary antibody (table 10). Secondary antibody was removed and cells were washed twice with 0.01% Triton X-100 in 1x PBS for 10 minutes each at RT. Cell nuclei were stained with Dapi solution (Merck #D9542) diluted 1:1000 in 1x PBS for five minutes and then washed again with 1x PBS for another five minutes at RT.

Finally, cells were kept in 1x PBS and stored at 4 °C. Microscopic pictures were acquired using the fluorescence microscope Zeiss Axio Imager Z1.

Table 8. Primary antibodies used in Immunohistochemistry/cytochemistry

Description	Species	Dilution
Foxo1 (Cell Signaling #2880)	Rabbit	1:200

Table 9. Conjugated and secondary antibodies used in immunohistochemistry/cytochemistry

Description	Species	Dilution
Alpha Smooth Muscle Actin FITC (Sigma #F3777**)**	mouse	1:500
Alpha Smooth Muscle Actin Cy3 (Sigma #C6198**)**	mouse	1:500
Anti-Rabbit IgG Alexa 488 (Invitrogen #A11070)	goat	1:1000
Anti-Rabbit IgG Alexa 594 (Invitrogen #A11012)	goat	1:1000

Table 10. Fluorescently labeled cytoskeletal stains

Description	Dilution
Phalloidin 633 (Invitrogen #A22284)	1:40

2.11.4 Electron microscopy

Carotids were perfused with 1x PBS followed by fixation solution (2% paraformaldehyde (Sigma #6148-1KG), 1.5% glutaraldehyde (Sigma #G5882) in 0.15 M HEPES buffer (Sigma #H3375), in ddH_20 pH 7.3), isolated and incubated in the same fixation solution for a minimum of 24 hours at 4°C. Next, samples were post-fixed using 1% osmium trioxide solution (Sigma #75633) and stained with uranyl acetate (Agar Scientific #AGR1260A). Carotids were then dehydrated through a series of gradient alcohol solutions. Finally, samples were embedded and mounted in Epoxy resin (Agar 100 Resin, Agar Scientific #AGR1031) and ultra-thin sections were cut using an ultramicrotome. Sections were imaged using TEM (Zeiss EM 900).

2.11.5 Morphological analysis of atherosclerotic plaques through light sheet microscopy: staining, clearing, and imaging

Microdissection of murine aortic arches was performed according to the protocol by Centa et al. (Centa et al., 2019). In brief, microdissection of murine aortic arches was performed under a stereomicroscope. First, the aortic bifurcation was dissected by lifting surrounding tissue with Dumont forceps and cutting under tension. The microdissection was further performed cranially, and the abdominal branches were cut away to free the aorta proximally through the aortic hiatus in the diaphragm. Next, the the adipose tissue covering the thoracic aorta was removed. Thereafter, the thymus was dorsally dissected to free the aortic arch with branches. Dissection of the carotid arteries was continued as distally as possible in the thoracic cavity. Finally, the aorta was cut away from the heart and the aortic arch was then dissected out of it and placed in a tube containing 1 mL of 4% formaldehyde overnight at 4 °C. Subsequent aortic arch tissue preparation, delipidation, permeabilization, whole mount immunostaining and tissue clearing were performed for light sheet microscopy imaging according to the protocol described by Chi *et al*. (Chi et al., 2018).

In brief, the fixed aortic arches were washed in 1x PBS for 1 hour, for three times. Fixed samples were then washed in 20%, 40%, 60%, 80% methanol in H_2O/0.1% Triton X-100/0.3 M glycine (B1N buffer, pH 7), and 100% methanol for 30 minutes each. Sample were then delipidated with 100% dichloromethane (DCM; Sigma-Aldrich) for 30 minutes, three times. After delipidation, samples were washed in 100% methanol for 30 minutes twice, and then in 80%, 60%, 40%, 20% methanol in B1N buffer for 30 minutes each. All procedures detailed above were carried out at 4°C whilst shaking. Samples were then washed twice in B1N for 30 minutes each followed by 1x PBS/0.1% Triton X-100/0.05% Tween 20/2 mg/ml heparin (PTwH buffer) for 1 hour twice to achieve sample permeabilization. For immunostaining, samples were incubated in primary antibody dilutions in PTxwH for 4 days. After primary antibody incubation, samples were washed in PTxwH for 5 min, 10 min, 15 min, 30 min, 1 hour, 2 hours, 4 hours, and overnight, and then incubated in secondary antibody dilutions in PTxwH for 4 days. Finally, samples were washed in PTwH for 5 min, 10 min, 15 min, 30 min, 1 hr, 2 hr, 4 hr, and overnight. Information on antibodies used for staining are available in tables 11 and 12. For tissue clearing, stained samples were dehydrated in 25%, 50%, 75%, 100%, 100% methanol/H_2O series for 30 minutes each at room

temperature. Following dehydration, samples were washed with 100% DCM for 30 minutes twice, followed by an overnight clearing step in dibenzyl ether (DBE; Sigma-Aldrich). Samples were stored at RT protected from light until imaging was performed. Aortic arches were imaged using an Ultramicroscope II (La Vision Biotec) with the ImSpector software (La Vision Biotec). The microscope was equipped with a MVX10 zoom body (Olympus), a 2x objective and a Zyla 4.2 PLUS sCMOS camera (Andor). A total magnification of 1 x together with 10 µm Z-steps were used for acquisition of images. Three-dimensional reconstruction was achieved using the Imaris file converter (Bitplane). Images were further processed for background subtraction and median tools using the Imaris software (Bitplane). Microdissection of aortic arches was performed together with Laia-Canes Esteve, Max-Planck-Institute for Heart and Lung Research. Further tissue processing and imaging was performed by Laia-Canes Esteve, Max-Planck-Institute for Heart and Lung Research.

2.11.6 Aortic root preparation hematoxylin and oil red O staining

Microdissection of murine aortic roots was performed according to the protocol by Centa et al. (Centa et al., 2019). Samples were processed for cryosectioning and stored at -80°C as described above. For oil red O staining, sections were thawed to room temperature for 10 to 15 mins, and washed with distilled water for 5 mins. Next, sections were submerged in a ready to use hematoxylin solution for 5 minutes followed by washing with tap water for 5 minutes. The tap water had to be exchanged several times during this wash step. Thereafter, sections were washed with distilled water for 5 minutes and successively submerged oil red O working solution (Stock solution: 1g Oil Red (C.I. 26125) was dissolved in 500 ml Isopropyl alcohol (2-propanol) for 24 hours with agitation, the solution was then filtered and stored protected from air. Working solution: 48 ml stock solution was diluted in 32 ml distilled water. Volumes of the working solution were adjusted as needed) for 15 minutes. For the last step of the staining, sections were dipped in and out of distilled water for 10 times. Finally, sections were mounted with Mowiol and imaged using the Ni-E ECLIPSE widefield microscope (Nikon). In short, images were acquired using a Ni-E ECLIPSE widefield microscope (Nikon) equipped with a SlideExpress 2 slideloader (Märzhäuser), a LED 100 coolwhite diascopic lightsource (Märzhäuser) and a DS-Ri2 Digital Microscope camera (Nikon) controlled by the NIS-AR software v.5.3 (Nikon). All acquisition

parameters (light sources, illumination time, camera gain etc.) were kept constant for the entire imaging experiment.

Image acquisition was automated using the NIS-AR JOBS module: Overview images were acquired using a CFI Plan Achromat UW 2 x objective (Nikon) and regions of interest selected for all slides. A 500 µm autofocus in the DAPI channel was performed in the middle of each region, followed by the acquisition of a large image using a CFI Plan Apochromat 10x Lambda objective (Nikon). The resulting images were processed using Image J. The staining and image analysis were performed together with Laia-Canes Esteve, Max-Planck-Institute for Heart and Lung Research. Imaging was performed by Laia-Canes Esteve, Max-Planck-Institute for Heart and Lung Research.

Table 11. Primary antibodies used for light sheet microscopy

Description	Dilution
CD31 (Invitrogen #PA5-32321)	1:100
CD68 (BioRad #MCA1957)	1:100
TOPRO (ThermoFischer #T3605)	1:5000

Table 12. Secondary antibodies used in light sheet microscopy

Description	Species	Dilution
Anti-Rat IgG Alexa 790 (Jackson Immuno Research Labs #712655153)	Donkey	1:200
Anti-Rabbit IgG Alexa 594 (Invitrogen #A11012)	goat	1:200

2.11.7 Migration *in vitro* scratch assay

PASMCs were isolated and grown from Ino80$^{lox/lox}$ SM22Cre^{pos} and Ino80$^{lox/lox}$ SM22Cre^{neg} as described above in section 2.10.1. The cell monolayer was scraped through both a vertical and horizontal line (creating a cross) using a p200 pipet tip.

Debris were removed by washing the cells with Smooth Muscle Cell Growth Medium 2 (Ready to use) (PromoCell #22062). Cells were eventually incubated in Smooth Muscle Cell Growth Medium 2 and placed in the IncuCyte Zoom Live Imaging System (Essen Bioscience). Cells were imaged every hour for 24 hours and wound size was determined using the Image J software. The recorded wound size was made of an average of three fields of view per well over the entire period mentioned.

2.11.8 Proliferation assay using EdU-kit

PASMCs were isolated and grown from Ino80$^{lox/lox}$ SM22Cre^{pos} and Ino80$^{lox/lox}$ SM22Cre^{neg} as described in Isolation of pulmonary arterial smooth muscle cells (PASMCs) section 2.10.1. Once confluence reached, cells were washed with 1x PBS and detached by incubating then in Trypsin (Sigma #T4049) for two and half minutes in a 5% CO_2, 37°C HeraCell150i (ThermoScientific) incubator. Cells were centrifuged at 12 500 RPM at RT and resuspended in fresh medium. The cells were next plated on a gelatine coated plate and 1:3.333 5-ethynyl-2´-deoxyuridine (ThermoFischer #C10339) was added on the cells at 1:1000 ratio. PASMCs were placed back into the incubator and EdU incorporation into the DNA was allowed to take place for 6 hours. EdU staining was performed according to manufacturer's instructions Click-iT^{TM} EdU Imaging Kits (ThermoFischer #C10339). Dapi diluted 1:1000 in 1x PBS was used at added onto the cells to stain for cell nuclei for 5 minutes at RT. Cells were washed with 1x PBS and stored in fresh 1x PBS at 4°C. Microscopic pictures were acquired using the fluorescence microscope Zeiss Axio Imager Z and number of EdU positive cells quantified using the Image J software.

2.12 Software used

Table 13. Software

Description	Manufacturer/Developer
Access, Excel, PowerPoint, Word	Microsoft
Adobe Illustrator 2022	Adobe Systems Incorporated
Adobe Reader	Adobe Systems Incorporated
BLAST	NCBI
CAT	Computer Administriertes Tierhaus (MPG)
Dataquest A.R.T 4.0	Data Sciences International
EndNote	Clarivate Analytics
Ensembl Genome Browser	European Molecular Biology Laboratory's European Bioinformatics Institute (EMBL-EBI)
GraphPad Prism 9	GraphPad Software, Inc.
GSEA 3 and 4	Broad Institute
ImageJ	Wayne Rasband
ImageLab	Bio-Rad Laboratories
IncuCyte ZOOM 2016 and 2018A	Essen BioScience
Integrated Genome Browser (IGV)	Broad Institute
Lab Chart 7	AD Instruments
Seqbuilder 17.3	DNASTAR Lasergene
Seqman Pro 17.3	DNASTAR Lasergene
StepOne Software v2.3	ThermoFisher
Zen 3.2	Zeiss

2.13 Statistical analysis

The number of samples per condition (n) was depicted on the figures themselves as well as stated in the figure legend of each figure, respectively. Every statistical analysis depicted in this work was completed using the Graph Pad Prism software (version 6 or version 9). Unless otherwise highlighted, all obtained values were plotted with standard error of the mean (SEM). Data sets containing over three replicates per group were tested for normal Gaussian distribution of values. If a Gaussian distribution of values was detected, a two-tailed student's t-test was performed. If a one-tailed student's t-test was used, this was highlighted in the figure legend of the said figures. respectively. Otherwise, a non-parametric test procedure was used and details about the statistical test then used can also be found in the figure legend of the said figures, respectively. Statistical significances were displayed as p-values and the significances reported in this work are shown below.

Table 14. p value annotation and significance

P value annotation	Significance
ns	Not significant $p > 0.05$
*	Significant $p < 0.05$
**	Significant $p < 0.01$
***	Significant $p < 0.001$
****	Significant $p < 0.0001$

3. Results

This study investigated the functions of the chromatin remodeler INO80 in VSMCs. To characterize the physiological and molecular consequences of the INO80 loss of function phenotype in VSMCs, the Ino80-encoding gene was inactivated in smooth muscle cells of mice using the Cre-loxP system. To analyse the physiological effects of the loss of Ino80 on VSMCs contractility, wire myography, telemetric blood pressure measurements and histological evaluation of arteries were performed. Molecular analysis of the INO80 loss of function was performed by means of affymetrix microarray analysis, RNA seq, INO80 Cut&Run, ATAC seq, gene set enrichment analysis, motif analysis, immunohistochemistry, cellular ROS quantification, western blot as well as *in vivo and in vitro* rescue experiments. Finally, to investigate the role of Ino80 in migration and proliferation, *in vivo* partial carotid ligation, *in vitro* scratch assay, affymetrix microarray analysis, immunostaining, and assessment of atherosclerosis development using the AAV8-PCSK9 murine model of high fat diet were performed. The next subsections will detail the reasoning behind and conclusions drawn from these experiments.

3.1 Constitutive deletion of Ino80 in smooth muscle cells

Ino80 is a ubiquitously expressed and evolutionary conserved protein(Conaway & Conaway, 2009; Flaus et al., 2006). Ino80 is located on the mouse genome on chromosome 2. To uncover the functions of Ino80 in mammalian development, Qiu *et al*. created a conditional KO allele of Ino80 in mice using the Cre-loxP system (Bouabe & Okkenhaug, 2013; Qiu et al., 2016). With this approach, exons 2-4 of the Ino80 gene were flanked by two loxP sites allowing for excision of the genomic DNA (in this instance exons 2-4 of the Ino80 gene) between these sites, upon tissue specific Cre recombinase expression ($Ino80^{lox/lox}$). To create a mouse line where Ino80 was specifically inactivated in smooth muscle cells, the $Ino80^{lox/lox}$ mice was crossed with mice constitutively expressing a smooth muscle specific Cre recombinase, namely the SM22Cre line (Holtwick et al., 2002). These transgenic mice express Cre recombinase under the control of the mouse smooth muscle protein 22-alpha (transgelin) promoter. Mice carrying the Ino80 deletion in smooth muscle cells were viable and born according to expected mendelian ratios.

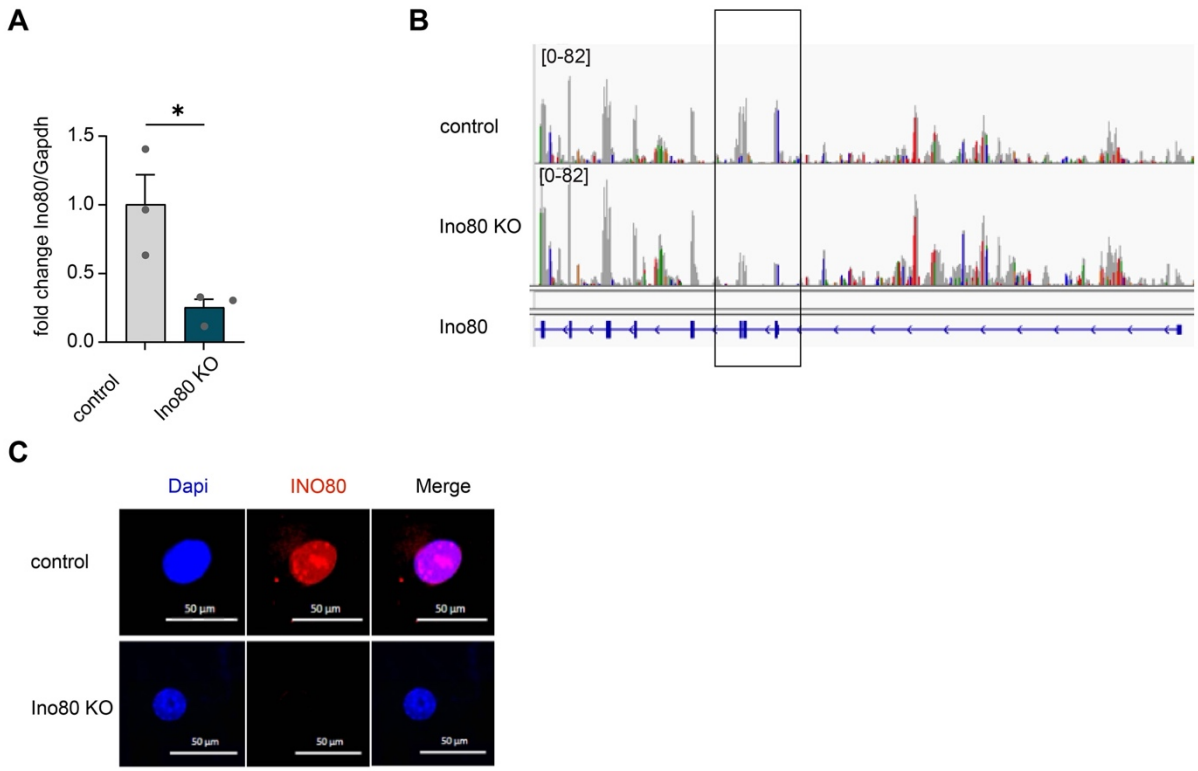

Figure 13. Validation of Ino80 knock out in smooth muscle cells *in vivo*.
A Quantitative Ino80 mRNA expression in $Ino80^{lox/lox}$ $SM22Cre^{neg}$ (control) and $Ino80^{lox/lox}$ $SM22Cre^{pos}$ (Ino80 KO) murine aortas was determined by RT-qPCR. Ino80 expression was normalised to gapdh expression as an internal control. n=3/3 animals. **B** Integrative genomics browser (IGV) snapshot depicting a part of the Ino80 encoding gene and RNA seq data for control and Ino80 KO murine aortas revealing a reduced detection of RNA coding for exons 2-4 (black box). The black box highlights exons 2-4 of the Ino80 encoding gene. n=3/3 animals. **C** Immunofluorescence images of pulmonary arterial smooth muscle cells (PASMCs) isolated from control and Ino80 KO mice. PASMCs were stained with Dapi (blue) and anti-Ino80 antibody (red). gapdh (glyceraldehyde-3-phosphate dehydrogenase), Ino80 (inositol requiring 80), IGV (integrative genomics viewer).

Loss of Ino80 in smooth muscle cells was confirmed by quantitative PCR (RT-qPCR) of aortas using primers flanking exons 2-4 of the Ino80 encoding gene. This analysis revealed a decrease of 80% of Ino80 expression in Ino80 KO aortas, in comparison with control (figure 13 A). Evaluation of aortic Ino80 RNA expression from control and Ino80 KO mice also showed a decrease of reads which overlap with exons 2, 3 and 4 of the Ino80 encoding gene (highlighted by a black box). Ino80 was deactivated using a smooth muscle specific Cre line (SM22 Cre) and was therefore knocked out in smooth muscle cells (Ino80 KO). Ino80 is ubiquitously expressed, and whilst aortas are mainly composed of smooth muscle cells, they also contain endothelial cells, fibroblasts, mesenchymal stem cells, pericytes and immune cells (Conaway & Conaway, 2009; Flaus et al., 2006; Li et al., 2021). Expression of Ino80 in non-smooth muscle cells of the Ino80 KO line are expected to remain unchanged in comparison with control. Thus, the remaining Ino80 expression observed in figure 13 A and B is

assumed to stem from non-smooth muscle cells found in the aorta. To further validate the loss of Ino80 in vascular smooth muscle cells, PASMCs isolated from control and Ino80 KO mice were stained for INO80 expression. Control PASMCs revealed strong nuclear INO80 expression. In contrast to this, INO80 KO PASMCs showed no expression of INO80 (figure 13 C). In contrast to figure 13 A and B, where Ino80 expression was evaluated from aortas which contain several other cell types in addition to smooth muscle cells, PASMCs are a population of pure vascular smooth muscle cells, hence why we detected no INO80 expression in the Ino80 KO PASMCs, thus remaining Ino80 expression in VSMCs can be excluded (figure 13 C).

Together, lack of Ino80 expression in smooth muscle cells in the Ino80 KO line was confirmed by RT-qPCR and RNA seq from aortas as well as INO80 PASMCs immunostaining. Ino80 aortic expression was significantly decreased upon loss of Ino80, and the remaining Ino80 expression was assumed to stem from aortic non-smooth muscle cells. No expression of INO80 was detected in PASMCs, a pure population of vascular smooth muscle cells, confirming our previous findings from the aortic evaluation of Ino80 expression and further validating that the remaining expression of aortic Ino80 expression in Ino80 KO line originates from non-smooth muscle cells. Therefore, Ino80 was successfully deleted in SMCs.

3.2 Loss of Ino80 leads to an increase in arterial luminal area, a decrease in vascular contractility and to a blunted blood pressure response

To evaluate whether loss of Ino80 led to morphological changes on the arterial level, sections of carotid arteries taken from Ino80 KO and control mice were stained for alpha smooth muscle actin. The thickness of alpha smooth muscle positive layer as well as the luminal area were analysed.

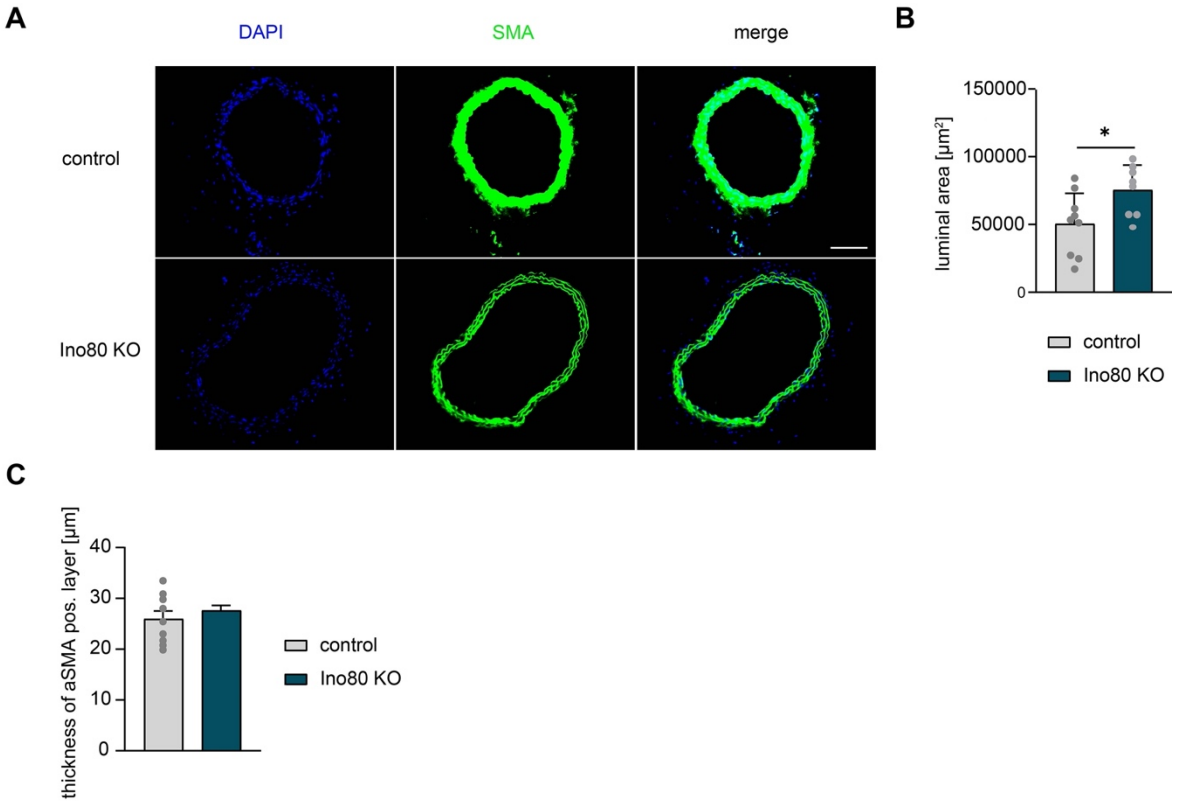

Figure 14. INO80 deletion causes an increase in the arterial luminal area.
A Representative image of Ino80$^{lox/lox}$ SM22Cre^{neg} (control) and Ino80$^{lox/lox}$ SM22Cre^{pos} (Ino80 KO) murine carotid sections stained with DAPI (blue) and anti-alpha smooth muscle cell actin (SMA) antibody. Scale bar 100 µm. **B-C** Statistical evaluation of the luminal area (B) and the alpha smooth muscle actin positive area from control and Ino80 KO mice carotid artery sections. (C). n=9/9 control and n=8/8 Ino80 KO animals. pos. layer (positive layer), DAPI (4',6-diamidino-2-phenylindole), aSMA (alpha smooth muscle actin), Ino80 (inositol requiring 80).

Assessment of representative images of Ino80 KO and control carotid murine sections shows that the luminal area of Ino80 KO carotid sections is larger than that of control mice (figure 14 A). Quantitative evaluation of the luminal area revealed that it was significantly increased in the Ino80 KO mice in comparison with control (figure 14 B). In contrast to this, the thickness of the alpha smooth muscle actin positive layer was

unchanged between Ino80 KO and control mice and remained around 25-27 µm (figure 14 C). Whilst the thickness of the alpha smooth muscle actin positive layer was unchanged in contrast to the control, the alpha smooth muscle actin signal was reduced in the Ino80 KO carotid murine sections in contrast to control (figure 14 A). Alpha smooth muscle actin (ACTA2) is an essential protein for smooth muscle contractility and motility (Wang et al., 2006). Additionally, arterial luminal area can affect vascular resistance and therefore might also have consequences on vascular contractility (Welsh et al., 2018). Therefore, the increase in luminal area together with the decrease in alpha smooth muscle actin signal suggest that loss Ino80 KO might affect smooth muscle contractility.

The observed increase in luminal area in addition to the decrease in alpha smooth muscle actin protein expression, observed in figure 14, indicate possible alterations in arterial contractility upon loss of Ino80. To investigate this, wire myography experiments using femoral artery segments from control and Ino80 KO mice were performed.

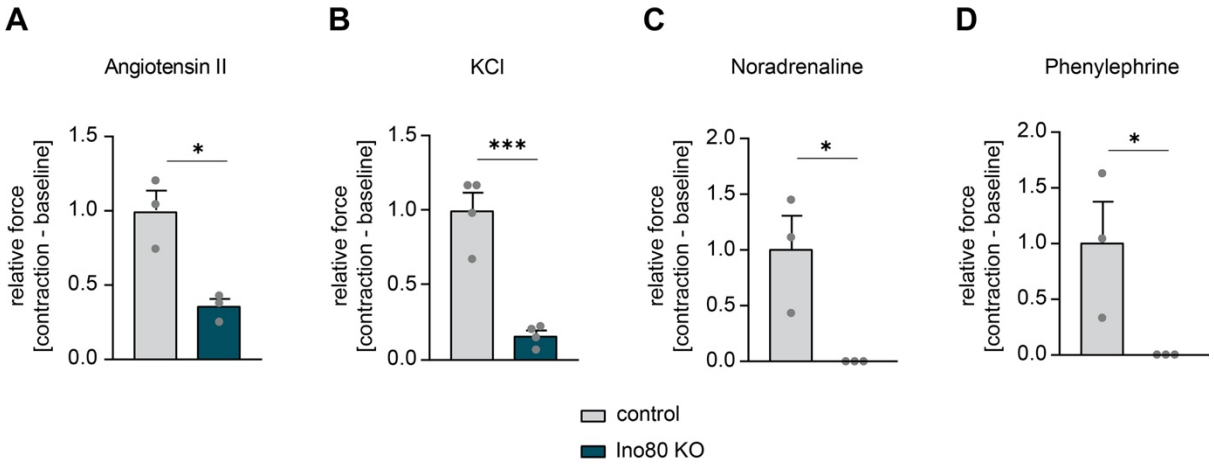

Figure 15. INO80 deficient arteries display a significant decrease in vascular contractility upon treatment with various vasoactive stimuli.
A-D Wire myography experiments using Ino80$^{lox/lox}$ SM22Cre^{neg} (control) and Ino80$^{lox/lox}$SM22Cre^{pos} (Ino80 KO) murine femoral artery segments. Statistical analysis of these experiments depicts the change in femoral artery tension (relative force [contraction-baseline]) upon addition of 10^{-2} µM angiotensin II (A), 100 mM KCl (B), 10^{-3} M noradrenaline (C) and 10^{-5} M phenylephrine (D) to stimulate vessel segment contractility. n=3/3 animals (A, C-D), n=4/4 animals (B). For statistical analysis of the femoral artery tension using phenylephrine treatment, a one-tailed unpaired student's t-test was used. Ino80 (inositol requiring 80).

Angiotensin II induced contraction in both control and Ino80 KO femoral artery segments, but the contraction induced was significantly reduced upon loss of Ino80 (figure 15 A). KCl treatment also induced contraction in both control and INO80 KO femoral artery segments however the induced contraction was significantly reduced upon loss of Ino80 (figure 15 B). Both Noradrenaline and Phenylephrine successfully induced contraction in control femoral artery segments but failed to induce contractility in Ino80 KO femoral artery segments (figure 15 C and D). Taken together, measurement of vascular contractility demonstrated a decrease in arterial contractility upon loss of Ino80, but with differential response to diverse type of stimuli. The observed reduction in smooth muscle contractility upon loss of Ino80 is in accordance with the observed increased luminal area and decreased alpha smooth muscle actin signal (figure 14). The discrepancy in contractility response between different stimuli might be explained by activation of diverse contractility pathways.

Loss of Ino80 led to a decrease in vascular contractility (figure 15). Vascular contractility is essential for blood pressure regulation. To evaluate the *in vivo* physiological consequences of reduced vascular contractility upon loss of Ino80, control and Ino80 KO mice were subjected to telemetric blood pressure measurement.

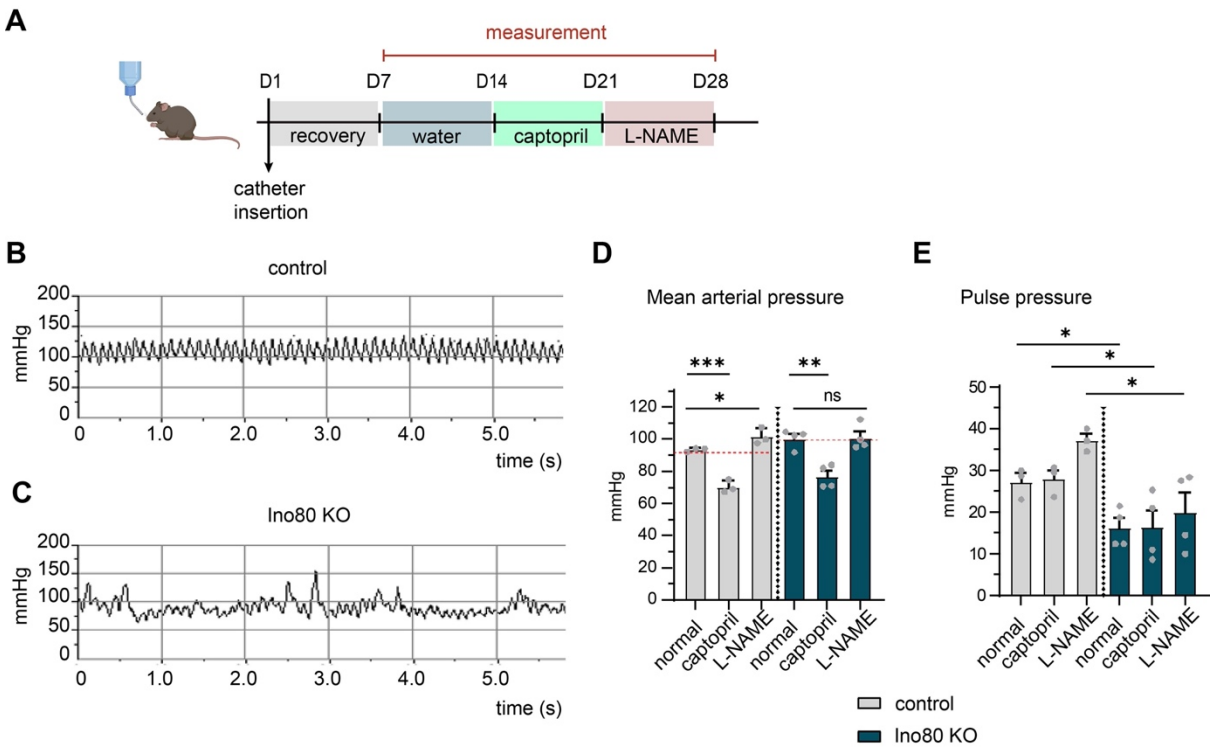

Figure 16. Loss of INO80 causes failure to increase blood pressure upon stimulus and to a decrease in pulse pressure.

A Experimental set up of telemetric blood pressure measurements conducted in Ino80$^{lox/lox}$SM22Cre^{neg} (control) and Ino80$^{lox/lox}$SM22Cre^{pos} (Ino80 KO) mice. Mice were given normal drinking water, captopril in drinking water (600 µg/ml) and L-NAME in drinking water (500 µg/ml) for 7 days at a time. **B-C** Continuous arterial blood pressure waveforms under normal physiological conditions from control (A) and Ino80 KO (B) mice. **D** Statistical analysis of the average mean arterial pressure (mmHg) over 7 days using normal drinking water, captopril in drinking water and L-NAME in drinking water from control and Ino80 KO mice. n=3/3 control and n=4/4 Ino80 KO animals. For statistical analysis of the comparison between the average mean arterial pressure of control animals under normal drinking water and L-NAME treatment, a one-tailed unpaired student's t-test was used. **E** Statistical analysis of the average pulse pressure (pulse pressure = systolic pressure – diastolic pressure) over 7 days in control and Ino80 KO mice using normal drinking water, captopril in drinking water and L-NAME in drinking water. n=3/3 control animals and n=4/4 Ino80 KO animals. For statistical analysis of the comparison between control and Ino80 KO animals under captopril treatment, a one-tailed unpaired student's t-test was used. Ino80 (inositol requiring 80), L-NAME (N (gamma)-nitro-L-arginine methyl ester), s (seconds).

Ino80 KO and control mice were subjected to telemetric blood pressure measurement under normal drinking water, captopril treatment, and L-NAME treatment over a period of seven days per condition (figure 16 A). Continuous arterial blood pressure waveforms under normal drinking water (normal condition) revealed an overall irregular narrow pulse pressure in the Ino80 KO mice (figure 16 C) in comparison with control mice. Nonetheless, arterial blood pressure waveforms of Ino80 KO mice also showed spikes where the pulse pressure was wider (figure 16 C). These spikes did not occur in the control mice (figure 16 B). Under normal drinking water (normal

condition) no significant difference in the mean arterial pressure was observed between Ino80 KO and control mice. Captopril (D-3-mercapto-2-methyl-propionyl-L-proline), a clinical angiotensin-converting enzyme inhibitor, blocks conversion of angiotensin I to the potent vasoconstrictor angiotensin II and inactivates simultaneously the vasodilator peptide bradykinin thereby lowering blood pressure (Odaka & Mizuochi, 2000). As expected, captopril treatment significantly reduced the mean arterial pressure in both Ino80 KO and control mice by around 20 mmHg. L-NAME (N^G-nitro-L-arginine methyl ester), a potent nitric oxide synthase inhibitor, reduces the bioavailability of nitric oxide, decreases the vasorelaxant activity and enhances contraction of the vascular tree thereby leading to an increase in blood pressure (Ignarro, 2002; Pechanova et al., 2020; Yadav et al., 2019). L-NAME treatment failed to increase blood pressure in the Ino80 KO mice in contrast to the control mice where the mean arterial pressure significant increased by 10 mmHg (figure 16 D). Finally, the average pulse pressure was significantly reduced by around 50 % in Ino80 KO mice in comparison with control mice under all three conditions (figure 16 E).

These experiments demonstrate that the basal blood pressure of Ino80 KO mice is disturbed, displaying a narrow average pulse pressure with intermittent widened pulse pressure. These might be explained by the decrease in smooth muscle contractility. Moreover, these findings also highlight the inability of smooth muscle cells to increase contractility upon stimulus (L-NAME treatment). Together, these findings confirm the decreased smooth muscle cell contractility in Ino80 KO mice *in vivo* accordingly with the wire myography results (figure 15).

3.3 Transcriptional regulation of identified INO80 associated genes in vascular smooth muscle cells

Several inter-species studies described that INO80 promotes transcriptional regulation of genes induced by different signaling pathways (Cao et al., 2015; Mizuguchi et al., 2004; Neuman et al., 2014; van Attikum et al., 2004; Yao et al., 2016). To examine the function of INO80 on global transcriptional regulation of VSMCs, gene expression analysis from control versus Ino80 KO aortas were performed.

A

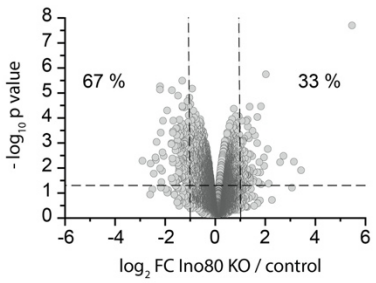

B

fold change	p value	gene	gene name
2.16	0.0514	Des	Desmin
1.08	0.6380	Cnn2	Calponin 2
1.01	0.8480	Acta2	Actin Alpha 2
0.97	0.4900	Tagln	Transgelin
0.95	0.4810	Cnn1	Calponin 1
0.89	0.2790	Cald1	Caldesmon 1
0.43	0.0004	Cnn3	Calponin 3
0.40	0.0230	Myocd	Myocardin
0.39	0.0004	Actg2	Actin gamma 2

Figure 17 INO80 regulates transcription of genes through both transcriptional activation and repression in aorta.

A Volcano plot depicting log_2 FC (fold change) of the RNA expression versus -log_{10} p value calculated using a modified t- test. This data was obtained from gene expression analysis using affymetrix microarray analysis of $Ino80^{lox/lox}SM22Cre^{neg}$ (control) and $Ino80^{lox/lox}SM22Cre^{pos}$ (Ino80 KO) murine aortas. n = 3/3 animals. **B** Table shows the fold change of smooth muscle specific gene expression from microarray based transcriptional analysis of $Ino80^{lox/lox}SM22Cre^{neg}$ (control) and $Ino80^{lox/lox}SM22Cre^{pos}$ (Ino80 KO). n=3/3 animals. p values (calculated using a modified t-test) for each fold change are described. FC (fold change), Ino80 (inositol requiring 80).

The volcano plot depicting the log_2 FC of the RNA expression of Ino80 KO/control versus -log_{10} p value revealed that the expression of the majority of the genes remained unchanged with a strong accumulation of genes between -1 and 1 log_2 FC. On other hand, the volcano plot also showed that 293 genes with a log_2 FC lower than -1 or higher than 1 were significantly deregulated upon loss of Ino80 in vascular smooth muscle cells. Interestingly, 67% of these genes were significantly downregulated, whilst 33% were significantly upregulated (figure 17 A). Evaluation of all significantly deregulated genes upon loss of Ino80 (without taking into consideration the log_2 FC) revealed that 5518 were significantly deregulated upon

loss of Ino80 in vascular smooth muscle cells. Of these genes, 55% were significantly downregulated and 45% were significantly upregulated. Several smooth muscle specific genes were also found to be deregulated upon loss of Ino80: desmin, calponin 3, myocardin and actin gamma2 (figure 17 B). However, only calponin 3, myocardin and actin gamma 2 were significantly downregulated in the Ino80 KO aortas in contrast to control. Calponin 2, actin alpha 2, transgelin, calponin 1 and caldesmon 1 remained unchanged (figure 17 B).
Together, these findings are in accordance with previous inter-species and inter-organ reports that Ino80 promotes transcriptional regulation of genes through both transcriptional activation and repression in vascular smooth muscle cells (Cao et al., 2015; Mizuguchi et al., 2004; Neuman et al., 2014; van Attikum et al., 2004; Yao et al., 2016). The downregulation of smooth muscle contractile genes observed upon loss of Ino80 might be responsible for the reduced contractility observed in figures 15 and 16. The question remains whether these observed transcriptional changes are primary targets of Ino80 or are due to secondary changes?

Ino80 promotes transcriptional regulation of genes through both transcriptional activation and repression in vascular smooth muscle cells (figure 17). To establish which genes are direct targets of Ino80 transcriptional regulation, a Cut and Run (CnR) experiment was performed on wildtype primary aortic smooth muscle cells using an INO80 antibody to identify binding targets of INO80. Furthermore, a motif analysis enrichment was also done to identify potential co-factors of INO80

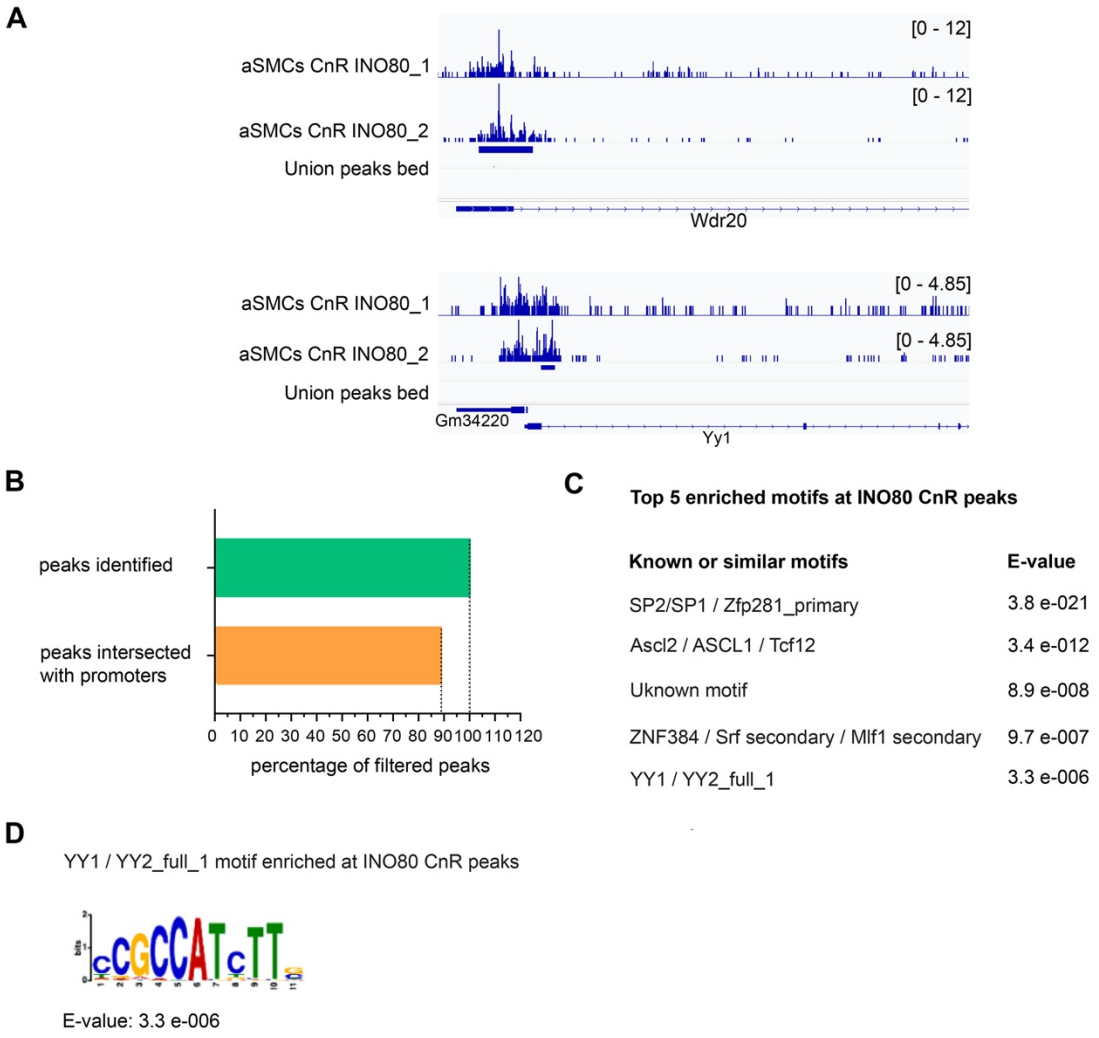

Figure 18. CnR reveals that INO80 mainly targets promoter regions of aortic smooth muscle cells and that these show an enrichment of YY1 motif, an interaction partner of INO80.

A Integrative genomics browser (IGV) snapshots depicting a part of the Wdr20 and Yy1 encoding genes from INO80 CnR of wildtype primary aortic smooth muscle cells (aSMCs) using an INO80 antibody. The upper IGV snapshot illustrates detection of a CnR INO80 peak at the Wdr20 promoter region, meanwhile the bottom IGV snapshot illustrates detection of a CnR INO80 peak at the Yy1 promoter region. n=2/2. Union peaks bed: called peaks between both samples. **B** Percentage of filtered peaks from the INO80 CnR which were identified and which were specifically intersected with promoter regions (TSS +- 5000 nt). INO80 CnR was performed using wildtype primary aortic smooth muscle cells and an INO80 antibody. n=2/2 **C** Top 5 significantly enriched motifs from motif-based analysis of INO80 CnR peaks. MEME-ChIP was applied on all peaks (center +- 250 nt) obtained from the INO80 CnR of wildtype primary aortic smooth muscle cells using an INO80 antibody. **D** YY1/YY2 full sequence motif. MEME ChIP based motif analysis showed that YY1/YY2 full sequence motif was significantly enriched at INO80 CnR peaks. INO80 CnR was performed using wildtype primary aortic smooth muscle cells and an INO80 antibody. n=2/2. aSMCs (aortic smooth muscle cells), CnR (cut and run), INO80 (inositol requiring 80), SP2/SP1 (specificity protein 1 / 2), Zfp281 (zinc finger protein 281), Ascl1 (achaete-scute family BHLH transcription factor 1), Ascl2 (achaete-scute family BHLH transcription factor 2), Tcf2 (transcription factor-2), ZNF384 (zinc finger protein 384), Srf (serum response factor), Mlf1 (myeloid leukemia factor 1), YY1 / YY2 (yin yang 1 / 2).

INO80 CnR on primary aortic smooth muscle cells revealed that the 89% of the INO80 peaks intersected with promoter regions (figure 18 B) as nicely illustrated by the two examples Wdr20 and Yy1, where the peaks were called at the promoter region of both genes respectively (figure 18 A). The INO80 peak at the Yy1 promoter overlaps with the promoter of Gm34220, nonetheless the peak is only called at the Yy1 promoter (figure 18 A). Previous studies described Yy1 to be an important co-factor of Ino80 transcriptional regulation (Yong Cai et al., 2007; Vella et al., 2012). Accordingly, motif enrichment analysis at INO80 CnR peaks revealed YY1 as one of the top 5 enriched motifs (figure 16 C). The motif analysis at INO80 CnR peaks was performed by Carsten Kuenne, Max-Planck Institute for Heart and Lung Research. Interestingly, a part of the top enriched motif at INO80 CnR peaks: SP1/SP2/Zfp281 "**CCGCC**" overlaps with the YY1 motif "**CCGCC**ATCTT". This could indicate, that this motif might only be a part of the YY1 motif and not necessarily an enrichment of a distinctive motif for SP1/SP2/Zfp281 (figure 18 C and D).
Together these findings show that INO80 primarily binds to promoters of genes and that these display an enrichment of the YY1 motif, a known INO80 co-factor for transcriptional regulation. This suggest that INO80 might be recruited to target sites through YY1 as previously reported (Y. Cai et al., 2007).

To determine whether INO80 binding correlates with transcriptional regulation, INO80 CnR data (figure 18) was combined to the microarray data (figure 17) to reveal which genes were direct targets of Ino80 transcriptional regulation. Furthermore, to evaluate the contribution of YY1 in transcriptional regulation by INO80, the next analysis also included the presence of a YY1 motif at the INO80 CnR peak for genes which were significantly regulated.

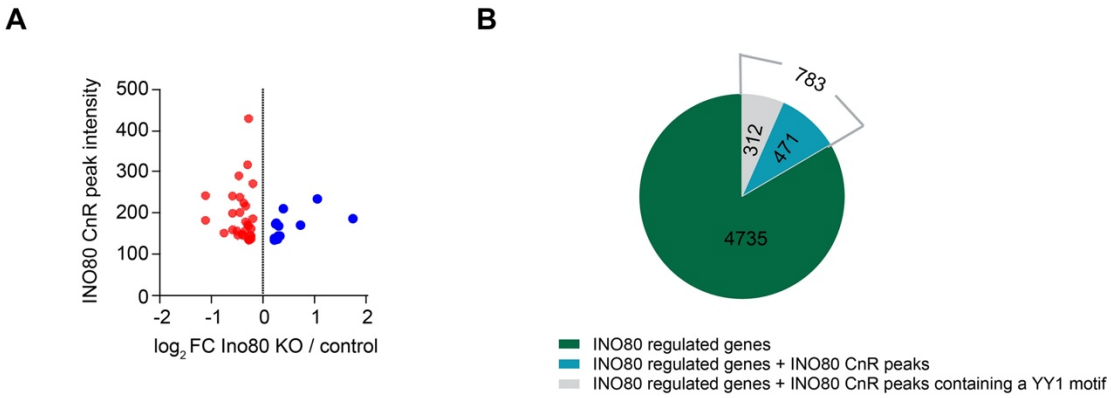

Figure 19. YY1 is an important co-factor of INO80 transcriptional regulation in vascular smooth muscle cells.

A Log_2 FC (fold change) of the RNA expression versus INO80 CnR peak intensity of the top 200 INO80 CnR peaks which were significantly regulated in the RNA microarray data set. FC results were obtained from gene expression analysis using microarray analysis of RNA from $Ino80^{lox/lox}SM22Cre^{neg}$ (control) and $Ino80^{lox/lox}SM22Cre^{pos}$ (Ino80 KO) murine aortas. n=3/3 animals. INO80 CnR was performed using wildtype primary aortic smooth muscle cells and an INO80 antibody. n=2/2. **B** Pie chart depicting the number of INO80 significantly regulated genes (from gene expression analysis using microarray analysis of $Ino80^{lox/lox}SM22Cre^{neg}$ (control) and $Ino80l^{ox/lox}SM22Cre^{pos}$ (Ino80 KO) murine aortas, the number of INO80 significantly regulated genes which contained an INO80 CnR peak at their promoter regions, the number of genes which were significantly regulated by INO80, contained both an INO80 CnR peak and a YY1 motif at the promoter region, and finally the number of genes which were significantly regulated by INO80 but contained neither an INO80 CnR peak nor a YY1 motif at their promoter region. FC (fold change), CnR (Cut and Run), INO80 (inositol requiring 80), YY1 (Yin Yang 1).

The majority of the top 200 INO80 associated genes, per say genes which were shown to be binding targets of INO80 (INO80CnR) and were found to be significantly regulated upon loss of Ino80 (microarray analysis), were downregulated upon loss of Ino80. Moreover, higher peak intensities of the top 200 INO80 CnR peaks were only downregulated upon loss of INO80, implying that INO80 binds stronger to its targets of transcriptional activation (figure 19 A). Together, these two points suggest that the direct function of INO80 is predominantly transcriptional activation (figure 19 A).

Ino80 KO in smooth muscle cells, led to a significant change in transcriptional regulation of 5518 genes. From these 5518 genes, 783 genes displayed an INO80 CnR peak. Finally, 312 genes out of the 783 genes (40%) which were transcriptionally regulated by INO80 and contained an INO80 CnR, comprised a YY1 motif at the INO80 peak CnR (figure 19 B). Conversely, the majority of INO80 significantly regulated genes were not binding targets of INO80, and might therefore only be indirectly regulated by INO80. The motif analysis at INO80 CnR peaks was performed by Carsten Kuenne, Max-Planck Institute for Heart and Lung Research

These findings suggest that YY1 binds to defined sequence motives in the DNA and thereby might, together with INO80, regulate transcriptional activity. Thus, YY1 is an important co-factor of INO80 transcriptional regulation.

3.4 INO80 controls vascular smooth muscle cell contractility through transcriptional regulation of myocardin

Loss of Ino80 in smooth muscle cells led to several contractility related phenotypical and morphological changes: narrow average pulse pressure, inability to acutely increase blood pressure, increased arterial luminal area and decreased contractility (figures 14-16). Loss of Ino80 also led to significant downregulation of several smooth muscle specific genes including myocardin, calponin 3, and actin gamma 2 (figure 17 B). Several reports demonstrate that myocardin is essential to the maintenance of a contractile VSMCs phenotype (Chen et al., 2002; Huang et al., 2015; Long et al., 2009; Nanda & Miano, 2012; Zhou & Herring, 2005). To examine the involvement of myocardin in the decreased contractility phenotype observed upon loss of Ino80, different experiments were performed. First, downregulation of myocardin upon loss of Ino80 was examined by means of western blot and ATAC seq. To discern whether myocardin was a binding target of INO80 transcriptional activation, INO80 CnR was analysed at the myocardin promoter. Since YY1 was found to be an important co-factor of transcriptional regulation in VSMCs (figure 18 C and figure 19 B), presence of a YY1 motif at the myocardin promoter was also examined. Finally, to evaluate the impact of YY1 on myocardin transcriptional regulation, yy1 was downregulated in primary aortic smooth muscle cells and expression of myocardin was measured in comparison to control.

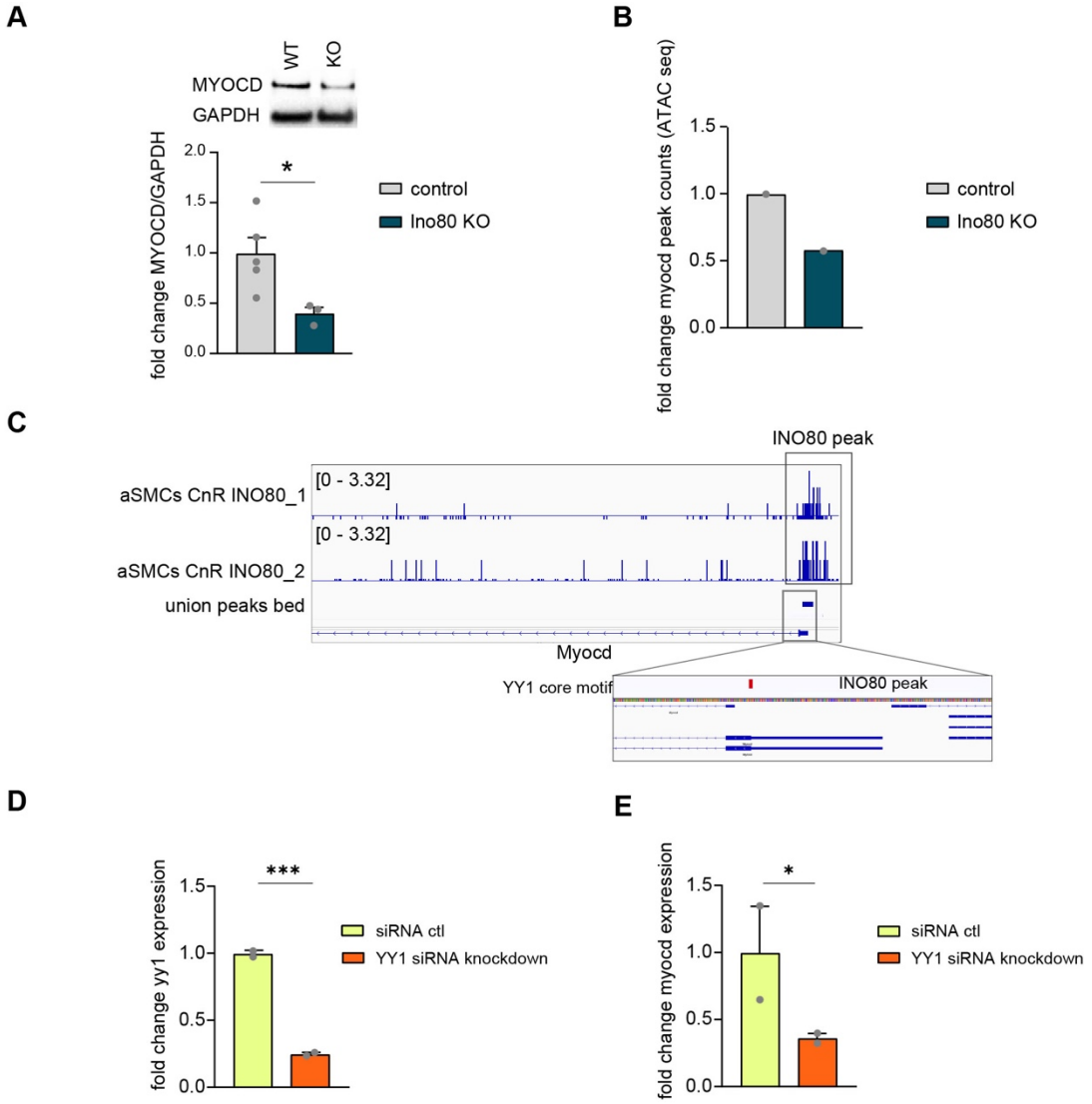

Figure 20. INO80 and YY1 transcriptionally regulate expression of myocardin and can directly bind the myocardin promoter.

A Western blot analysis of protein lysates from Ino80$^{lox/lox}$SM22Cre^{neg} (control), and Ino80$^{lox/lox}$SM22Cre^{pos} (Ino80 KO) using MYOCD (105 kDa) and GAPDH (37 kDa) antibodies. GAPDH served as a loading control and for normalization. n=4/4 control, n=3/3 Ino80 KO. **B** Fold change in myocardin (Myocd) peak counts using ATAC seq analysis from DNA preparations of Ino80$^{lox/lox}$SM22Cre^{neg} (control) and Ino80$^{lox/lox}$SM22Cre^{pos} (Ino80 KO) primary aortic smooth muscle cells. n=1/1. **C** CnR experiment was performed using wildtype primary aortic smooth muscle cells and an INO80 antibody. The upper integrative genomics browser (IGV) snapshot illustrates detection of a CnR INO80 peak at the myocardin (Myocd) promoter (highlighted through a black box). Furthermore, the "Find motif" analysis tool from IGV, revealed the presence of a YY1 core motif at the Myocd promoter, 92 bps away from the INO80 CnR peak, as illustrated by the bottom IGV snapshot. n=2/2. **D-E**. Statistical analysis of fold change in Yy1 expression (D) and Myocd (E) obtained from RNA sequencing reads of Yy1 siRNA versus siRNA control (negative control) transfected primary aortic smooth muscle cells. n=2/2. Myocd (myocardin), gapdh (glyceraldehyde-3-phosphate dehydrogenase), CnR (Cut and Run), INO80 (inositol requiring 80), YY1 (Yin Yang 1), IGV (integrative genomics viewer).

Downregulation of myocardin upon loss of Ino80 was confirmed by means of western blot analysis from control and Ino80 KO aortas as well as ATAC seq from primary aortic smooth muscle cells of Ino80 KO and control mice (figure 20 A and B). This is in correlation with the microarray results where myocardin was reduced by 50% upon loss of Ino80 (figure 17 B). INO80 Cut and Run experiments from wildtype primary aortic smooth muscle cells revealed the presence of an INO80 peak and the myocardin promoter. Furthermore, motif enrichment analysis revealed the presence of a YY1 core motif (figure 18 D) at the promoter of myocardin (its position is highlighted in red). The distance between the end of the INO80 Cut and Run peak and the beginning of the YY1 core motif was of 92 base pairs (figure 20 C). siRNA mediated YY1 downregulation in wildtype primary aortic smooth muscle cells was validated by RNA seq (figure 20 D). RNA seq transcriptomic analysis of YY1 siRNA treated versus control siRNA treated wildtype primary aortic smooth muscle cells showed that myocardin was significantly downregulated upon YY1 downregulation in comparison with the control.
Together these results indicate that YY1 might be binding to the myocardin promoter where it recruits INO80 and together INO80 and YY1 regulate transcriptional activation of myocardin.

Myocardin is a co-activator of serum response factor (SRF)-dependent gene expression in smooth muscle cells and cardiac muscle by binding of CArG box at gene promoters (Wang et al., 2001). The majority of contractile VSMCs gene markers contain a CArG box and can thus be transcriptionally regulated by the myocardin-SRF complex (Miano, 2002; Wang et al., 2001). Myocardin is transcriptionally regulated by INO80 and YY1 (figure 20) and loss of Ino80 causes downregulation of arterial contractility (results part 3.2). To evaluate the function of this potent transcriptional coactivator in the regulation of other contractile vascular smooth muscle cell genes and therefore on contractility, myocardin was overexpressed *in vitro* in pulmonary arterial smooth muscle cells (PASMCs) of control and Ino80 mice.
For this purpose, the smooth muscle specific isoform of myocardin (MYOCD_v3) was cloned into a vector containing a cytomegalovirus CMV promoter, kanamycin resistance for selection in bacteria and cell culture as well as an internal ribosomal entry site (IRES) driven green fluorescent protein (eGFP) cassette to monitor cellular transfection efficiency (appendix figure 36) (Imamura et al., 2010). The control plasmid

was lacking the myocardin insertion. Quantitative RT-qPCRs using specific taqman probes for three different contractile genes were performed in the presence and absence of myocardin overexpression in Ino80 KO and control PASMCs.

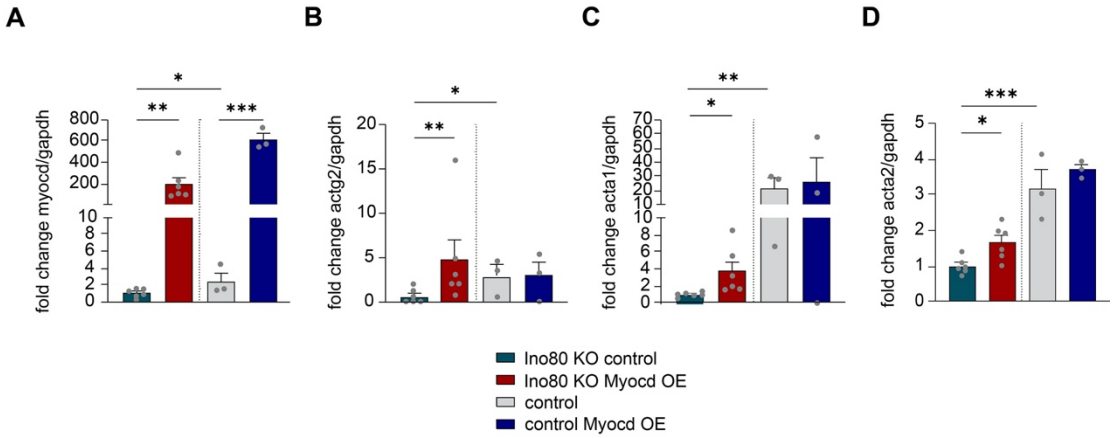

Figure 21. Overexpression of myocardin *in vitro* rescues the expression of contractile genes upon loss of INO80.

A-D RT-qPCR of Ino80$^{lox/lox}$SM22Cre^{neg} (control) and Ino80$^{lox/lox}$SM22Cre^{pos} (Ino80 KO) pulmonary arterial smooth muscle cells transfected with the myocardin overexpression (myocd OE) vector or with a control plasmid were performed using taqman probes for myocd (A), actg2 (B), acta1 (C) and acta2 (D). Expression of each gene was normalized to gapdh as an internal control. n=6/6 Ino80 KO, n=3/3 control. For statistical analysis of myocd fold change expression between Ino80 KO control and control cells, a one-tailed unpaired student's t-test was used. For statistical analysis of myocd and actg2 fold change expression between Ino80 KO control and Ino80 KO Myocd OE cells, a Mann-Whitney test was used. Myocd (myocardin), actg2 (actin gamma 2), acta1 (actin alpha 1), acta2 (actin alpha 2), gapdh (glyceraldehyde-3-phosphate dehydrogenase), OE (overexpression).

The RT-qPCR results corroborate significant downregulation of myocardin expression in Ino80 KO in contrast to control (figure 21 A) as demonstrated by the microarray data (figure 17), western blot analysis and ATAC seq data (figure 20 A-B). Furthermore, it also confirms successful overexpression of myocardin in both control Myocd OE and Ino80 KO Myocd OE cells in comparison to control transfected cells (figure 21 A). Actg2, acta1 and acta2 were all found to be significantly downregulated in Ino80 KO control in comparison to control transfected PASMCs (figure 21 A-D). Myocardin overexpression led to an upregulation of actg2 (figure 21 B), acta1 (figure 21 C) and acta2 (figure 21 D) in Ino80 KO Myocd OE PASMCs in comparison with Ino80 KO control. The expression of actg2 (figure 21 B), acta1 (figure 21 C) and acta2 (figure 21 D) were unchanged upon myocardin overexpression in control Myocd OE PASMCs in comparison to control. These results strongly support the claim that reduced myocardin expression upon loss of Ino80 in VSMCs is the cause for the reduced

expression of several other smooth muscle specific genes, namely actg2, acta1, acta2.

Taken together, this data show that loss of Ino80 leads to the downregulation of myocardin, a key contractile gene that can rescue the expression of other downregulated contractile genes (acta2, actg2, acta1) and which are together essential to vascular contractility. Downregulation of important contractile genes triggers arterial morphological changes, an important decrease in arterial contractility and thereby can lead to dysfunctional blood pressure levels. Upon loss of INO80 or downregulation of YY1, transcriptional activation of myocardin by the complex doesn't take place leading to downregulation of myocardin expression (figure 19) and to a decrease in arterial contractility and disturbances in blood pressure regulation (figures 15 and 16). Mechanistically, YY1 might recruit INO80 to the myocardin promoter where they together regulate transcriptional activation of myocardin (figure 19).

3.5 INO80 regulates vascular smooth muscle cell metabolism through DNA repair

In addition to the analysis of microarray data for Ino80 KO and control aortas, and evaluation of smooth muscle related genes (parts 3.2 and 3.3), we were interested in identifying pathways and processes which are associated with the function of Ino80 in smooth muscle cells. Whitin this context, the transcriptomics data was further analyzed using the Gene Set Enrichment Analysis (GSEA) software to evaluate significant differences in specific gene sets (Subramanian et al., 2005); (Mootha et al., 2003).

A

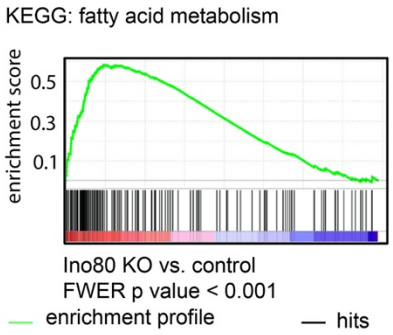

B

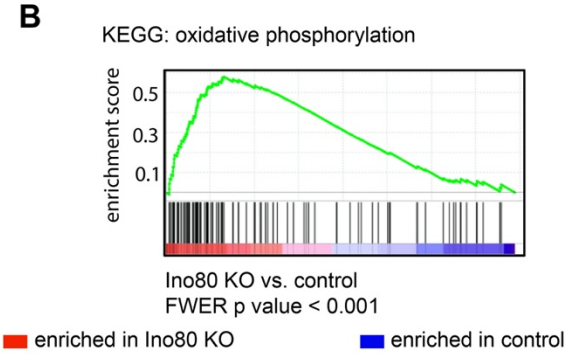

C

Cellular components: top 10 enriched gene sets in Ino80 KO

gene set	NES	FWER p-value
Mitochondrial membrane part	2.73	< 0.001
Microbody	2.63	< 0.001
Organelle inner membrane	2.58	< 0.001
Microbody part	2.58	< 0.001
Oxidoreductase complex	2.56	< 0.001
Respirasome	2.55	< 0.001
Inner mitochondrial membrane protein complex	2.53	< 0.001
Mitochondrial matrix	2.51	< 0.001
Microbody membrane	2.49	< 0.001
Mitochondrial protein complex	2.45	< 0.001

D

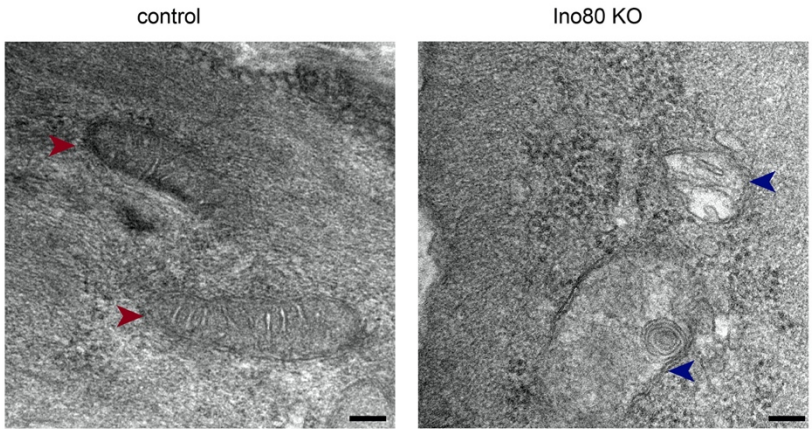

Figure 22. Loss of INO80 in vascular smooth muscle cells induces expression of fatty metabolism and oxidative phosphorylation related genes and disrupts mitochondrial structure.

A-B Enrichment plots from GSEA of microarray based transcriptional analysis of Ino80$^{lox/lox}$ SM22Cre^{neg} (control) and Ino80$^{lox/lox}$ SM22Cre^{pos} (Ino80 KO) murine aortas. A Fatty acid metabolism pathway. B oxidative phosphorylation pathway. n=3/3 animals. **C** Table depicts the top 10 cellular components enriched gene sets in Ino80 KO in contrast to control from GSEA of microarray based transcriptional analysis of Ino80$^{lox/lox}$ SM22Cre^{neg} (control) and Ino80$^{lox/lox}$ SM22Cre^{pos} (Ino80 KO) murine aortas. n=3/3 animals **D** Representative ultrastructural images of mitochondrial structure histological examination from Ino80$^{lox/lox}$ SM22Cre^{neg} (control) and Ino80$^{lox/lox}$ SM22Cre^{pos} (Ino80 KO) murine carotids obtained by electron microscopy. n=3/3 Ino80 KO and n=2/2 control carotids were examined. Scale bar 100 nm. Red arrows point to normal morphological structure of mitochondria. Blue arrows point to non-physiological mitochondria. KEGG (Kyoto Encyclopedia of Genes and Genomes), GSEA (Gene set enrichment analysis), NES (normalized enrichment score), FWER (family-wise error rate).

Gene set enrichment analysis of microarray data for Ino80 KO and control aortas revealed a significant enrichment in fatty acid metabolism (figure 22 A) and oxidative phosphorylation (figure 22 B) upon loss of Ino80 in comparison with control. Furthermore, this analysis unveiled significant upregulation of mitochondrial structure and mitochondrial respiration related gene sets in the Ino80 KO aortas in contrast to the control (figure 22 C). Inspection of the ultrastructure of smooth muscle mitochondria from control smooth muscle cells of carotid arteries exhibited normal morphological features: a double membrane system consisting of an inner membrane (containing invaginated cristae) and of an outer mitochondrial membrane separated by an intermembrane space (red arrows). In contrast to this, mitochondria from Ino80 KO smooth muscle carotids displayed alterations in the mitochondrial area with vesicular, swollen mitochondria displaying unorganized cristae in the inner membrane and formation of mitochondrial spheroids (blue arrows) (figure 22 D).
Thus, deletion of INO80 in vascular smooth muscle cells leads to a switch in metabolism by inducing the expression of fatty metabolism and oxidative phosphorylation related genes. Moreover, loss of Ino80 dramatically disrupts mitochondrial structure which might explain the enrichments in mitochondrial structure and mitochondrial respiration related gene sets as a mean to rescue the function of the non-physiological mitochondria.

For insight into pathways and specific genes which might be behind the observed metabolic changes upon loss of INO80 in SMCs, the transcriptomics data was further analyzed for transcription factor target enrichment in Ino80 KO in contrast to control.

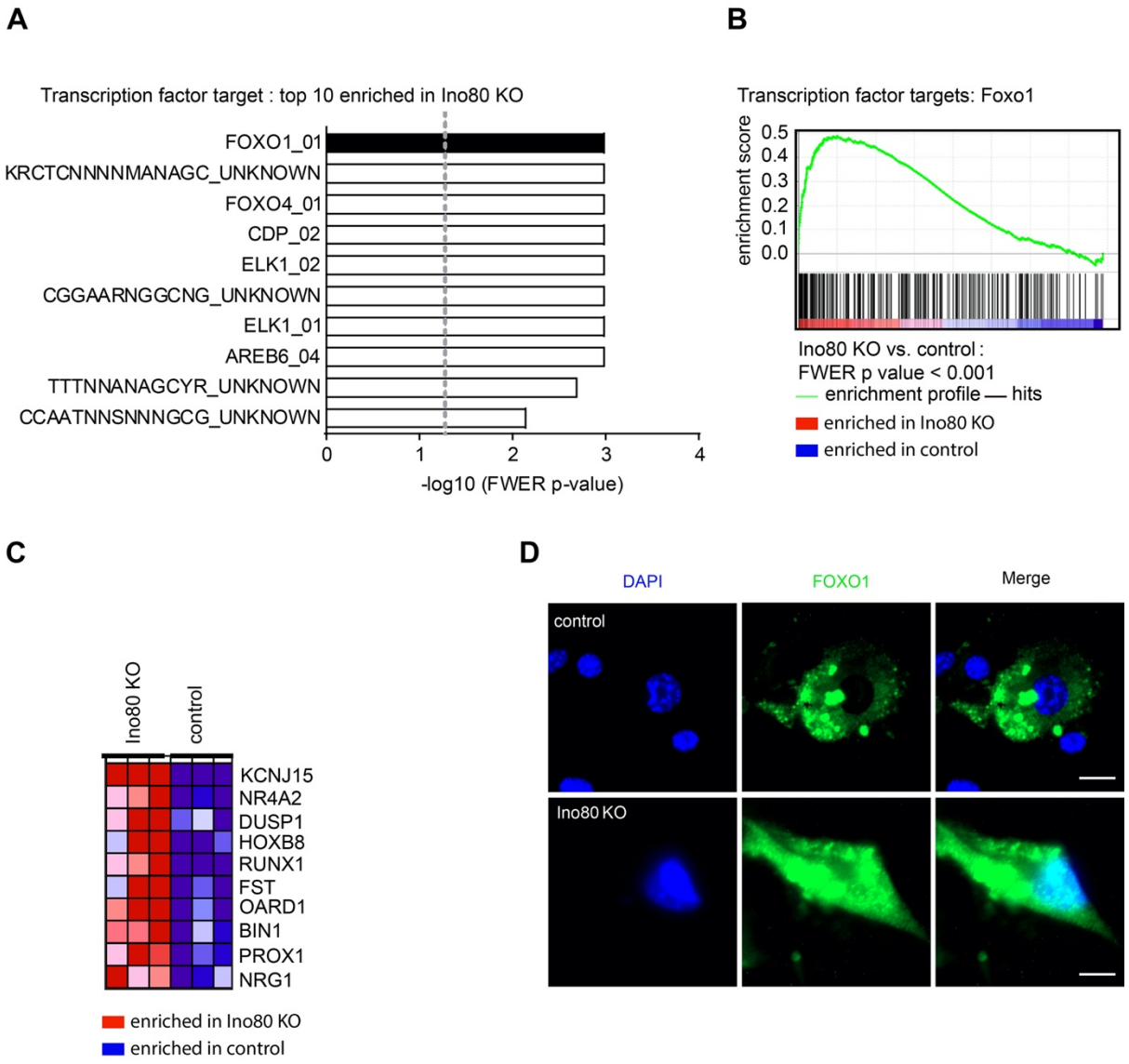

Figure 23. INO80 controls FOXO1 subcellular localization and transcriptional activity in vascular smooth muscle cells.

A Top 10 transcription factor target enriched gene sets in Ino80 KO from GSEA of microarray based transcriptional analysis of Ino80$^{lox/lox}$ SM22Cre^{neg} (control) and Ino80$^{lox/lox}$ SM22Cre^{pos} (Ino80 KO) murine aortas. n=3/3 animals. **B** Enrichment plot of the transcription factor target Foxo1 from GSEA of microarray based transcriptional analysis of Ino80$^{lox/lox}$ SM22Cre^{neg} (control) and Ino80$^{lox/lox}$ SM22Cre^{pos} (Ino80 KO) murine aortas. n=3/3 animals. **C** Heat map of the 10 most upregulated genes of the respective gene set depicted in B. n=3/3 animals. **D** Representative images of pulmonary arterial smooth muscle cells isolated from Ino80$^{lox/lox}$ SM22Cre^{neg} (control) and Ino80$^{lox/lox}$ SM22Cre^{pos} (Ino80 KO) mice stained with DAPI (blue) and anti-FOXO1 antibody (green). Scale bar 10µm. Ino80 (inositol requiring 80), DAPI (4',6-diamidino-2-phenylindole), FOXO1 (forkhead box O1), FOXO4 (forkhead box O4), INO80 (inositol requiring 80), FWER (family-wise error rate), KCNJ15 (potassium inwardly rectifying channel subfamily j member 15), NR4A2 (nuclear receptor 4A2), DUSP1 (dual specificity phosphatase 1), HOXB8 (Homeobox B8), RUNX1 (RUNX family transcption factor 1), FST (follistatin), OARD1 (O-acyl-ADP-ribose deacylase 1), BIN1 (bridging integrator 1), PROX1 (Prospero Homeobox 1), NRG1 (neuregulin 1).

Gene set enrichment analysis of microarrays from Ino80 KO and control aortas revealed an enrichment of transcription factor targets of FOXO1 to be the top significantly enriched pathway in the transcription factor targets gene sets upon loss of Ino80 in comparison with control (figure 23 A-B). The top 10 transcriptional target genes of FOXO1 were strongly enriched in aortas upon loss of Ino80 in SMCs (figure 23 C). Subcellular localization of FOXO1 is essential to transcriptional activation of FOXO1 targets. Staining of FOXO1 in pulmonary arterial smooth muscle cells (PASMCs) revealed that FOXO1 was located in the cytoplasm of control pulmonary arterial smooth muscle cells. Conversely, FOXO1 expression was increased and switched to a nuclear localization upon loss of INO80 in Ino80 KO PASMCs (figure 23 D). Thus, this data shows that loss of Ino80 led to a switch in FOXO1 subcellular localization to the nucleus thereby inducing transcriptional activation of FOXO1 target genes.

Stöhr et al. created a conditional KO allele of Foxo1 in mice using the Cre-loxP system (Bouabe & Okkenhaug, 2013; Stöhr et al., 2013). With this approach, exons 2 and 3 of the Foxo1 gene were flanked by loxP sites which can be excised using tissue specific Cre recombinase expression ($Foxo1^{lox/lox}$). FOXO1 subcellular localization switched to the nucleus upon loss of Ino80 in smooth muscle cells, leading to an increase in the transcription of its targets (figure 23). FOXO1 transcriptionally activates various metabolic diseases whereby it regulates metabolic responses to different environmental cues (Eijkelenboom & Burgering, 2013; Link & Fernandez-Marcos, 2017; Maiese, 2015). To determine whether FOXO1 was responsible for the metabolic changes observed upon loss of Ino80 in SMCs (figure 22), a mouse line with a deletion of Ino80 and Foxo1 specifically in smooth muscle cells was generated by mating $Ino80^{lox/lox}$ $SM22Cre^{pos}$ mice with $Foxo1^{lox/lox}$. Mice carrying both the Ino80 and Foxo1 deletions in smooth muscle cells were viable and born according to expected mendelian ratios.

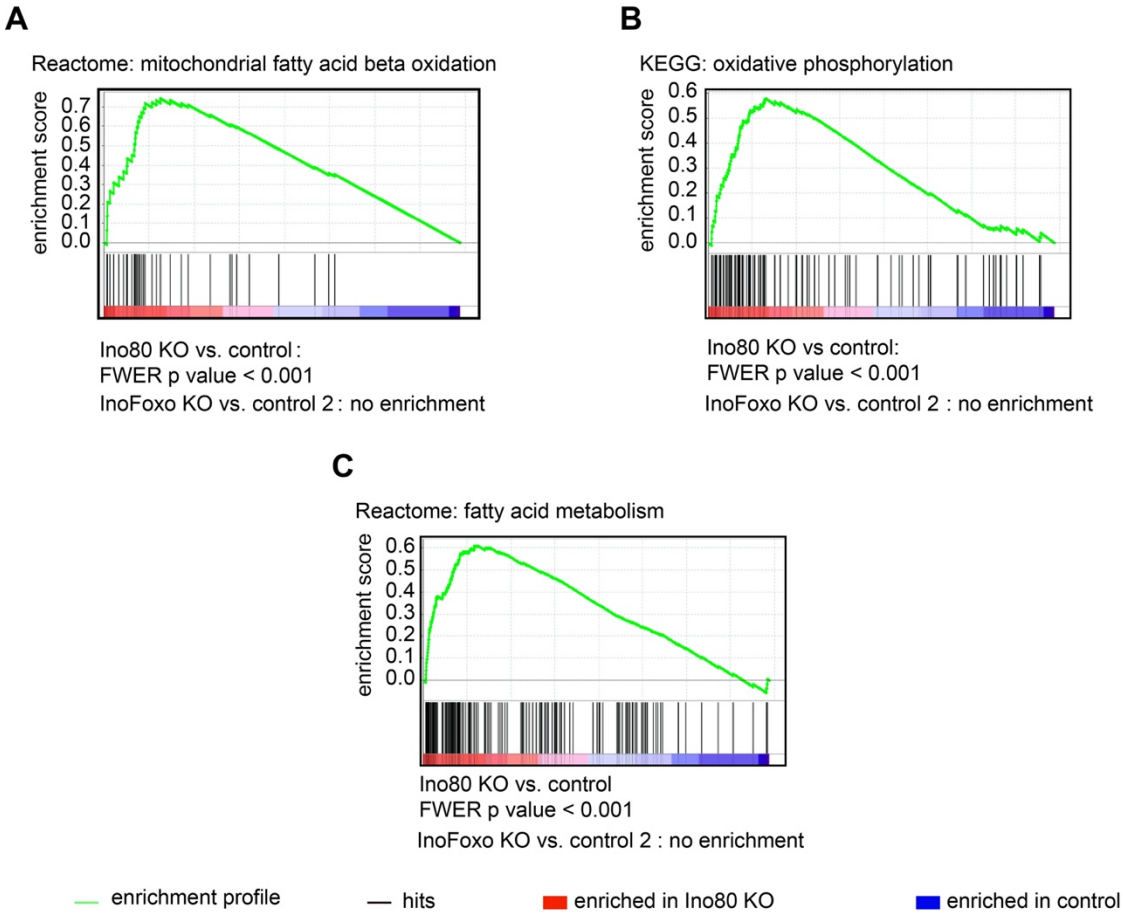

Figure 24. FOXO1 knockout rescues the metabolism phenotype incurred upon loss of INO80.

A-C Enrichment plots from GSEA of RNA seq based transcriptional analysis of $Ino80^{lox/lox}$ $SM22Cre^{neg}$ (control) vs. $Ino80^{lox/lox}$ $SM22Cre^{pos}$ (Ino80 KO) as well as $Ino80^{lox/lox}$ $Foxo1^{lox/lox}$ $SM22Cre^{neg}$ (control 2) vs. $Ino80^{lox/lox}$ $Foxo1^{lox/lox}SM22Cre^{pos}$ (Foxo1 KO) murine aortas. A Mitochondrial fatty acid beta oxidation pathway. B oxidative phosphorylation pathway. C Fatty acid metabolism. n=3/3 animals. Vs. (versus), KEGG (Kyoto Encyclopedia of Genes and Genomes), Ino80 (inositol requiring 80), FWER (family-wise error rate), FOXO1 (forkhead box O1).

Gene set enrichment analysis of additional RNA seq data of control and Ino80 KO murine aortas using reactome and KEGG gene sets confirmed a switch into fatty acid metabolism and an increase in oxidative phosphorylation upon loss of Ino80 (figure 24 A-C) in accordance with the independently obtained microarray data and the respective GSEA (figure 22 A-B). Interestingly, additional deletion of Foxo1 abrogated these enrichments indicating that Foxo1 activity is responsible for the observed metabolic switch (increased fatty acid metabolism and oxidative phosphorylation) upon loss of Ino80 in SMCs.

These results indicate that deletion of Ino80 controls protein abundance and alters subcellular localization/activity of FOXO1. Since foxo1 is not regulated on the

transcriptional level upon loss of Ino80, the question arises how does loss of INO80 activate FOXO1.

Ino80 has previously been demonstrated to have an important role in DNA damage repair (Papamichos-Chronakis et al., 2006; van Attikum et al., 2007). On the other hand, DNA damage has been shown to lead to reactive oxygen species (ROS) production in mammalian cells (Kang et al., 2012; Niocel et al., 2019), and moreover ROS has also been shown to induce FOXO1 activation in mammalian cells *in vivo* (Ragu et al., 2023). Together, these facts suggest a regulatory cascade upon deletion of INO80 starting with a decrease in DNA repair causing DNA damage accumulation and consequently instigating an increase in ROS production, ultimately leading to the translocation of FOXO1 to the nucleus of VSMCs and thereby to a switch in VSMC metabolism activity. Thus, we sought to characterize the function of INO80 in DNA damage repair and to assess whether this regulates FOXO1 activity in VSMCs.

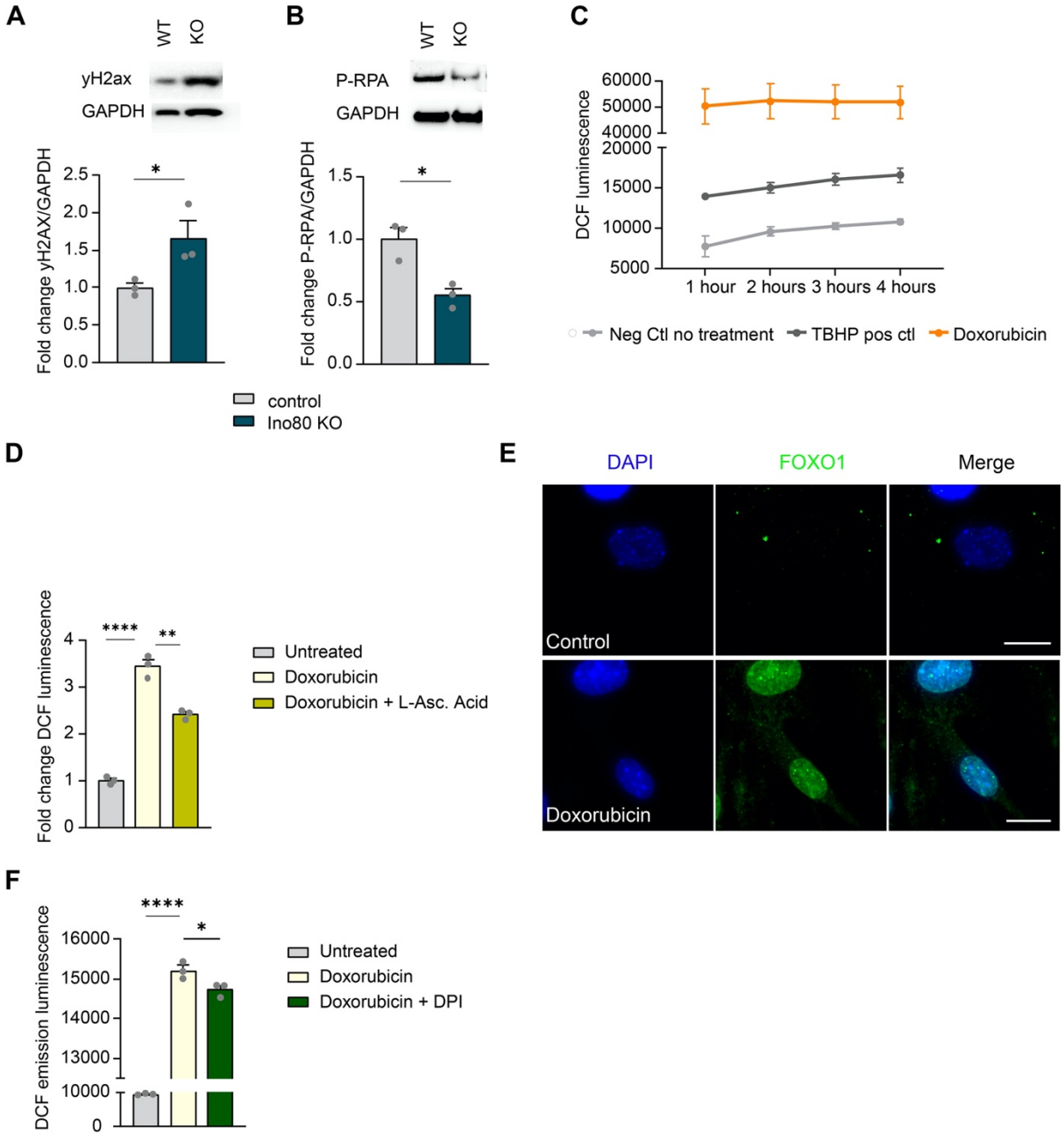

Figure 25. Loss of Ino80 leads to an increase in DNA damage induced ROS and causes FOXO1 nuclear translocation.

A-B Western blot analysis of yH2AX (17 kDa) (A) and P-RPA (32 kDa) (B) from aortic protein lysates of Ino80$^{lox/lox}$ SM22Cre^{neg} (control) and Ino80$^{lox/lox}$ SM22Cre^{pos} (Ino80 KO) mice. GAPDH (37 kDa) served as a loading control and for normalization. n=3/3 animals. **C** Analysis of ROS production in primary wildtype aortic smooth muscle cells under treatment with 8.5 µM doxorubicin and 100 µM TBHP (positive control) treatments. Untreated primary wildtype aortic smooth muscle cells were used as a negative control. Cells were treated with the indicated conditions for four hours in a buffer compatible with the assay. Cellular ROS generations were measured by luminescence using a DCFDA/H2CFDA cellular ROS detection kit. DCF luminescence is representative of ROS generation levels. n=3/3. **D** ROS production analysis of wildtype primary aortic smooth muscle cells treated with 8.5 µM doxorubicin and a mix of 8.5 µM doxorubicin + 15 µM L-ascorbic acid (L-Asc. Acid) for 4 hours. Untreated cells were used as a negative control. Cells were treated with the indicated conditions for four hours in a buffer compatible with the assay. Cellular ROS generation was measured by luminescence using a

DCFDA/H2CFDA cellular ROS detection kit. DCF luminescence is representative of ROS generation levels. n=3/3. **E** Representative images of primary wildtype aortic smooth muscle cells treated with 8.5μM doxorubicin and untreated control. Cells were stained with DAPI (blue) and anti-FOXO1 antibody (green). Scale bar 20 μm. **F** Analysis of ROS production in primary aortic smooth muscle cells treated with 2.125 μM doxorubicin and a mix of 2.125 μM doxorubicin and 200 μM DPI for two hours in an assay compatible buffer. Untreated cells were used as a negative control. Cellular ROS generation was measured by luminescence using a DCFDA/H2CFDA cellular ROS detection kit. DCF luminescence is representative of ROS generation levels. n=3/3. yH2AX (gamma histone 2AX), P-RPA (phospho replication protein A), Ino80 (inositol requiring 80), DAPI (4',6-diamidino-2-phenylindole), FOXO1 (forkhead box O1), GAPDH (glyceraldehyde-3-phosphate dehydrogenase), DCF (dichlorodihydrofluorescein), H2CFDA **(**dichlorodihydrofluorescein diacetate), ROS (reactive oxygen species), TBHP (tert-Butyl hydroperoxide), L-Asc. Acid (L-ascorbic acid), DPI (Diphenyleneiodonium chloride).

Loss of Ino80 in smooth muscle cells resulted in an increase in y-H2AX, a marker of double strand breaks (DSBs), as well as to a decrease in P-RPA protein levels, a marker for DSB resection with an essential function in homologous repair of DSBs, by western blot, in comparison with the control. This demonstrates that deletion of Ino80 causes a decrease in DNA repair, and an accumulation in DNA damage (figure 25 A-B). DCFDA reactive oxygen species assay using primary wildtype aortic smooth muscle cells (aSMCs) shows that treatment with doxorubicin, a topoisomerase II inhibitor-leading to double strand break formation, led to an increase in ROS production (DCF luminescence) in comparison with the untreated control, showing that DNA damage induces ROS production in vascular smooth muscle cells (figure 25 C-D). DCFDA ROS assay using aSMCs treated with doxorubicin in contrast with a mix of doxorubicin and L- ascorbic acid, a ROS scavenger, demonstrates that L-ascorbic acid can significantly reduce doxorubicin induced ROS production as expected, validating the functionality of the assay (figure 25 D). Furthermore, aSMCs treatment with doxorubicin resulted in an increase in FOXO1 expression and to its translocation into the nucleus, showing that DNA damage induced ROS regulates the subcellular localisation of FOXO1 and thereby FOXO1 activity (figure 25 E). Activation of NOX enzymes has been suggested to lead to ROS production upon DNA damage induction (Kang et al., 2012; Niocel et al., 2019). Treatment of aSMCs with DPI, a NOX enzyme inhibitor, can significantly reduce but not totally abrogate doxorubicin induced ROS production (DCF luminescence), suggesting that NOX enzymes play a role in DNA damage induced ROS production (figure 25 F).

These findings demonstrate that loss of Ino80 induces a reduction in DNA repair, an increase in DSB formation, and thus an accumulation in DNA damage. Ino80 has

previously been demonstrated to have an important role in DNA damage repair (Papamichos-Chronakis et al., 2006; van Attikum et al., 2007) and these findings have also validated this in smooth muscle cells of the aortas. Moreover, these results established that DNA damage in aortic smooth muscle cells induces ROS production partially through NOX enzymes activation and leads to nuclear translocation of FOXO1.

To further validate that ROS production is responsible for the observed increase in FOXO1 expression as well as to the switch in FOXO1 subcellular localization, control pulmonary arterial smooth muscle cells were treated with the ROS inducing agent H_20_2 at different concentrations and FOXO1 subcellular localization was analyzed by immunofluorescence.

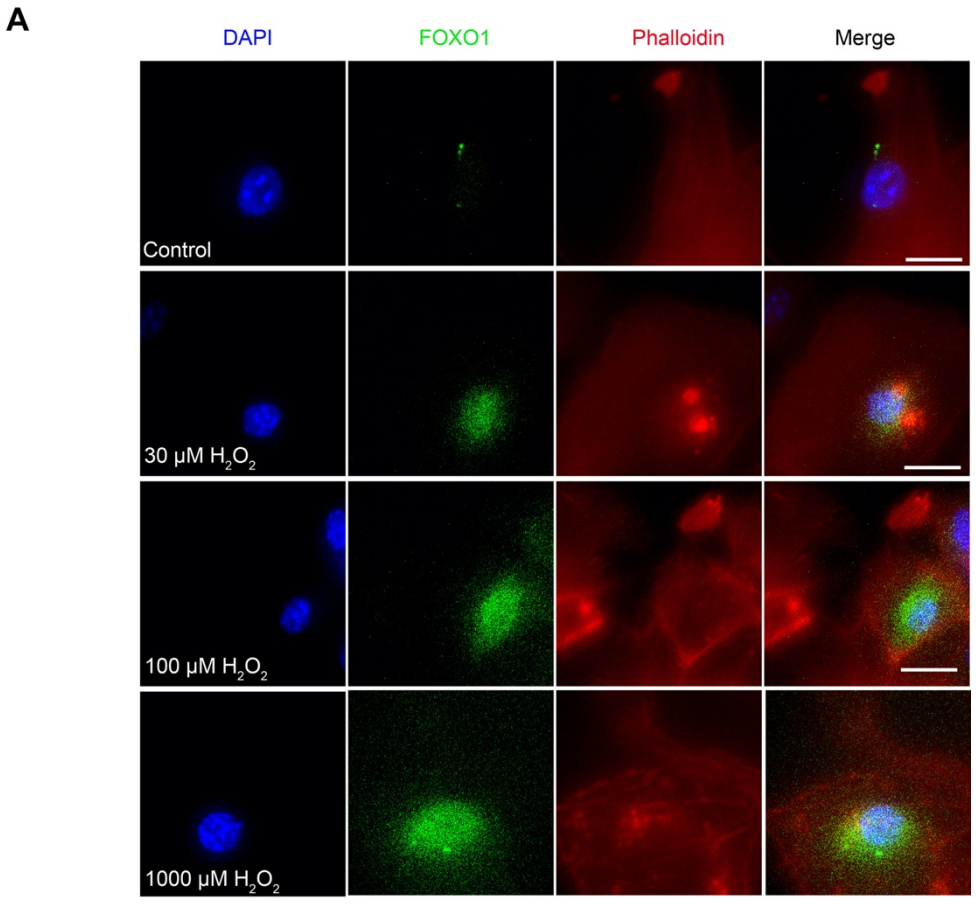

Figure 26. H_2O_2 treatment recapitulates the FOXO1 nuclear subcellular localization switch observed upon loss of INO80 in vascular smooth muscle cells.

Immunofluorescence images of pulmonary arterial smooth muscle cells isolated from $Ino80^{lox/lox}$ $SM22Cre^{neg}$ (control) mice treated with different concentrations of H_20_2: 30 μM, 100 μM and a 1000 μM

respectively for three hours. Untreated control cells were used as negative control. Cells were stained with DAPI (blue), anti-FOXO1 antibody (green) and Phalloidin. Scale bar 20µm. DAPI (4',6-diamidino-2-phenylindole), FOXO1 (forkhead box O1), Ino80 (inositol requiring 80).

Control primary pulmonary arterial smooth muscle cells (PASMCs) treatment with H_2O_2, a ROS inducing agent, led to a switch in the subcellular localisation of FOXO1 to the nucleus as well as to an increase in FOXO1 protein expression in a dose dependent manner in comparison with the untreated control (figure 26). The F-actin microfilaments structure of the cells stained by Phalloidin were unchanged after H_20_2 treatment (figure 26).

This shows that the increase in FOXO1 expression and switch in subcellular localization observed upon loss of Ino80 (figure 23 D) and upon DNA damage induction (figure 25 E) are a consequence of DNA damage-induced ROS production and are not due to other DNA damage effects unrelated to ROS production. The mechanism (s) by which ROS production causes translocation of FOXO1 to the nucleus are however unclear.

In the presence of oxidative stress, c-Jun N-terminal kinases (JNKs) have been reported to phosphorylate FOXO1 and FOXO4 proteins resulting in their translocation from the cytoplasm to the nucleus (Essers et al., 2004; Grabiec et al., 2015). Moreover, FOXO1 dependent DNA damage repair has been reported to be regulated through c-Jun N-terminal kinases (JNKs) (Ju et al., 2014). Therefore, FOXO1 might also be activated by JNKs upon DNA damage induced ROS in smooth muscle cells. To test this, the effects of the loss of INO80 on JNK phosphorylation and expression, as well as the consequences of the loss of FOXO1 and inhibition of the JNK regulated AP1 complex (composed of FOS and JUN) in vascular smooth muscle cells were analyzed.

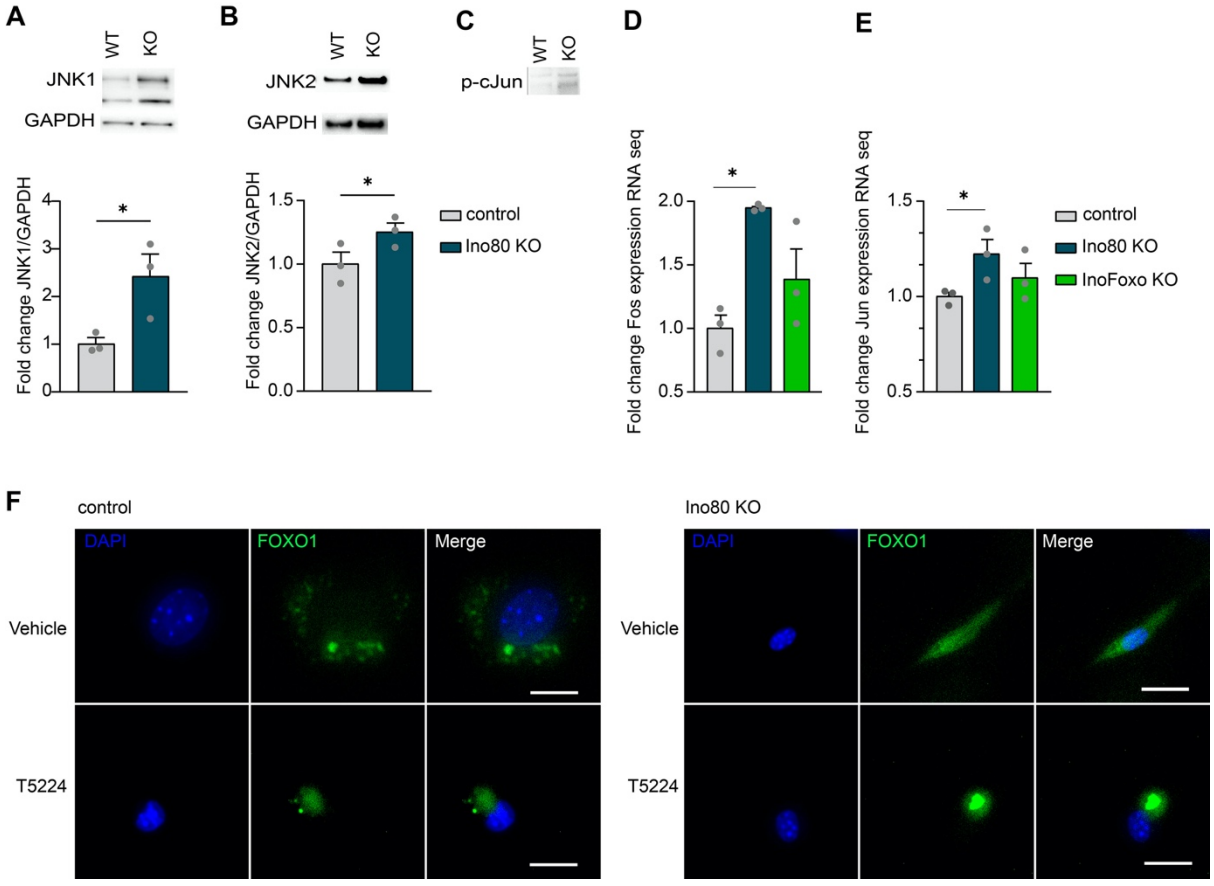

Figure 27. JNK1 and JNK2 are upregulated upon loss of INO80 and can control FOXO1 subcellular localization in vascular smooth muscle cells.

A-C Western blot analysis of JNK1 (47kDa) (A), JNK2 (55 kDa) (B) and p-cJun (48 kDa) (C) in aortic protein lysates of Ino80$^{lox/lox}$ SM22Cre^{neg} (control) and Ino80$^{lox/lox}$ SM22Cre^{pos} (Ino80 KO) mice. GAPDH (37 kDa) served as a loading control and for normalization. A and B n=3/3 animals, C n=1/1 animal. **D-E** Statistical analysis of fold change in Fos (D) and Jun (E) RNA expression levels from Ino80$^{lox/lox}$ SM22Cre^{neg} (control), Ino80$^{lox/lox}$ SM22Cre^{pos} (Ino80 KO) as well Ino80$^{lox/lox}$ Foxo1$^{lox/lox}$ SM22Cre^{pos} (InoFoxo KO) murine aortas. n=3/3 animals. **F** Immunofluorescence images of pulmonary arterial smooth muscle cells isolated from Ino80$^{lox/lox}$ SM22Cre^{neg} (control) and Ino80$^{lox/lox}$ SM22Cre^{pos} (Ino80 KO) mice. Cells were treated with 30 µM T5224 or with vehicle (DMSO) for 24 hours and stained with DAPI (blue) and anti-FOXO1 antibody (green). Scale bar 20 µM. Ino80 (inositol requiring 80), DAPI (4',6-diamidino-2-phenylindole), FOXO1 (forkhead box O1), JNK1 (mapk8: mitogen-activated protein kinase 8), JNK2 (mapk9: mitogen-activated protein kinase 9), p-cJUN (phosphor jun proto-oncogene), Fos (fos proto-oncogene), Jun (jun proto-oncogene), GAPDH (glyceraldehyde-3-phosphate dehydrogenase).

JNK1 and JNK2 protein expression were found to be significantly upregulated upon loss of Ino80 in aorta in comparison with the control by means of western blot analysis (figure 27 A-B). Additionally, phosphorylation of c-Jun (p-cJun) was also found to be upregulated in the Ino80 KO aortas compared to control (figure 27 C). The AP1 complex (composed of Jun and Fos) has been reported to be regulated by and to regulate JNKs (Hess et al., 2004; Karin et al., 1997; Martindale & Holbrook, 2002;

Torres, 2003; Ueda et al., 2002). Fos and Jun were found to be significantly upregulated in the Ino80 KO compared to control (figure 27 D-E). Interestingly, Foxo1 knockout after Ino80 smooth muscle cell knockout could rescue the observed enrichments in Fos and Jun RNA expression, indicating that there is a feedback regulation from FOXO1 expression back to the expression of JNK enzymes possibly through FOXO1 dependent metabolism regulation (figure 27 D-E). Moreover, inhibition of Fos and Jun in Ino80 KO PASMCs by T5224 treatment, an AP1 inhibitor, led to the translocation of FOXO1 from the nucleus to the cytoplasm in contrast with vehicle treated Ino80 KO PASMCs where FOXO1 nuclear localization was unchanged, showing that AP1 activity also regulates FOXO1 subcellular localization and activity (figure 27 F). Treatment of control PASMCs with T5224 had no effect on the subcellular localization of FOXO1 which remained cytoplasmic (figure 27 F). This figure shows that loss of Ino80 leads to upregulation of JNKs which control the expression and activity of the AP1 complex (accordingly with previous reports), and of FOXO1. Furthermore, FOXO1 and AP1 can regulate each other's expression and are therefore part of the genetic regulatory network which is activated upon loss of Ino80.

Taken together, DNA damage accumulation upon loss of INO80 leads to an increase in DNA damage induced ROS production which possibly triggers activation of JNK enzymes through an increase in both expression and phosphorylation (figure 25-27). These findings suggest that activated JNKs induce FOXO1 translocation into the nucleus resulting in a switch of metabolic related genes (figure 22-24 and 27). The AP1 complex composed of FOS and JUN is regulated by the activation of JNKs, and can also regulate and be regulated by FOXO1 through a feedback loop most probably involving JNKs (figure 27 D-F).

3.6 Loss of INO80 accelerates atherosclerotic lesion development

Atherosclerosis is characterized by the deposition and accumulation of lipids between the intimal and medial layers of blood vessels, infiltration of macrophages in the blood vessels as well as migration of VSMCs in the plaque and VSMCs differentiation into foam cells (Chen et al., 2010); (Gistera & Hansson, 2017; Libby et al., 2019). Interventions to treat atherosclerosis such as balloon angioplasty can lead to aggressive post-injury restenosis of the vessel and thus recurrence of the ischemic symptoms (Brown et al., 2018). An essential underlying mechanism of restenosis and atherosclerosis is the switch of VSMCs from a contractile to a synthetic state characterized by enhanced VSMCs proliferation and migration (Bochaton-Piallat et al., 1993; Wallitt et al., 2007). Loss of Ino80 led to a reduction in VSMCs contractility (figure 15), due to the downregulation of myocardin (figures 17 B, figure 20-21) as well as the deregulation of several smooth muscle cell specific markers (figure 17 B). To determine whether Ino80 has a function in VSMCs migration and proliferation, Ino80 KO and control adult mice were subjected to a partial carotid ligation followed by EdU injections. To assess smooth muscle migration and proliferation, the thickness of the alpha smooth muscle actin positive layer and luminal area of the ligated carotids were measured. For proliferation EdU staining followed by enumeration of EdU positive smooth muscle cells were performed (figure 28-29).

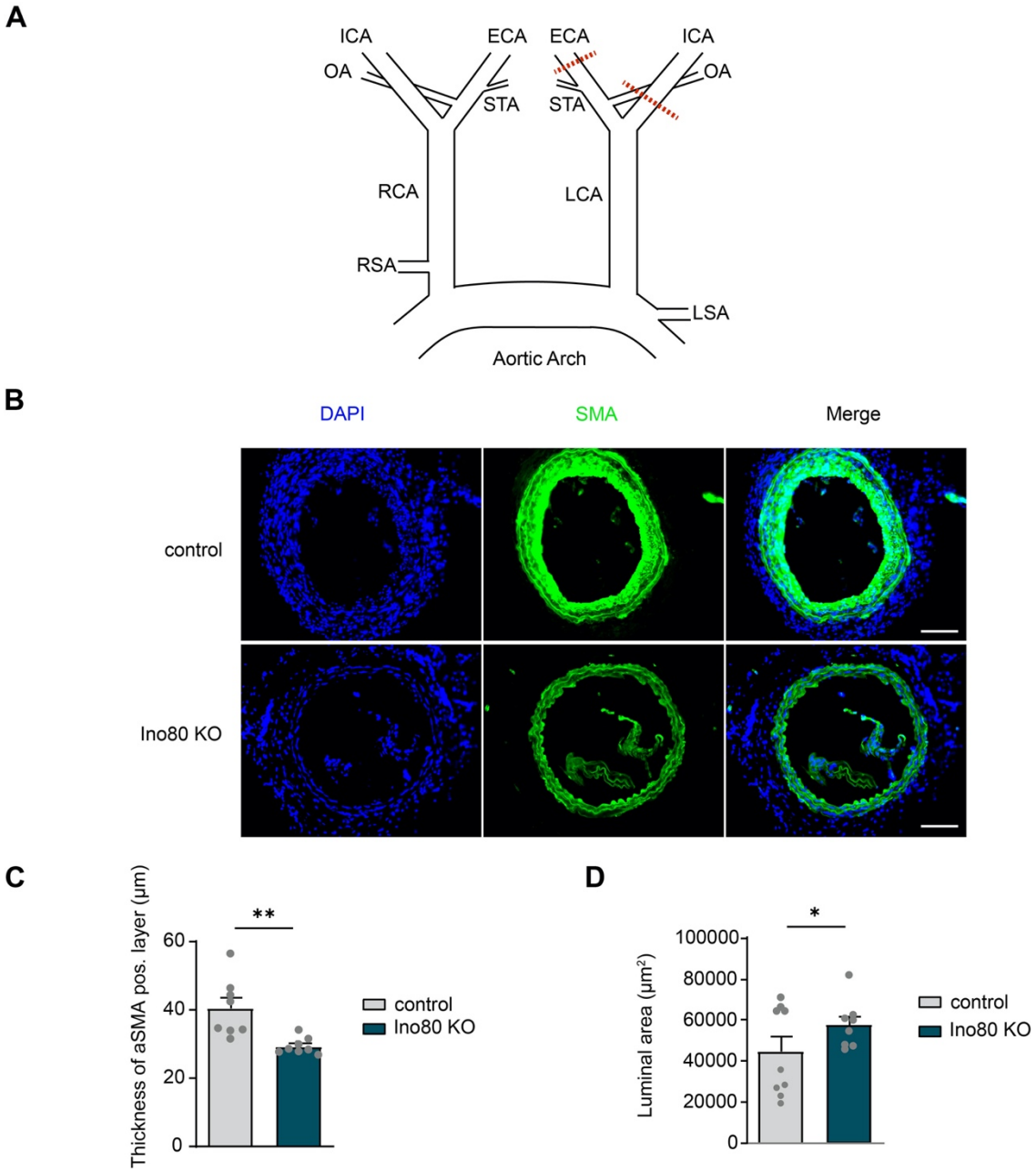

Figure 28. INO80 deletion leads to a decrease in the thickness of SMCs layer and to an increase in the luminal area following partial carotid artery ligation.

A Schematic representation of carotid anatomy and partial carotid ligation. Three branches of the left common carotid artery namely (LCA), namely the external carotid artery (ECA), the internal carotid artery (ICA) and the occipital artery (OA) were ligated in Ino80$^{lox/lox}$ SM22Cre^{neg} (control) and Ino80$^{lox/lox}$ SM22Cre^{pos} (Ino80 KO) mice. **B** Representative images of Ino80$^{lox/lox}$ SM22Cre^{neg} (control) and Ino80$^{lox/lox}$ SM22Cre^{pos} (Ino80 KO) partially ligated carotid arteries post staining with DAPI (blue) and anti-SMA antibody (alpha smooth muscle actin) (green). **C-D** Statistical analysis of the thickness of aSMA (alpha smooth muscle actin) positive layer (C) and of the luminal area (D) in Ino80$^{lox/lox}$ SM22Cre^{neg} (control) and Ino80$^{lox/lox}$ SM22Cre^{pos} (Ino80 KO). n=9/9 control animals and n=8/8 Ino80 KO animals. For statistical analysis of the luminal area between control and Ino80 KO carotids, a one-tailed unpaired student's t-test was used. Ino80 (inositol requiring 80), DAPI (4',6-diamidino-2-phenylindole), SMA (alpha smooth muscle actin), aSMA pos. layer (alpha smooth muscle actin positive layer), RCA (right common carotid artery), RSA (right subclavian artery), LSA (left subclavian artery), LCA (left

common carotid artery namely), ECA (the external carotid artery), ICA (the internal carotid artery), (OA) the occipital artery.

Ino80 KO and control mice were subjected to partial carotid ligations (figure 28 A). The carotid ligations surgeries were performed by Marion Wiesnet, Max-Planck Institute for Heart and Lung Research. To determine whether the thickness of the smooth muscle layer and luminal area of the arteries were affected by Ino80 KO, carotids were stained with SMA and DAPI. Upon carotid ligation, the thickness of alpha smooth muscle actin positive layer was significantly reduced by around 10 µm in the Ino80 KO mice compared to control (figure 28 B-C). Moreover, the luminal area was increased by around 25% in the Ino80 KO ligated carotid arteries compared to control (figure 28 D). Together, loss of Ino80 caused a thinner smooth muscle layer and wider arteries upon *in vivo* partial carotid ligation and suggests that upon loss of Ino80 VSMCs might show decreased migration and proliferation *in vivo*.

To determine the contribution of proliferation in the thinner VSMCs wall and wider lumen upon partial carotid ligation (figure 28), VSMCs cells with an overlapping EdU signal in addition to alpha smooth muscle actin signal (SMA) were considered to be proliferating.

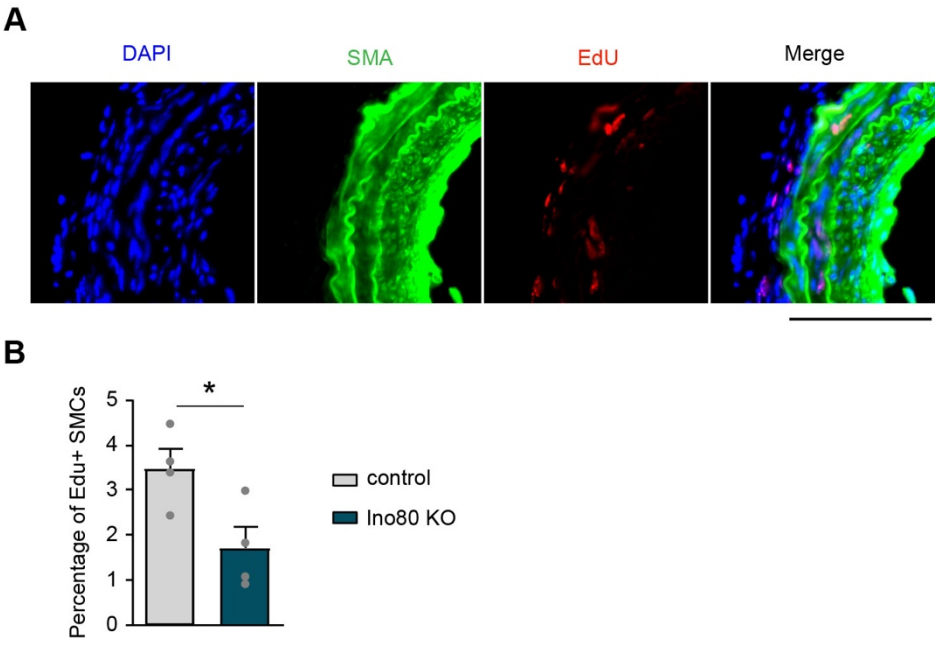

Figure 29. Arteries lacking INO80 display a defect in vascular smooth muscle cell proliferation upon partial carotid artery ligation.

A Immunofluorescence image of Edu stained partially ligated carotid artery from Ino80$^{lox/lox}$ SM22Cre^{neg} (control) mice. Carotid sections were stained with DAPI (blue), anti-SMA antibody (green), and EdU (red). **B** Statistical analysis of the percentage of EdU positive smooth muscle cells in Ino80$^{lox/lox}$ SM22Cre^{neg} (control) and Ino80$^{lox/lox}$ SM22Cre^{pos} (Ino80 KO) partially ligated murine carotid artery sections. n=4/4 animals. For statistical analysis of the percentage of Edu positive SMCs between control and Ino80 KO ligated carotids, a one-tailed unpaired student's t-test was used. Ino80 (inositol requiring 80), DAPI (4',6-diamidino-2-phenylindole), SMA (smooth muscle actin), EdU (5-ethynyl-2′-deoxyuridine), Edu+ (Edu positive), SMCs (smooth muscle cells).

Evaluation of the amount of EdU incorporation in partially ligated carotids of Ino80 KO animals was significantly reduced (50%) compared to control, suggesting that loss of Ino80 leads to a decrease in VSMCs proliferation *in vivo* (figure 29 B). Thus, deletion of Ino80 in VSMCs leads to both a decrease in VSMCs migration and proliferation *in vivo* in the model of partial carotid artery ligation.

The thickness of the VSMC layer as well as the proliferation rate of VSMCs were reduced in Ino80 KO ligated carotids in comparison with the control (figure 28 C-D). In order to assess the involvement of the loss of Ino80 in the migration of vascular smooth muscle cells, isolated PASMCs were subjected to a scratch assay (wound assay). The scratch assay is an *in vitro* technique of cell migration assay where a monolayer of cells is grown to confluence and is subjected to a scratch (or a wound) creating a cell free zone in the monolayer. Cells can then migrate into the scratched region and cell migration can be quantified.

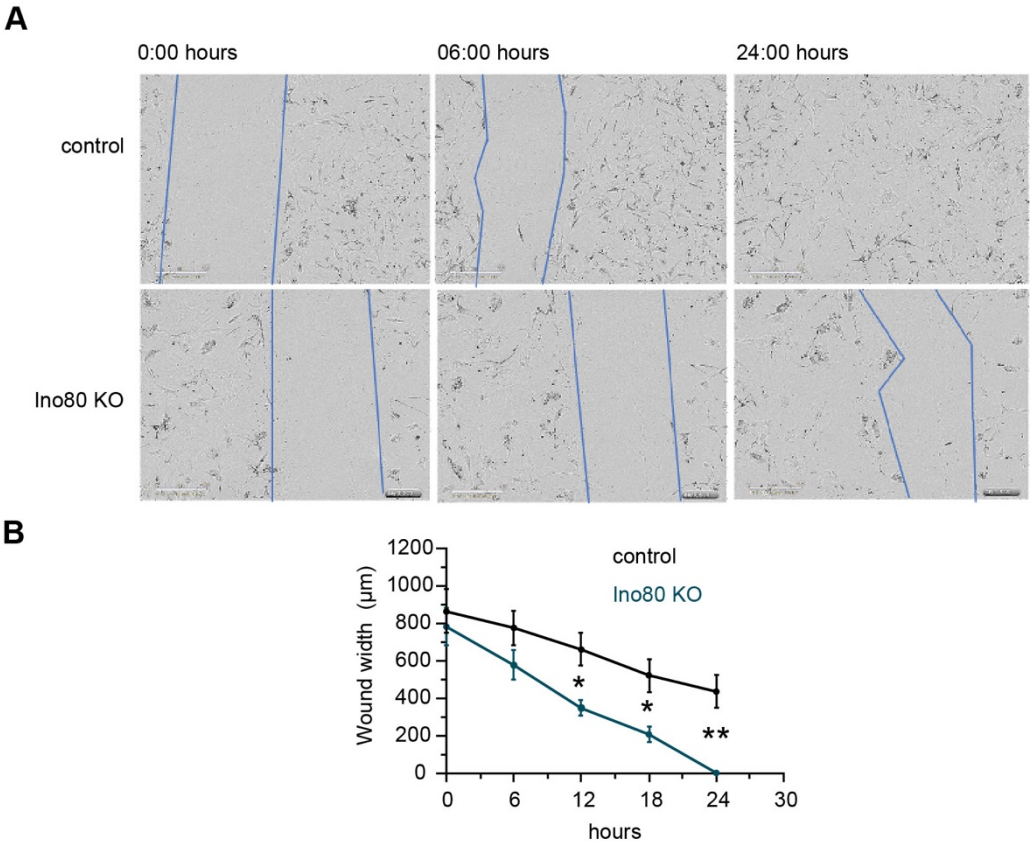

Figure 30. Loss of INO80 leads to an increase in vascular smooth muscle cells *in vitro*

A Representative images of Ino80$^{lox/lox}$ SM22Cre^{neg} (control) and Ino80$^{lox/lox}$ SM22Cre^{pos} (Ino80 KO) pulmonary arterial smooth muscle cells (PASMCs) scratch assay time lapse at 0, 6 and 24 hours. In each image, the leading edges were marked in blue using Image J. Scale 300µm. **B** Statistical evaluation of wound closure time of Ino80$^{lox/lox}$ SM22Cre^{neg} (control) and Ino80$^{lox/lox}$ SM22Cre^{pos} (Ino80 KO) PASMCs scratch assay during a 30 hours interval using Image J. n=3/3. For statistical analysis of the wound width between control and Ino80 KO cells, a multiple unpaired t-test was used. Ino80 (inositol requiring 80).

At 0 and 6 hours, the wound width was not significantly different between Ino80 KO PASMCs compared to control, allowing for comparable starting conditions in both Ino80 KO and control cells (figure 30 A and B) However, the width of the wound became significantly reduced (by over 300 µm) in Ino80 KO PASMCs in comparison with the control after 12 and 18 hours (figure 30 B). Finally, the wound completely closed in the Ino80 KO PASMCs in contrast to WT where it was still over 400 µm large after 24 hours, demonstrating that loss of Ino80 causes an increase in VSMCs migration *in vitro* (figure 30 B). This finding is in contrast to the *in vivo* partial carotid ligation results that loss of Ino80 led to a decrease in VSMCs migration and proliferation (figure 28-29). The discrepancy between both *in vitro* and *in vivo* findings

might be attributed to the fact that VSMCs upon loss of Ino80 are not correctly responding to environmental stimuli.

Loss of Ino80 in SMCs revealed a decrease in VSMCs migration *in vivo* (figure 28) but in contrast showed an increase in VSMCs migration *in vitro (*figure 30). VSMCs migration has an essential function in atherosclerosis development During atherosclerosis development, macrophages infiltrate the blood vessels and VSMCs migrate into the plaque and differentiate into foam cell like VSMCs (Gistera & Hansson, 2017; Libby et al., 2019). Interestingly, it has been reported that 40% of foam cells found within advanced human coronary atherosclerotic lesions express both SMC marker ACTA2 and the macrophage marker CD68 (Allahverdian et al., 2014). Therefore, the expression of Cd68 was examined both on the RNA (by affymetrix microarray analysis) as well as on the protein level (by immunostaining) from Ino80$^{lox/lox}$SM22Cre^{neg} (control) and Ino80$^{lox/lox}$SM22Cre^{pos} (Ino80 KO) arteries.

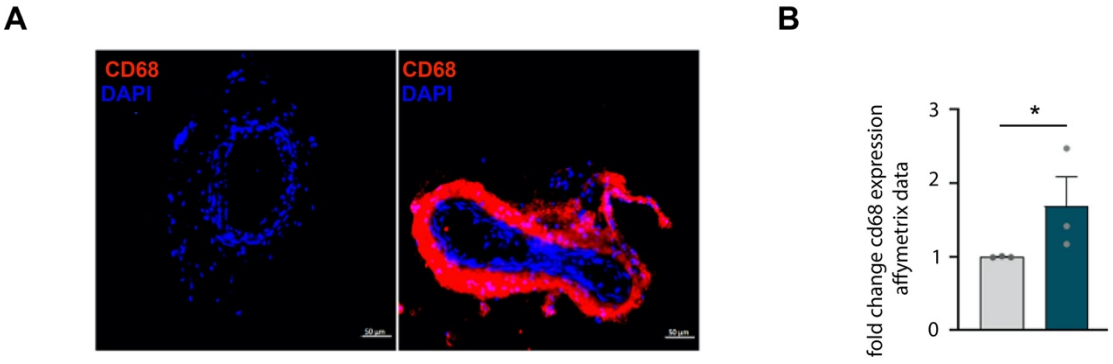

Figure 31. Deletion of INO80 leads to foam cell like vascular smooth muscle cells.

A Representative images of Ino80$^{lox/lox}$ SM22Cre^{neg} (control) (left panel) and Ino80$^{lox/lox}$ SM22Cre^{pos} (Ino80 KO) (right panel) femoral artery sections, stained with DAPI (blue) and anti-CD68 antibody (red). Scale = 50 µm. **B** Quantification of CD68 expression fold change obtained from microarray based transcriptional analysis of Ino80$^{lox/lox}$ SM22Cre^{neg} (control) and Ino80$^{lox/lox}$ SM22Cre^{pos} (Ino80 KO) murine aortas. n=3/3 animals. Ino80 (inositol requiring 80).

Femoral arteries of Ino80 KO mice revealed a strong expression of CD68 (a macrophage a foam cell marker) in contrast to control (figure 31 A). CD68 was not observed in control femoral arteries stained for CD68 expression (figure 31 A). Evaluation of cd68 expression by microarray analysis from aortas confirmed an increase in cd68 expression in Ino80 KO compared to control, thereby suggesting that VSMCs lacking Ino80 display a feature of VSMCs-derived macrophages (figure 31 B).

These cells are not macrophage derived VSMCs but rather VSMCs expressing the cd68 marker (a foam cell marker).

The alterations in VSMCs migration and proliferation, as well as the observed increase of CD68 expression upon loss of Ino80, support the hypothesis that Ino80 might play a role in atherosclerotic plaque development. To examine the contribution of Ino80 in atherosclerosis development, a murine atherosclerosis model was used. For this purpose, Ino80 KO and control mice were intravenously injected with AAV8_PCSK9 and challenged with high fat diet (HFD) for 14 consecutive days (high fat murine model). measurement of atherosclerotic plaque volume was performed using aortic arches from Ino80 KO and control high fat murine mice model (AAV8-PCSK9) using light sheet microscopy.

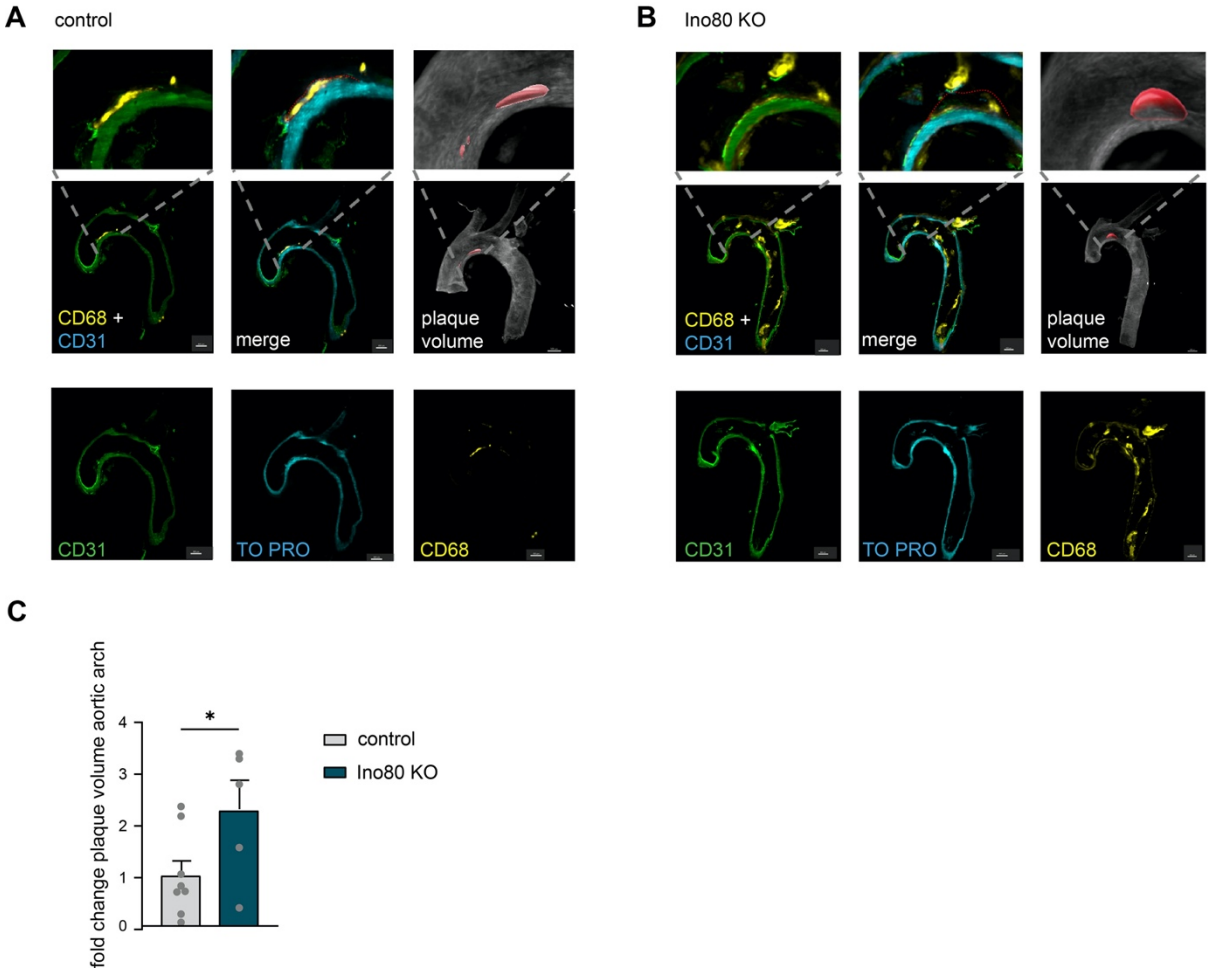

Figure 32. Atherosclerotic lesions in the aortic arch are larger upon loss of INO80 in a murine model of high-fat diet.

A-B Representative optical sections of aortic arches isolated from Ino80$^{lox/lox}$ SM22Cre^{neg} (control) and Ino80$^{lox/lox}$ SM22Cre^{pos} (Ino80 KO) mice injected with AAV8_PCSK9 and fed with HFD for 14 weeks,

obtained using light sheet microscopy together with three-dimensional reconstruction by the Imaris software. Aortic arches were stained with anti-CD31 antibody (green), TO PRO (blue) and anti-CD68 antibody (yellow) (these can be visualized in the bottom panels). The top panels shows atherosclerotic plaque delineated (in red) by CD31 and CD68 staining. Scale 400 µm. Middle right panel from A and B: automatic segmentation of the atherosclerotic plaque volume in the 3D space of the aortic arch, labeled in red. Scale 500 µm. **C** Quantification of atherosclerotic plaque volume within the aortic arch of $Ino80^{lox/lox}$ $SM22Cre^{neg}$ (control) and $Ino80^{lox/lox}$ $SM22Cre^{pos}$ (Ino80 KO) mice injected with AAV8_PCSK9 and fed with HFD for 14 weeks. n=8/8 control animals and n=5/5 Ino80 KO animals. For statistical analysis of the fold change in plaque volume between control and Ino80 KO aortic arches, a one-tailed unpaired student's t-test was used. Ino80 (inositol requiring 80), HFD (high fat diet).

Aortic arches were stained for markers of interest to identify the atherosclerotic plaque: CD31 for endothelial cells, CD68 to macrophages and TO PRO for cell nuclei (figure 32 A). In order to evaluate plaque volume, atherosclerotic plaques were manually annotated using these three cell markers and three-dimensional reconstruction was performed using the Imaris software (figure 32 A). The aortic arch plaque volume was found to be significantly increased, upon loss of Ino80 in an AAV8-PCSK9 murine high fat model in comparison with control, demonstrating that loss of Ino80 leads to an increase in aortic arch atherosclerotic plaque development (figure 32 B). Vector preparations were a gift from Oliver J. Mueller, Kiel University. Staining, imaging and plaque volume measurements of the aortic arches were performed by Laia-Canes Esteve, Max-Planck Institute for Heart and Lung Research.

The results of the light sheet microscopy established that loss of Ino80 (in a high fat murine model) leads to an increase of atherosclerotic plaque burden in the aortic arch in comparison with control. In order to further validate this finding, atherosclerotic plaque size was quantified from lipid rich regions of aortic roots of Ino80 KO and control high fat murine models stained with oil red O (figure 33 A).

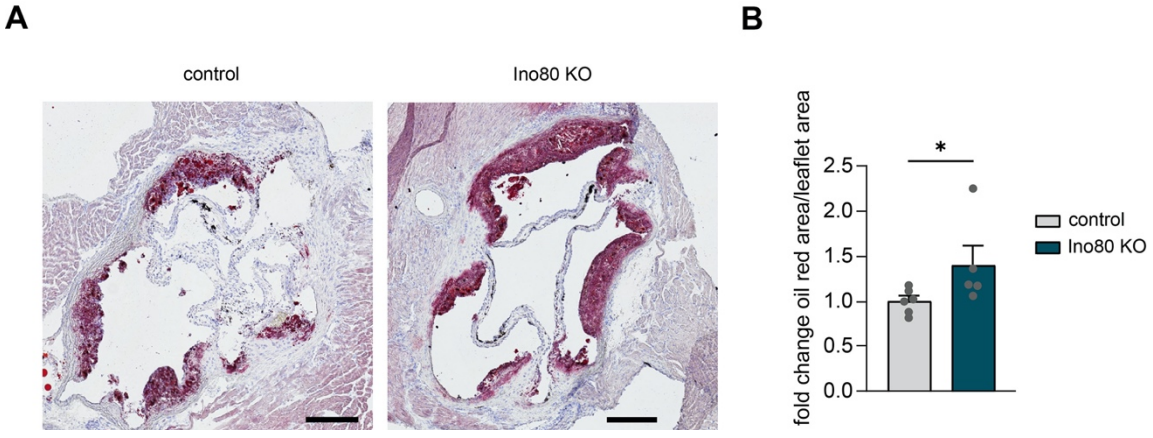

Figure 33. Loss of INO80 accelerates atherosclerotic lesion development in the aortic arch of murine model of high-fat diet.

A Representative images of Oil red O (red color stains lipid) and hematoxylin (blue color stains cell nuclei) staining of aortic root sections from Ino80$^{lox/lox}$ SM22Cre^{neg} (control) and Ino80$^{lox/lox}$ SM22Cre^{pos} (Ino80 KO) mice injected with AAV8_PCSK9 and fed with HFD for 14 weeks. Scale bar 200 µm. **B** Quantification of lipid- rich regions by Oil red O staining in aortic root leaflets of Ino80$^{lox/lox}$ SM22Cre^{neg} (control) and Ino80$^{lox/lox}$ SM22Cre^{pos} (Ino80 KO) mice injected with AAV8_PCSK9 and fed with HFD for 14 weeks was performed using the Fiji image analysis software. n=6/6 control animals and n=5/5 Ino80 KO animals. For statistical analysis a Mann-Whitney test was used. Ino80 (inositol requiring 80), HFD (high fat diet).

Ino80 KO mice exhibited a significant increase in oil red O staining of lipid rich regions in the aortic root in comparison to control in a murine model of high-fat diet, showing that loss of Ino80 in SMCs leads to an increase in atherosclerotic plaque size (figure 33 B). This data corroborates the increase in plaque volume of Ino80 KO aortic arches (figure 32 B). Vector preparations were a gift from Oliver J. Mueller, Kiel University. Staining of the aortic roots was performed together with Laia-Canes Esteve. Imaging of the aortic roots was performed by Laia-Canes Esteve, Max-Planck Institute for Heart and Lung Research. Measurement of plaque area was performed by myself.

Collectively, this data shows that Ino80 regulates vascular smooth muscle cell phenotypic migration, induces the expression of the foam cell marker cd68 and ultimately leads to an increase in atherosclerotic plaque development.

4. Discussion

The aim of this work was to characterize the functions of the INO80 chromatin remodelling complex in adult smooth muscle cells of the cardiovascular system.

In this study, multiple lines of evidence suggest that different core functions of the chromatin remodelling complex INO80 regulate specific phenotypical features in vascular smooth muscle cells (VSMCs). Global analysis of the function of Ino80 in VSMCs transcriptional regulation revealed that YY1 is a major co-factor of INO80 transcription regulation. This study determined that INO80 binds the promoter region of myocardin and regulates its transcriptional activation together with YY1. Moreover, it established that INO80 controls VSMC metabolism through regulation of DNA damage response. Finally, this work demonstrated that loss of INO80 accelerates atherosclerotic development using the AAV8-PCSK9 murine model of high fat diet possibly as a consequence of myocardin downregulation.

4.1. Ino80 regulates vascular smooth muscle cell physiological function

4.1.1 Various vasoactive stimuli show different levels of reduced contractile responses in Ino80 KO arteries due to the heterogeneity of targeted pathways

Resistance arteries are responsible for local distribution of vascular tone and blood flow thereby defining vascular resistance (Christensen & Mulvany, 2001). Three essential parameters determine blood flow resistance. These include vessel diameter, arterial length, and blood viscosity. Vessel diameter is the most critical feature of the aforementioned parameters, since it is a function of vasomotor tone through adaptation to contraction and dilation of VSMCs (Christensen & Mulvany, 2001). Primary examination of the structural consequences of the loss of Ino80 in VSMCs revealed an increase in arterial luminal area upon Ino80 KO but no changes in the thickness of the smooth muscle cell layer. According to Poiseuille's law, vessel resistance is inversely proportional to the lumen diameter to the fourth power (Touyz & Schiffrin, 2000). This suggests that changes in lumen diameter can have a substantial effect on vascular resistance and therefore on contractility (Welsh et al., 2018). In accordance with this, measurement of vascular contractility revealed a decrease in femoral artery contractility upon stimulation with angiotensin II and KCl in Ino80 KO arteries compared to the control. Intriguingly, arteries stimulated with

vasopressors (phenylephrine and epinephrine) showed a complete loss of contractile response in Ino80 KO arteries in contrast to the control. This discrepancy can be explained by the heterogeneity of targeted pathways between KCl, angiotensin II, epinephrine and phenylephrine. KCl induces contraction through direct membrane depolarization causing Ca^{2+} entry through voltage-operated Ca^{2+} channels which leads to activation of Ca^{2+} dependent MLC kinase and increases MLC phosphorylation (Driska et al., 1981; Ganitkevich & Isenberg, 1991; Nelson et al., 1988; Ratz & Murphy, 1987; Van Breemen et al., 1972). Phosphorylated myosin subsequently binds actin fibers leading to fiber contraction and alteration of vessel resistance and diameter (Bravo-Sagua et al., 2020). Therefore, KCl-induced stimulus-response coupling mechanism activates VSMCs contractility through a simple mechanism independent of GPCRs. In contrast to this, angiotensin II induces VSMCs contractility through three different pathways. Angiotensin II is the biologically active component of the renin-angiotensin-aldosterone- system (RAAS) and can bind angiotensin type 1 and 2 receptors (AT_1 and AT_2). In VSMCs, angiotensin II primarily binds AT_1 receptors. The angiotensin II signaling cascade via the AT_1 receptor is a consequence of the activation of the G-protein and signaling pathways involving $G_{q/11}$, G_i, G_{12}, and G_{13} (Higuchi et al., 2007; Ohtsu et al., 2006). The AT_1 receptor signals through three main cascades activating downstream signaling involving specific increase in Ca^{2+} signalling, which results ultimately in contraction of VSMCs as described above for KCl (Bennett et al., 2016; Te Riet et al., 2015; Touyz & Berry, 2002). The first cascade takes place through activation of the classical phospholipase C (PLC) which causes cleavage of inositol trisphosphate (IP_3) and sustained production of diacylglycerol (DAG), which in turn modulates Ca^{2+} mobilization from the sarcoplasmic reticulum and stimulates protein kinase C (PKC) (Ushio-Fukai et al., 1998). The increase in intracellular Ca^{2+} causes calmodulin-activated phosphorylation of MLC leading to VSMCs contraction (Touyz & Berry, 2002). The second cascade occurs through activation of phospholipase D (PLD) and also culminates in DAG generation; but unlike PLC, PLD hydrolyzes phosphatidylcholine. Sustained activation of PLD leads to the generation of phosphatidic acid (PA) and subsequent production of DAG by phosphatidic acid phosphohydrolase. Ang II-induced activation of PLD in VSMC is PKC independent, but involves tyrosine kinase dependent intracellular Ca^{2+} mobilization and Ca^{2+} influx and thereby induces VSMCs contractility (Billah, 1993; Dhalla et al., 1997; Touyz & Schiffrin, 1999). The final AT_1 angiotensin II dependent

signaling starts with the activation of phospholipase A_2 (PLA_2), which is responsible for arachidonic acid (AA) release from phospholipids. Activated PLA_2 and its metabolites subsequently activate Ras/MAPK-dependent signaling pathways, amplifying PLA_2 activity and inducing further generation of arachidonic acid through a positive feedback mechanism. AA is metabolized by cyclooxygenases, lipoxygenases or cytochrome P450 oxygenases to various eicosanoids in vascular and renal tissues. Ang II-generated eicosanoids also regulate vascular contraction and growth, possibly through MAPK and redox-sensitive pathways activation (Bonventre, 1992; Nasjletti, 1998). Conversely, epinephrine and phenylephrine are alpha 1 adrenergic receptor agonist and alpha1/beta1 adrenergic receptor agonist respectively (Cooper, 2008; Russell, 2019; VanValkinburgh et al., 2024). Adrenergic receptor agonists can induce contraction through activation of trimeric G proteins linked G proteins G_q and $G_{12/13}$ leading to generation of various cell messengers which are key players of the PLC/IP_3/DAG pathway and of the Rhoa/Rho-kinase pathway (Hofmann, 2021; Sakurada et al., 2001; Somlyo & Somlyo, 2000; Uehata et al., 1997). Thereby, IP_3 stimulates calcium release from intracellular stores that binds to calmodulin and activates MLCK leading to VSMCs contraction, meanwhile calcium-independent regulation of smooth muscle tone is achieved by Rho-kinase-dependent inhibition of MLCP activity at constant calcium level generating an increase in phospho-rMLC and achieving VSMCs contraction (Hofmann, 2021). Whilst angiotensin II, epinephrine and norepinephrine share certain regulatory events (involving activation of GPCRs and DAG) which culminate in VSMCs contraction, they certainly also induce different molecular players which would explain the difference in contractility induction observed with the different treatments. To try and address the difference in generated contractility upon the use of various vasoactive stimuli, the expression of genes known to be involved in downstream pathways related to direct adrenergic stimulation of contractility were analyzed, but no direct INO80 target could be identified. The difference in generated contractility upon use of diverse vasoactive stimuli might therefore be due to secondary effects of direct Ino80 target gene regulation.

4.1.2 Ino80 alters VSMCs pulse propagation through the artery

Evaluation of the physiological consequences of the reduced contractility observed upon loss of Ino80 revealed a decrease in the average pulse pressure under normal

physiological conditions in the Ino80 KO mice in comparison with control. Interestingly, arterial blood pressure waveforms of Ino80 KO mice also showed spikes where the pulse pressure was wider. Arterial elasticity is a major determinant of pulse pressure, and is characterized by arterial resistance (Briet & Schiffrin, 2013). In the arterial tree, pressure pulsations are reduced by the elasticity of the vessels (based on the windkessel effect: model describing the hemodynamics of the arterial system in terms of resistance and compliance) and the pulse is propagated along blood vessels in the form of a wave (Westerhof et al., 2009). Blood is pumped from the heart into the entrance of the aorta, where pressure rises, the vessel wall is then stretched leading to an increase in wall tension. As the rate of cardiac ejection slows down, the pressure slowly reduces, and the distended wall return towards its equilibrium position. The inertia of the fluid keeps it moving forwards following the decrease in driving pressure. The next section of the wall becomes simultaneously distended and once it recoils, the fluid driven out distends to the next section of the arterial wall which also recoils sending it to the next section and so on (Caro et al., 2011). Indeed, the elastic function of arteries creates a wave-propagation phenomenon. VSMCs can alter their contractile state through changes in diameter and hemodynamical resistance. This allows for blood flow to be distributed to various vascular beds according to immediate local metabolic requirements. Since VSMCs upon Ino80 KO show a significant reduction in contractility this would directly impact the propagation of the pulse through the artery and would explain the decreased average pulse pressure since the pulse would mainly be propagated through the inertia of the fluid. The observed wide pulse pressure peaks might be accounted for by the accumulation of the pulse at certain sections of the artery due to the poor VSMCs contractility.

4.1.3 Deletion of Ino80 results in the formation of non-physiological VSMCs depicted by reduced contractility and unsuited responsiveness to environmental cues

Investigation into the physiological consequences of the reduced contractility revealed a failure to increase blood pressure following administration of the nitric oxide synthase inhibitor L-NAME (L-arginine analogue N^{ω}-nitro-l-arginine methyl ester, a nitric oxide (NO) inhibitor) in the Ino80 KO animals. The inability of Ino80 KO arteries to induce a vasoconstrictor response upon L-NAME treatment argues that resistance vessels of

Ino80 KO mice also lack the ability to promote further contraction in response to surrounding physiological stimuli, which nicely confirms the wire myography findings *in vivo*, but are still able to undertake further relaxation following captopril treatment (an angiotensin I converting enzyme inhibitor). An alternative explanation is that NO generally cannot induce vasorelaxation in Ino80 KO arteries since their intrinsic myogenic tone is minimal or absent which would be in agreement with the increased arterial lumen diameter observed upon loss Ino80. The fact that Ino80 KO arteries do not properly respond to environmental stimuli was also observed during the partial carotid ligation assay, where Ino80 KO VSMCs showed a decrease in proliferation. Upon injury, VSMCs conventionally switch from a contractile to synthetic phenotype where VSMCs exhibit proliferative and migratory features (Sinha et al., 2014). In this example however, VSMCs ability to proliferate and migrate *in vivo* were reduced. The finding that inactivation of Ino80 led to a decrease in VSMCs contractility but not to a switch towards a synthetic phenotype was unexpected. The gene expression of various contractile and synthetic smooth muscle cell markers was found to be deregulated, but showed no clear phenotypical switch which corroborates the physiological findings. Taken together with the blood pressure results, these findings suggest that loss of Ino80 leads to an impairment of VSMCs function where VSMCs are in a non-physiological “sick” cell state, unable to properly respond to environmental stimuli.

4.2. The function of INO80 in vascular smooth muscle cells transcriptional regulation

4.2.1. YY1 is an essential co-factor of INO80 transcriptional regulation

The INO80 complex is a conserved chromatin remodeling complex composed of over 15 different subunits, which perform various functions including transcriptional regulation (Aramayo et al., 2018; Chen et al., 2011; Jin et al., 2005; Shen et al., 2000; Tosi et al., 2013). Mice carrying the Ino80 deletion in smooth muscle cells were viable and born according to mendelian ratios. INO80 complex composition adapts to the dynamic requirements of cell stage associated functions. Due to the lack of DNA-binding domains, chromatin remodelers need coordination with other factors to recognize specific DNA sequences and achieve various biological functions. Indeed, the interaction of INO80 with different subunits such as YY1 has been previously described to support cell type-specific transcriptional regulation. For instance, in mouse embryonic stem cells, YY1 was reported to present genome-wide PcG-independent activities while remaining stably associated with the INO80 chromatin remodeling complex (Vella et al., 2012). In a human cell line, YY1 was described to function with INO80 to gain access to target promoters and to act as an essential transcriptional co-activator (Yong Cai et al., 2007). In this study, microarray analysis, INO80 CutnRun, GSEA, and motif analysis were integrated to define the likely direct targets of INO80 transcriptional regulation. Deletion of Ino80 in VSMCs led to significant changes in transcriptional regulation of 5518 genes, of which 783 were found to be binding targets of INO80 These 783 genes are considered to be primary targets of INO80 transcriptional regulation, since they show both significant regulation by Ino80 and are binding targets of INO80 (contain an INO80 CnR peak). Regulation of the remaining 4735 genes could result partly from secondary effects and, or from dependence on other transcription factors, co-factors or chromatin modifiers which are regulated by primary Ino80 target genes. This study was centered around evaluating the direct targets of Ino80 which were transcriptionally regulated, and therefore focused on these 783 target genes. Interestingly, strongly associated Ino80 genes were found to be exclusively targets of Ino80 transcriptional activation. Moreover, further analysis of Ino80 transcriptionally regulated direct targets, revealed an enrichment of the YY1 motif at around 40 % of these genes confirming previous findings which claimed that YY1 is an important co-factor for INO80 transcriptional

regulation (Yong Cai et al., 2007; Vella et al., 2012). This data suggests coactivation between YY1 and INO80 whereby INO80 is likely recruited to these target sites through YY1. It would be interesting to explore the biological functions of further TFs which might be involved in this transcriptional network to gain further insight into the mechanisms of INO80 VSMCs transcriptional regulation.

4.2.2 INO80 transcriptional regulation of VSMCs and nucleosome mobility

Globally, the INO80 complex acts as a master coordinator of transcriptional regulation in VSMCs. Indeed, INO80 transcriptionally regulated targets genes were found to be targets of both transcriptional activation and repression which is in correlation with previous findings. For example, transcriptome analysis of the loss of Ino80 in isogenic yeast strains revealed that 668 genes were upregulated and 488 genes were reduced by at least 1.5-fold (van Attikum et al., 2004). Moreover, loss of the catalytic Ino80 subunit in yeast reveled mis-regulation of 15% of the yeast genome (half of which was upregulated and the other half downregulated). The dual transcriptional regulation by INO80 might be due to changes in nucleosome mobility as a key controlling mechanism in gene regulation. Sliding of nucleosomes along the DNA, or transfer of a nucleosome from a segment of DNA to an adjacent one could modulate nucleosome mobility. Decreasing nucleosome mobility might allow “stepping around” a transcribing RNA polymerase (thereby repressing RNA polymerase activity) or making a binding site for TF/activator unavailable. Conversely, increasing mobility of nucleosomes would increase the availability of a binding site for a TF/activator thereby regulating transcriptional activity of target genes (Kingston, 1996; Soutoglou & Misteli, 2007; Studitsky et al., 1994). The INO80 complex has been established to alter nucleosome positioning both *in vivo* and *in vitro*. By using energy derived from ATP hydrolysis, INO80 can alter histone-DNA interactions resulting in nucleosome translocation (sliding), ejection, and reconfiguration (Clapier et al., 2017; Jin et al., 2005; Shen et al., 2003; Udugama et al., 2011). In yeast, INO80 was shown to recognize and establish NFRs, to correctly position the -1 and +1 nucleosomes relative to the TSS, as well as reposition nucleosomes after their mobilization by the elongation transcription machinery (Krietenstein et al., 2016; Yen et al., 2013). To date, the chromatin remodeling function of mammalian INO80 in terms of nucleosome positioning mapping has not been shown. It would be of particular interest to evaluate

how nucleosome positioning by INO80 regulates active organization and allosteric regulation of the first level chromatin and how this might correlate with transcriptional regulation in VSMCs. Moreover, this might shed some light on which subunits of the INO80 complex are essential to its nucleosome positioning function. Genome-wide nucleosome positioning is commonly performed using micrococcal nuclease digestion based high throughput sequencing (MNase-seq) (Hughes & Rando, 2014). Typically, MNase based methods allow for estimation of nucleosome positioning as an average of the bulk nucleosome population (Kevin Struhl & Eran Segal, 2013; Zhang & Pugh, 2011). This method can however be misleading since averaging nucleosomes which have overlapping positions in a large portion of the cell population over a heterogenous nucleosome positions in the rest of the cells would result in a discrepancy between the consensus center of nucleosomes and the most representative nucleosome positions (Zhou et al., 2016). This variability may be due to biological changes within a cell population or to different degrees of digestion of the same nucleosome by MNase. Determining the exact location of individual nucleosomes within a mammalian cell population remains a challenge and hence, in the future novel analytical methods and tools need to be developed to accurately determine nucleosome positioning.

4.2.3. INO80 is recruited by YY1 to the myocardin promoter and together they regulate transcriptional activation of myocardin

Gene expression analysis and protein analysis comparing Ino80 KO and control aortas revealed deregulation of various several genes including smooth muscle cell contractile and synthetic specific genes. By means of gene expression analysis, protein analysis from aortas as well as an INO80 Cut and Run from primary aortic smooth muscle cells, myocardin was identified as an INO80 target which was significantly downregulated upon loss of Ino80. Furthermore, a YY1 core motif was identified at the promoter of myocardin and downregulation of YY1 *in vitro* resulted in a decrease of myocardin expression suggesting that myocardin is also a target of YY1. Global analysis of YY1 is an essential co-factor for INO80 transcriptional regulation. This analysis was based on genes which were significantly transcriptionally regulated by INO80, were direct targets of INO80 (contained an INO80 CnR peak) and included a YY1 motif at the INO80 CnR peak. In the case of myocardin, both YY1 and INO80 co-localize at the myocardin promoter, nonetheless, the YY1 motif was identified

around 92 bps away from the INO80 CnR peak. The INO80 complex is a megadalton large modular complex with a 3D structure that can be modified upon binding, therefore the small distance observed between the location of the INO80 CnR peak and the YY1 motif can be merely due to the conformation of the complex upon binding to the myocardin promoter (Knoll et al., 2018; Su et al., 2016). Nevertheless, this fact emphasizes that YY1 might be playing an even larger role in VSMCs global transcriptional regulation of INO80 targets than the analysis described in 4.2.1, since INO80 targets which contain a YY1 motif at their promoter region (without it being including within the INO80 peak) were not considered. This work didn't not assess whether INO80 or YY1 first bind to the myocardin promoter. Based on a previous report, this data would suggest that YY1 recruits INO80 to the myocardin promoter to activate its transcription (Yong Cai et al., 2007).

4.2.4. Myocardin downregulation is responsible for the reduced arterial contractility upon loss of Ino80

Myocardin is a co-activator of serum response factor (SRF)-dependent gene expression in smooth muscle cells and cardiac muscle through binding of CArG box at gene promoters (Wang et al., 2001). Virtually, all marker genes of the VSMCs differentiated (contractile) phenotype contain one or more CArG box within 1 ± 2 kb of the transcription start site and therefore can be regulated by the myocardin-SRF complex (Miano, 2002; Wang et al., 2001). Myocardin expression was described to be sufficient for inducing a functional competent SMC phenotype based on ultrastructural and physiological evaluations (including calcium flux and slow wave contraction) (Jiang et al., 2010; Long et al., 2008; Raphel et al., 2012). Jointly, several papers have reported that myocardin directs a SMC differentiation program by showing that myocardin expression is reduced in de-differentiated (synthetic) SMC, that myocardin induces activation of SMC promoters and endogenous SMC marker genes, and finally that myocardin overexpression leads to attenuation of SMCs growth (a feature of SMCs synthetic phenotype) (Chen et al., 2002; Long et al., 2009; Nanda & Miano, 2012; Zhou & Herring, 2005). Intriguingly, ectopic expression of myocardin on its own was sufficient to convert a non-SMC into a SMC-like phenotype *in vivo*(McDonald, 2005). Overexpression of myocardin in PASMCs of Ino80 KO mice resulted in the rescue of a subset of contractile (differentiated) VSMC specific genes observed by RT-

qPCR gene expression analysis, consistent with previous reports (Long et al., 2009; Wystub et al., 2013). These findings suggest that transcriptional activation of myocardin by INO80 and YY1 is essential for vascular smooth muscle cells contractility. YY1 most likely recruits INO80 to the myocardin promoter to activate its transcription thereby inducing expression of other VSMCs contractile genes (such as Acta2, Actg2). Upon loss of Ino80 or yy1, myocardin expression is decreased resulting in downregulation of contractile VSMCs markers, also reflected by deregulation of synthetic VSMCs gene expression and ultimately leads to a VSMCs "sick" state where the cells are neither properly contractile nor synthetic and cannot correctly respond to environmental stimuli (figure 35). Therefore,this VSMCs "sick" state is presumably responsible for the observed reduced contractility and dysfunctional blood pressure upon loss of Ino80 in VSMCs.

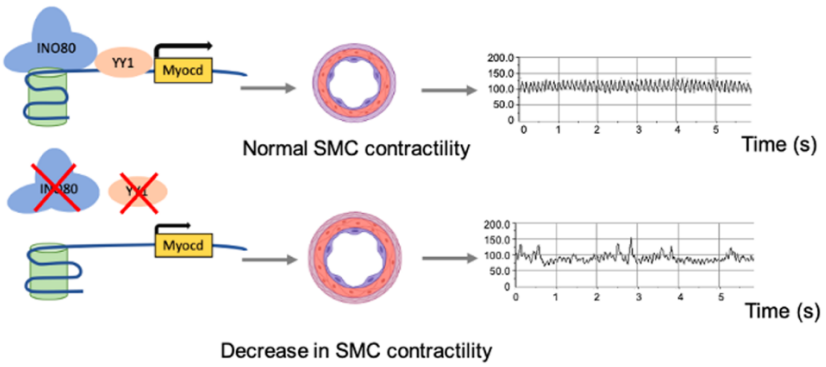

Figure 34. Regulation of myocardin expression by INO80 and its co-factor YY1 is essential to vascular contractility.
YY1 recruits INO80 to the myocardin promoter and together the INO80-YY1 complex regulate myocd expression. Myocardin is critical for normal vascular SMC contractility and maintenance of normal arterial pulse waveforms. Myocd (myocardin), INO80 (inositol requiring 80), YY1 (Yin Yang 1), s (seconds), SMC (smooth muscle cell).

Of course, downregulation of myocardin does not account for all effects of Ino80 KO in VSMCs as illustrated by the deregulation of 783 genes, which are not all targets of myocardin transcription. Rather, it is the most probable target of INO80/YY1 transcriptional regulation which can be responsible for the observed phenotype acquired upon loss of Ino80. It would be interesting to investigate whether overexpression of myocardin *in vivo* can rescue the reduced vascular contractility and dysfunctional blood pressure observed upon loss of Ino80 in SMCs. It is important to also mention that the transcriptional regulation of these 783 genes was not confirmed

on the protein level and might therefore have no effect on cellular function if proteins levels are not accordingly regulated. Alternatively, transcriptional regulation of these genes might be representative of the dynamic auto-regulation transcriptional program that takes place upon loss of Ino80 to maintain VSMCs homeostasis. Nevertheless, we cannot exclude that deregulation of various VSMCs marker genes as well as other INO80 target genes could not accrue to the development of the non-physiological “sick” VSMCs phenotype observed upon loss of Ino80.

4.3. Loss of INO80 mediated DNA repair is essential to the maintenance of vascular smooth muscle cell metabolism through FOXO1

4.3.1. Deletion of Ino80 in smooth muscle cells leads to a switch in metabolism and impairs mitochondrial morphology

Gene set enrichment analysis of microarray data from aortas, uncovered an increase in fatty acid metabolism and oxidative phosphorylation as well as mitochondrial respiratory complexes upon loss of Ino80. Metabolic reprogramming has emerged as an essential key regulator of VSMCs phenotypic switch and cell specific signal transduction processes (Metallo & Vander Heiden, 2010; Morales et al., 2014; Shi et al., 2020). In VSMCs, fatty acid oxidation (FAO) is coordinated with glucose metabolism. Thereby, the energy produced from aerobic glycolysis can be supplied by FAO, and glycolysis activity can be controlled by the feedback of FAO products (Barron et al., 1994). FAO of fatty acyl-CoA esters is performed in four enzymatic reactions that generate nicotinamide (NADH), flavin adenine dinucleotide ($FADH_2$), and acetyl-CoA.

Fatty acids are transported via the blood as non-esterified fatty acids bound to lipoproteins or serum albumin (Hirsch et al., 1998). Inside the cell, acyl-CoA synthetases activate fatty acid by converting it from its non-esterified form to a fatty acyl-CoA ester. Fatty acyl-CoA esters then enter the mitochondria via the carnitine shuttle system to undergo FAO (Kompare & Rizzo, 2008). FAO metabolizes fatty acyl-CoAs resulting in the production of one acetyl-CoA molecule, two electrons derived from NADH and $FADH_2$ and a fatty acyl-CoA ester shortened by two carbon atoms (Nsiah-Sefaa & McKenzie, 2016). Electrons derived from NADH and $FADH_2$ are then utilized by the five oxidative phosphorylation (OXPHOS) complexes I–V (CI–V) to produce ATP (Nsiah-Sefaa & McKenzie, 2016; Yu et al., 2017). Complexes I-IV transfer electrons released from the reduced forms of NADH and $FADH_2$ via a sequence of exergonic redox reactions which contribute to the generation of the electrochemical gradient across the inner mitochondrial membrane (Tang et al., 2020). The proton gradient drives the translocation of protons from the intermembrane space back into the matrix through ATP synthase (complex V) which catalyzes the conversion of ADP to ATP (Tang et al., 2020). Therefore, an increase in fatty acid metabolism would also lead to an increase in OXPHOS. Throughout VSMC phenotypic transition, synthetic VSMCs display a decreased glucose oxidation and an upregulated FAO. The

increase in FAO in synthetic VSMCs can be accounted for the need of added energy for VSMCs to achieve rapid proliferation, migration, synthesis and secretion of extra cellular matrix (Sartore et al., 2013; Scheede-Bergdahl & Bergdahl, 2017). Previous studies have reported that metabolic switching can regulate the progression of VSMCs dependent vascular diseases. In fact, inhibition of mitochondrial respiratory complex I and II resulted in improvement of neointimal hyperplasia following arterial injury (Yin et al., 2019). Furthermore, a more recent study described an increase in OXPHOS in both high phosphate and uremic serum induced calcification (Shi et al., 2022). The increased FAO and OXPHOS observed upon deletion of INO80 further corroborate the observed loss of contractile phenotype towards a VSMCs “sick” state seen upon Ino80 deletion.

Initially, the discovery of severely disturbed VSMCs mitochondrial cristae ultrastructure seen upon loss Ino80 was surprising to us since oxidative phosphorylation and electron transport take place in the deeply invaginated cristae of the inner mitochondrial membrane (Kirkinezos et al., 2005; R. W. Gilkerson, 2003; Vogel et al., 2006). The observed enrichment in the expression of oxidative phosphorylation gene sets upon loss of Ino80, might however be a consequence of a compensatory effect maintained by undamaged mitochondria to counteract the impaired functions of the disturbed mitochondria. Alternatively, the increase in FAO and OXPHOS upon loss of Ino80 might not be reflected on the protein level and could therefore only be taking place on the gene expression level as a compensatory mechanism. Functional metabolic assays should be performed to confirm or refute this. Moreover, oxidative stress through chronic ROS exposure produced by DNA damage accumulation upon loss of Ino80 is presumably the cause for the disruption of mitochondria ultrastructure as previously reported (Sultana et al., 2006; Valko et al., 2007; Wei et al., 2001).

4.3.2. FOXO1 is responsible for the metabolic switch observed upon loss of Ino80

In order to gain insights into the molecular mechanisms resulting in the metabolic switch observed upon loss of Ino80, analysis of transcription factor targets by gene set enrichment analysis was performed. FOXO1 transcription targets were found to be the most enriched gene set upon deletion of Ino80. FOXO1 activity is dependent on subcellular localisation as it requires nuclear DNA to produce cellular effects (Lees et

al., 2023). Accordingly, we observed that FOXO1 subcellular localization was switched to a nuclear localization upon loss of Ino80, rendering FOXO1 transcriptionally active. FOXO1 regulates the responses to environmental changes, including metabolic and oxidative stress to maintain tissue homeostasis, through regulation of its mRNA expression and diverse PTMs such as phosphorylation (Eijkelenboom & Burgering, 2013; Essaghir et al., 2009; van der Horst & Burgering, 2007; Yamagata et al., 2008). FOXO1 has been reported to transcriptionally activate various metabolic diseases, including gluconeogenesis, glycogenolysis, adipogenesis and thermogenesis (Dong, 2017; Eijkelenboom & Burgering, 2013; Link & Fernandez-Marcos, 2017; Maiese, 2015; Wagatsuma et al., 2016; Xing et al., 2018). Additional Foxo1 knockout after Ino80 KO rescues the metabolic phenotype incurred upon loss of Ino80. Thus, FOXO1 hyper-activation is responsible for the metabolic changes observed upon Ino80 deletion.

So far, the Phosphoinositide 3-kinase/protein kinase B (PI3K/PKB) mediated phosphorylation of FOXO1 in response to insulin or growth factors is the best described and most common form of FOXO1 PTM and is achieved by phosphorylation of three FOXO1 conserved residues (Biggs et al., 1999; Peng et al., 2020). Upon loss of Ino80, both Foxo1 mRNA expression and PI3K/PKB induced FOXO1 PTMs were unchanged. The data suggests that FOXO1 is activated by JNK, in response to oxidative stress generated by DNA damage accumulation caused by the loss of Ino80. The next sub-section will specify the mechanisms behind this.

4.3.3. DNA damage accumulation upon loss of Ino80 causes an increase in ROS production and engenders an upregulation in FOXO1 activity

The ‘chromatin barrier’ consists of DNA packaged into chromatin which makes efficient DSB detection and repair challenging (Goodarzi & Jeggo, 2012). Several papers have shown that to resolve this issue, the chromatin remodeler INO80 though its various functions can bind and remove DSBs, degrade histone proteins and RNAPII under damage conditions, and together with other factors initiate DNA damage repair (Au et al., 2011; Bjergbaek et al., 2005; Falbo et al., 2009; Horigome et al., 2014; Lafon et al., 2015; Lambert et al., 2010; Papamichos-Chronakis et al., 2006; Poli et al., 2016; Tsukuda et al., 2005; van Attikum et al., 2007).

RPA phosphorylation induced in response to DNA damage is commonly used as a readout of DSB resection (Binz et al., 2003; Binz et al., 2004). RPA itself plays an essential role in homologous repair of DSBs through recruitment of a cascade of proteins including radiation sensitivity gene 52 (RAD 52) as well as RAD 51 resulting in the repair of the DSB (Borgstahl et al., 2014; Creeden et al., 2021; Deng et al., 2009; Prakash & Borgstahl, 2012; Wright et al., 2018). Accordingly, deletion of Ino80 in VSMCs resulted in an increase in the DSB DNA damage-induced phosphorylated histone H2A (γ-H2AX) and to a decrease in the DNA repair-associated phosphorylation of the human replication protein A (P-RPA).

The presence of cellular ROS has been established to cause DNA damage, meanwhile the possibility that DNA damage induces ROS production has been only shown in a few studies (Kang et al., 2012; Niocel et al., 2019; Rowe et al., 2008). Treatment of VSMCs with doxorubicin, a topoisomerase II inhibitor which leads to DSB formation, caused an increase in ROS production, thus demonstrating that DNA damage induces ROS production in line with previous reports (Kang et al., 2012; Niocel et al., 2019). Moreover, FOXO1 expression was found to be increased and switched to a nuclear subcellular localization upon doxorubicin-induced DNA damage. Additionally, treatment of VSMCs with H_2O_2, a ROS inducing agent, led to the increase in FOXO1 expression and to the translocation of FOXO1 expression into the nucleus. Thus, these findings confirm that the increase in FOXO1 expression and switch in subcellular localization observed upon loss of Ino80 are a consequence of DNA damage-induced ROS production.

Various DNA-damaging compounds were shown to drive ROS production through a Rac1-dependent mechanism that ultimately led to the activation of Nox enzymes (Kang et al., 2012; Niocel et al., 2019). In line with this proposed mechanism, the contribution of NAD (P)H oxidases (Nox enzymes) in ROS production upon loss of Ino80 was tested. Inhibition of Nox following DNA damage induction in VSMCs decreased ROS production but didn't completely abrogate ROS production. Thus, Nox activation might play a role in DNA damage induced ROS production but is not the only pathway which regulates it. The exact mechanism by which DNA damage induces ROS production in VSMCs is yet unclear and warrants further investigation.

It has been well established that ROS are potent inducers of Jun N-terminal kinases (JNKs) which activate the AP-1 complex composed of fos and jun, which also in turn regulates the activity of JNKs through a negative feedback mechanism (Hess et al.,

2004; Karin et al., 1997; Martindale & Holbrook, 2002; Torres, 2003; Ueda et al., 2002). In the presence of oxidative stress, JNKs have been described to phosphorylate FOXO1 leading to its translocation from the cytoplasm to the nucleus, rendering it transcriptionally active (Grabiec et al., 2015; Ragu et al., 2023; Shen et al., 2010). In agreement with previous reports, loss of Ino80 leads to an increase in the expression of jun and fos (AP-1 complex), known to be regulated by and to regulate JNKs, as well as to an upregulation of JNK1 and JNK2 phosphorylation. Finally, the data demonstrates that FOXO1 activity can be regulated by the AP-1 complex most likely by JNK regulation though a negative feedback mechanism (figure 36). Moreover, FOXO1 activity also controls transcriptional activity of the AP-1 complex likely through subsequent regulation of mitochondrial and metabolism related genes, ROS generation and JNKs activation (figure 36).

These findings suggest that loss of the DNA repair function of Ino80 results in DNA damage accumulation causing an increase in ROS production, converging in the activation of JNKs and FOXO1, and subsequently resulting in a metabolic switch in VSMCs (figure 36).

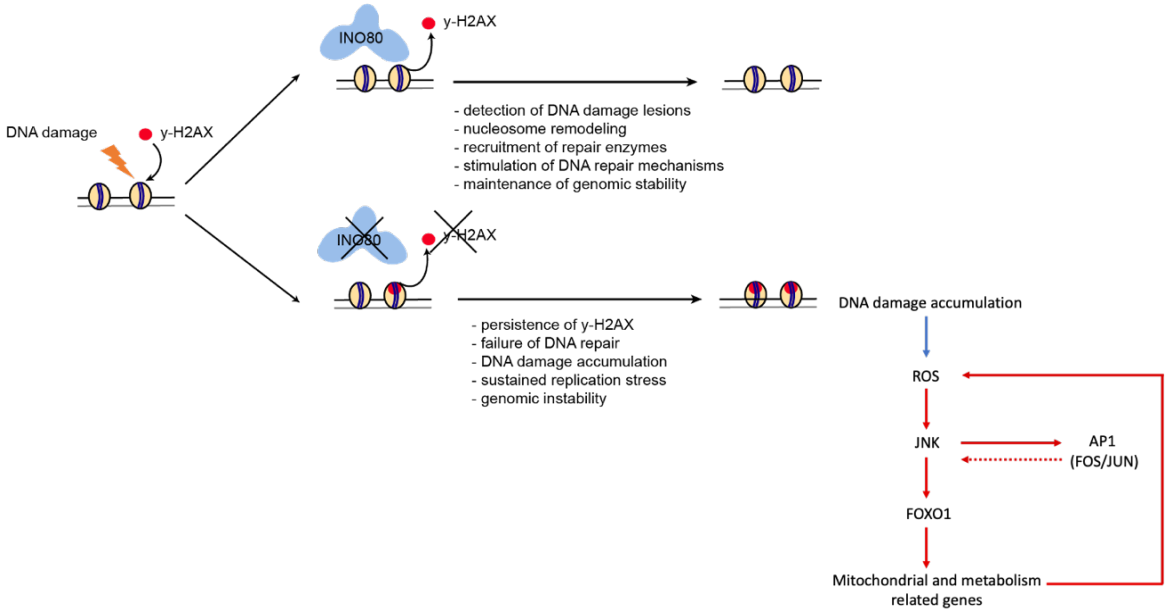

Figure 35. Model representing the function of INO80 in DNA repair and how this regulates vascular smooth muscle cell metabolism.

Ino80 (inositol requiring 80), γH2AX (gamma histone 2AX), ROS (reactive oxygen species), JNK (Jun N-terminal kinase), AP1 (activator protein 1), FOS (fos proto-oncogene), JUN (jun proto-oncogene), FOXO1 (forkhead box O1).

Interestingly, loss of INO80 in endothelial cells or muscle stem cells did not result in an oxidative stress-induced metabolic switch observed in VSMCs (Rhee et al., 2018;

Schutt et al., 2020). Previous reports collectively illustrate the fundamental concept that cellular responses to oxidative stress are contingent on the cell type affected, per say terminally quiescent, fully differentiated, or differentiated cells (Cepinskas G. , 1994; Flores S. C. , 1997; Kaufmann, 1989; Kim et al., 2018; Liu, 1989; Walker P. R. , 1991). This discrepancy in DNA damage induced ROS production between different cells types upon deletion of Ino80, may be related to cell-specific variation in oxidative stress responses which could be associated with cell vulnerability and cell specific physiological roles. Alternatively, it might be due to the fact that different cell types display differential efficiencies in the expression of genes related to antioxidant defense mechanisms (Kim et al., 2018).

In summary, we identified a novel mechanism where DNA repair by INO80 controls VSMCs metabolism through regulation of DNA damage-induced oxidative stress.

4.4. Smooth muscle INO80 prevents atherosclerosis development

Atherosclerosis is a major public health issue, and its associated clinical complications, such as myocardial infarction or stroke are the leading causes of worldwide morbidity and mortality (Xia et al., 2017). Atherosclerosis is a multi-factorial, chronic inflammatory disease involving interactions between cells which reside within the vascular wall as well as infiltrating immune cells of both the innate and adaptive immune system. Within the vascular wall, contractile quiescent VSMCs undergo a phenotypical switch and convert to a proliferative synthetic and migratory phenotype during atherosclerosis development. Furthermore, VSMCs can undergo a process of inflammatory activation, whereby VSMCs are transformed into VSMCs-derived foam cells, take up oxidized lipids and interact with infiltrating immune cells to further spread inflammation (Allahverdian et al., 2014; Miao et al., 2022).

Under normal conditions, VSMCs of Ino80 mutants revealed co-expression of ACTA2 and CD68, a macrophage marker, which indicates that VSMCs lacking Ino80 display a feature of VSMCs-derived macrophages. Furthermore, VSMCs lacking Ino80 displayed an increased *in vitro* migration. In contrast to this, i*n vivo* analysis of the synthetic features of VSMCs upon loss of Ino80 by carotid ligation assay revealed a decrease in VSMCs migration and proliferation. This contradictory finding may be attributed to non-physiological “sick” state of VSMCs lacking Ino80, whereby VSMCs do not correctly respond to environmental stimuli.

In the present study, loss of Ino80 in VSMCs led to downregulation of myocardin to haploinsufficiency levels. Myocardin has been established as a central negative regulator of VSMC inflammatory activation and pathological vascular disease (Ackers-Johnson et al., 2015). Myocardin haploinsufficiency was found to promote accelerated inflammation and atherosclerosis in hypercholesterolemic mice, in contrast to myocardin-normal controls (Ackers-Johnson et al., 2015). Furthermore, overexpression of myocardin in VSMCs reduced the expression of various inflammatory cytokines, chemokines, adhesion molecules, and upregulated anti-inflammatory mediators (Ackers-Johnson et al., 2015). Another report also associated Ino80 to increased atherosclerosis. A Ser818Cys mutation in INO80D, a subunit of the human INO80 chromatin remodeling complex, was found to induce premature atherosclerosis in humans amongst other syndromes of accelerated arterial ageing (K. Shameer et al., 2014). Certainly, this report does not mimic an Ino80 KO but nonetheless correlates defects in expression of the INO80 complex with

atherosclerosis development. It would be very interesting to examine the expression of the INO80 complex in VSMCs of human atherosclerotic plaques in comparison with human VSMCs of healthy arteries using scRNA seq to better precisely assess the impact of the Ino80 complex on atherosclerosis development in humans.

Nonetheless, in line with these reports, loss of INO80 was found to accelerate atherosclerotic development using the AAV8-PCSK9 murine model of high fat diet.

Together, these findings suggest that loss of INO80 accelerates atherosclerotic lesion development through downregulation of myocardin which amplifies inflammatory responses and lipid uptake. Myocardin expression reduces the production of pro-inflammatory cytokines, chemokines and adhesion molecules as well as pro-inflammatory pathway mediators such as CEBPB and CEBPD (Ackers-Johnson et al., 2015; Baccam et al., 2003; Poli, 1998; Sato et al., 2007). Evaluation of the changes in the expression of pro-inflammatory markers expression during atherosclerotic development upon loss of INO80 in VSMCs would enable further validation of this model. To further corroborate this, myocardin overexpression could be induced in the Ino80 VSMCs loss of function high fat diet murine model, to rescue the increase in atherosclerotic development observed upon loss of Ino80.

On the other hand, the increase in VSMCs oxidative stress upon loss of Ino80 might also contribute to the observed increase in atherosclerosis. Indeed, trapped LDL particles in the subendothelial space of vessel walls can be oxidised by ROS to form oxidised LDL which stimulates an inflammatory response, a fundamental step in atherosclerosis development (Batty et al., 2022). Therefore, increased ROS production upon loss of the DNA repair function of INO80 could lead to an increase in oxidized LDL and thereby to an upregulation of the inflammatory response. FOXO1 hyper-activation was found to be responsible for the metabolic changes observed upon Ino80 deletion, and might also regulate ROS generation. It would be interesting to investigate whether Foxo1 deletion in addition to loss of Ino80 in SMCs could rescue the increased atherosclerotic burden observed upon loss of Ino80 in SMCs.

4.5. Conclusion

In summary, this study was the first to characterize the functions of Ino80 in VSMCs in mice. The ATP-dependent INO80 chromatin remodeling complex is expressed from yeast to humans and plays a role in transcription regulation, DNA replication and DNA damage repair, three essential processes that are fundamental for cellular integrity. INO80's dynamic multi-subunit architecture though association with specialized subunits, as well as targeting of the complex to specific genes through transcription factors such as YY1, or post-translational modifications of specific subunits of the complex enables the complex to fulfill these diverse functions.

This work demonstrates how two essential functions of the INO80 chromatin remodelling complex contribute to different aspects of the INO80 loss of function phenotype in VSMCs. Global analysis of the function of INO80 in VSMCs transcriptional regulation, revealed that Ino80 plays a major role on transcriptional regulation of VSMCs and that YY1 is a fundamental co-factor of INO80 transcription regulation. Moreover, we established that the transcriptional regulation function of INO80 and YY1 regulates the expression of myocardin, a key contractility gene, which results in a decrease of VSMCs contractility, unfitting responsiveness to environmental stimuli and dysfunctional blood pressure. Additionally, we report that the DNA repair function of INO80 is essential to the regulation of VSMCs metabolism, and loss of this function leads to a switch in VSMCs metabolism through FOXO1 activation. This novel observation has not been described in any other mammalian Ino80 loss of function models using other cell types. We believe this phenomenon to be specific to VSMCs and speculate that it might occur due to the dynamic phenotypic nature of VSMCs which either show higher sensitivity to oxidative stress or are unable to reduce oxidative stress as effectively as other cell types. These changes in VSMCs function upon loss of Ino80 are most likely responsible for the increase in atherosclerosis development observed upon loss of Ino80

This study highlights how involvement of the INO80 complex in various cell specific functions takes place through tightly controlled regulatory mechanisms. Finally, these findings emphasize the significance of INO80-dependent functions on the basic physical and functional roles of VSMCs.

References

1. Ackers-Johnson, M., Talasila, A., Sage, A. P., Long, X., Bot, I., Morrell, N. W., Bennett, M. R., Miano, J. M., & Sinha, S. (2015). Myocardin Regulates Vascular Smooth Muscle Cell Inflammatory Activation and Disease. *Arteriosclerosis, Thrombosis, and Vascular Biology*, *35*(4), 817-828. https://doi.org/10.1161/atvbaha.114.305218
2. Adam, M., Robert, F., Larochelle, M., & Gaudreau, L. (2001). H2A.Z is required for global chromatin integrity and for recruitment of RNA polymerase II under specific conditions. *Mol Cell Biol*, *21*(18), 6270-6279. https://doi.org/10.1128/MCB.21.18.6270-6279.2001
3. Adam, S., Dabin, J., Chevallier, O., Leroy, O., Baldeyron, C., Corpet, A., Lomonte, P., Renaud, O., Almouzni, G., & Polo, S. E. (2016). Real-Time Tracking of Parental Histones Reveals Their Contribution to Chromatin Integrity Following DNA Damage. *Mol Cell*, *64*(1), 65-78. https://doi.org/10.1016/j.molcel.2016.08.019
4. Aikawa, Y., Morimoto, K., Yamamoto, T., Chaki, H., Hashiramoto, A., Narita, H., Hirono, S., & Shiozawa, S. (2008). Treatment of arthritis with a selective inhibitor of c-Fos/activator protein-1. *Nature Biotechnology*, *26*(7), 817-823. https://doi.org/10.1038/nbt1412
5. Albert, I., Mavrich, T. N., Tomsho, L. P., Qi, J., Zanton, S. J., Schuster, S. C., & Pugh, B. F. (2007). Translational and rotational settings of H2A.Z nucleosomes across the Saccharomyces cerevisiae genome. *Nature*, *446*(7135), 572-576. https://doi.org/10.1038/nature05632
6. Allahverdian, S., Chaabane, C., Boukais, K., Francis, G. A., & Bochaton-Piallat, M. L. (2018). Smooth muscle cell fate and plasticity in atherosclerosis. *Cardiovasc Res*, *114*(4), 540-550. https://doi.org/10.1093/cvr/cvy022
7. Allahverdian, S., Chehroudi, A. C., McManus, B. M., Abraham, T., & Francis, G. A. (2014). Contribution of Intimal Smooth Muscle Cells to Cholesterol Accumulation and Macrophage-Like Cells in Human Atherosclerosis. *Circulation*, *129*(15), 1551-1559. https://doi.org/10.1161/circulationaha.113.005015
8. Allshire, R. C., & Madhani, H. D. (2018). Ten principles of heterochromatin formation and function. *Nat Rev Mol Cell Biol*, *19*(4), 229-244. https://doi.org/10.1038/nrm.2017.119
9. Amitai, A., Seeber, A., Gasser, S. M., & Holcman, D. (2017). Visualization of Chromatin Decompaction and Break Site Extrusion as Predicted by Statistical Polymer Modeling of Single-Locus Trajectories. *Cell Rep*, *18*(5), 1200-1214. https://doi.org/10.1016/j.celrep.2017.01.018
10. Annunziato, A. (2008). DNA Packaging: Nucleosomes and Chromatin. *1*(1), 2.
11. Aramayo, R. J., Willhoft, O., Ayala, R., Bythell-Douglas, R., Wigley, D. B., & Zhang, X. (2018). Cryo-EM structures of the human INO80 chromatin-remodeling complex. *Nature Structural & Molecular Biology*, *25*(1), 37-44. https://doi.org/10.1038/s41594-017-0003-7
12. Au, T. J., Rodriguez, J., Vincent, J. A., & Tsukiyama, T. (2011). ATP-Dependent Chromatin Remodeling Factors Tune S Phase Checkpoint Activity. *Molecular and Cellular Biology*, *31*(22), 4454-4463. https://doi.org/10.1128/mcb.05931-11
13. Avila-Flores, A., Arranz-Nicolas, J., & Merida, I. (2019). Transcriptional Activity of FOXO Transcription Factors Measured by Luciferase Assays. *Methods Mol Biol*, *1890*, 91-102. https://doi.org/10.1007/978-1-4939-8900-3_8

14. Baccam, M., Woo, S. Y., Vinson, C., & Bishop, G. A. (2003). CD40-mediated transcriptional regulation of the IL-6 gene in B lymphocytes: involvement of NF-kappa B, AP-1, and C/EBP. *J Immunol*, *170*(6), 3099-3108. https://doi.org/10.4049/jimmunol.170.6.3099
15. Bailey, T. L., Johnson, J., Grant, C. E., & Noble, W. S. (2015). The MEME Suite. *Nucleic Acids Res*, *43*(W1), W39-49. https://doi.org/10.1093/nar/gkv416
16. Bannister, A. J., & Kouzarides, T. (2011). Regulation of chromatin by histone modifications. *Cell Research*, *21*(3), 381-395. https://doi.org/10.1038/cr.2011.22
17. Barbaric, S., Luckenbach, T., Schmid, A., Blaschke, D., Hörz, W., & Korber, P. (2007). Redundancy of Chromatin Remodeling Pathways for the Induction of the Yeast PHO5 Promoter in Vivo. *Journal of Biological Chemistry*, *282*(38), 27610-27621. https://doi.org/10.1074/jbc.m700623200
18. Barron, J. T., Kopp, S. J., Tow, J., & Parrillo, J. E. (1994). Fatty acid, tricarboxylic acid cycle metabolites, and energy metabolism in vascular smooth muscle. *Am J Physiol*, *267*(2 Pt 2), H764-769. https://doi.org/10.1152/ajpheart.1994.267.2.H764
19. Bastos de Oliveira, F. M., Kim, D., Cussiol, J. R., Das, J., Jeong, M. C., Doerfler, L., Schmidt, K. H., Yu, H., & Smolka, M. B. (2015). Phosphoproteomics reveals distinct modes of Mec1/ATR signaling during DNA replication. *Mol Cell*, *57*(6), 1124-1132. https://doi.org/10.1016/j.molcel.2015.01.043
20. Batty, M., Bennett, M. R., & Yu, E. (2022). The Role of Oxidative Stress in Atherosclerosis. *Cells*, *11*(23), 3843. https://doi.org/10.3390/cells11233843
21. Bedford, M. T., & Clarke, S. G. (2009). Protein arginine methylation in mammals: who, what, and why. *Mol Cell*, *33*(1), 1-13. https://doi.org/10.1016/j.molcel.2008.12.013
22. Bennett, M. R., Sinha, S., & Owens, G. K. (2016). Vascular Smooth Muscle Cells in Atherosclerosis. *Circ Res*, *118*(4), 692-702. https://doi.org/10.1161/CIRCRESAHA.115.306361
23. Beshnova, D. A., Cherstvy, A. G., Vainshtein, Y., & Teif, V. B. (2014). Regulation of the Nucleosome Repeat Length In Vivo by the DNA Sequence, Protein Concentrations and Long-Range Interactions. *PLoS Computational Biology*, *10*(7), e1003698. https://doi.org/10.1371/journal.pcbi.1003698
24. Biggs, W. H., 3rd, Meisenhelder, J., Hunter, T., Cavenee, W. K., & Arden, K. C. (1999). Protein kinase B/Akt-mediated phosphorylation promotes nuclear exclusion of the winged helix transcription factor FKHR1. *Proc Natl Acad Sci U S A*, *96*(13), 7421-7426. https://doi.org/10.1073/pnas.96.13.7421
25. Billah, M. M. (1993). Phospholipase D and cell signaling. *Curr Opin Immunol*, *5*(1), 114-123. https://doi.org/10.1016/0952-7915(93)90090-f
26. Billups, D., Billups, B., Challiss, R. A., & Nahorski, S. R. (2006). Modulation of Gq-protein-coupled inositol trisphosphate and Ca2+ signaling by the membrane potential. *J Neurosci*, *26*(39), 9983-9995. https://doi.org/10.1523/JNEUROSCI.2773-06.2006
27. Binz, S. K., Lao, Y., Lowry, D. F., & Wold, M. S. (2003). The Phosphorylation Domain of the 32-kDa Subunit of Replication Protein A (RPA) Modulates RPA-DNA Interactions. *Journal of Biological Chemistry*, *278*(37), 35584-35591. https://doi.org/10.1074/jbc.m305388200
28. Binz, S. K., Sheehan, A. M., & Wold, M. S. (2004). Replication protein A phosphorylation and the cellular response to DNA damage. *DNA Repair (Amst)*, *3*(8-9), 1015-1024. https://doi.org/10.1016/j.dnarep.2004.03.028

29. Bjergbaek, L., Cobb, J. A., Tsai-Pflugfelder, M., & Gasser, S. M. (2005). Mechanistically distinct roles for Sgs1p in checkpoint activation and replication fork maintenance. *EMBO J*, *24*(2), 405-417. https://doi.org/10.1038/sj.emboj.7600511
30. Bjørklund, M. M., Hollensen, A. K., Hagensen, M. K., Dagnæs-Hansen, F., Christoffersen, C., Mikkelsen, J. G., & Bentzon, J. F. (2014). Induction of Atherosclerosis in Mice and Hamsters Without Germline Genetic Engineering. *Circulation Research*, *114*(11), 1684-1689. https://doi.org/10.1161/circresaha.114.302937
31. Bochaton-Piallat, M. L., Gabbiani, F., Ropraz, P., & Gabbiani, G. (1993). Age influences the replicative activity and the differentiation features of cultured rat aortic smooth muscle cell populations and clones. *Arteriosclerosis and Thrombosis: A Journal of Vascular Biology*, *13*(10), 1449-1455. https://doi.org/10.1161/01.atv.13.10.1449
32. Bolger, A. M., Lohse, M., & Usadel, B. (2014). Trimmomatic: a flexible trimmer for Illumina sequence data. *Bioinformatics*, *30*(15), 2114-2120. https://doi.org/10.1093/bioinformatics/btu170
33. Bolz, S. S., Vogel, L., Sollinger, D., Derwand, R., de Wit, C., Loirand, G., & Pohl, U. (2003). Nitric oxide-induced decrease in calcium sensitivity of resistance arteries is attributable to activation of the myosin light chain phosphatase and antagonized by the RhoA/Rho kinase pathway. *Circulation*, *107*(24), 3081-3087. https://doi.org/10.1161/01.CIR.0000074202.19612.8C
34. Bonventre, J. V. (1992). Phospholipase A2 and signal transduction. *J Am Soc Nephrol*, *3*(2), 128-150. https://doi.org/10.1681/ASN.V32128
35. Borgstahl, G. E., Brader, K., Mosel, A., Liu, S., Kremmer, E., Goettsch, K. A., Kolar, C., Nasheuer, H. P., & Oakley, G. G. (2014). Interplay of DNA damage and cell cycle signaling at the level of human replication protein A. *DNA Repair (Amst)*, *21*, 12-23. https://doi.org/10.1016/j.dnarep.2014.05.005
36. Bouabe, H., & Okkenhaug, K. (2013). Gene targeting in mice: a review. *Methods Mol Biol*, *1064*, 315-336. https://doi.org/10.1007/978-1-62703-601-6_23
37. Brahma, S., Udugama, M. I., Kim, J., Hada, A., Bhardwaj, S. K., Hailu, S. G., Lee, T. H., & Bartholomew, B. (2017). INO80 exchanges H2A.Z for H2A by translocating on DNA proximal to histone dimers. *Nat Commun*, *8*, 15616. https://doi.org/10.1038/ncomms15616
38. Bravo-Sagua, R., Parra, V., Munoz-Cordova, F., Sanchez-Aguilera, P., Garrido, V., Contreras-Ferrat, A., Chiong, M., & Lavandero, S. (2020). Sarcoplasmic reticulum and calcium signaling in muscle cells: Homeostasis and disease. *Int Rev Cell Mol Biol*, *350*, 197-264. https://doi.org/10.1016/bs.ircmb.2019.12.007
39. Brehove, M., Wang, T., North, J., Luo, Y., Dreher, S. J., Shimko, J. C., Ottesen, J. J., Luger, K., & Poirier, M. G. (2015). Histone core phosphorylation regulates DNA accessibility. *J Biol Chem*, *290*(37), 22612-22621. https://doi.org/10.1074/jbc.M115.661363
40. Briet, M., & Schiffrin, E. L. (2013). Treatment of Arterial Remodeling in Essential Hypertension. *Current Hypertension Reports*, *15*(1), 3-9. https://doi.org/10.1007/s11906-012-0325-0
41. Brown, A. K., & Webb, A. E. (2018). Regulation of FOXO Factors in Mammalian Cells. *Curr Top Dev Biol*, *127*, 165-192. https://doi.org/10.1016/bs.ctdb.2017.10.006
42. Brown, B. A., Williams, H., Bond, A. R., Angelini, G. D., Johnson, J. L., & George, S. J. (2018). Carotid artery ligation induced intimal thickening and proliferation is

unaffected by ageing. *Journal of Cell Communication and Signaling*, *12*(3), 529-537. https://doi.org/10.1007/s12079-017-0431-5

43. Brunet, A., Bonni, A., Zigmond, M. J., Lin, M. Z., Juo, P., Hu, L. S., Anderson, M. J., Arden, K. C., Blenis, J., & Greenberg, M. E. (1999). Akt promotes cell survival by phosphorylating and inhibiting a Forkhead transcription factor. *Cell*, *96*(6), 857-868. https://doi.org/10.1016/s0092-8674(00)80595-4
44. Brunet, A., Park, J., Tran, H., Hu, L. S., Hemmings, B. A., & Greenberg, M. E. (2001). Protein kinase SGK mediates survival signals by phosphorylating the forkhead transcription factor FKHRL1 (FOXO3a). *Mol Cell Biol*, *21*(3), 952-965. https://doi.org/10.1128/MCB.21.3.952-965.2001
45. Buenrostro, J. D., Giresi, P. G., Zaba, L. C., Chang, H. Y., & Greenleaf, W. J. (2013). Transposition of native chromatin for fast and sensitive epigenomic profiling of open chromatin, DNA-binding proteins and nucleosome position. *Nat Methods*, *10*(12), 1213-1218. https://doi.org/10.1038/nmeth.2688
46. Bure, I. V., & Nemtsova, M. V. (2023). Mutual Regulation of ncRNAs and Chromatin Remodeling Complexes in Normal and Pathological Conditions. *Int J Mol Sci*, *24*(9). https://doi.org/10.3390/ijms24097848
47. Burgering, B. M. (2008). A brief introduction to FOXOlogy. *Oncogene*, *27*(16), 2258-2262. https://doi.org/10.1038/onc.2008.29
48. Burgess, R. C., Rahman, S., Lisby, M., Rothstein, R., & Zhao, X. (2007). The Slx5-Slx8 complex affects sumoylation of DNA repair proteins and negatively regulates recombination. *Mol Cell Biol*, *27*(17), 6153-6162. https://doi.org/10.1128/MCB.00787-07
49. Cai, Y., Jin, J., Yao, T., Gottschalk, A. J., Swanson, S. K., Wu, S., Shi, Y., Washburn, M. P., Florens, L., Conaway, R. C., & Conaway, J. W. (2007). YY1 functions with INO80 to activate transcription. *Nat Struct Mol Biol*, *14*(9), 872-874. https://doi.org/10.1038/nsmb1276
50. Cai, Y., Jin, J., Yao, T., Gottschalk, A. J., Swanson, S. K., Wu, S., Shi, Y., Washburn, M. P., Florens, L., Conaway, R. C., & Conaway, J. W. (2007). YY1 functions with INO80 to activate transcription. *Nature Structural & Molecular Biology*, *14*(9), 872-874. https://doi.org/10.1038/nsmb1276
51. Calissi, G., Lam, E. W. F., & Link, W. (2021). Therapeutic strategies targeting FOXO transcription factors. *Nature Reviews Drug Discovery*, *20*(1), 21-38. https://doi.org/10.1038/s41573-020-0088-2
52. Campbell, G., and Campbell, J. (1995). Development of the Vessel Wall: Overview, in The Smooth Muscle Cell Molecular and Biolgoical Responses to the Extracellular Matrix In S. Schwartz, and Mecham, R. (Ed.), (pp. 1-10). Academic Press.
53. Campbell, G. R., & Campbell, J. H. (1985). Smooth muscle phenotypic changes in arterial wall homeostasis: implications for the pathogenesis of atherosclerosis. *Exp Mol Pathol*, *42*(2), 139-162. https://doi.org/10.1016/0014-4800(85)90023-1
54. Campbell, J. H. a. C., G. R. . (1987). Phenotypic modulation of smooth muscle cells in culture. In: Vascular Smooth Muscle Cells in Culture. In J. H. a. C. Campbell, G. R. (Ed.), (Vol. 1, pp. 39–55). CRC Press Inc.
55. Cao, L., Ding, J., Dong, L., Zhao, J., Su, J., Wang, L., Sui, Y., Zhao, T., Wang, F., Jin, J., & Cai, Y. (2015). Negative Regulation of p21Waf1/Cip1 by Human INO80 Chromatin Remodeling Complex Is Implicated in Cell Cycle Phase G2/M Arrest and Abnormal Chromosome Stability. *PLoS One*, *10*(9), e0137411. https://doi.org/10.1371/journal.pone.0137411

56. Caro, C. G., Pedley , T. J., Schroter, R. C., & Seed, W. A. (2011). *The systemic arteries. In: The Mechanics of the Circulation*.
57. Centa, M., Ketelhuth, D. F. J., Malin, S., & Gistera, A. (2019). Quantification of Atherosclerosis in Mice. *J Vis Exp*(148). https://doi.org/10.3791/59828
58. Cepinskas G. , K. P. R., Aw T. Y. (1994). The cytotoxicity of peroxidized omega-3 lipids on cultured human epithelial cells is related to the development of cellular GSH-dependent antioxidant systems. *Gastroenterology*, *107*, 80-86.
59. Chagin, V. O., Casas-Delucchi, C. S., Reinhart, M., Schermelleh, L., Markaki, Y., Maiser, A., Bolius, J. J., Bensimon, A., Fillies, M., Domaing, P., Rozanov, Y. M., Leonhardt, H., & Cardoso, M. C. (2016). 4D Visualization of replication foci in mammalian cells corresponding to individual replicons. *Nat Commun*, *7*, 11231. https://doi.org/10.1038/ncomms11231
60. Chamley-Campbell J, C. G. R., Ross R. (1979). <chamley-campbell-et-al-1979-the-smooth-muscle-cell-in-culture.pdf>. *Physiological Reviews*, *59*.
61. Chen, J., Kitchen, C. M., Streb, J. W., & Miano, J. M. (2002). Myocardin: a component of a molecular switch for smooth muscle differentiation. *J Mol Cell Cardiol*, *34*(10), 1345-1356. https://doi.org/10.1006/jmcc.2002.2086
62. Chen, L., Cai, Y., Jin, J., Florens, L., Swanson, S. K., Washburn, M. P., Conaway, J. W., & Conaway, R. C. (2011). Subunit organization of the human INO80 chromatin remodeling complex: an evolutionarily conserved core complex catalyzes ATP-dependent nucleosome remodeling. *J Biol Chem*, *286*(13), 11283-11289. https://doi.org/10.1074/jbc.M111.222505
63. Chen, Z., Ichetovkin, M., Kurtz, M., Zycband, E., Kawka, D., Woods, J., He, X., Plump, A. S., & Hailman, E. (2010). Cholesterol in human atherosclerotic plaque is a marker for underlying disease state and plaque vulnerability. *Lipids Health Dis*, *9*, 61. https://doi.org/10.1186/1476-511X-9-61
64. Chen, Z., Liu, M., Li, L., & Chen, L. (2018). Involvement of the Warburg effect in non-tumor diseases processes. *J Cell Physiol*, *233*(4), 2839-2849. https://doi.org/10.1002/jcp.25998
65. Cheng, J. C., Cheng, H. P., Tsai, I. C., & Jiang, M. J. (2013). ROS-mediated downregulation of MYPT1 in smooth muscle cells: a potential mechanism for the aberrant contractility in atherosclerosis. *Lab Invest*, *93*(4), 422-433. https://doi.org/10.1038/labinvest.2013.40
66. Chi, J., Crane, A., Wu, Z., & Cohen, P. (2018). Adipo-Clear: A Tissue Clearing Method for Three-Dimensional Imaging of Adipose Tissue. *J Vis Exp*(137). https://doi.org/10.3791/58271
67. Christensen, K. L., & Mulvany, M. J. (2001). Location of Resistance Arteries. *Journal of Vascular Research*, *38*(1), 1-12. https://doi.org/10.1159/000051024
68. Clapier C. R., C. B. R. (2014). Chromatin Remodeling Complexes. In *Fundamentals of Chromatin* (pp. 69–146). Springer Link.
69. Clapier, C. R., & Cairns, B. R. (2009). The biology of chromatin remodeling complexes. *Annu Rev Biochem*, *78*, 273-304. https://doi.org/10.1146/annurev.biochem.77.062706.153223
70. Clapier, C. R., Iwasa, J., Cairns, B. R., & Peterson, C. L. (2017). Mechanisms of action and regulation of ATP-dependent chromatin-remodelling complexes. *Nat Rev Mol Cell Biol*, *18*(7), 407-422. https://doi.org/10.1038/nrm.2017.26
71. Conaway, R. C., & Conaway, J. W. (2009). The INO80 chromatin remodeling complex in transcription, replication and repair. *Trends Biochem Sci*, *34*(2), 71-77. https://doi.org/10.1016/j.tibs.2008.10.010

72. Cooper, B. E. (2008). Review and update on inotropes and vasopressors. *AACN Adv Crit Care*, *19*(1), 5-13; quiz 14-15. https://doi.org/10.1097/01.AACN.0000310743.32298.1d
73. Cosgrove, M. S., Boeke, J. D., & Wolberger, C. (2004). Regulated nucleosome mobility and the histone code. *Nature Structural & Molecular Biology*, *11*(11), 1037-1043. https://doi.org/10.1038/nsmb851
74. Creeden, J. F., Nanavaty, N. S., Einloth, K. R., Gillman, C. E., Stanbery, L., Hamouda, D. M., Dworkin, L., & Nemunaitis, J. (2021). Homologous recombination proficiency in ovarian and breast cancer patients. *BMC Cancer*, *21*(1), 1154. https://doi.org/10.1186/s12885-021-08863-9
75. Davey, C. A., Sargent, D. F., Luger, K., Maeder, A. W., & Richmond, T. J. (2002). Solvent mediated interactions in the structure of the nucleosome core particle at 1.9 a resolution. *J Mol Biol*, *319*(5), 1097-1113. https://doi.org/10.1016/S0022-2836(02)00386-8
76. Davies, J. D., Carpenter, K. L., Challis, I. R., Figg, N. L., McNair, R., Proudfoot, D., Weissberg, P. L., & Shanahan, C. M. (2005). Adipocytic differentiation and liver x receptor pathways regulate the accumulation of triacylglycerols in human vascular smooth muscle cells. *J Biol Chem*, *280*(5), 3911-3919. https://doi.org/10.1074/jbc.M410075200
77. Deng, X., Prakash, A., Dhar, K., Baia, G. S., Kolar, C., Oakley, G. G., & Borgstahl, G. E. (2009). Human replication protein A-Rad52-single-stranded DNA complex: stoichiometry and evidence for strand transfer regulation by phosphorylation. *Biochemistry*, *48*(28), 6633-6643. https://doi.org/10.1021/bi900564k
78. Deng, Z., Cao, P., Wan, M. M., & Sui, G. (2010). Yin Yang 1: a multifaceted protein beyond a transcription factor. *Transcription*, *1*(2), 81-84. https://doi.org/10.4161/trns.1.2.12375
79. Dhalla, N. S., Xu, Y. J., Sheu, S. S., Tappia, P. S., & Panagia, V. (1997). Phosphatidic acid: a potential signal transducer for cardiac hypertrophy. *J Mol Cell Cardiol*, *29*(11), 2865-2871. https://doi.org/10.1006/jmcc.1997.0522
80. DiFiore, J. V., Ptacek, T. S., Wang, Y., Li, B., Simon, J. M., & Strahl, B. D. (2020). Unique and Shared Roles for Histone H3K36 Methylation States in Transcription Regulation Functions. *Cell Rep*, *31*(10), 107751. https://doi.org/10.1016/j.celrep.2020.107751
81. Dikalov, S. I., & Ungvari, Z. (2013). Role of mitochondrial oxidative stress in hypertension. *Am J Physiol Heart Circ Physiol*, *305*(10), H1417-1427. https://doi.org/10.1152/ajpheart.00089.2013
82. Dobin, A., Davis, C. A., Schlesinger, F., Drenkow, J., Zaleski, C., Jha, S., Batut, P., Chaisson, M., & Gingeras, T. R. (2013). STAR: ultrafast universal RNA-seq aligner. *Bioinformatics*, *29*(1), 15-21. https://doi.org/10.1093/bioinformatics/bts635
83. Dong, X. C. (2017). FOXO transcription factors in non-alcoholic fatty liver disease. *Liver Res*, *1*(3), 168-173. https://doi.org/10.1016/j.livres.2017.11.004
84. Draker, R., Ng, M. K., Sarcinella, E., Ignatchenko, V., Kislinger, T., & Cheung, P. (2012). A combination of H2A.Z and H4 acetylation recruits Brd2 to chromatin during transcriptional activation. *PLoS Genet*, *8*(11), e1003047. https://doi.org/10.1371/journal.pgen.1003047
85. Driska, S. P., Aksoy, M. O., & Murphy, R. A. (1981). Myosin light chain phosphorylation associated with contraction in arterial smooth muscle. *Am J Physiol*, *240*(5), C222-233. https://doi.org/10.1152/ajpcell.1981.240.5.C222

86. Durham, A. L., Speer, M. Y., Scatena, M., Giachelli, C. M., & Shanahan, C. M. (2018). Role of smooth muscle cells in vascular calcification: implications in atherosclerosis and arterial stiffness. *Cardiovasc Res*, *114*(4), 590-600. https://doi.org/10.1093/cvr/cvy010
87. Ebbert, R., Birkmann, A., & Schuller, H. J. (1999). The product of the SNF2/SWI2 paralogue INO80 of Saccharomyces cerevisiae required for efficient expression of various yeast structural genes is part of a high-molecular-weight protein complex. *Mol Microbiol*, *32*(4), 741-751. https://doi.org/10.1046/j.1365-2958.1999.01390.x
88. Eijkelenboom, A., & Burgering, B. M. (2013). FOXOs: signalling integrators for homeostasis maintenance. *Nat Rev Mol Cell Biol*, *14*(2), 83-97. https://doi.org/10.1038/nrm3507
89. Esler, M., Lambert, E., & Schlaich, M. (2010). Point: Chronic activation of the sympathetic nervous system is the dominant contributor to systemic hypertension. *J Appl Physiol (1985)*, *109*(6), 1996-1998; discussion 2016. https://doi.org/10.1152/japplphysiol.00182.2010
90. Essaghir, A., Dif, N., Marbehant, C. Y., Coffer, P. J., & Demoulin, J. B. (2009). The transcription of FOXO genes is stimulated by FOXO3 and repressed by growth factors. *J Biol Chem*, *284*(16), 10334-10342. https://doi.org/10.1074/jbc.M808848200
91. Essers, M. A., Weijzen, S., de Vries-Smits, A. M., Saarloos, I., de Ruiter, N. D., Bos, J. L., & Burgering, B. M. (2004). FOXO transcription factor activation by oxidative stress mediated by the small GTPase Ral and JNK. *EMBO J*, *23*(24), 4802-4812. https://doi.org/10.1038/sj.emboj.7600476
92. Falbo, K. B., Alabert, C., Katou, Y., Wu, S., Han, J., Wehr, T., Xiao, J., He, X., Zhang, Z., Shi, Y., Shirahige, K., Pasero, P., & Shen, X. (2009). Involvement of a chromatin remodeling complex in damage tolerance during DNA replication. *Nat Struct Mol Biol*, *16*(11), 1167-1172. https://doi.org/10.1038/nsmb.1686
93. Flaus, A., Martin, D. M., Barton, G. J., & Owen-Hughes, T. (2006). Identification of multiple distinct Snf2 subfamilies with conserved structural motifs. *Nucleic Acids Res*, *34*(10), 2887-2905. https://doi.org/10.1093/nar/gkl295
94. Flemming, W. (1882). Zellsubstanz, Kern und Zelltheilung. In Vogel (Ed.).
95. Flores S. C. , M. J. M. (1997). Redox regulation by the HIV-1 Tat transcriptional factor. In C. S. Harbor (Ed.), (pp. 117-138). Cold Spring Harbor Laboratory Press.
96. Flotow, H., Graves, P. R., Wang, A. Q., Fiol, C. J., Roeske, R. W., & Roach, P. J. (1990). Phosphate groups as substrate determinants for casein kinase I action. *J Biol Chem*, *265*(24), 14264-14269. https://www.ncbi.nlm.nih.gov/pubmed/2117608
97. https://www.sciencedirect.com/science/article/pii/S0021925818772955?via%3Dihub
98. Furuyama, T., Nakazawa, T., Nakano, I., & Mori, N. (2000). Identification of the differential distribution patterns of mRNAs and consensus binding sequences for mouse DAF-16 homologues. *Biochem J*, *349*(Pt 2), 629-634. https://doi.org/10.1042/0264-6021:3490629
99. Ganitkevich, V. Y., & Isenberg, G. (1991). Depolarization-mediated intracellular calcium transients in isolated smooth muscle cells of guinea-pig urinary bladder. *J Physiol*, *435*, 187-205. https://doi.org/10.1113/jphysiol.1991.sp018505
100. Giaimo, B. D., Ferrante, F., Herchenröther, A., Hake, S. B., & Borggrefe, T. (2019). The histone variant H2A.Z in gene regulation. *Epigenetics & Chromatin*, *12*(1). https://doi.org/10.1186/s13072-019-0274-9

101. Gistera, A., & Hansson, G. K. (2017). The immunology of atherosclerosis. *Nat Rev Nephrol*, *13*(6), 368-380. https://doi.org/10.1038/nrneph.2017.51
102. Goodarzi, A. A., & Jeggo, P. A. (2012). The Heterochromatic Barrier to DNA Double Strand Break Repair: How to Get the Entry Visa. *International Journal of Molecular Sciences*, *13*(12), 11844-11860. https://doi.org/10.3390/ijms130911844
103. Grabiec, A. M., Angiolilli, C., Hartkamp, L. M., van Baarsen, L. G., Tak, P. P., & Reedquist, K. A. (2015). JNK-dependent downregulation of FoxO1 is required to promote the survival of fibroblast-like synoviocytes in rheumatoid arthritis. *Ann Rheum Dis*, *74*(9), 1763-1771. https://doi.org/10.1136/annrheumdis-2013-203610
104. Greer, E. L., Oskoui, P. R., Banko, M. R., Maniar, J. M., Gygi, M. P., Gygi, S. P., & Brunet, A. (2007). The energy sensor AMP-activated protein kinase directly regulates the mammalian FOXO3 transcription factor. *J Biol Chem*, *282*(41), 30107-30119. https://doi.org/10.1074/jbc.M705325200
105. Hargreaves, D. C., & Crabtree, G. R. (2011). ATP-dependent chromatin remodeling: genetics, genomics and mechanisms. *Cell Res*, *21*(3), 396-420. https://doi.org/10.1038/cr.2011.32
106. Hauer, M. H., Seeber, A., Singh, V., Thierry, R., Sack, R., Amitai, A., Kryzhanovska, M., Eglinger, J., Holcman, D., Owen-Hughes, T., & Gasser, S. M. (2017). Histone degradation in response to DNA damage enhances chromatin dynamics and recombination rates. *Nat Struct Mol Biol*, *24*(2), 99-107. https://doi.org/10.1038/nsmb.3347
107. He, W. Q., Peng, Y. J., Zhang, W. C., Lv, N., Tang, J., Chen, C., Zhang, C. H., Gao, S., Chen, H. Q., Zhi, G., Feil, R., Kamm, K. E., Stull, J. T., Gao, X., & Zhu, M. S. (2008). Myosin light chain kinase is central to smooth muscle contraction and required for gastrointestinal motility in mice. *Gastroenterology*, *135*(2), 610-620. https://doi.org/10.1053/j.gastro.2008.05.032
108. Hedin, U., & Thyberg, J. (1987). Plasma fibronectin promotes modulation of arterial smooth-muscle cells from contractile to synthetic phenotype. *Differentiation*, *33*(3), 239-246. https://doi.org/10.1111/j.1432-0436.1987.tb01563.x
109. Herrera, A. M., McParland, B. E., Bienkowska, A., Tait, R., Pare, P. D., & Seow, C. Y. (2005). 'Sarcomeres' of smooth muscle: functional characteristics and ultrastructural evidence. *J Cell Sci*, *118*(Pt 11), 2381-2392. https://doi.org/10.1242/jcs.02368
110. Herzog, W., & Ait-Haddou, R. (2002). Considerations on muscle contraction. *J Electromyogr Kinesiol*, *12*(6), 425-433. https://doi.org/10.1016/s1050-6411(02)00036-6
111. Hess, J., Angel, P., & Schorpp-Kistner, M. (2004). AP-1 subunits: quarrel and harmony among siblings. *J Cell Sci*, *117*(Pt 25), 5965-5973. https://doi.org/10.1242/jcs.01589
112. Higuchi, S., Ohtsu, H., Suzuki, H., Shirai, H., Frank, G. D., & Eguchi, S. (2007). Angiotensin II signal transduction through the AT1 receptor: novel insights into mechanisms and pathophysiology. *Clin Sci (Lond)*, *112*(8), 417-428. https://doi.org/10.1042/CS20060342
113. Hintermair, C., Heidemann, M., Koch, F., Descostes, N., Gut, M., Gut, I., Fenouil, R., Ferrier, P., Flatley, A., Kremmer, E., Chapman, R. D., Andrau, J. C., & Eick, D. (2012). Threonine-4 of mammalian RNA polymerase II CTD is targeted by

Polo-like kinase 3 and required for transcriptional elongation. *EMBO J*, *31*(12), 2784-2797. https://doi.org/10.1038/emboj.2012.123

114. Hirsch, D., Stahl, A., & Lodish, H. F. (1998). A family of fatty acid transporters conserved from mycobacterium to man. *Proc Natl Acad Sci U S A*, *95*(15), 8625-8629. https://doi.org/10.1073/pnas.95.15.8625
115. Ho, K. K., McGuire, V. A., Koo, C. Y., Muir, K. W., de Olano, N., Maifoshie, E., Kelly, D. J., McGovern, U. B., Monteiro, L. J., Gomes, A. R., Nebreda, A. R., Campbell, D. G., Arthur, J. S., & Lam, E. W. (2012). Phosphorylation of FOXO3a on Ser-7 by p38 promotes its nuclear localization in response to doxorubicin. *J Biol Chem*, *287*(2), 1545-1555. https://doi.org/10.1074/jbc.M111.284224
116. Ho, L., & Crabtree, G. R. (2010). Chromatin remodelling during development. *Nature*, *463*(7280), 474-484. https://doi.org/10.1038/nature08911
117. Hofmann, F. (2021). Encyclopedia of Molecular Pharmacology. In S. Offermanns & W. Rosenthal (Eds.), (pp. 1445–1450). Springer. https://doi.org/10.1007/978-3-030-57401-7
118. Hogan, C. J., Aligianni, S., Durand-Dubief, M., Persson, J., Will, W. R., Webster, J., Wheeler, L., Mathews, C. K., Elderkin, S., Oxley, D., Ekwall, K., & Varga-Weisz, P. D. (2010). Fission yeast Iec1-ino80-mediated nucleosome eviction regulates nucleotide and phosphate metabolism. *Mol Cell Biol*, *30*(3), 657-674. https://doi.org/10.1128/MCB.01117-09
119. Holtwick, R., Gotthardt, M., Skryabin, B., Steinmetz, M., Potthast, R., Zetsche, B., Hammer, R. E., Herz, J., & Kuhn, M. (2002). Smooth muscle-selective deletion of guanylyl cyclase-A prevents the acute but not chronic effects of ANP on blood pressure. *Proceedings of the National Academy of Sciences*, *99*(10), 7142-7147. https://doi.org/10.1073/pnas.102650499
120. **H**olzapfel G A, G. T. C. (2000). A New Constitutive Framework for Arterial Wall Mechanics and a Comparative Study of Material Models. *Journal of Elasticity 61*, 1.
121. Hong, S. H., Lee, K. S., Kwak, S. J., Kim, A. K., Bai, H., Jung, M. S., Kwon, O. Y., Song, W. J., Tatar, M., & Yu, K. (2012). Minibrain/Dyrk1a regulates food intake through the Sir2-FOXO-sNPF/NPY pathway in Drosophila and mammals. *PLoS Genet*, *8*(8), e1002857. https://doi.org/10.1371/journal.pgen.1002857
122. Horigome, C., Bustard, D. E., Marcomini, I., Delgoshaie, N., Tsai-Pflugfelder, M., Cobb, J. A., & Gasser, S. M. (2016). PolySUMOylation by Siz2 and Mms21 triggers relocation of DNA breaks to nuclear pores through the Slx5/Slx8 STUbL. *Genes Dev*, *30*(8), 931-945. https://doi.org/10.1101/gad.277665.116
123. Horigome, C., Oma, Y., Konishi, T., Schmid, R., Marcomini, I., Hauer, M. H., Dion, V., Harata, M., & Gasser, S. M. (2014). SWR1 and INO80 chromatin remodelers contribute to DNA double-strand break perinuclear anchorage site choice. *Mol Cell*, *55*(4), 626-639. https://doi.org/10.1016/j.molcel.2014.06.027
124. Hu, M. C., Lee, D. F., Xia, W., Golfman, L. S., Ou-Yang, F., Yang, J. Y., Zou, Y., Bao, S., Hanada, N., Saso, H., Kobayashi, R., & Hung, M. C. (2004). IkappaB kinase promotes tumorigenesis through inhibition of forkhead FOXO3a. *Cell*, *117*(2), 225-237. https://doi.org/10.1016/s0092-8674(04)00302-2
125. Huang, H., Regan, K. M., Lou, Z., Chen, J., & Tindall, D. J. (2006). CDK2-dependent phosphorylation of FOXO1 as an apoptotic response to DNA damage. *Science*, *314*(5797), 294-297. https://doi.org/10.1126/science.1130512
126. Huang, J., Wang, T., Wright, A. C., Yang, J., Zhou, S., Li, L., Yang, J., Small, A., & Parmacek, M. S. (2015). Myocardin is required for maintenance of vascular and visceral smooth muscle homeostasis during postnatal development.

Proceedings of the National Academy of Sciences, *112*(14), 4447-4452. https://doi.org/10.1073/pnas.1420363112
127. Hughes, A. L., & Rando, O. J. (2014). Mechanisms Underlying Nucleosome Positioning In Vivo. *Annual Review of Biophysics*, *43*(1), 41-63. https://doi.org/10.1146/annurev-biophys-051013-023114
128. Hustedt, N., Seeber, A., Sack, R., Tsai-Pflugfelder, M., Bhullar, B., Vlaming, H., van Leeuwen, F., Guenole, A., van Attikum, H., Srivas, R., Ideker, T., Shimada, K., & Gasser, S. M. (2015). Yeast PP4 interacts with ATR homolog Ddc2-Mec1 and regulates checkpoint signaling. *Mol Cell*, *57*(2), 273-289. https://doi.org/10.1016/j.molcel.2014.11.016
129. Hyde-DeRuyscher, R. P., Jennings, E., & Shenk, T. (1995). DNA binding sites for the transcriptional activator/repressor YY1. *Nucleic Acids Res*, *23*(21), 4457-4465. https://doi.org/10.1093/nar/23.21.4457
130. Ignarro, L. J. (2002). Nitric oxide as a unique signaling molecule in the vascular system: a historical overview. *J Physiol Pharmacol*, *53*(4 Pt 1), 503-514. https://www.ncbi.nlm.nih.gov/pubmed/12512688
131. Imamura, M., Long, X., Nanda, V., & Miano, J. M. (2010). Expression and functional activity of four myocardin isoforms. *Gene*, *464*(1-2), 1-10. https://doi.org/10.1016/j.gene.2010.03.012
132. Iwasaki, W., Miya, Y., Horikoshi, N., Osakabe, A., Taguchi, H., Tachiwana, H., Shibata, T., Kagawa, W., & Kurumizaka, H. (2013). Contribution of histone N-terminal tails to the structure and stability of nucleosomes. *FEBS Open Bio*, *3*, 363-369. https://doi.org/10.1016/j.fob.2013.08.007
133. Jeronimo, C., Watanabe, S., Craig, Craig, & Robert, F. (2015). The Histone Chaperones FACT and Spt6 Restrict H2A.Z from Intragenic Locations. *Molecular Cell*, *58*(6), 1113-1123. https://doi.org/10.1016/j.molcel.2015.03.030
134. Jiang, Y., Yin, H., & Zheng, X. L. (2010). MicroRNA-1 inhibits myocardin-induced contractility of human vascular smooth muscle cells. *Journal of Cellular Physiology*, *225*(2), 506-511. https://doi.org/10.1002/jcp.22230
135. Jin, C., Zang, C., Wei, G., Cui, K., Peng, W., Zhao, K., & Felsenfeld, G. (2009). H3.3/H2A.Z double variant-containing nucleosomes mark 'nucleosome-free regions' of active promoters and other regulatory regions. *Nat Genet*, *41*(8), 941-945. https://doi.org/10.1038/ng.409
136. Jin, J., Cai, Y., Yao, T., Gottschalk, A. J., Florens, L., Swanson, S. K., Gutierrez, J. L., Coleman, M. K., Workman, J. L., Mushegian, A., Washburn, M. P., Conaway, R. C., & Conaway, J. W. (2005). A mammalian chromatin remodeling complex with similarities to the yeast INO80 complex. *J Biol Chem*, *280*(50), 41207-41212. https://doi.org/10.1074/jbc.M509128200
137. Jonsson, Z. O., Jha, S., Wohlschlegel, J. A., & Dutta, A. (2004). Rvb1p/Rvb2p recruit Arp5p and assemble a functional Ino80 chromatin remodeling complex. *Mol Cell*, *16*(3), 465-477. https://doi.org/10.1016/j.molcel.2004.09.033
138. Ju, Y., Xu, T., Zhang, H., & Yu, A. (2014). FOXO1-dependent DNA damage repair is regulated by JNK in lung cancer cells. *Int J Oncol*, *44*(4), 1284-1292. https://doi.org/10.3892/ijo.2014.2269
139. Jungmann A, L. B., Rommelaere J, Katus H A, Mueller O J. (2017). Protocol for Efficient Generation and Characterization of Adeno-Associated Viral Vectors. *Human Gene Therapy Methods*, *28*(5), 235-246. https://doi.org/10.1089/hgtb.2017.192
140. Kang, M. A., So, E. Y., Simons, A. L., Spitz, D. R., & Ouchi, T. (2012). DNA damage induces reactive oxygen species generation through the H2AX-

Nox1/Rac1 pathway. *Cell Death Dis*, *3*(1), e249. https://doi.org/10.1038/cddis.2011.134
141. Karin, M., Liu, Z., & Zandi, E. (1997). AP-1 function and regulation. *Curr Opin Cell Biol*, *9*(2), 240-246. https://doi.org/10.1016/s0955-0674(97)80068-3
142. Kaufmann, S. H. (1989). Induction of endonucleolytic DNA cleavage in human acute myelogenous leukemia cells by etoposide, camptothecin, and other cytotoxic anticancer drugs: a cautionary note. *Cancer Research*, *49*, 5870-5878.
143. Kim, J., Kim, H., & Son, C. (2018). Tissue-Specific Profiling of Oxidative Stress-Associated Transcriptome in a Healthy Mouse Model. *International Journal of Molecular Sciences*, *19*(10), 3174. https://doi.org/10.3390/ijms19103174
144. Kim, M. J., Seo, J., Cho, K. I., Yoon, S. J., Choi, J. H., & Shin, M. S. (2016). Echocardiographic Assessment of Structural and Hemodynamic Changes in Hypertension-Related Pregnancy. *J Cardiovasc Ultrasound*, *24*(1), 28-34. https://doi.org/10.4250/jcu.2016.24.1.28
145. Kingston, R. E., Bunker C. A., Imbalzano A. N. (1996). Repression and activation by multiprotein complexes that alter chromatin structure. *Genes & Development*, *10*, 905-920. https://genesdev.cshlp.org/content/10/8/905.full.pdf
146. Kirkinezos, I. G., Bacman, S. R., Hernandez, D., Oca-Cossio, J., Arias, L. J., Perez-Pinzon, M. A., Bradley, W. G., & Moraes, C. T. (2005). CytochromecAssociation with the Inner Mitochondrial Membrane Is Impaired in the CNS of G93A-SOD1 Mice. *The Journal of Neuroscience*, *25*(1), 164-172. https://doi.org/10.1523/jneurosci.3829-04.2005
147. Klopf, E., Paskova, L., Sole, C., Mas, G., Petryshyn, A., Posas, F., Wintersberger, U., Ammerer, G., & Schuller, C. (2009). Cooperation between the INO80 complex and histone chaperones determines adaptation of stress gene transcription in the yeast Saccharomyces cerevisiae. *Mol Cell Biol*, *29*(18), 4994-5007. https://doi.org/10.1128/MCB.01858-08
148. Klopf, E., Schmidt, H. A., Clauder-Munster, S., Steinmetz, L. M., & Schuller, C. (2017). INO80 represses osmostress induced gene expression by resetting promoter proximal nucleosomes. *Nucleic Acids Res*, *45*(7), 3752-3766. https://doi.org/10.1093/nar/gkw1292
149. Klymenko, T., Papp, B., Fischle, W., Kocher, T., Schelder, M., Fritsch, C., Wild, B., Wilm, M., & Muller, J. (2006). A Polycomb group protein complex with sequence-specific DNA-binding and selective methyl-lysine-binding activities. *Genes Dev*, *20*(9), 1110-1122. https://doi.org/10.1101/gad.377406
150. Knoll, K. R., Eustermann, S., Niebauer, V., Oberbeckmann, E., Stoehr, G., Schall, K., Tosi, A., Schwarz, M., Buchfellner, A., Korber, P., & Hopfner, K.-P. (2018). The nuclear actin-containing Arp8 module is a linker DNA sensor driving INO80 chromatin remodeling. *Nature Structural & Molecular Biology*, *25*(9), 823-832. https://doi.org/10.1038/s41594-018-0115-8
151. Kompare, M., & Rizzo, W. B. (2008). Mitochondrial fatty-acid oxidation disorders. *Semin Pediatr Neurol*, *15*(3), 140-149. https://doi.org/10.1016/j.spen.2008.05.008
152. Krietenstein, N., Wal, M., Watanabe, S., Park, B., Peterson, C. L., Pugh, B. F., & Korber, P. (2016). Genomic Nucleosome Organization Reconstituted with Pure Proteins. *Cell*, *167*(3), 709-721 e712. https://doi.org/10.1016/j.cell.2016.09.045
153. Kunert, F., Metzner, F. J., Jung, J., Hopfler, M., Woike, S., Schall, K., Kostrewa, D., Moldt, M., Chen, J. X., Bantele, S., Pfander, B., Eustermann, S., & Hopfner, K. P. (2022). Structural mechanism of extranucleosomal DNA readout by the

INO80 complex. *Sci Adv*, *8*(49), eadd3189. https://doi.org/10.1126/sciadv.add3189
154. Lacolley, P., Regnault, V., Nicoletti, A., Li, Z., & Michel, J. B. (2012). The vascular smooth muscle cell in arterial pathology: a cell that can take on multiple roles. *Cardiovasc Res*, *95*(2), 194-204. https://doi.org/10.1093/cvr/cvs135
155. Lafon, A., Taranum, S., Pietrocola, F., Dingli, F., Loew, D., Brahma, S., Bartholomew, B., & Papamichos-Chronakis, M. (2015). INO80 Chromatin Remodeler Facilitates Release of RNA Polymerase II from Chromatin for Ubiquitin-Mediated Proteasomal Degradation. *Mol Cell*, *60*(5), 784-796. https://doi.org/10.1016/j.molcel.2015.10.028
156. Lai, A. Y., & Wade, P. A. (2011). Cancer biology and NuRD: a multifaceted chromatin remodelling complex. *Nat Rev Cancer*, *11*(8), 588-596. https://doi.org/10.1038/nrc3091
157. Lambert, S., Mizuno, K., Blaisonneau, J., Martineau, S., Chanet, R., Freon, K., Murray, J. M., Carr, A. M., & Baldacci, G. (2010). Homologous recombination restarts blocked replication forks at the expense of genome rearrangements by template exchange. *Mol Cell*, *39*(3), 346-359. https://doi.org/10.1016/j.molcel.2010.07.015
158. Lan, F., & Shi, Y. (2009). Epigenetic regulation: methylation of histone and non-histone proteins. *Sci China C Life Sci*, *52*(4), 311-322. https://doi.org/10.1007/s11427-009-0054-z
159. Lee, H. S., Lee, S. A., Hur, S. K., Seo, J. W., & Kwon, J. (2014). Stabilization and targeting of INO80 to replication forks by BAP1 during normal DNA synthesis. *Nat Commun*, *5*, 5128. https://doi.org/10.1038/ncomms6128
160. Lee, J. H., Kim, E. W., Croteau, D. L., & Bohr, V. A. (2020). Heterochromatin: an epigenetic point of view in aging. *Exp Mol Med*, *52*(9), 1466-1474. https://doi.org/10.1038/s12276-020-00497-4
161. Lee, K. J., Czech, L., Waypa, G. B., & Farrow, K. N. (2013). Isolation of Pulmonary Artery Smooth Muscle Cells from Neonatal Mice. *Journal of Visualized Experiments*(80). https://doi.org/10.3791/50889
162. Lees, J., Hay, J., Moles, M. W., & Michie, A. M. (2023). The discrete roles of individual FOXO transcription factor family members in B-cell malignancies. *Front Immunol*, *14*, 1179101. https://doi.org/10.3389/fimmu.2023.1179101
163. Lehtinen, M. K., Yuan, Z., Boag, P. R., Yang, Y., Villen, J., Becker, E. B., DiBacco, S., de la Iglesia, N., Gygi, S., Blackwell, T. K., & Bonni, A. (2006). A conserved MST-FOXO signaling pathway mediates oxidative-stress responses and extends life span. *Cell*, *125*(5), 987-1001. https://doi.org/10.1016/j.cell.2006.03.046
164. Li, G., & Widom, J. (2004). Nucleosomes facilitate their own invasion. *Nat Struct Mol Biol*, *11*(8), 763-769. https://doi.org/10.1038/nsmb801
165. Li, Y., LeMaire, S. A., & Shen, Y. H. (2021). Molecular and Cellular Dynamics of Aortic Aneurysms Revealed by Single-Cell Transcriptomics. *Arterioscler Thromb Vasc Biol*, *41*(11), 2671-2680. https://doi.org/10.1161/ATVBAHA.121.315852
166. Liao, Y., Smyth, G. K., & Shi, W. (2014). featureCounts: an efficient general purpose program for assigning sequence reads to genomic features. *Bioinformatics*, *30*(7), 923-930. https://doi.org/10.1093/bioinformatics/btt656
167. Libby, P., Buring, J. E., Badimon, L., Hansson, G. K., Deanfield, J., Bittencourt, M. S., Tokgozoglu, L., & Lewis, E. F. (2019). Atherosclerosis. *Nat Rev Dis Primers*, *5*(1), 56. https://doi.org/10.1038/s41572-019-0106-z

168. Link, W. (2019). Introduction to FOXO Biology. *Methods Mol Biol*, *1890*, 1-9. https://doi.org/10.1007/978-1-4939-8900-3_1
169. Link, W., & Fernandez-Marcos, P. J. (2017). FOXO transcription factors at the interface of metabolism and cancer. *Int J Cancer*, *141*(12), 2379-2391. https://doi.org/10.1002/ijc.30840
170. Liu, H., Schmidt-Supprian, M., Shi, Y., Hobeika, E., Barteneva, N., Jumaa, H., Pelanda, R., Reth, M., Skok, J., Rajewsky, K., & Shi, Y. (2007). Yin Yang 1 is a critical regulator of B-cell development. *Genes & Development*, *21*(10), 1179-1189. https://doi.org/10.1101/gad.1529307
171. Liu, L. F. (1989). DNA topoisomerase poisonous as antitumor drugs. *Annu Rev Biochem*, *58*, 351-375.
172. Liu, P., Kao, T. P., & Huang, H. (2008). CDK1 promotes cell proliferation and survival via phosphorylation and inhibition of FOXO1 transcription factor. *Oncogene*, *27*(34), 4733-4744. https://doi.org/10.1038/onc.2008.104
173. Livak, K. J., & Schmittgen, T. D. (2001). Analysis of relative gene expression data using real-time quantitative PCR and the 2(-Delta Delta C(T)) Method. *Methods*, *25*(4), 402-408. https://doi.org/10.1006/meth.2001.1262
174. Long, X., Bell, R. D., Gerthoffer, W. T., Zlokovic, B. V., & Miano, J. M. (2008). Myocardin Is Sufficient for a Smooth Muscle-Like Contractile Phenotype. *Arteriosclerosis, Thrombosis, and Vascular Biology*, *28*(8), 1505-1510. https://doi.org/10.1161/atvbaha.108.166066
175. Long, X., Tharp, D. L., Georger, M. A., Slivano, O. J., Lee, M. Y., Wamhoff, B. R., Bowles, D. K., & Miano, J. M. (2009). The Smooth Muscle Cell-restricted KCNMB1 Ion Channel Subunit Is a Direct Transcriptional Target of Serum Response Factor and Myocardin. *Journal of Biological Chemistry*, *284*(48), 33671-33682. https://doi.org/10.1074/jbc.m109.050419
176. Love, M. I., Huber, W., & Anders, S. (2014). Moderated estimation of fold change and dispersion for RNA-seq data with DESeq2. *Genome Biol*, *15*(12), 550. https://doi.org/10.1186/s13059-014-0550-8
177. Luger, K., Dechassa, M. L., & Tremethick, D. J. (2012). New insights into nucleosome and chromatin structure: an ordered state or a disordered affair? *Nature Reviews Molecular Cell Biology*, *13*(7), 436-447. https://doi.org/10.1038/nrm3382
178. Luger, K., Mader, A. W., Richmond, R. K., Sargent, D. F., & Richmond, T. J. (1997). Crystal structure of the nucleosome core particle at 2.8 A resolution. *Nature*, *389*(6648), 251-260. https://doi.org/10.1038/38444
179. Maiese, K. (2015). FoxO Transcription Factors and Regenerative Pathways in Diabetes Mellitus. *Curr Neurovasc Res*, *12*(4), 404-413. https://doi.org/10.2174/1567202612666150807112524
180. Manthorpe M , C.-J. F., Hartikka J, Felgner J, Rundell A, Margalith M, Dwarki V. (1993). Gene therapy by intramuscular injection of plasmid DNA: studies on firefly luciferase gene expression in mice *Human gene therapy*, *4*, 419. https://www.liebertpub.com/doi/pdf/10.1089/hum.1993.4.4-419?download=true
181. Marquardt, S., Escalante-Chong, R., Pho, N., Wang, J., Churchman, L. S., Springer, M., & Buratowski, S. (2014). A Chromatin-Based Mechanism for Limiting Divergent Noncoding Transcription. *Cell*, *158*(2), 462. https://doi.org/10.1016/j.cell.2014.06.038
182. Martindale, J. L., & Holbrook, N. J. (2002). Cellular response to oxidative stress: signaling for suicide and survival. *J Cell Physiol*, *192*(1), 1-15. https://doi.org/10.1002/jcp.10119

183. Matchkov, V. V., Kudryavtseva, O., & Aalkjaer, C. (2012). Intracellular Ca(2)(+) signalling and phenotype of vascular smooth muscle cells. *Basic Clin Pharmacol Toxicol*, *110*(1), 42-48. https://doi.org/10.1111/j.1742-7843.2011.00818.x
184. McDonald, O. G. (2005). Control of SRF binding to CArG box chromatin regulates smooth muscle gene expression in vivo. *Journal of Clinical Investigation*, *116*(1), 36-48. https://doi.org/10.1172/jci26505
185. Metallo, C. M., & Vander Heiden, M. G. (2010). Metabolism strikes back: metabolic flux regulates cell signaling: Figure 1. *Genes & Development*, *24*(24), 2717-2722. https://doi.org/10.1101/gad.2010510
186. Miano, J. M. (2002). Mammalian Smooth Muscle Differentiation: Origins, Markers and Transcriptional Control. In (pp. 39-59). Springer Berlin Heidelberg. https://doi.org/10.1007/978-3-540-45686-5_2
187. Miano, J. M. (2015). Myocardin in biology and disease. *J Biomed Res*, *29*(1), 3-19. https://doi.org/10.7555/JBR.29.20140151
188. Miao, G., Zhao, X., Chan, S. L., Zhang, L., Li, Y., Zhang, Y., Zhang, L., & Wang, B. (2022). Vascular smooth muscle cell c-Fos is critical for foam cell formation and atherosclerosis. *Metabolism*, *132*, 155213. https://doi.org/10.1016/j.metabol.2022.155213
189. Millan-Zambrano, G., Burton, A., Bannister, A. J., & Schneider, R. (2022). Histone post-translational modifications - cause and consequence of genome function. *Nat Rev Genet*, *23*(9), 563-580. https://doi.org/10.1038/s41576-022-00468-7
190. Mizuguchi, G., Shen, X., Landry, J., Wu, W. H., Sen, S., & Wu, C. (2004). ATP-driven exchange of histone H2AZ variant catalyzed by SWR1 chromatin remodeling complex. *Science*, *303*(5656), 343-348. https://doi.org/10.1126/science.1090701
191. Mootha, V. K., Lindgren, C. M., Eriksson, K. F., Subramanian, A., Sihag, S., Lehar, J., Puigserver, P., Carlsson, E., Ridderstrale, M., Laurila, E., Houstis, N., Daly, M. J., Patterson, N., Mesirov, J. P., Golub, T. R., Tamayo, P., Spiegelman, B., Lander, E. S., Hirschhorn, J. N., . . . Groop, L. C. (2003). PGC-1alpha-responsive genes involved in oxidative phosphorylation are coordinately downregulated in human diabetes. *Nat Genet*, *34*(3), 267-273. https://doi.org/10.1038/ng1180
192. Morales, P. E., Torres, G., Sotomayor-Flores, C., Pena-Oyarzun, D., Rivera-Mejias, P., Paredes, F., & Chiong, M. (2014). GLP-1 promotes mitochondrial metabolism in vascular smooth muscle cells by enhancing endoplasmic reticulum-mitochondria coupling. *Biochem Biophys Res Commun*, *446*(1), 410-416. https://doi.org/10.1016/j.bbrc.2014.03.004
193. Morrison, A. J. (2017). Genome maintenance functions of the INO80 chromatin remodeller. *Philosophical Transactions of the Royal Society B: Biological Sciences*, *372*(1731), 20160289. https://doi.org/10.1098/rstb.2016.0289
194. Morrison, A. J., Highland, J., Krogan, N. J., Arbel-Eden, A., Greenblatt, J. F., Haber, J. E., & Shen, X. (2004). INO80 and γ-H2AX Interaction Links ATP-Dependent Chromatin Remodeling to DNA Damage Repair. *Cell*, *119*(6), 767-775. https://doi.org/10.1016/j.cell.2004.11.037
195. Morrison, A. J., Kim, J. A., Person, M. D., Highland, J., Xiao, J., Wehr, T. S., Hensley, S., Bao, Y., Shen, J., Collins, S. R., Weissman, J. S., Delrow, J., Krogan, N. J., Haber, J. E., & Shen, X. (2007). Mec1/Tel1 phosphorylation of the INO80 chromatin remodeling complex influences DNA damage checkpoint responses. *Cell*, *130*(3), 499-511. https://doi.org/10.1016/j.cell.2007.06.010

196. Morrison, O., & Thakur, J. (2021). Molecular Complexes at Euchromatin, Heterochromatin and Centromeric Chromatin. *Int J Mol Sci*, *22*(13). https://doi.org/10.3390/ijms22136922
197. Mulvihill, E. R., Jaeger, J., Sengupta, R., Ruzzo, W. L., Reimer, C., Lukito, S., & Schwartz, S. M. (2004). Atherosclerotic plaque smooth muscle cells have a distinct phenotype. *Arterioscler Thromb Vasc Biol*, *24*(7), 1283-1289. https://doi.org/10.1161/01.ATV.0000132401.12275.0c
198. Nagai, S., Dubrana, K., Tsai-Pflugfelder, M., Davidson, M. B., Roberts, T. M., Brown, G. W., Varela, E., Hediger, F., Gasser, S. M., & Krogan, N. J. (2008). Functional targeting of DNA damage to a nuclear pore-associated SUMO-dependent ubiquitin ligase. *Science*, *322*(5901), 597-602. https://doi.org/10.1126/science.1162790
199. Nakano-Kurimoto, R., Ikeda, K., Uraoka, M., Nakagawa, Y., Yutaka, K., Koide, M., Takahashi, T., Matoba, S., Yamada, H., Okigaki, M., & Matsubara, H. (2009). Replicative senescence of vascular smooth muscle cells enhances the calcification through initiating the osteoblastic transition. *Am J Physiol Heart Circ Physiol*, *297*(5), H1673-1684. https://doi.org/10.1152/ajpheart.00455.2009
200. Nam, D., Ni, C. W., Rezvan, A., Suo, J., Budzyn, K., Llanos, A., Harrison, D. G., Giddens, D. P., & Jo, H. (2010). A model of disturbed flow-induced atherosclerosis in mouse carotid artery by partial ligation and a simple method of RNA isolation from carotid endothelium. *J Vis Exp*(40). https://doi.org/10.3791/1861
201. Nanda, V., & Miano, J. M. (2012). Leiomodin 1, a New Serum Response Factor-dependent Target Gene Expressed Preferentially in Differentiated Smooth Muscle Cells. *Journal of Biological Chemistry*, *287*(4), 2459-2467. https://doi.org/10.1074/jbc.m111.302224
202. Nasjletti, A. (1998). The Role of Eicosanoids in Angiotensin-Dependent Hypertension. *Hypertension*, *31*(1), 194-200. https://doi.org/https://doi.org/10.1161/01.HYP.31.1.194
203. Nelson, M. T., Standen, N. B., Brayden, J. E., & Worley, J. F., 3rd. (1988). Noradrenaline contracts arteries by activating voltage-dependent calcium channels. *Nature*, *336*(6197), 382-385. https://doi.org/10.1038/336382a0
204. Neuman, S. D., Ihry, R. J., Gruetzmacher, K. M., & Bashirullah, A. (2014). INO80-dependent regression of ecdysone-induced transcriptional responses regulates developmental timing in Drosophila. *Dev Biol*, *387*(2), 229-239. https://doi.org/10.1016/j.ydbio.2014.01.006
205. Neumann, F. R., Dion, V., Gehlen, L. R., Tsai-Pflugfelder, M., Schmid, R., Taddei, A., & Gasser, S. M. (2012). Targeted INO80 enhances subnuclear chromatin movement and ectopic homologous recombination. *Genes Dev*, *26*(4), 369-383. https://doi.org/10.1101/gad.176156.111
206. Ng, S. S., Yue, W. W., Oppermann, U., & Klose, R. J. (2009). Dynamic protein methylation in chromatin biology. *Cell Mol Life Sci*, *66*(3), 407-422. https://doi.org/10.1007/s00018-008-8303-z
207. Nguyen, N., Zhang, X., Olashaw, N., & Seto, E. (2004). Molecular cloning and functional characterization of the transcription factor YY2. *J Biol Chem*, *279*(24), 25927-25934. https://doi.org/10.1074/jbc.M402525200
208. Nicholson, S., Whitehouse, H., Naidoo, K., & Byers, R. J. (2011). Yin Yang 1 in human cancer. *Crit Rev Oncog*, *16*(3-4), 245-260. https://doi.org/10.1615/critrevoncog.v16.i3-4.80

209. Niocel, M., Appourchaux, R., Nguyen, X. N., Delpeuch, M., & Cimarelli, A. (2019). The DNA damage induced by the Cytosine Deaminase APOBEC3A Leads to the production of ROS. *Sci Rep*, *9*(1), 4714. https://doi.org/10.1038/s41598-019-40941-8
210. Nsiah-Sefaa, A., & McKenzie, M. (2016). Combined defects in oxidative phosphorylation and fatty acid beta-oxidation in mitochondrial disease. *Biosci Rep*, *36*(2). https://doi.org/10.1042/BSR20150295
211. O'Rourke, C., Shelton, G., Hutcheson, J. D., Burke, M. F., Martyn, T., Thayer, T. E., Shakartzi, H. R., Buswell, M. D., Tainsh, R. E., Yu, B., Bagchi, A., Rhee, D. K., Wu, C., Derwall, M., Buys, E. S., Yu, P. B., Bloch, K. D., Aikawa, E., Bloch, D. B., & Malhotra, R. (2016). Calcification of Vascular Smooth Muscle Cells and Imaging of Aortic Calcification and Inflammation. *J Vis Exp*(111). https://doi.org/10.3791/54017
212. Obsil, T., & Obsilova, V. (2008). Structure/function relationships underlying regulation of FOXO transcription factors. *Oncogene*, *27*(16), 2263-2275. https://doi.org/10.1038/onc.2008.20
213. Odaka, C., & Mizuochi, T. (2000). Angiotensin-converting enzyme inhibitor captopril prevents activation-induced apoptosis by interfering with T cell activation signals. *Clin Exp Immunol*, *121*(3), 515-522. https://doi.org/10.1046/j.1365-2249.2000.01323.x
214. Ogiwara, H., Enomoto, T., & Seki, M. (2007). The INO80 chromatin remodeling complex functions in sister chromatid cohesion. *Cell Cycle*, *6*(9), 1090-1095. https://doi.org/10.4161/cc.6.9.4130
215. Ohtsu, H., Suzuki, H., Nakashima, H., Dhobale, S., Frank, G. D., Motley, E. D., & Eguchi, S. (2006). Angiotensin II signal transduction through small GTP-binding proteins: mechanism and significance in vascular smooth muscle cells. *Hypertension*, *48*(4), 534-540. https://doi.org/10.1161/01.HYP.0000237975.90870.eb
216. Olins, A. L., & Olins, D. E. (1974). Spheroid chromatin units (v bodies). *Science*, *183*(4122), 330-332. https://doi.org/10.1126/science.183.4122.330
217. Orr, A. W., Hastings, N. E., Blackman, B. R., & Wamhoff, B. R. (2010). Complex regulation and function of the inflammatory smooth muscle cell phenotype in atherosclerosis. *J Vasc Res*, *47*(2), 168-180. https://doi.org/10.1159/000250095
218. Owens, G. K. (1995). Regulation of differentiation of vascular smooth muscle cells. *Physiol Rev*, *75*(3), 487-517. https://doi.org/10.1152/physrev.1995.75.3.487
219. Owens, G. K., Kumar, M. S., & Wamhoff, B. R. (2004). Molecular regulation of vascular smooth muscle cell differentiation in development and disease. *Physiol Rev*, *84*(3), 767-801. https://doi.org/10.1152/physrev.00041.2003
220. Papamichos-Chronakis, M., Krebs, J. E., & Peterson, C. L. (2006). Interplay between Ino80 and Swr1 chromatin remodeling enzymes regulates cell cycle checkpoint adaptation in response to DNA damage. *Genes Dev*, *20*(17), 2437-2449. https://doi.org/10.1101/gad.1440206
221. Papamichos-Chronakis, M., & Peterson, C. L. (2008). The Ino80 chromatin-remodeling enzyme regulates replisome function and stability. *Nat Struct Mol Biol*, *15*(4), 338-345. https://doi.org/10.1038/nsmb.1413
222. Papamichos-Chronakis, M., Watanabe, S., Rando, O. J., & Peterson, C. L. (2011). Global regulation of H2A.Z localization by the INO80 chromatin-remodeling enzyme is essential for genome integrity. *Cell*, *144*(2), 200-213. https://doi.org/10.1016/j.cell.2010.12.021

223. Papin, C., Humbert, O., Kalashnikova, A., Eckert, K., Morera, S., Kas, E., & Grigoriev, M. (2010). 3'- to 5' DNA unwinding by TIP49b proteins. *FEBS J*, *277*(12), 2705-2714. https://doi.org/10.1111/j.1742-464X.2010.07687.x
224. Pechanova, O., Vrankova, S., & Cebova, M. (2020). Chronic L-Name-Treatment Produces Hypertension by Different Mechanisms in Peripheral Tissues and Brain: Role of Central eNOS. *Pathophysiology*, *27*(1), 46-54. https://doi.org/10.3390/pathophysiology27010007
225. Peng, S., Li, W., Hou, N., & Huang, N. (2020). A Review of FoxO1-Regulated Metabolic Diseases and Related Drug Discoveries. *Cells*, *9*(1), 184. https://doi.org/10.3390/cells9010184
226. Poirier, M. G., Bussiek, M., Langowski, J., & Widom, J. (2008). Spontaneous access to DNA target sites in folded chromatin fibers. *J Mol Biol*, *379*(4), 772-786. https://doi.org/10.1016/j.jmb.2008.04.025
227. Poirier, M. G., Oh, E., Tims, H. S., & Widom, J. (2009). Dynamics and function of compact nucleosome arrays. *Nat Struct Mol Biol*, *16*(9), 938-944. https://doi.org/10.1038/nsmb.1650
228. Poli, J., Gasser, S. M., & Papamichos-Chronakis, M. (2017). The INO80 remodeller in transcription, replication and repair. *Philos Trans R Soc Lond B Biol Sci*, *372*(1731). https://doi.org/10.1098/rstb.2016.0290
229. Poli, J., Gerhold, C. B., Tosi, A., Hustedt, N., Seeber, A., Sack, R., Herzog, F., Pasero, P., Shimada, K., Hopfner, K. P., & Gasser, S. M. (2016). Mec1, INO80, and the PAF1 complex cooperate to limit transcription replication conflicts through RNAPII removal during replication stress. *Genes Dev*, *30*(3), 337-354. https://doi.org/10.1101/gad.273813.115
230. Poli, V. (1998). The role of C/EBP isoforms in the control of inflammatory and native immunity functions. *J Biol Chem*, *273*(45), 29279-29282. https://doi.org/10.1074/jbc.273.45.29279
231. Potente, M., Urbich, C., Sasaki, K., Hofmann, W. K., Heeschen, C., Aicher, A., Kollipara, R., DePinho, R. A., Zeiher, A. M., & Dimmeler, S. (2005). Involvement of Foxo transcription factors in angiogenesis and postnatal neovascularization. *J Clin Invest*, *115*(9), 2382-2392. https://doi.org/10.1172/JCI23126
232. Prakash, A., & Borgstahl, G. E. (2012). The structure and function of replication protein A in DNA replication. *Subcell Biochem*, *62*, 171-196. https://doi.org/10.1007/978-94-007-4572-8_10
233. Qiu, Z., Elsayed, Z., Peterkin, V., Alkatib, S., Bennett, D., & Landry, J. W. (2016). Ino80 is essential for proximal-distal axis asymmetry in part by regulating Bmp4 expression. *BMC Biology*, *14*(1). https://doi.org/10.1186/s12915-016-0238-5
234. R. W. Gilkerson, J. M. L. S., R. A. Capaldi. (2003). The cristal membrane of mitochondria is the principal siteof oxidative phosphorylation. *Federation of European Biochemical Societies*, *546*, 355-358. https://doi.org/10.1016/s0014-5793
235. Radman-Livaja, M., & Rando, O. J. (2010). Nucleosome positioning: how is it established, and why does it matter? *Dev Biol*, *339*(2), 258-266. https://doi.org/10.1016/j.ydbio.2009.06.012
236. Ragu, S., Droin, N., Matos-Rodrigues, G., Barascu, A., Caillat, S., Zarkovic, G., Siberchicot, C., Dardillac, E., Gelot, C., Guirouilh-Barbat, J., Radicella, J. P., Ishchenko, A. A., Ravanat, J. L., Solary, E., & Lopez, B. S. (2023). A noncanonical response to replication stress protects genome stability through ROS production, in an adaptive manner. *Cell Death Differ*, *30*(5), 1349-1365. https://doi.org/10.1038/s41418-023-01141-0

237. Raphel, L., Talasila, A., Cheung, C., & Sinha, S. (2012). Myocardin Overexpression Is Sufficient for Promoting the Development of a Mature Smooth Muscle Cell-Like Phenotype from Human Embryonic Stem Cells. *PLoS One*, *7*(8), e44052. https://doi.org/10.1371/journal.pone.0044052
238. Ratz, P. H., & Murphy, R. A. (1987). Contributions of intracellular and extracellular Ca2+ pools to activation of myosin phosphorylation and stress in swine carotid media. *Circ Res*, *60*(3), 410-421. https://doi.org/10.1161/01.res.60.3.410
239. Rena, G., Woods, Y. L., Prescott, A. R., Peggie, M., Unterman, T. G., Williams, M. R., & Cohen, P. (2002). Two novel phosphorylation sites on FKHR that are critical for its nuclear exclusion. *EMBO J*, *21*(9), 2263-2271. https://doi.org/10.1093/emboj/21.9.2263
240. Rhee, S., Chung, J. I., King, D. A., D'Amato, G., Paik, D. T., Duan, A., Chang, A., Nagelberg, D., Sharma, B., Jeong, Y., Diehn, M., Wu, J. C., Morrison, A. J., & Red-Horse, K. (2018). Endothelial deletion of Ino80 disrupts coronary angiogenesis and causes congenital heart disease. *Nat Commun*, *9*(1), 368. https://doi.org/10.1038/s41467-017-02796-3
241. Rhodin, J. A. G. (1980). Architecture of the Vessel Wall. In *Comprehensive Physiology* (pp. 1-31). https://doi.org/https://doi.org/10.1002/cphy.cp020201
242. Rohs, R., West, S. M., Sosinsky, A., Liu, P., Mann, R. S., & Honig, B. (2009). The role of DNA shape in protein-DNA recognition. *Nature*, *461*(7268), 1248-1253. https://doi.org/10.1038/nature08473
243. Rowe, L. A., Degtyareva, N., & Doetsch, P. W. (2008). DNA damage-induced reactive oxygen species (ROS) stress response in Saccharomyces cerevisiae. *Free Radic Biol Med*, *45*(8), 1167-1177. https://doi.org/10.1016/j.freeradbiomed.2008.07.018
244. Russell, J. A. (2019). Vasopressor therapy in critically ill patients with shock. *Intensive Care Medicine*, *45*(11), 1503-1517. https://doi.org/10.1007/s00134-019-05801-z
245. Ryu, T., Spatola, B., Delabaere, L., Bowlin, K., Hopp, H., Kunitake, R., Karpen, G. H., & Chiolo, I. (2015). Heterochromatic breaks move to the nuclear periphery to continue recombinational repair. *Nat Cell Biol*, *17*(11), 1401-1411. https://doi.org/10.1038/ncb3258
246. Rzucidlo, E. M., Martin, K. A., & Powell, R. J. (2007). Regulation of vascular smooth muscle cell differentiation. *J Vasc Surg*, *45 Suppl A*, A25-32. https://doi.org/10.1016/j.jvs.2007.03.001
247. Sakurada, S., Okamoto, H., Takuwa, N., Sugimoto, N., & Takuwa, Y. (2001). Rho activation in excitatory agonist-stimulated vascular smooth muscle. *Am J Physiol Cell Physiol*, *281*(2), C571-578. https://doi.org/10.1152/ajpcell.2001.281.2.C571
248. Salih, D. A., & Brunet, A. (2008). FoxO transcription factors in the maintenance of cellular homeostasis during aging. *Curr Opin Cell Biol*, *20*(2), 126-136. https://doi.org/10.1016/j.ceb.2008.02.005
249. Samouillan, V., Dandurand, J., Nasarre, L., Badimon, L., Lacabanne, C., & Llorente-Cortes, V. (2012). Lipid loading of human vascular smooth muscle cells induces changes in tropoelastin protein levels and physical structure. *Biophys J*, *103*(3), 532-540. https://doi.org/10.1016/j.bpj.2012.06.034
250. Sartore, G., Piarulli, F., Ragazzi, E., Burlina, S., Chilelli, N. C., Sarais, C., Marin, R., Manzato, E., Fedele, D., & Lapolla, A. (2013). Subclinical diastolic dysfunction in type 2 diabetic patients with and without carotid atherosclerosis:

relationship with glyco-oxidation, lipid-oxidation and antioxidant status. *Int J Cardiol*, *163*(2), 201-205. https://doi.org/10.1016/j.ijcard.2011.06.026
251. Sato, Y., Nishio, Y., Sekine, O., Kodama, K., Nagai, Y., Nakamura, T., Maegawa, H., & Kashiwagi, A. (2007). Increased expression of CCAAT/enhancer binding protein-beta and -delta and monocyte chemoattractant protein-1 genes in aortas from hyperinsulinaemic rats. *Diabetologia*, *50*(2), 481-489. https://doi.org/10.1007/s00125-006-0480-4
252. Schalch, T., Duda, S., Sargent, D. F., & Richmond, T. J. (2005). X-ray structure of a tetranucleosome and its implications for the chromatin fibre. *Nature*, *436*(7047), 138-141. https://doi.org/10.1038/nature03686
253. Scheede-Bergdahl, C., & Bergdahl, A. (2017). Adaptation of mitochondrial expression and ATP production in dedifferentiating vascular smooth muscle cells. *Can J Physiol Pharmacol*, *95*(12), 1473-1479. https://doi.org/10.1139/cjpp-2017-0227
254. Schutt, C., Hallmann, A., Hachim, S., Klockner, I., Valussi, M., Atzberger, A., Graumann, J., Braun, T., & Boettger, T. (2020). Linc-MYH configures INO80 to regulate muscle stem cell numbers and skeletal muscle hypertrophy. *EMBO J*, *39*(22), e105098. https://doi.org/10.15252/embj.2020105098
255. Seeber, A., Dion, V., & Gasser, S. M. (2013). Checkpoint kinases and the INO80 nucleosome remodeling complex enhance global chromatin mobility in response to DNA damage. *Genes Dev*, *27*(18), 1999-2008. https://doi.org/10.1101/gad.222992.113
256. Seeber, A., & Gasser, S. M. (2017). Chromatin organization and dynamics in double-strand break repair. *Curr Opin Genet Dev*, *43*, 9-16. https://doi.org/10.1016/j.gde.2016.10.005
257. Shameer, K., Klee, E. W., Dalenberg, A. K., & Kullo, I. J. (2014). Whole Exome Sequencing Implicates an INO80D Mutation in a Syndrome of Aortic Hypoplasia, Premature Atherosclerosis, and Arterial Stiffness. *Circulation: Cardiovascular Genetics*, *7*(5), 607-614. https://doi.org/10.1161/circgenetics.113.000233
258. Shameer, K., Klee, E. W., Dalenberg, A. K., & Kullo, I. J. (2014). Whole exome sequencing implicates an INO80D mutation in a syndrome of aortic hypoplasia, premature atherosclerosis, and arterial stiffness. *Circ Cardiovasc Genet*, *7*(5), 607-614. https://doi.org/10.1161/CIRCGENETICS.113.000233
259. Shanahan, C. M., Crouthamel, M. H., Kapustin, A., & Giachelli, C. M. (2011). Arterial calcification in chronic kidney disease: key roles for calcium and phosphate. *Circ Res*, *109*(6), 697-711. https://doi.org/10.1161/CIRCRESAHA.110.234914
260. Shen, B., Chao, L., & Chao, J. (2010). Pivotal role of JNK-dependent FOXO1 activation in downregulation of kallistatin expression by oxidative stress. *Am J Physiol Heart Circ Physiol*, *298*(3), H1048-1054. https://doi.org/10.1152/ajpheart.00826.2009
261. Shen, X., & Gorovsky, M. A. (1996). Linker histone H1 regulates specific gene expression but not global transcription in vivo. *Cell*, *86*(3), 475-483. https://doi.org/10.1016/s0092-8674(00)80120-8
262. Shen, X., Mizuguchi, G., Hamiche, A., & Wu, C. (2000). A chromatin remodelling complex involved in transcription and DNA processing. *Nature*, *406*(6795), 541-544. https://doi.org/10.1038/35020123

263. Shen, X., Ranallo, R., Choi, E., & Wu, C. (2003). Involvement of actin-related proteins in ATP-dependent chromatin remodeling. *Mol Cell*, *12*(1), 147-155. https://doi.org/10.1016/s1097-2765(03)00264-8
264. Shi, J., Yang, Y., Cheng, A., Xu, G., & He, F. (2020). Metabolism of vascular smooth muscle cells in vascular diseases. *Am J Physiol Heart Circ Physiol*, *319*(3), H613-H631. https://doi.org/10.1152/ajpheart.00220.2020
265. Shi, J., Yang, Y., Wang, Y. N., Li, Q., Xing, X., Cheng, A. Y., Zhan, X. N., Li, J., Xu, G., & He, F. (2022). Oxidative phosphorylation promotes vascular calcification in chronic kidney disease. *Cell Death Dis*, *13*(3), 229. https://doi.org/10.1038/s41419-022-04679-y
266. Shi, Y., Seto, E., Chang, L. S., & Shenk, T. (1991). Transcriptional repression by YY1, a human GLI-Kruppel-related protein, and relief of repression by adenovirus E1A protein. *Cell*, *67*(2), 377-388. https://doi.org/10.1016/0092-8674(91)90189-6
267. Shimada, K., Oma, Y., Schleker, T., Kugou, K., Ohta, K., Harata, M., & Gasser, S. M. (2008). Ino80 chromatin remodeling complex promotes recovery of stalled replication forks. *Curr Biol*, *18*(8), 566-575. https://doi.org/10.1016/j.cub.2008.03.049
268. Silver, F. H., Christiansen, D. L., & Buntin, C. M. (1989). Mechanical properties of the aorta: a review. *Crit Rev Biomed Eng*, *17*(4), 323-358. https://www.ncbi.nlm.nih.gov/pubmed/2676341
269. Sinha, S., Iyer, D., & Granata, A. (2014). Embryonic origins of human vascular smooth muscle cells: implications for in vitro modeling and clinical application. *Cell Mol Life Sci*, *71*(12), 2271-2288. https://doi.org/10.1007/s00018-013-1554-3
270. Smale, S. T., & Kadonaga, J. T. (2003). The RNA polymerase II core promoter. *Annu Rev Biochem*, *72*, 449-479. https://doi.org/10.1146/annurev.biochem.72.121801.161520
271. Sobue, K., Hayashi, K., & Nishida, W. (1999). Expressional regulation of smooth muscle cell-specific genes in association with phenotypic modulation. *Mol Cell Biochem*, *190*(1-2), 105-118. https://www.ncbi.nlm.nih.gov/pubmed/10098977
272. Somlyo, A. P., & Somlyo, A. V. (2000). Signal transduction by G-proteins, rho-kinase and protein phosphatase to smooth muscle and non-muscle myosin II. *J Physiol*, *522 Pt 2*(Pt 2), 177-185. https://doi.org/10.1111/j.1469-7793.2000.t01-2-00177.x
273. Sonntag, F., Köther, K., Schmidt, K., Weghofer, M., Raupp, C., Nieto, K., Kuck, A., Gerlach, B., Böttcher, B., Müller, O. J., Lux, K., Hörer, M., & Kleinschmidt, J. A. (2011). The Assembly-Activating Protein Promotes Capsid Assembly of Different Adeno-Associated Virus Serotypes. *Journal of Virology*, *85*(23), 12686-12697. https://doi.org/10.1128/jvi.05359-11
274. Soundararajan, M., Roos, A. K., Savitsky, P., Filippakopoulos, P., Kettenbach, A. N., Olsen, J. V., Gerber, S. A., Eswaran, J., Knapp, S., & Elkins, J. M. (2013). Structures of Down syndrome kinases, DYRKs, reveal mechanisms of kinase activation and substrate recognition. *Structure*, *21*(6), 986-996. https://doi.org/10.1016/j.str.2013.03.012
275. Soutoglou, E., & Misteli, T. (2007). Mobility and immobility of chromatin in transcription and genome stability. *Curr Opin Genet Dev*, *17*(5), 435-442. https://doi.org/10.1016/j.gde.2007.08.004

276. Sprague, A. H., & Khalil, R. A. (2009). Inflammatory cytokines in vascular dysfunction and vascular disease. *Biochem Pharmacol*, *78*(6), 539-552. https://doi.org/10.1016/j.bcp.2009.04.029
277. Steger, D. J., Haswell, E. S., Miller, A. L., Wente, S. R., & O'Shea, E. K. (2003). Regulation of chromatin remodeling by inositol polyphosphates. *Science*, *299*(5603), 114-116. https://doi.org/10.1126/science.1078062
278. Sterner, D. E., & Berger, S. L. (2000). Acetylation of histones and transcription-related factors. *Microbiol Mol Biol Rev*, *64*(2), 435-459. https://doi.org/10.1128/MMBR.64.2.435-459.2000
279. Stöhr, O., Schilbach, K., Moll, L., Hettich, M. M., Freude, S., Wunderlich, F. T., Ernst, M., Zemva, J., Brüning, J. C., Krone, W., Udelhoven, M., & Schubert, M. (2013). Insulin receptor signaling mediates APP processing and β-amyloid accumulation without altering survival in a transgenic mouse model of Alzheimer's disease. *AGE*, *35*(1), 83-101. https://doi.org/10.1007/s11357-011-9333-2
280. Strecker, J., Gupta, G. D., Zhang, W., Bashkurov, M., Landry, M. C., Pelletier, L., & Durocher, D. (2016). DNA damage signalling targets the kinetochore to promote chromatin mobility. *Nat Cell Biol*, *18*(3), 281-290. https://doi.org/10.1038/ncb3308
281. Struhl, K., & Segal, E. (2013). Determinants of nucleosome positioning. *Nat Struct Mol Biol*, *20*(3), 267-273. https://doi.org/10.1038/nsmb.2506
282. Struhl, K., & Segal, E. (2013). Determinants of nucleosome positioning. *Nature Structural & Molecular Biology*, *20*(3), 267-273. https://doi.org/10.1038/nsmb.2506
283. Studitsky, V. M., Clark, D. J., & Felsenfeld, G. (1994). A histone octamer can step around a transcribing polymerase without leaving the template. *Cell*, *76*(2), 371-382. https://doi.org/10.1016/0092-8674(94)90343-3
284. Su, J., Sui, Y., Ding, J., Li, F., Shen, S., Yang, Y., Lu, Z., Wang, F., Cao, L., Liu, X., Jin, J., & Cai, Y. (2016). Human INO80/YY1 chromatin remodeling complex transcriptionally regulates the BRCA2- and CDKN1A-interacting protein (BCCIP) in cells. *Protein & Cell*, *7*(10), 749-760. https://doi.org/10.1007/s13238-016-0306-1
285. Subramanian, A., Tamayo, P., Mootha, V. K., Mukherjee, S., Ebert, B. L., Gillette, M. A., Paulovich, A., Pomeroy, S. L., Golub, T. R., Lander, E. S., & Mesirov, J. P. (2005). Gene set enrichment analysis: a knowledge-based approach for interpreting genome-wide expression profiles. *Proc Natl Acad Sci U S A*, *102*(43), 15545-15550. https://doi.org/10.1073/pnas.0506580102
286. Sultana, R., Poon, H. F., Cai, J., Pierce, W. M., Merchant, M., Klein, J. B., Markesbery, W. R., & Butterfield, D. A. (2006). Identification of nitrated proteins in Alzheimer's disease brain using a redox proteomics approach. *Neurobiol Dis*, *22*(1), 76-87. https://doi.org/10.1016/j.nbd.2005.10.004
287. Sunayama, J., Tsuruta, F., Masuyama, N., & Gotoh, Y. (2005). JNK antagonizes Akt-mediated survival signals by phosphorylating 14-3-3. *J Cell Biol*, *170*(2), 295-304. https://doi.org/10.1083/jcb.200409117
288. Swirski, F. K., & Nahrendorf, M. (2014). Do vascular smooth muscle cells differentiate to macrophages in atherosclerotic lesions? *Circ Res*, *115*(7), 605-606. https://doi.org/10.1161/CIRCRESAHA.114.304925
289. Szerlong, H., Hinata, K., Viswanathan, R., Erdjument-Bromage, H., Tempst, P., & Cairns, B. R. (2008). The HSA domain binds nuclear actin-related proteins to

regulate chromatin-remodeling ATPases. *Nat Struct Mol Biol*, *15*(5), 469-476. https://doi.org/10.1038/nsmb.1403

290. Taddei, A., Van Houwe, G., Hediger, F., Kalck, V., Cubizolles, F., Schober, H., & Gasser, S. M. (2006). Nuclear pore association confers optimal expression levels for an inducible yeast gene. *Nature*, *441*(7094), 774-778. https://doi.org/10.1038/nature04845
291. Tang, D. D. (2015). Critical role of actin-associated proteins in smooth muscle contraction, cell proliferation, airway hyperresponsiveness and airway remodeling. *Respir Res*, *16*, 134. https://doi.org/10.1186/s12931-015-0296-1
292. Tang, J. X., Thompson, K., Taylor, R. W., & Olahova, M. (2020). Mitochondrial OXPHOS Biogenesis: Co-Regulation of Protein Synthesis, Import, and Assembly Pathways. *Int J Mol Sci*, *21*(11). https://doi.org/10.3390/ijms21113820
293. Taylor, C. W., & Tovey, S. C. (2010). IP(3) receptors: toward understanding their activation. *Cold Spring Harb Perspect Biol*, *2*(12), a004010. https://doi.org/10.1101/cshperspect.a004010
294. Te Riet, L., van Esch, J. H., Roks, A. J., van den Meiracker, A. H., & Danser, A. H. (2015). Hypertension: renin-angiotensin-aldosterone system alterations. *Circ Res*, *116*(6), 960-975. https://doi.org/10.1161/CIRCRESAHA.116.303587
295. Thoma, F., & Koller, T. (1977). Influence of histone H1 on chromatin structure. *Cell*, *12*(1), 101-107. https://doi.org/10.1016/0092-8674(77)90188-x
296. Torres, M. (2003). Mitogen-activated protein kinase pathways in redox signaling. *Front Biosci*, *8*, d369-391. https://doi.org/10.2741/999
297. Tosi, A., Haas, C., Herzog, F., Gilmozzi, A., Berninghausen, O., Ungewickell, C., Christian, Lakomek, K., Aebersold, R., Beckmann, R., & Hopfner, K.-P. (2013). Structure and Subunit Topology of the INO80 Chromatin Remodeler and Its Nucleosome Complex. *Cell*, *154*(6), 1207-1219. https://doi.org/10.1016/j.cell.2013.08.016
298. Touyz, R. M., Alves-Lopes, R., Rios, F. J., Camargo, L. L., Anagnostopoulou, A., Arner, A., & Montezano, A. C. (2018). Vascular smooth muscle contraction in hypertension. *Cardiovasc Res*, *114*(4), 529-539. https://doi.org/10.1093/cvr/cvy023
299. Touyz, R. M., & Berry, C. (2002). Recent advances in angiotensin II signaling. *Braz J Med Biol Res*, *35*(9), 1001-1015. https://doi.org/10.1590/s0100-879x2002000900001
300. Touyz, R. M., & Schiffrin, E. L. (1999). Ang II-stimulated superoxide production is mediated via phospholipase D in human vascular smooth muscle cells. *Hypertension*, *34*(4 Pt 2), 976-982. https://doi.org/10.1161/01.hyp.34.4.976
301. Touyz, R. M., & Schiffrin, E. L. (2000). Signal transduction mechanisms mediating the physiological and pathophysiological actions of angiotensin II in vascular smooth muscle cells. *Pharmacol Rev*, *52*(4), 639-672. https://www.ncbi.nlm.nih.gov/pubmed/11121512
302. Tramantano, M., Sun, L., Au, C., Labuz, D., Liu, Z., Chou, M., Shen, C., & Luk, E. (2016). Constitutive turnover of histone H2A.Z at yeast promoters requires the preinitiation complex. *Elife*, *5*. https://doi.org/10.7554/eLife.14243
303. Trojer, P., & Reinberg, D. (2007). Facultative heterochromatin: is there a distinctive molecular signature? *Mol Cell*, *28*(1), 1-13. https://doi.org/10.1016/j.molcel.2007.09.011
304. Tsukuda, T., Fleming, A. B., Nickoloff, J. A., & Osley, M. A. (2005). Chromatin remodelling at a DNA double-strand break site in Saccharomyces cerevisiae. *Nature*, *438*(7066), 379-383. https://doi.org/10.1038/nature04148

305. Tyagi, M., Imam, N., Verma, K., & Patel, A. K. (2016). Chromatin remodelers: We are the drivers!! *Nucleus*, *7*(4), 388-404. https://doi.org/10.1080/19491034.2016.1211217
306. Udugama, M., Sabri, A., & Bartholomew, B. (2011). The INO80 ATP-dependent chromatin remodeling complex is a nucleosome spacing factor. *Mol Cell Biol*, *31*(4), 662-673. https://doi.org/10.1128/MCB.01035-10
307. Ueda, S., Masutani, H., Nakamura, H., Tanaka, T., Ueno, M., & Yodoi, J. (2002). Redox control of cell death. *Antioxid Redox Signal*, *4*(3), 405-414. https://doi.org/10.1089/15230860260196209
308. Uehata, M., Ishizaki, T., Satoh, H., Ono, T., Kawahara, T., Morishita, T., Tamakawa, H., Yamagami, K., Inui, J., Maekawa, M., & Narumiya, S. (1997). Calcium sensitization of smooth muscle mediated by a Rho-associated protein kinase in hypertension. *Nature*, *389*(6654), 990-994. https://doi.org/10.1038/40187
309. Ushio-Fukai, M., Griendling, K. K., Akers, M., Lyons, P. R., & Alexander, R. W. (1998). Temporal dispersion of activation of phospholipase C-beta1 and -gamma isoforms by angiotensin II in vascular smooth muscle cells. Role of alphaq/11, alpha12, and beta gamma G protein subunits. *J Biol Chem*, *273*(31), 19772-19777. https://doi.org/10.1074/jbc.273.31.19772
310. Valko, M., Leibfritz, D., Moncol, J., Cronin, M. T., Mazur, M., & Telser, J. (2007). Free radicals and antioxidants in normal physiological functions and human disease. *Int J Biochem Cell Biol*, *39*(1), 44-84. https://doi.org/10.1016/j.biocel.2006.07.001
311. van Attikum, H., Fritsch, O., & Gasser, S. M. (2007). Distinct roles for SWR1 and INO80 chromatin remodeling complexes at chromosomal double-strand breaks. *EMBO J*, *26*(18), 4113-4125. https://doi.org/10.1038/sj.emboj.7601835
312. van Attikum, H., Fritsch, O., Hohn, B., & Gasser, S. M. (2004). Recruitment of the INO80 complex by H2A phosphorylation links ATP-dependent chromatin remodeling with DNA double-strand break repair. *Cell*, *119*(6), 777-788. https://doi.org/10.1016/j.cell.2004.11.033
313. Van Breemen, C., Farinas, B. R., Gerba, P., & McNaughton, E. D. (1972). Excitation-contraction coupling in rabbit aorta studied by the lanthanum method for measuring cellular calcium influx. *Circ Res*, *30*(1), 44-54. https://doi.org/10.1161/01.res.30.1.44
314. van der Horst, A., & Burgering, B. M. (2007). Stressing the role of FoxO proteins in lifespan and disease. *Nat Rev Mol Cell Biol*, *8*(6), 440-450. https://doi.org/10.1038/nrm2190
315. van Holde, K., & Zlatanova, J. (2007). Chromatin fiber structure: Where is the problem now? *Semin Cell Dev Biol*, *18*(5), 651-658. https://doi.org/10.1016/j.semcdb.2007.08.005
316. Vanhoutte, P. M., Shimokawa, H., Feletou, M., & Tang, E. H. (2017). Endothelial dysfunction and vascular disease - a 30th anniversary update. *Acta Physiol (Oxf)*, *219*(1), 22-96. https://doi.org/10.1111/apha.12646
317. VanValkinburgh, D., Kerndt, C. C., & Hashmi, M. F. (2024). Inotropes and Vasopressors. In *StatPearls*. https://www.ncbi.nlm.nih.gov/pubmed/29494018
318. Vassileva, I., Yanakieva, I., Peycheva, M., Gospodinov, A., & Anachkova, B. (2014). The mammalian INO80 chromatin remodeling complex is required for replication stress recovery. *Nucleic Acids Res*, *42*(14), 9074-9086. https://doi.org/10.1093/nar/gku605

319. Vella, P., Barozzi, I., Cuomo, A., Bonaldi, T., & Pasini, D. (2012). Yin Yang 1 extends the Myc-related transcription factors network in embryonic stem cells. *Nucleic Acids Res*, *40*(8), 3403-3418. https://doi.org/10.1093/nar/gkr1290
320. Venkatesh, S., Smolle, M., Li, H., Gogol, M. M., Saint, M., Kumar, S., Natarajan, K., & Workman, J. L. (2012). Set2 methylation of histone H3 lysine 36 suppresses histone exchange on transcribed genes. *Nature*, *489*(7416), 452-455. https://doi.org/10.1038/nature11326
321. Venkatesh, S., & Workman, J. L. (2015). Histone exchange, chromatin structure and the regulation of transcription. *Nat Rev Mol Cell Biol*, *16*(3), 178-189. https://doi.org/10.1038/nrm3941
322. Verheul, T. C. J., van Hijfte, L., Perenthaler, E., & Barakat, T. S. (2020). The Why of YY1: Mechanisms of Transcriptional Regulation by Yin Yang 1. *Front Cell Dev Biol*, *8*, 592164. https://doi.org/10.3389/fcell.2020.592164
323. Vincent, J. A., Kwong, T. J., & Tsukiyama, T. (2008). ATP-dependent chromatin remodeling shapes the DNA replication landscape. *Nat Struct Mol Biol*, *15*(5), 477-484. https://doi.org/10.1038/nsmb.1419
324. Vogel, F., BornhöVd, C., Neupert, W., & Reichert, A. S. (2006). Dynamic subcompartmentalization of the mitochondrial inner membrane. *The Journal of Cell Biology*, *175*(2), 237-247. https://doi.org/10.1083/jcb.200605138
325. Wagatsuma, A., Shiozuka, M., Takayama, Y., Hoshino, T., Mabuchi, K., & Matsuda, R. (2016). Effects of ageing on expression of the muscle-specific E3 ubiquitin ligases and Akt-dependent regulation of Foxo transcription factors in skeletal muscle. *Mol Cell Biochem*, *412*(1-2), 59-72. https://doi.org/10.1007/s11010-015-2608-7
326. Walker P. R. , S. C., Youdale T. , Leblanc J. , Whitfield J. F. , Sikorska M. (1991). Topoisomerase II-reactive chemotherapeutic drugs induce apoptosis in thymocytes. *Cancer Research*, *51*, 1078-1085.
327. Wallitt, E. J. W., Jevon, M., & Hornick, P. I. (2007). Therapeutics of Vein Graft Intimal Hyperplasia: 100 Years On. *The Annals of Thoracic Surgery*, *84*(1), 317-323. https://doi.org/10.1016/j.athoracsur.2007.02.035
328. Wang, D., Chang, P. S., Wang, Z., Sutherland, L., Richardson, J. A., Small, E., Krieg, P. A., & Olson, E. N. (2001). Activation of cardiac gene expression by myocardin, a transcriptional cofactor for serum response factor. *Cell*, *105*(7), 851-862. https://doi.org/10.1016/s0092-8674(01)00404-4
329. Wang, J., Wu, X., Wei, C., Huang, X., Ma, Q., Huang, X., Faiola, F., Guallar, D., Fidalgo, M., Huang, T., Peng, D., Chen, L., Yu, H., Li, X., Sun, J., Liu, X., Cai, X., Chen, X., Wang, L., . . . Ding, J. (2018). YY1 Positively Regulates Transcription by Targeting Promoters and Super-Enhancers through the BAF Complex in Embryonic Stem Cells. *Stem Cell Reports*, *10*(4), 1324-1339. https://doi.org/10.1016/j.stemcr.2018.02.004
330. Wang, J., Zohar, R., & McCulloch, C. A. (2006). Multiple roles of alpha-smooth muscle actin in mechanotransduction. *Exp Cell Res*, *312*(3), 205-214. https://doi.org/10.1016/j.yexcr.2005.11.004
331. Wang, Y., Zhu, P., Luo, J., Wang, J., Liu, Z., Wu, W., Du, Y., Ye, B., Wang, D., He, L., Ren, W., Wang, J., Sun, X., Chen, R., Tian, Y., & Fan, Z. (2019). LncRNA HAND2-AS1 promotes liver cancer stem cell self-renewal via BMP signaling. *EMBO J*, *38*(17), e101110. https://doi.org/10.15252/embj.2018101110
332. Wang, Z., Wang, D. Z., Pipes, G. C., & Olson, E. N. (2003). Myocardin is a master regulator of smooth muscle gene expression. *Proc Natl Acad Sci U S A*, *100*(12), 7129-7134. https://doi.org/10.1073/pnas.1232341100

333. Weber, C. M., Ramachandran, S., & Henikoff, S. (2014). Nucleosomes are context-specific, H2A.Z-modulated barriers to RNA polymerase. *Mol Cell*, *53*(5), 819-830. https://doi.org/10.1016/j.molcel.2014.02.014
334. Wei, Y. H., Lu, C. Y., Wei, C. Y., Ma, Y. S., & Lee, H. C. (2001). Oxidative stress in human aging and mitochondrial disease-consequences of defective mitochondrial respiration and impaired antioxidant enzyme system. *Chin J Physiol*, *44*(1), 1-11. https://www.ncbi.nlm.nih.gov/pubmed/11403514
335. Weintraub, H. (1978). The nucleosome repeat length increases during erythropoiesis in the chick. *Nucleic Acids Res*, *5*(4), 1179-1188. https://doi.org/10.1093/nar/5.4.1179
336. Welsh, D. G., Tran, C. H. T., Hald, B. O., & Sancho, M. (2018). The Conducted Vasomotor Response: Function, Biophysical Basis, and Pharmacological Control. *Annual Review of Pharmacology and Toxicology*, *58*(1), 391-410. https://doi.org/10.1146/annurev-pharmtox-010617-052623
337. Westerhof, N., Lankhaar, J. W., & Westerhof, B. E. (2009). The arterial Windkessel. *Med Biol Eng Comput*, *47*(2), 131-141. https://doi.org/10.1007/s11517-008-0359-2
338. Whetstine, J. R., Nottke, A., Lan, F., Huarte, M., Smolikov, S., Chen, Z., Spooner, E., Li, E., Zhang, G., Colaiacovo, M., & Shi, Y. (2006). Reversal of histone lysine trimethylation by the JMJD2 family of histone demethylases. *Cell*, *125*(3), 467-481. https://doi.org/10.1016/j.cell.2006.03.028
339. Wilkinson, F., Pratt, H., & Atchison, M. L. (2010). PcG recruitment by the YY1 REPO domain can be mediated by Yaf2. *J Cell Biochem*, *109*(3), 478-486. https://doi.org/10.1002/jcb.22424
340. Wilkinson, F. H., Park, K., & Atchison, M. L. (2006). Polycomb recruitment to DNA in vivo by the YY1 REPO domain. *Proc Natl Acad Sci U S A*, *103*(51), 19296-19301. https://doi.org/10.1073/pnas.0603564103
341. Wilson, B. G., & Roberts, C. W. (2011). SWI/SNF nucleosome remodellers and cancer. *Nat Rev Cancer*, *11*(7), 481-492. https://doi.org/10.1038/nrc3068
342. Woodcock, C. L., Safer, J. P., & Stanchfield, J. E. (1976). Structural repeating units in chromatin. I. Evidence for their general occurrence. *Exp Cell Res*, *97*, 101-110. https://doi.org/10.1016/0014-4827(76)90659-5
343. Woods, Y. L., Rena, G., Morrice, N., Barthel, A., Becker, W., Guo, S., Unterman, T. G., & Cohen, P. (2001). The kinase DYRK1A phosphorylates the transcription factor FKHR at Ser329 in vitro, a novel in vivo phosphorylation site. *Biochem J*, *355*(Pt 3), 597-607. https://doi.org/10.1042/bj3550597
344. Wright, W. D., Shah, S. S., & Heyer, W. D. (2018). Homologous recombination and the repair of DNA double-strand breaks. *J Biol Chem*, *293*(27), 10524-10535. https://doi.org/10.1074/jbc.TM118.000372
345. Wu, S., Shi, Y., Mulligan, P., Gay, F., Landry, J., Liu, H., Lu, J., Qi, H. H., Wang, W., Nickoloff, J. A., Wu, C., & Shi, Y. (2007). A YY1-INO80 complex regulates genomic stability through homologous recombination-based repair. *Nat Struct Mol Biol*, *14*(12), 1165-1172. https://doi.org/10.1038/nsmb1332
346. Wystub, K., Besser, J., Bachmann, A., Boettger, T., & Braun, T. (2013). miR-1/133a Clusters Cooperatively Specify the Cardiomyogenic Lineage by Adjustment of Myocardin Levels during Embryonic Heart Development. *PLoS Genetics*, *9*(9), e1003793. https://doi.org/10.1371/journal.pgen.1003793
347. Xia, X. D., Zhou, Z., Yu, X. H., Zheng, X. L., & Tang, C. K. (2017). Myocardin: A novel player in atherosclerosis. *Atherosclerosis*, *257*, 266-278. https://doi.org/10.1016/j.atherosclerosis.2016.12.002

348. Xing, Y. Q., Li, A., Yang, Y., Li, X. X., Zhang, L. N., & Guo, H. C. (2018). The regulation of FOXO1 and its role in disease progression. *Life Sci*, *193*, 124-131. https://doi.org/10.1016/j.lfs.2017.11.030
349. Xu, Y., Ayrapetov, M. K., Xu, C., Gursoy-Yuzugullu, O., Hu, Y., & Price, B. D. (2012). Histone H2A.Z controls a critical chromatin remodeling step required for DNA double-strand break repair. *Mol Cell*, *48*(5), 723-733. https://doi.org/10.1016/j.molcel.2012.09.026
350. Xue, Y., Van, C., Pradhan, S. K., Su, T., Gehrke, J., Kuryan, B. G., Kitada, T., Vashisht, A., Tran, N., Wohlschlegel, J., Peterson, C. L., Kurdistani, S. K., & Carey, M. F. (2015). The Ino80 complex prevents invasion of euchromatin into silent chromatin. *Genes Dev*, *29*(4), 350-355. https://doi.org/10.1101/gad.256255.114
351. Yadav, V. R., Teng, B., & Mustafa, S. J. (2019). Enhanced A(1) adenosine receptor-induced vascular contractions in mesenteric artery and aorta of in L-NAME mouse model of hypertension. *Eur J Pharmacol*, *842*, 111-117. https://doi.org/10.1016/j.ejphar.2018.10.024
352. Yamagata, K., Daitoku, H., Takahashi, Y., Namiki, K., Hisatake, K., Kako, K., Mukai, H., Kasuya, Y., & Fukamizu, A. (2008). Arginine methylation of FOXO transcription factors inhibits their phosphorylation by Akt. *Mol Cell*, *32*(2), 221-231. https://doi.org/10.1016/j.molcel.2008.09.013
353. Yang, J. Y., Zong, C. S., Xia, W., Yamaguchi, H., Ding, Q., Xie, X., Lang, J. Y., Lai, C. C., Chang, C. J., Huang, W. C., Huang, H., Kuo, H. P., Lee, D. F., Li, L. Y., Lien, H. C., Cheng, X., Chang, K. J., Hsiao, C. D., Tsai, F. J., . . . Hung, M. C. (2008). ERK promotes tumorigenesis by inhibiting FOXO3a via MDM2-mediated degradation. *Nat Cell Biol*, *10*(2), 138-148. https://doi.org/10.1038/ncb1676
354. Yant, S. R., Zhu, W., Millinoff, D., Slightom, J. L., Goodman, M., & Gumucio, D. L. (1995). High affinity YY1 binding motifs: identification of two core types (ACAT and CCAT) and distribution of potential binding sites within the human beta globin cluster. *Nucleic Acids Res*, *23*(21), 4353-4362. https://doi.org/10.1093/nar/23.21.4353
355. Yao, T., Song, L., Jin, J., Cai, Y., Takahashi, H., Swanson, S. K., Washburn, M. P., Florens, L., Conaway, R. C., Cohen, R. E., & Conaway, J. W. (2008). Distinct modes of regulation of the Uch37 deubiquitinating enzyme in the proteasome and in the Ino80 chromatin-remodeling complex. *Mol Cell*, *31*(6), 909-917. https://doi.org/10.1016/j.molcel.2008.08.027
356. Yao, W., King, D. A., Beckwith, S. L., Gowans, G. J., Yen, K., Zhou, C., & Morrison, A. J. (2016). The INO80 Complex Requires the Arp5-Ies6 Subcomplex for Chromatin Remodeling and Metabolic Regulation. *Mol Cell Biol*, *36*(6), 979-991. https://doi.org/10.1128/MCB.00801-15
357. Yen, K., Vinayachandran, V., Batta, K., Koerber, R. T., & Pugh, B. F. (2012). Genome-wide nucleosome specificity and directionality of chromatin remodelers. *Cell*, *149*(7), 1461-1473. https://doi.org/10.1016/j.cell.2012.04.036
358. Yen, K., Vinayachandran, V., & Pugh, B. F. (2013). SWR-C and INO80 chromatin remodelers recognize nucleosome-free regions near +1 nucleosomes. *Cell*, *154*(6), 1246-1256. https://doi.org/10.1016/j.cell.2013.08.043
359. Yin, J., Xia, W., Wu, M., Zhang, Y., Huang, S., Zhang, A., & Jia, Z. (2019). Inhibition of mitochondrial complex I activity attenuates neointimal hyperplasia by inhibiting smooth muscle cell proliferation and migration. *Chem Biol Interact*, *304*, 73-82. https://doi.org/10.1016/j.cbi.2019.03.002

360. Yu, E. P. K., Reinhold, J., Yu, H., Starks, L., Uryga, A. K., Foote, K., Finigan, A., Figg, N., Pung, Y. F., Logan, A., Murphy, M. P., & Bennett, M. (2017). Mitochondrial Respiration Is Reduced in Atherosclerosis, Promoting Necrotic Core Formation and Reducing Relative Fibrous Cap Thickness. *Arterioscler Thromb Vasc Biol*, *37*(12), 2322-2332. https://doi.org/10.1161/ATVBAHA.117.310042
361. Yuan, Z., Becker, E. B., Merlo, P., Yamada, T., DiBacco, S., Konishi, Y., Schaefer, E. M., & Bonni, A. (2008). Activation of FOXO1 by Cdk1 in cycling cells and postmitotic neurons. *Science*, *319*(5870), 1665-1668. https://doi.org/10.1126/science.1152337
362. Zamponi, G. W., & Currie, K. P. (2013). Regulation of Ca(V)2 calcium channels by G protein coupled receptors. *Biochim Biophys Acta*, *1828*(7), 1629-1643. https://doi.org/10.1016/j.bbamem.2012.10.004
363. Zhang, J. J., Zhu, Y., Zhang, X. F., Liu, D. F., Wang, Y., Yang, C., Shi, G. D., Peng, Y. P., Zhang, K., Tian, L., Miao, Y., & Jiang, K. R. (2017). Yin Yang-1 suppresses pancreatic ductal adenocarcinoma cell proliferation and tumor growth by regulating SOX2OT-SOX2 axis. *Cancer Lett*, *408*, 144-154. https://doi.org/10.1016/j.canlet.2017.08.032
364. Zhang, Y., Liu, T., Meyer, C. A., Eeckhoute, J., Johnson, D. S., Bernstein, B. E., Nusbaum, C., Myers, R. M., Brown, M., Li, W., & Liu, X. S. (2008). Model-based analysis of ChIP-Seq (MACS). *Genome Biol*, *9*(9), R137. https://doi.org/10.1186/gb-2008-9-9-r137
365. Zhang, Z., & Pugh, B. F. (2011). High-Resolution Genome-wide Mapping of the Primary Structure of Chromatin. *Cell*, *144*(2), 175-186. https://doi.org/10.1016/j.cell.2011.01.003
366. Zhou, J., & Herring, B. P. (2005). Mechanisms Responsible for the Promoter-specific Effects of Myocardin. *Journal of Biological Chemistry*, *280*(11), 10861-10869. https://doi.org/10.1074/jbc.m411586200
367. Zhou, K., Gaullier, G., & Luger, K. (2019). Nucleosome structure and dynamics are coming of age. *Nat Struct Mol Biol*, *26*(1), 3-13. https://doi.org/10.1038/s41594-018-0166-x
368. Zhou, X., Blocker, A. W., Airoldi, E. M., & O'Shea, E. K. (2016). A computational approach to map nucleosome positions and alternative chromatin states with base pair resolution. *Elife*, *5*. https://doi.org/10.7554/eLife.16970
369. Zhuge, Y., Zhang, J., Qian, F., Wen, Z., Niu, C., Xu, K., Ji, H., Rong, X., Chu, M., & Jia, C. (2020). Role of smooth muscle cells in Cardiovascular Disease. *Int J Biol Sci*, *16*(14), 2741-2751. https://doi.org/10.7150/ijbs.49871
370. Zlatanova, J., Bishop, T. C., Victor, J. M., Jackson, V., & van Holde, K. (2009). The nucleosome family: dynamic and growing. *Structure*, *17*(2), 160-171. https://doi.org/10.1016/j.str.2008.12.016

Appendix

A

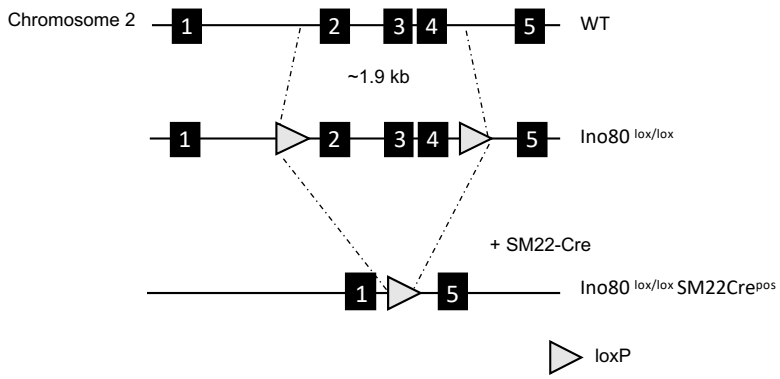

B

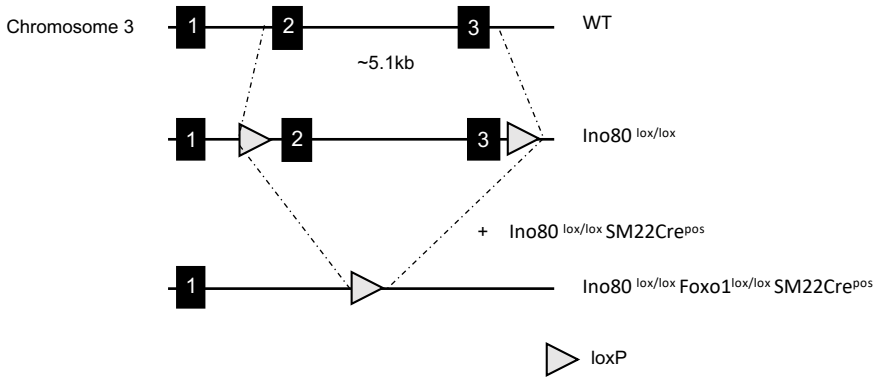

Figure 36. Schematic representation of the mating strategy for Ino80 and Foxo1 deletion in smooth muscle cells using the Cre-loxP system.

A Schematic representation of the genomic locus of Ino80. Exons 2-4 of the Ino80 coding region was flanked with loxP sequences (grey triangles) to allow for Cre-dependent deletion. Smooth muscle cell-specific Ino80 knockout was performed by breeding the Ino80$^{lox/lox}$ (Qiu et al., 2016) with SM22-Cre transgenic mice (Holtwick et al., 2002). **B** Schematic representation of the genomic locus of Foxo1. Exons 2 and 3 of the Foxo1 coding region was flanked with loxP sequences (grey triangles) to allow for Cre-dependent deletion (Stöhr et al., 2013). In order to induce Foxo1 knockout in addition to Ino80 knockout in smooth muscle cells, Foxo1$^{lox/lox}$ was bred with Ino80$^{lox/lox}$SM22Cre^{pos} transgenic mice.

A

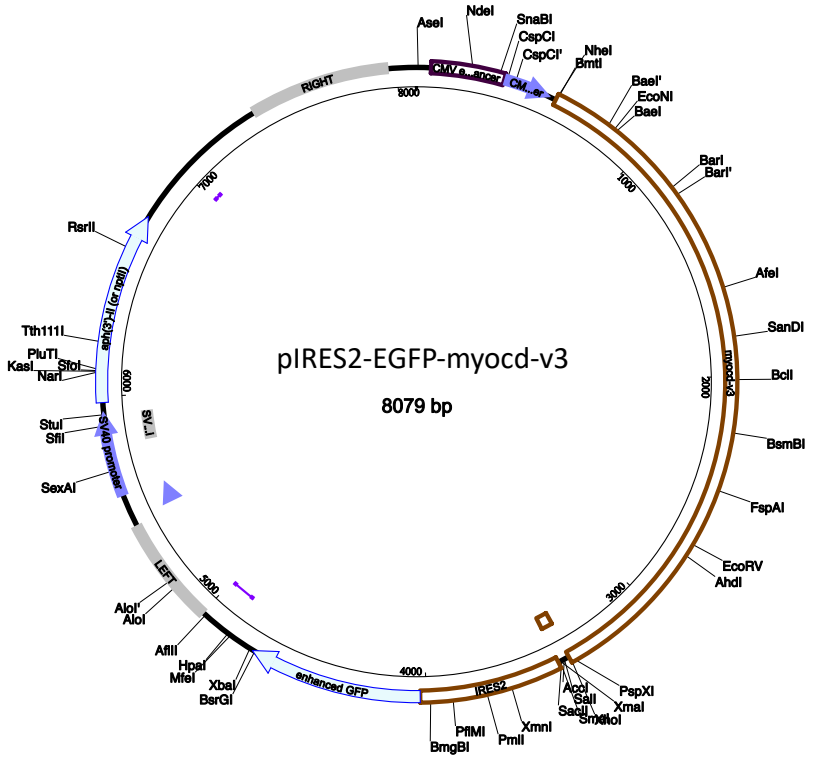

B

Type	Name	Range (bp)	Strand	Length (bp)	Description
enhancer	CMV enhancer	61..364	top	304	CMV enhancer
promoter	CMV promoter	365..568	top	204	CMV promoter
polyA_signal	HSV TK poly (A) signal	7001..7048	top	48	HSV TK poly (A) signal
misc_feature	IRES2	3438..4024	top	587	IRES2
rep_origin	LEFT	complement (4995..5450)	bottom	456	f1 ori
misc_feature	MCS	3384..3436	top	53	MCS
rep_origin	RIGHT	7377..7965	top	589	ori
rep_origin	SV40 ori	5791..5926	top	136	SV40 ori
polyA_signal	SV40 poly (A) signal	4867..4988	top	122	SV40 poly (A) signal
promoter	SV40 promoter	5583..5940	top	358	SV40 promoter
CDS	aph (3')-II (or nptII)	5975..6769	top	795	aminoglycoside phosphotransferase from Tn5
promoter	bla	5477..5581	top	105	bla
CDS	enhanced GFP	4025..4744	top	720	enhanced GFP
misc_feature	myocd-v3	591..3389	top	2799	myocd-v3
source	synthetic DNA construct	1..8079	top	8079	synthetic DNA construct

Figure 37. Plasmid map and features list of the pIRES2-EGFP-myocardin-v3 used for the myocardin overexpression construct.

A Myocardin smooth muscle cell specific variant (Imamura et al., 2010) was inserted into the multiple cloning site using NheI and XhoI cloning sites resulting in a 8079 bp vector. **B** Features list of the pIRES2-EGFP-myocardin-v3 construct.

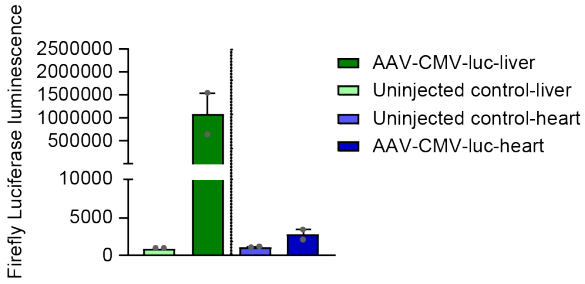

Figure 38. AAV8 achieves efficient liver specific transduction upon intravenous injection in mice.

Expression of firefly luciferase measured by luminescence *in vitro* from liver and heart tissue two days following AAV8-ssCMV-Luc intravenous injection versus un-injected. AAV (adeno-associated viral vectors), Luc (luciferase), CMV (cytomegalovirus promoter). n=1/1. Vector preparations were a gift from Oliver J. Mueller, Kiel University.

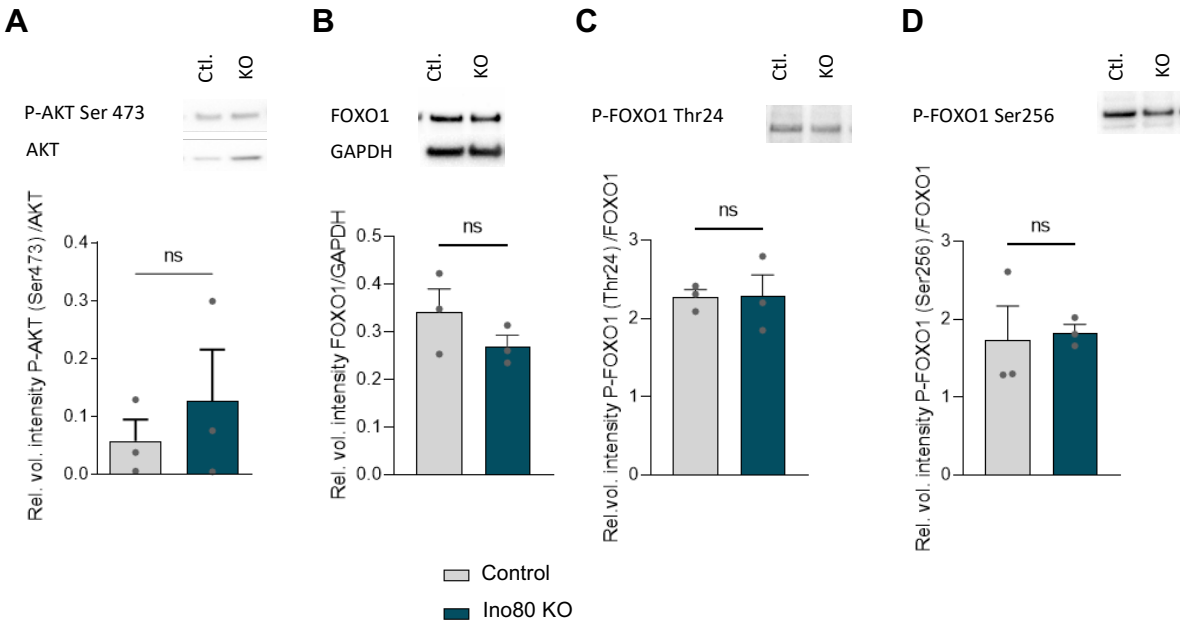

Figure 39. The Akt pathway is not involved in the increased FOXO1 activity observed upon loss of Ino80 in vascular smooth muscle cells.

A-D Western blot analysis of protein lysates from Ino80$^{lox/lox}$SM22Cre^{neg} (control), and Ino80$^{lox/lox}$SM22Cre^{pos} (Ino80 KO). n=3/3 murine aortas using the following antibodies. A Phospho-AKT Ser 473 (60 kDa) and AKT (60 kDa), B FOXO1 (78-82 kDa) and GAPDH (37 kDa), C FOXO1 (78-82 kDa) and Phospho-FOXO1 Thr 24 (78-82 kDa) D FOXO1 (78-82 kDa) and Phospho-FOXO1 Ser 256 (82 kDa). Ctl. (control), GAPDH served as a loading control and for normalization. FOXO1 (forkhead box O1), AKT (protein kinase B), INO80 (inositol requiring 80), Ser (serine), Thr (Threonine)

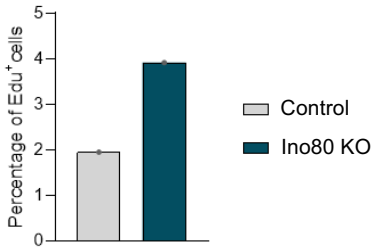

Figure 40. Loss of Ino80 leads to an increase in VSMCs proliferation *in vitro.*
Statistical analysis of the percentage of Edu positive pulmonary arterial smooth muscle cells isolated from Ino80$^{lox/lox}$ SM22Cre^{neg} (control) and Ino80$^{lox/lox}$ SM22Cre^{pos} (Ino80 KO) and stained for EdU. Ino80 (inositol requiring 80), EdU (5-ethynyl-2′-deoxyuridine), Edu+ (Edu positive). n=1/1.

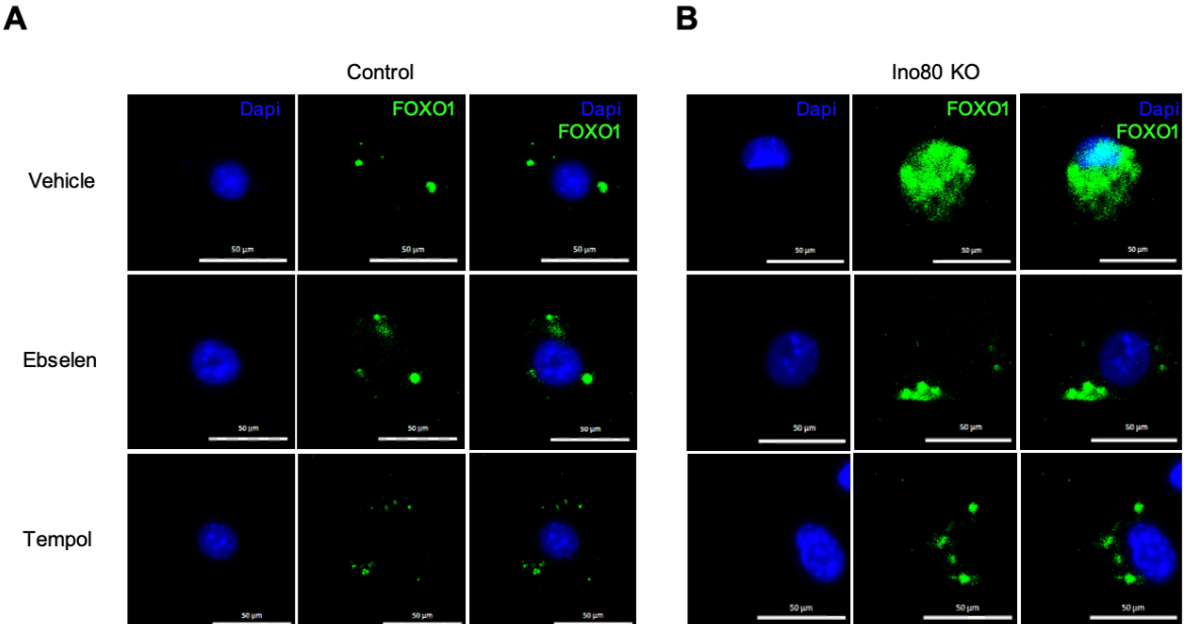

Figure 41. Treatment with ROS scavengers can abrogate the switch in FOXO1 subcellular localization observed upon loss of Ino80.
A-B Representative images of pulmonary arterial smooth muscle cells isolated from Ino80$^{lox/lox}$ SM22Cre^{neg} (control) and Ino80$^{lox/lox}$ SM22Cre^{pos} (Ino80 KO) mice treated with vehicle (DMSO), 1μM Ebselen or 3mM Tempol respectively for 24 hours. Vehicle treated cells were used as a negative control. Cells were stained for DAPI (blue) and anti-FOXO1 antibody (green). Scale bar 50 μm. Ino80 (inositol requiring 80), FOXO1 (forkhead box O1).

Acknowledgments

First, I would like to express my sincere gratitude to Prof. Dr. Thomas Boettger for the opportunity to work on this project, his expertise, continuous support, guidance and patience throughout my PhD.

Many thanks also go to Prof. Dr. Dr. Thomas Braun for allowing me to pursue my PhD in his department. I am also grateful for the suggestions and support during the seminars but also for challenging my ideas and pushing me to develop my critical thinking.

I am also grateful to Prof. Dr. Reinhard Dammann and Prof. Dr. Lienhard Schmitz for supervising my dissertation at the University of Giessen and for their suggestions during the thesis advisory committee meetings.

I would also like to thank my group members for their help, discussions and suggestions. Special thanks go to Theresa and Christian. Theresa, for the constant friendship, encouragements and discussions throughout the last years and Christian for the support at the beginning of my PhD. Moreover, I would like to thank Jonas, Dafina, Simon and Stephanie for their help with genotyping.

Special thanks also go to the staff of the animal house for their work and all my colleagues from the Department of Cardiac Development and Remodeling, especially to Marion who performed the mouse surgeries and to Laia for her help with the atherosclerosis development work.

Last but foremost, my biggest thanks to my family and friends, for all the support and understanding you have shown me. To my husband Driss, thank you for helping me stay focused and motivated, it has been a great comfort and relief to know you were taking such good care of our son when I couldn't. Thank you for taking care of us the way you do. To my son Elias, thank you for keeping my spirits high with your love and big smile. To my parents, brother and sisters, thank you for the constant support, motivation and encouragements, it has been a true source of strength.